

**Instituto de Neurociencias de Alicante
Universidad Miguel Hernandez**

Thesis manuscript for:

PhD in Neurosciences title

**Assessing the action of GluK1 overexpression
on synaptic strength and plasticity in a mouse
model of Down syndrome**

Wilfrid Mazier

Supervised by:
Prof. Juan Lerma

Year 2014

Prof. Juan Lerma Gómez, Director del Instituto de Neurociencias de Alicante, Centro Mixto de la Universidad Miguel Hernández, UMH y de la Agencia Estatal Consejo Superior de Investigaciones Científicas, CSIC

CERTIFICA:

Que la Tesis Doctoral titulada” *“Assesing the action of GluK1 overexpression of synaptic strength and plasticity in a mouse model of down syndrome”* ha sido realizada por D. Wilfrid Bernard Mazier, bajo su misma dirección y supervisión como Profesor de Investigación CSIC en el Instituto de Neurociencias, UMH-CSIC, y da su conformidad para que sea presentada ante la Comisión de Doctorado de la Universidad Miguel Hernández.

Y para que así conste a los efectos oportunos, firma el presente certificado, en Sant Joan d’Alacant, a 28 de febrero de 2014


Juan Lerma
Director
Instituto Neurociencias, UMH-CSIC



Prof. Juan Lerma Gómez, Profesor de Investigación de la Agencia Estatal Consejo Superior de Investigaciones Científicas, CSIC

CERTIFICA:

Que la Tesis Doctoral titulada” *“Assesing the action of GluK1 overexpression of synaptic strength and plasticity in a mouse model of down syndrome”* ha sido realizada por D. Wilfrid Bernard Mazier, bajo su inmediata dirección y supervisión en el Instituto de Neurociencias, UMH-CSIC, y que presenta para la obtención del grado de Doctor por la Universidad Miguel Hernández.

Y para que así conste a los efectos oportunos, firma el presente certificado, en Sant Joan d’Alacant, a 28 de febrero de 2014



Juan Lerma
Profesor Investigación CSIC
Instituto Neurociencias, UMH-CSIC



To Anaïs & my family



ACKNOWLEDGEMENTS

My thanks first go to my supervisor Professor Juan Lerma who opened me the doors of his institute and lab to permit me to do these PhD project. Thanks for his help and advices correcting the various abstracts, posters and finally this manuscript.

Many thanks also to Dr Ana Paternain, alias *Ana checking*, who kindly and patiently taught me *in vitro* electrophysiology, data analysis and many others professional skills. Thanks also to Monica Llinares for her very precious help in animal genotyping especially in this last moments. Many thanks to Dr. Isabel Aller and Ester Pico for their help and advices during molecular biology experiments. I also want to thank all the others lab members: Jon, Joana, Ricardo, Sergio, Valeria and the Instituto de Neurociencias de Alicante's staff. Thanks to all these persons I also finally managed to speak an understandable Spanish.

I am also grateful to Dr Keith Phillips and Dr. John Isaac from Eli Lilly Company for having welcomed me 6 months in their team and given me the opportunity to acquire skills in animal behavior and *in vitro* electrophysiology. This short internship allows me to appreciate Science in a private company. I also thank Dr Anthony Blockeel and Dr Johanna Jackson for their warm welcoming and help during this stage.

I would like to show my gratitude to the coordinators of the SyMBad Marie Curie program: Dr Christophe Mulle and Dr Antonella Caminiti for the organization of this great european PhD program.

I really want to thank my friends: Pierrick (*Piwi, petit chat, baba-pas-cool*), Mehdi (*enfant du soleil*), Julien (*Abdou*), Johnathan (*Zapinou*), Amandine (*Saucisse*), Till (*Tillus*), Zeus (*Mr Fahrenheit*), Gabriele (*Gabri*) and all the others for suffering me all these months. I would also like to thank all the people and friends met during these three last years in Alicante and in UK.

Many thanks to my parents, my sister and my brother for their support and patience even at more than 1500kms of distance.

Finally and most importantly, I would like to thank my lovely girlfriend Anaïs for her massive support and incredible patience during these three and half years of long distance relationship. Now I am really happy and in a hurry to go back living close to her.

Preamble

The main cognitive functions like language speaking, memory and thinking are dependent on the correct function of the brain. The central nervous system is a great network made by interconnected cells that can be glial or neuronal cells. To communicate between them, neural cells exchange information via a specialized structure called synapse. In the presynaptic neuron, depolarization of the cell body can generate an electrical signal, the action potential, which is conducted along the axon till the synaptic apparatus. At this level, action potentials are transformed into a chemical messenger by releasing neurotransmitters to the extracellular fluid. They cross the synaptic cleft to reach the “postsynaptic” neuron, specifically suited for the reception of this messenger. Activation of the receptor machinery gives birth to a new electrical signal in the postsynaptic neuron that will run towards the cell body, where multiple signals may be integrated. Correct communication between the different neurons or groups of neurons is mandatory for adequate cognitive functions. That is why the study of the mechanisms involved in the synaptic transmission is crucial to understand how the brain works and generate cognition. My main thesis project, carried out at the “Instituto de Neurociencias de Alicante”, aimed at improving our knowledge about the role of kainate receptors and figure out their level of implication in the Down syndrome pathophysiology, a syndrome where cognitive abilities are compromised.

This thesis has been done within the SyMBaD ("Synapses: from Molecules to higher Brain function and Diseases") international research Marie Curie program (7th framework). This program aimed to teach sophisticated techniques required for the study of synapses and extends from molecules through higher brain function to diseases.

This program was also focused on building constructive interactions between academia and the industry in Neurosciences. That's why during this 36 months fellowship, I did a 6 months internship in a private company: Eli Lilly and Co (Erl Wood Manor, Surrey, United Kingdom). This stage gave an international and industrial vision to my research experience. In this company my project was also focused on neuronal communication in health and disease. The objective was to “characterize the abnormal neuronal network activity in a rat model of schizophrenia”. A short report of this internship will be presented as an Appendix at the end of this manuscript.

Abstract

Kainate receptors belong to one subfamily of the glutamatergic receptors. This receptor family is composed by homo- or heterodimers of five different types of subunits named GluK1 to GluK5. The human gene coding for the kainate receptor subunit GluK1 (*GRIK1*) is located on the human chromosome 21 that triplicates in Down syndrome. In animal models of this disease, *Grik1* is situated on the short triplicated segment of chromosome 16, the orthologous of human chromosome 21. Previous work on trisomic models has found an imbalance between excitatory and inhibitory hippocampal synaptic activity.

In this study, we used Ts2Cje mouse model to investigate a putative link between a GluK1 excess of function and altered synaptic properties in the hippocampus of trisomic mice.

Trisomic animals were differentiated from their diploid littermates (DLM) by multiplex qPCR. RTqPCR analysis revealed that *Grik1* mRNA levels are increased by more than 50% in different structures of the trisomic brain. Despite the lack of GluK1 specific antibody, we found in electrophysiological experiments that the extra gene-copy produces an increase of GluK1 functional protein at the membrane of trisomic neurons. Hippocampal patch clamp recordings from CA1 neurons revealed significant increase in basal and evoked inhibitory drive onto pyramidal cells and interneurons from trisomic mice. Ts2Cje animals also presented impaired synaptic plasticity in hippocampal CA1 pyramidal cells. We also observed that GluK1 selective drugs may rescue the over-inhibition phenotype observed in trisomic mice. Our data support the implication of GluK1-containing kainate receptors in the control of network activity in the area CA1 of the hippocampus which is altered in Down syndrome. Further molecular and pharmacological experiments will reveal more details about the effect of GluK1 overexpression on synaptic physiology and pathophysiology of this disease.

Resumen (en Castellano)

Los receptores al kainato pertenecen a la familia de los receptores glutamatergicos. Esta familia de receptores se compone de homo- y heterodimers de cinco diferentes subunidades, del GluK1 al GluK5. El gene codificando para la subunidad GluK1 (*GRIK1*) está localizado sobre el cromosoma 21 triplicado en el síndrome de Down. En modelos animales de esta patología, *Grik1* está localizado en el corte trozo triplicado of del cromosoma 16, el ortólogo of del cromosoma humano 21. Precedente estudios han demostrado la existencia de un desequilibrio entre excitación y inhibición en la actividad sináptica del hipocampo de estos modelos.

En este trabajo, hemos utilizado el modelo Ts2cje para investigar sobre una relación entre un exceso de función de GluK1 y la alteración de la transmisión sináptica el hipocampo de ratones trisomicos. Ts2Cje animales fueron distinguidos de las crías disomicas por multiplex qPCR. RTqPCR análisis ha revelado que *Grik1* ARNm niveles están incrementados por 50% en las diferentes estructuras del cerebro trisomico. Aunque no existe ninguno especifico anticuerpo para GluK1, hemos demostrado haciendo electrophisiologia que una extra copia del gen aumenta la cantidad de proteína funcional a la membrana de las neuronas trisomicas. Patch clamp registros hechos en la región CA1 del hipocampo han revelado un incremento significativo de la inhibición basal y evocada de las células piramidales y de las interneuronas en ratones trisomicos. Ts2Cje animales también presentaban una alteración de la plasticidad sináptica en las células piramidales de CA1. Hemos demostrado que la farmacología selectiva para GluK1 puede reducir el fenotipo de sobre inhibición observado en ratones trisomicos.

Nuestros resultados soportan la implicación de los receptores al kainato conteniendo GluK1 en el control de la actividad de la red CA1 alterada en el síndrome de Down. Los siguientes experimentos moleculares y farmacológicos revelaran más detalles sobre el efecto de la sobre expresión de GluK1 sobre la fisiología sináptica y fisiopatología de esta enfermedad.



WORK COMMUNICATIONS
LIST OF ABBREVIATIONS

POSTER PRESENTATIONS

Mazier W., Paternain A.V. and Lerma J.G. GluK1 overexpression in a mouse model of Down syndrome results in an increase of inhibitory synaptic transmission. European Synapse Meeting, 28-30 August 2013, Bordeaux, France

Mazier W., Paternain A.V. and Lerma J.G. Assessing the action on synaptic strength and plasticity of GluK1 overexpression in a Down's syndrome animal model. 8th FENS Forum of Neuroscience, 14-18 July 2012, Barcelona, Spain

Mazier W., Paternain A.V. and Lerma J.G. Assessing the action on synaptic strength and plasticity of GluK1 overexpression in a Down's syndrome animal model. International symposium on ionotropic glutamate receptors, 16-17 February 2012, Valencia, Spain

ORAL PRESENTATIONS

Cellular and systems unit seminar - Instituto de Neurociencias de Alicante, Spain

Annual SyMBaD Marie Curie reports

Introduction seminar - June 2013, Nutri Neuro, University Bordeaux II, France

LIST OF ABBREVIATIONS

ACET	<i>S</i> -1-(2-Amino-2-carboxyethyl)-3-(2-carboxy-5-phenylthiophene-3-yl-methyl)-5-methylpyrimidine-2,4-dione
AMPAR	α -amino-3-hydroxy-5-methyl-4-isoxazolepropionic acid receptors
AP	Action Potential
App	Amyloid protein precursor
ATPA	2-Amino-3-(3-hydroxy-5- <i>tert</i> -butylisoxazol-4-yl) Propanoic Acid)

CA	Cornu Ammonis or Ammun's horn
CC	Cyclophilin
CNS	Central Nervous System
CNQX	6-cyano-7-nitroquinoxaline
CT	Cycle Threshold

DEPC	Diethylpyrocarbonate
DNA	DesoxyriboNucleic Acid
DNQX	6,7-dinitroquinoxaline-2,3-dione
DG	Dentate Gyrus
DS	Down Syndrome
DSCR	Down Syndrome critical Region 1

EC	Entorhinal Cortex
eEPSC	evoked Excitatory PostSynaptic Current
eIPSC	evoked Inhibitory Post Synaptic Currents
EPSC	Excitatory PostSynaptic Current

fEPSP	field excitatory post synaptic potentials
FV	Fiber Volley
FRET	Fluorescence Resonance Energy Transfer

GABA	Gamma-AminoButyric Acid
GluK1	Glutamatergic ionotropic Kainate receptor subunit 1
GluK1-KARs	GluK1-containing kainate receptors

HFS	High Frequency Stimulation
HSA21	Homo Sapiens 21 chromosome

iGluR	ionotropic Glutamate Receptors
--------------	--------------------------------

KAR	Kainate Receptor
------------	------------------

LFP	Local Fiel Potential
------------	----------------------

LFS	Low Frequency Stimulation
LTD	Long-Term Depression
LTP	Long-Term Potentiation
mGluR	metabotropic Glutamate Receptors
mIPSC	miniature Inhibitory Post Synaptic Currents
mRNA	messenger RiboNucleic Acid
MMU	<i>mus musculus</i> chromosome
NBQX	2,3-dihydroxy-6-nitro-7-sulphamoyl-benzo(F)quinoxaline
NMDAR	N-methyl-D-aspartate receptors
PKC	Protein Kinase C
PPD	Paired-Pulse Depression
PPF	Paired-Pulse Facilitation
PPR	Paired-Pulse Ratio
PSD	Post Synaptic Density
qPCR	quantitative Polymerization Chain Reaction
rpm	rounds per minute
RNA	RiboNucleic Acid
RNA^{tot}	RiboNucleic Acid total
rRNA	ribosomal RiboNucleic Acid
RT	Reverse Transcription
Sc	Schaffer collaterals
sIPSC	spontaneous Inhibitory Post Synaptic Currents
T_M	TransMembrane domain
UBP310	S)-1-(2-Amino-2-carboxyethyl)-3-(2-carboxy-thiophene-3-yl-methyl)-5-methylpyrimidine-2,4-dione



TABLE OF CONTENTS
Miguel
Hernández

I. Introduction.....	1
1. The Down syndrome.....	1
1.1. Generalities	1
1.1.1. History	1
1.1.2. Epidemiology, diagnostic, etiology	1
1.1.3. Pathophysiology of Down syndrome.....	3
1.2. The triplicated chromosome: HSA21	4
1.2.1. Chromosome cartography.....	5
1.2.2. Gene expression and proteomic	5
1.2.3. Orthology	7
2. The hippocampus.....	7
3. The synapse	9
3.1. Generalities	9
3.2. The glutamatergic synapse.....	10
3.2.1. Morphology and classification.....	10
3.2.2. The glutamate receptors	10
3.2.2.1. Ionotropic glutamate receptors	10
3.2.2.2. Metabotropic glutamate receptors	10
3.2.3. Excitatory synaptic plasticity.....	13
3.2.3.1. Short term plasticity.....	13
3.2.3.2. Long term plasticity	13
3.2.3.3. Role of synaptic plasticity.....	14
3.3. The inhibitory synapse.....	15
3.3.1. Generalities.	15
3.3.2. The different types of GABA receptors.....	15
3.3.3. Inhibitory synapse plasticity	16
4. The kainate receptors	17
4.1. Generalities	17
4.2. Structure and composition of KARs subunits.....	17
4.2.1. Structure and pharmacology	17
4.2.2. Molecular cloning and recombinant KARs	18

4.2.3. Kainate receptors distribution	20
4.3. Kainate receptors physiology.....	22
4.3.1. Mediation of the synaptic transmission	22
4.3.2. Regulation of the synaptic transmission	23
4.3.3. Regulation of neuronal excitability.....	28
4.4. Pathophysiology of kainate receptors	28
5. Mouse models of Down syndrome.....	32
5.1. Transgenic models	33
5.2. Partial and full models	33
6. Down syndrome as a synaptopathy.....	37
7. Aim of the thesis project.....	39
II. Materials and Methods.....	41
1. Animal model: the Ts2Cje mouse	43
2. Animal genotyping	45
3. Evaluation of mRNA levels: RT-qPCR.....	47
4. Quantification of KARs protein levels	52
5. <i>In vitro</i> electrophysiology	53
5.1. Setting up the experiment	53
5.2. Whole cell patch clamp experiments	55
5.3. Extracellular field recording experiments.....	56
5.4. Kainate receptors selective pharmacology	57
5.5. Data analysis	57
III. Results.....	59
1. Ts2Cje production and genotyping.....	61
2. Increased GluK1 mRNA levels	62
3. Changes in KARs protein levels.....	63
4. Overexpression of functional GluK1 in CA1 interneurons	65
5. Increased basal inhibitory synaptic transmission in CA1 pyramidal cells	66
6. Enhanced basal inhibitory synaptic transmission in SR interneurons	73

7. Augmented basal inhibitory synaptic transmission in SO interneurons.....	76
8. Impaired evoked inhibitory synaptic transmission.....	78
9. Altered synaptic plasticity in Ts2Cje hippocampus CA1.....	82
IV. Discussion.....	89
1. Animal production and genotyping.....	91
2. GluK1 mRNA levels are increased in Ts2Cje.....	92
3. Protein quantification highlights changes in KARs levels in Ts2Cje.....	92
4. GluK1 levels are increased at interneuron membrane.....	93
5. Increased basal inhibitory neurotransmission in the area CA1.....	93
6. Impaired evoked inhibitory synaptic transmission in the area CA1.....	96
7. Deficient synaptic plasticity in area CA1.....	97
V. General conclusion.....	99
VI. Conclusiones en Castellano.....	104
VII. Bibliography.....	105
VIII. Appendix: Eli Lilly private internship report.....	123
1. Introduction.....	125
2. Materials and Methods.....	135
3. Results.....	140
4. Discussion.....	145
5. Appendix bibliography.....	147



INTRODUCTION

1. The Down syndrome

1.1. Generalities

Down syndrome (DS), also known as Trisomy 21, is a genetic disorder and the main genetic cause of mental disability. Clinical and genetic description of the disease came out with Science progress during XIX and XX centuries. It has been the first discovered chromosome aberration and the first demonstration of a link between genotype and phenotype.

1.1.1 History

The first clinical description of DS was reported in 1838 by Jean-Etienne Esquirol (French psychiatrist) who named this syndrome as *Idiocy*. Then in 1844, Edouard Segouin (French physician and educationist) in *Idiocy and its treatment by the physiological method* made a more specific and detailed description of the illness. Finally the first complete clinical description of DS was reported by John Langdon Down (British physician) in *Observation on an ethnic classification of idiots* (Down, 1866). In view of the typical patient face shape, he first called the disease *Mongoloid Idiocy*. The genetic characterization came one century after Esquirol first description. In 1959, a French team composed by Raymond Turpin, Jérôme Lejeune and Marthe Gauthier established the karyotypes of 3 young patients and observed for the first time the chromosome aberration at the origin of the syndrome: the chromosome 21 (HSA21) extra copy (figure 1).

1.1.2 Epidemiology, diagnostic, etiology

Epidemiology

DS is the most common viable chromosome aberration in humans. There are approximately 60 millions of persons who have DS. Following improved medical care, particularly with heart problems, the life expectancy among persons with DS has increased from 12 years in 1912, to 60 years nowadays. Globally, DS prevalence is about 1.4 per 1000 live births and results in about 17,000 deaths per year in the United States. The chance of having a pregnancy with DS increases with the mother's age (figure 2A) (Yoon et al., 1996).

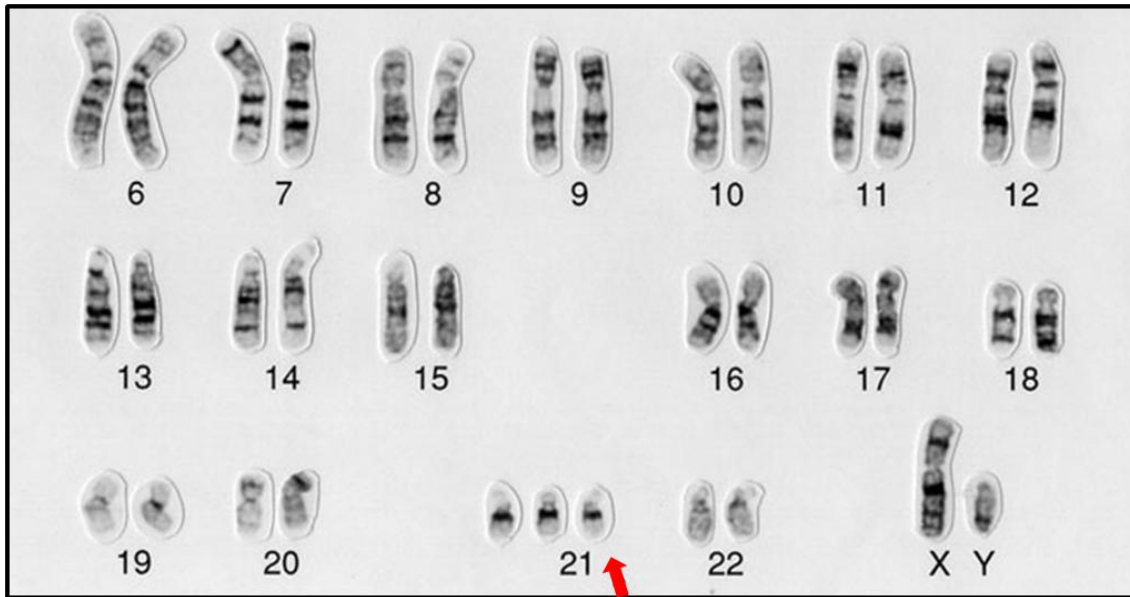


Figure 1: DS karyotype of a human male (formula: 47,XY,+21). This male has a full chromosome collection plus an extra chromosome 21 (red arrow). *Wessex Reg. Genetics Centre / Wellcome Images*

Diagnostic

Even if age of the first pregnancy increases, the DS incidence is decreasing in several countries. This is due to improvement of DS detection after prenatal screening. A number of tests can be used, with varying levels of accuracy and invasiveness. If screening is positive either amniocentesis or chorionic villous sampling is required to confirm the diagnosis.

Etiology

In 92.5% of the cases, trisomy is free and homogeneous, because the extra HSA21 comes from a meiotic non-disjunction during gametogenesis (generally in the female egg cell) and because the triplication is present in all cells of the organism. In 2.5% of the cases, trisomy can also be due to a translocation of the HSA21 on another chromosome. Half of these cases are parental transmission; the other half arise *de novo*. In the majority of the cases, the translocation is Robertsonian. Supernumerary HSA21 is fused with an acrocentric chromosome (e.g. 13, 14, 15, 21, 22). The main form of Robertsonian translocation observed is 14-21. A reciprocal translocation between HSA21 long arm and another chromosome can also occur. A free trisomy in mosaic is observed in 3% of the cases. Here two populations of cells co-exist: one is normal and the other contains an extra chromosome. This form of trisomy comes from a mitotic accident (non-disjunction or loss of one chromosome) during first cellular divisions of

the initial zygote that can be either normal (46, XX or XY) or with an extra chromosome 21 (47, XX, +21 or 47, XY, +21).

1.1.3 Pathophysiology of Down syndrome

DS patients present a large spectrum of clinical symptoms implying all systems at structural and functional levels. Symptoms severity varies from one individual to the other and from one trisomy type to the other.

Intellectual disability and neurological issues

Trisomy represents around 30% of total mental illness in human. Intellectual disability is “the” preponderant and invariable phenotype of the disease. It is also the most handicapping. All individuals are characterized by cognitive disorders and low intellectual quotient that make them dependent from others people in their daily life. An adapted and early care, can improve considerably their intellectual performance (Dierssen et al. 2009).

Psychomotor and cognitive delay

Early childhood is characterized by a slow psychomotor development. For instance DS children learn to walk one year later than normal children (Ulrich et al., 2001). DS children present problems in the posture maintenance due to a generalized hypotonia, ligament laxity and defect in the mechanisms controlling the posture. A serious delay in language comprehension and expression is also reported. However DS patient present normal capacities to learn simple tasks (cognitive executive functions, like spatial navigation for example) (Rowe et al., 2006).

Behavior disorders

DS patients can exhibit behavioral troubles, notably anxiety, depression (Walker et al., 2011) and attention deficit hyperactivity disorder. In rare cases, autistic disorders and aggressive behavior can be observed. However DS patients are generally very sociable and affective (Roizen and Patterson, 2003).

Morphological abnormalities

DS patients usually present facial dimorphism and musculoskeletal anomalies. At birth the face is round and flat (figure 2C) and the cranial skull is small with flat occiput (figure 10B), concurrent with cerebral malformations (figure 2B).

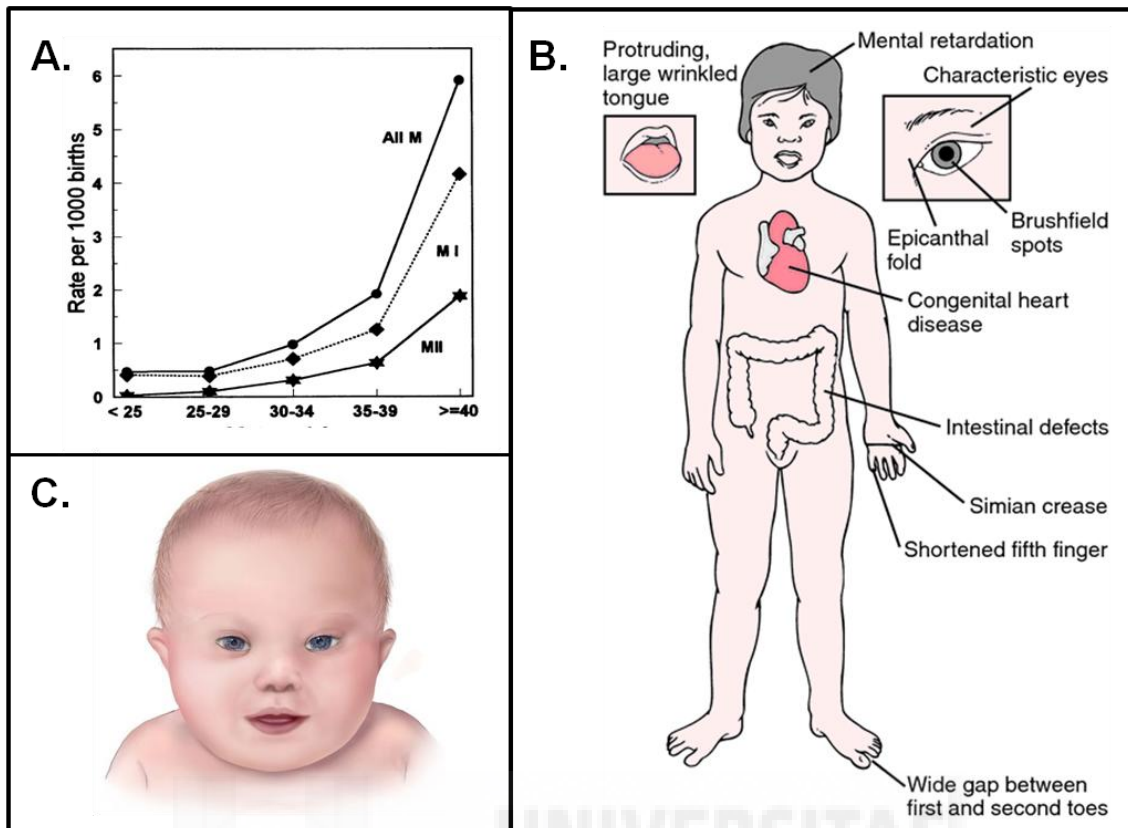


Figure 2: (A) Estimated birth-prevalence rates of maternally derived trisomy 21 by maternal age. Atlanta, Georgia, 1989-1993. All M= maternally derived cases; MI= maternal meiosis cases; MII= maternal meiosis II cases (Yoon *et al*, 1996). (B) Recapitulative schema presenting the main clinical signs associated with DS. (C) A drawing of the facial features of DS cdc.gov/ncbddd/birthdefects/DownSyndrome.

In general adult DS patients have microcephaly, the regions selectively reduced are the frontal lobe, the hippocampus and the cerebellum (Rachidi and Lopes, 2007). Inversely the size of the subcortical gray matter and the parahippocampal gyrus are augmented (Pinter *et al*., 2001). The cerebral alterations are in direct relationship with the intellectual delay observed in the disease. DS is frequently associated to cardiac insufficiency, gastrointestinal problems, immune system alterations and an accelerated ageing associated with Alzheimer disease.

1.2. The triplicated chromosome: HSA21

HSA21 is the smallest of the 23 chromosomes, that's likely why its triplication is viable. HSA21 genes sequencing and analysis are crucial to understand the genetic mechanisms responsible for DS.

1.2.1 Chromosome cartography

The full HSA21 sequence has been published in 2000 (Hattori et al., 2000). HSA21 is an acrocentric chromosome, with a long arm, HSA21q, and a short arm, HSA21p. All the genes present on HSA21 are not known yet, but around 3% of the sequence seems to be coding. On HSA21q around 240 genes could code for proteins (Antonarakis et al., 2004). The gene repartition along the chromosome is not homogeneous; around 60 genes are located at the proximal half of HSA21q whereas all the others are on the distal part. Some rare cases of partial trisomy allowed the elaboration of a relationship between genotype and phenotype. These links have been more precisely drawn thanks to the generation of several rodent models. A region sufficient to induce phenotype preponderance for the disease has been pointed out and named the *Down Syndrome critical Region (DSCR)* (Korenberg et al., 1994). It contains 20 genes, 2.8Mb and it is localized on 21q22.2 band. Another region involved in facial dimorphism and cardiac malformation has been delimited and called *Down syndrome congenital heart disease* (Korenberg et al., 1992).

1.2.2. Gene expression and proteomic

Functions of the proteins coded by HSA21 genes are not fully known. Ontological analysis demonstrates that they act in at least a hundred of biological processes. Around 15 genes are referenced as transcription factors or molecules able to interact with DNA, 11 genes are involved a signal transduction, 8 code for cell adhesion proteins and 7 implicated in the mitochondrial function. A list of 122 genes has been proposed in 2000 (table 1; Gardiner and Davisson, 2000). Interestingly, *GRIK1*, the gene coding for GluK1 kainate receptors subunit, is located in the DSCR.

1.2.3. Orthology

Comparative genomics is a potent tool to decode human genome. The conserved and functional sequences that are transcribed can be identified. A good starting point to do the comparison is laboratory mouse *mus musculus*. The genomic sequence has been decrypted in both human HSA21 and mouse, then comparative analysis have been made in syntenic sequences (Dermitzakis et al., 2002). The orthologous regions (conserved from mouse to human) are located on 3 distinct chromosomes in the mouse (MMU for *mus musculus*):

Functional categories	Nb of genes	Functional assignments
Transcription factors, regulators, and modulators	17	GABPA, BACH1, RUNX1, SIM2, ERG, ETS2 (transcription factors); ZNF294, ZNF295, Pred65, *ZNF298, APECED (zinc fingers); KIAA0136 (leucine zipper); GCFC (GC-rich binding protein); SON (DNA binding domain); PKNOX1 (homeobox); HSF2BP (heat shock transcription factor binding protein); NRIP1 (modulator of transcriptional activation by estrogen)
Chromatin structure	4	H2BFS (histone 2B), HMG14 (high mobility group), CHAF1B (chromatin assembly factor), PCNT (pericentrin, an integral component of the pericentriolar matrix of the centrosome)
Proteases and protease inhibitors	6	BACE (beta-site APP cleaving enzyme); TMPRSS2, TMPRSS3 (transmembrane serine proteases); ADAMTS1, ADAMTS5 (metalloproteinases); CSTB (protease inhibitor)
Ubiquitin pathway	4	USP25, USP16 (ubiquitin proteases); UBE2G2 (ubiquitin conjugating enzyme); SMT3A (ubiquitin-like)
Interferons and immune response	9	IFNAR1, IFNAR2, IL10RB, IFNGR2 (receptors/auxiliary factors); MX1, MX2 (interferon-induced); CCT8 (T-complex subunit), TIAM1 (T-lymphoma invasion and metastasis inducing protein), TCP10L (T-complex protein 10 like)
Kinases	8	ENK (enterokinase); MAKV, MNB, KID2 (serine/threonine); PHK (pyridoxal kinase), PFKL (phosphofructokinase); *ANKRD3 (ankyrin-like with kinase domains); PRKCBP2 (protein kinase C binding protein)
Phosphatases	2	SYNJ1 (polyphosphoinositide phosphatase); PDE9A (cyclic phosphodiesterase)
RNA processing	5	rA4 (SR protein), U2AF35 (splicing factor), RED1 (editase), PCBP3 (poly(C)-binding protein); *RBM11 (RNA-binding motif)
Adhesion molecules	4	NCAM2 (neural cell), DSCAM; ITGB2 (lymphocyte); c21orf43 (similar to endothelial tight junction molecule)
Channels	7	GRIK1 (glutamate receptor, calcium channel); KCNE1, KCNE2, KNCJ6, KNCJ15 (potassium); *CLIC11 (chloride); TRPC7 (calcium)
Receptors	5	CXADR (Coxsackie and adenovirus); Claudins 8, 14, 17 (Claustidia); Pred12 (mannose)
Transporters	2	SLC5A3 (Na-myoinositol); ABCG1 (ATP-binding cassette)
Energy metabolism	4	ATP50 (ATP synthase oligomycin-sensitivity conferral protein); ATP5A (ATPase-coupling factor 6); NDUFV3 (NADH-ubiquinone oxidoreductase subunit precursor); CRYZL1 (quinine oxidoreductase)
Structural	4	CRYA (lens protein); COL18, COL6A1, COL6A2 (collagens)
Methyl transferases	3	DNMT3L (cytosine methyl transferase), HRMT111 (protein arginine methyl transferase); Pred28 (AF139682) (N6-DNA methyltransferase) SH3 domain 3 ITSN, SH3BGR, UBASH3A
One carbon metabolism	4	GART (purine biosynthesis), CBS (cystathionine- β -synthetase), FTCD (formiminotransferase cyclodeaminase), SLC19A1 (reduced folate carrier)
Oxygen metabolism	3	SOD1 (superoxide dismutase); CBR1, CBR3 (carbonyl reductases)
Miscellaneous	28	HLCS (holocarboxylase synthase); LSS (lanosterol synthetase); B3GALT5 (galactosyl transferase); *AGPAT3 (acyltransferase); STCH (microsomal stress protein); ANA/BTG3 (cell cycle control); MCM3 (DNA replication associated factor); APP (Alzheimer's amyloid precursor); WDR4, WDR9 (WD repeat containing proteins); TFF1, 2, 3 (trefoil proteins); UMODL1 (uromodulin); *Pred5 (lipase); *Pred3 (keratinocyte growth factor); KIAA0653, *IgSF5 (Ig domain); TMEM1, *Pred44 (transmembrane domains); TRPD (tetratricopeptide repeat containing); S100b (Ca binding); PWP2 (periodic tryptophan protein); DSCR1 (proline rich); DSCR2 (leucine rich); WRB (tryptophan rich protein); Pred22 (tRNA synthetase); SCL37A1 (glycerol phosphate permease)

Table 1: Categories of functional genes of HSA21. *Adapted from Gardiner and Davisson, 2000*

- MMU16, syntenic with a 154 genes region in HSA21q.
- MMU17 corresponds to a 23 genes region in HSA21q.
- MMU10 corresponds to a 58 genes region in HSA21q.

This comparative analysis allowed highlighting of big quantity of sequences conserved more than 70% of homology between human and mouse.

1.2.4 Gene dosage and Down syndrome critical region

As the common characteristic of DS patient is the presence of an extra HSA21, investigators focused their research on the consequences of gene triplication. The “gene dosage effect” is well established now. With the development of fast and efficient transcriptome analysis methods, like DNA chip, a global increase of triplicated genes has been reported (FitzPatrick et al., 2002). However, in 2007 a study on *postmortem* human tissues demonstrated that only 25% of the triplicated genes are actually overexpressed compare to control individuals (Lockstone et al., 2007). Results concerning the expression variability of disomic genes in DS individuals were more divergent.

Despite this observation, the “gene dosage effect” remains the most accepted hypothesis to explain DS phenotype. Alterations characteristic of the disease could directly result from the overexpression of one gene or a group of genes located on the triplicated chromosome. Indeed the description of the DSCR argues in favor of this hypothesis and proposes the idea of “candidate genes” associated with particular phenotypes. To validate this hypothesis, it is important to keep on investigating on animal model of DS and improve our knowledge on mechanisms responsible for pathological phenotype.

2. The hippocampus

“Hippocampus” comes from the latin word for “seahorse” because of the curly shape similar to the one exhibit by the sea animal (figure 3A). In 1742, Garengeot also named it “cornu Ammonis” because he found shape similarities with the Ammun’s horn, a mythological music instrument. The brain contains two hippocampi lying within the medial temporal lobes, which is a fold of the cerebral cortex edge (figure 3C).

Hippocampus is made of two thin neuronal layers rolled up in them self: one is the dentate gyrus (DG) and the other is the Ammun's horn (CA). Hippocampus circuitry can be assimilated to a three checkpoints circuit (figure 3B). Briefly, the major hippocampus input is the perforant pathway, a group of axons coming from the enthorinal cortex (EC) that connect with the granule cells of the DG. Then these neurons send their axons, called "mossy fibers", towards the CA3 pyramidal cells. Axons emerging from CA3 cells are sent onto two different targets: one is the contralateral hippocampus CA3, via the fornix, the other is ipsilateral CA1 pyramidal cell via the Schaffer collateral pathway. Finally CA1 neurons send their axons back through the subiculum to the EC to close the loop.

The hippocampus is involved in cognitive processes, in particular memory. This idea derived from several cases of lesioned hippocampus, but in particular from the studies performed with "Patient H.M.". In 1957, to release this patient from chronic epileptic seizures, surgeons destroyed both hippocampi from H.M. temporal lobe. The consequence was a persistent and severe impairment of memory formation (Scoville and Milner, 2000). In the following years, other patients with similar levels of hippocampal damage and amnesia (caused by accident or disease) were studied. However, a vast knowledge about hippocampus and memory has been accumulated from experiments made in rodents to study the physiology of activity-driven changes in neural connectivity in the hippocampus. These studies confirmed implication of this structure in declarative memory formation, spatial memory and contextual memory (see Bear et al. 2001 for a review). The simple, well-organized architecture made the hippocampus a suitable structure to study neurotransmission in the mammalian brain. At the end of the 60's it was discovered that it is possible to remove the hippocampus from the rest of the brain, cut it into slices and maintain them alive for several hours. Thanks to optic microscopy, it was possible to visualize the different hippocampal areas in these preparations. On these slices, fiber pathways can be easily electrically stimulated in order to study neural communication.

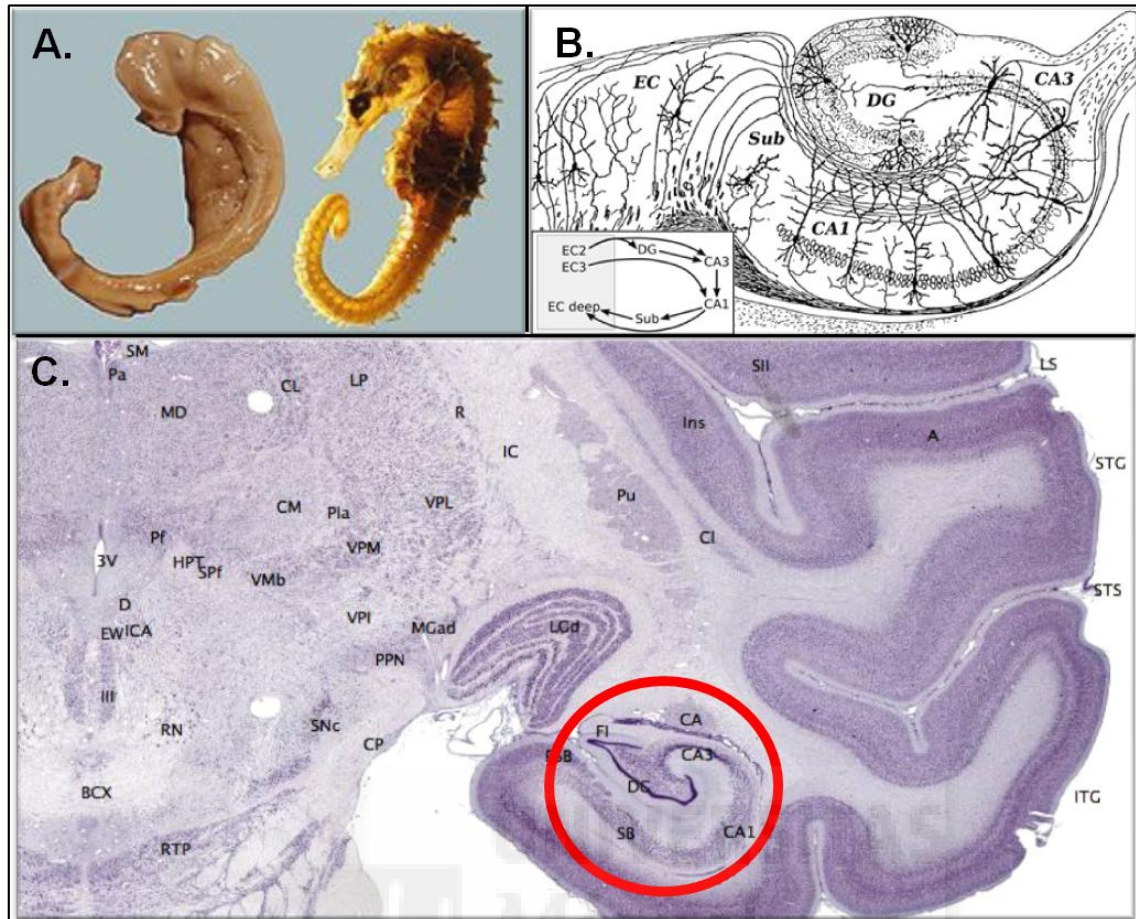


Figure 3: (A) Shape comparison between human hippocampus (left) and seahorse (right). *Photo made in 1980 by the Hungarian neuroscientist László Seress*!. (B) Basic circuit of the hippocampus, as drawn by Santiago Ramon y Cajal (Cajal 1884) (C) Nissl-stained coronal section of the macaque monkey brain showing the hippocampus location (red circle). *brainmaps.org*. CA: cornu Ammoni; DG: dentate gyrus; Sub: subiculum; EC: entorhinal cortex.

3. The Synapse

3.1. Generalities

In the adult vertebrate CNS, the major part of the synaptic transmission is chemical. Presynaptic element contains the synaptic vesicles filled with neurotransmitters. When an action potential (AP) arrives in the presynaptic terminal, neurotransmitters are released into the synaptic cleft after fusion of the synaptic vesicles with the plasma membrane. On the other side of the synaptic cleft, the postsynaptic membrane presents the neurotransmitter receptors. In the case of ligand operated channels, binding of the neurotransmitter to its receptor induces the opening of the channel and the ionic flow

throughout. Synaptic transmission can be excitatory or inhibitory and/or modulatory. The amino acid glutamate is the main excitatory neurotransmitter in the brain, whereas gamma-aminobutyric acid (GABA) mediates inhibitory transmission. Homeostasis of the nervous system depends on the balance between these two systems. Pathologies like epilepsy, amnesia, anxiety, hyperalgesia or psychosis are all associated with neurotransmission dysfunctions in the brain (Meldrum, 2000).

3.2. The glutamatergic synapse

3.2.1. Morphology and classification

The majority of glutamatergic synapses in the CNS are formed on membranous protrusions of the dendritic compartment called “dendritic spines” and classified after their shape. Synapses can also be classified on the basis of the postsynaptic element location: axodendritic, axosomatic, axoaxonic or dendrodendritic. Following the classification by Gray (Gray, 1969), under electronic microscopy, Type I synapses appears asymmetrical with large dense postsynaptic zone, so called postsynaptic density (PSD). In contrast, Type II synapses are inhibitory and look like symmetrical synapses because they lack a specialized thick PSD (Bear et al., 2001).

3.2.2. The glutamate receptors

Based on their transduction mechanisms, glutamate receptors have been separated in “ionotropic”, a family of receptors forming an ion channel (iGluR), and “metabotropic” that are G-protein coupled receptors (mGluR).

3.2.2.1 Ionotropic glutamate receptors

The first subunit of a iGluR was cloned in 1989 (Hollmann et al., 1989). The iGluRs are transmembrane proteins that form a channel permeable to cations, mainly Na^+ and K^+ and sometimes to Ca^{2+} . The iGluRs are ligand gated ion channels, i.e. glutamate binding induces a conformational change that results in the opening of the channel (Burnashev et al., 1996). These channel receptors are tetrameric complexes composed by different subunit combinations (Rosenmund et al., 1998). All iGluR subunits share a common structure: one extracellular N-terminal domain, 4 membrane segments (only 3 crossing completely the membrane) and one intracellular C-terminal domain (figure 4A). There

are 4 families of iGluRs classified after their respective pharmacological characteristics: the N-methyl-D-aspartate receptors (NMDAR), α -amino-3-hydroxy-5-methyl-4-isoxazolepropionic acid receptors (AMPA), the kainate iGluR (KAR) and delta iGluR.

The NMDA iGluRs

NMDARs are a combination of 4 subunits. There are 6 different subunits: GluN1, GluN2A, GluN2B, GluN2C, GluN2D and GluN3. The GluN1 subunit is an essential component of all NMDA receptor complexes and is associated with GluN2 and/or GluN3 subunits to generate a large number of different NMDARs, having differing pharmacological and biological properties. GluN2 and GluN3 do not form functional receptors by themselves (Carroll and Zukin, 2002). The NMDARs are permeable to Na^+ , K^+ and Ca^{2+} . Interestingly, NMDARs require the presence of a co-agonist on GluN1 subunit, the glycine, to reach the active state (figure 4B) (Johnson and Ascher, 1987). Activation of NMDARs is also voltage-dependent, a result of ion channel block by extracellular Mg^{2+} at membrane resting potential (-70mV). A membrane depolarization (around -40mV) is necessary to remove Mg^{2+} block from the pore and let charges to flow through the channel (Nowak et al., 1984). Thus, NMDARs are “molecular coincidence detectors”, because their opening is dependent on the simultaneous activation of the presynapse and the postsynapse. This property puts NMDARs at the center of a certain form of neural plasticity, the long term potentiation (LTP) (Harris et al., 1984; Nicoll et al., 1988).

The AMPA iGluRs

AMPA receptors are the main actors of the fast synaptic transmission. Four genes code for 4 different AMPAR subunits: GluA1, GluA2, GluA3 and GluA4. The majority of AMPARs include the GluA2 subunit, heteromerized with GluA1 or GluA3. GluA4 is only expressed during a short period during development (Carroll et al., 2001). These receptors are mainly permeable to Na^+ and K^+ and some types to Ca^{2+} . Alternative splicing of AMPAR subunits mRNA generate a large variety of C-terminals, as a consequence AMPARs present a variety of different phosphorylation and interaction sites (figure 4C) (Luscher and Frerking, 2001). The density of AMPARs in the PSD determines the strength of synaptic transmission. It has been reported that insertion of AMPARs in PSD is one of the necessary mechanisms for LTP expression (Shi et al., 1999).

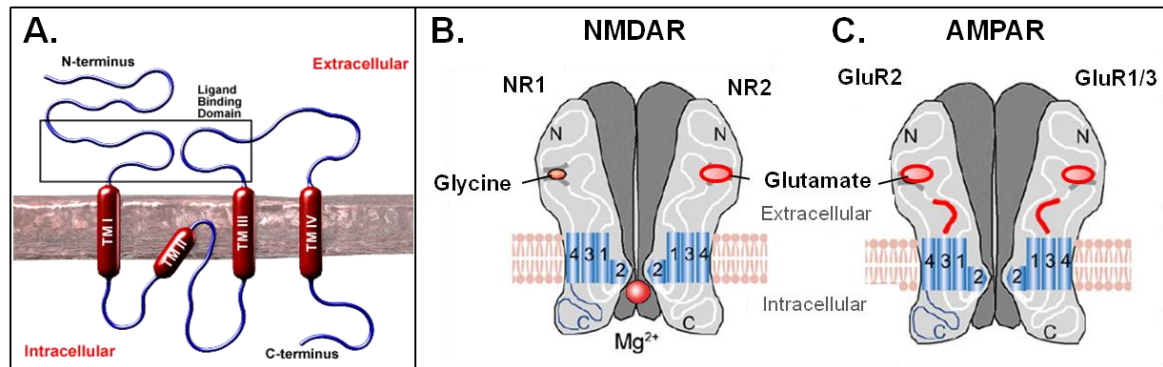


Figure 4: (A) General structure of an ionotropic glutamate receptor subunit. The large N-terminal domain is extracellular while the shorter C-terminal domain is intracellular. *bris.ac.uk*. (B) NMDAR representation. Glutamate binds NR2/3 subunits whereas glycine binds NR1. Mg²⁺ block is located at the intercellular side of the receptor. (C) AMPAR representation. Red line indicates typical alternative splicing region of the molecule.

The Delta iGluRs

The delta receptor is the less known and investigated family of iGluR. They are composed by 2 different subunits: GluD1 and GluD2. They have been involved in cerebellar function and high-frequency hearing and it appears to serve structural functions at synapses. Although no function has been yet ascribed for these subunits (Yuzaki, 2003). Recently it has been suggested that delta receptors have functional gating machineries and ion permeation pathways similar but not identical to those of AMPA and kainate receptors (Orth et al., 2013).

3.2.2.2 Metabotropic glutamate receptors

mGluRs are G-protein coupled receptors (GPCRs) that have been subdivided into three groups, based on sequence similarity, pharmacology and intracellular signaling mechanisms. Group I mGluRs (mGluR1 and mGluR5) are coupled via Gq protein to the phospholipase C (PLC), the protein kinase C (PKC) and intracellular calcium signaling, while group II (mGluR2 and mGluR3) and group III receptors (mGlu4, mGlu6, mGlu7 and mGlu8) are negatively coupled to adenylyl cyclase (AC) and positively to PKA via Gi/Go protein. mGluR subunit protein possesses 7-transmembrane domains. Like the other G protein-coupled receptors, mGluR can be assemble as homodimers (Romano et al., 1996). mGluRs are widely expressed in the CNS, mGluRI are mainly presynaptic and mGluRII postsynaptic whereas mGluRIII can be find in both side of the synaptic cleft. Functionally mGluRs can mediate and regulate

the synaptic transmission via different effectors like PKC, Inositol triphosphate, calcium or ionotropic channels (Niswender and Conn, 2010).

3.2.3. Excitatory synaptic plasticity

Synaptic plasticity can be defined as the capacity of the synapse to adapt its activity depending on the different stimulations it receives and synaptic environment. Classically, synaptic plasticity is classified according to the type of modification, potentiation or depression, and the durability of the modification, short term or long term (Kandel et al., 2000). Modifications can operate on the presynaptic side to control neurotransmitter released quantity, release probability or reuptake (Liu, 2003). On the postsynaptic side, neurotransmitters receptors are the main target of the regulatory mechanisms. Receptors numbers, coupling or biophysical properties determine the efficacy of the synaptic transmission (McGee and Brecht, 2003). Changes in the diffusion capacity of the receptors in the postsynaptic membrane can also influence synaptic transmission (Choquet and Triller, 2003). The total number of active synapses is also an important source a synaptic transmission fluctuation at a cellular scale (Harris, 1999).

3.2.3.1. Short term plasticity

The mechanism involved, mainly presynaptic, can decrease (depression) or increase (facilitation, augmentation) synaptic transmission. Short term depression (STD) is mainly due to a depletion of the readily releasable pool of neurotransmitter. Inhibition of vesicular fusion due to Ca^{2+} influx reduction could also be an explanation of the release inactivation (Zucker and Regehr, 2002). Some postsynaptic mechanisms can also be involved, like the saturation or the desensitization of the receptors. Short term potentiation (STP) is mainly due to the increase of residual Ca^{2+} in the presynaptic element that increases neurotransmitter release probability after repeated activation of presynaptic fibers (Zucker and Regehr, 2002).

3.2.3.2. Long term plasticity

Different types of long term plasticity have been discovered mainly in the hippocampus and the cerebellum. Bliss and Lomo observed that a repeated stimulation to the perforant pathway, induced a durable potentiation of the transmission in the DG (Bliss

and Lomo, 1973). Since then numerous studies focused on the cellular and molecular mechanisms responsible for this process.

Long term potentiation (LTP)

Induction of LTP can be dependent from pre- or postsynaptic mechanisms. The most prominent one is the NMDAR-dependent LTP that is induced after a precise sequence of events. First during sustained activity, AMPAR and NMDAR are simultaneously activated. Second, the entry of Ca^{2+} in the dendrite activates complex intracellular cascades, notably CaMKII. Once activated, CaMKII phosphorylates AMPARs. Phosphorylation of AMPAR modifies their conductance and trafficking to the membrane. The result is a durable increase of the synaptic strength after incorporation of new AMPAR to the synapse (Collingridge et al., 1983; Lisman et al., 2012). LTP can also be explained by other mechanisms like the unmasking of synapses that were silent before the LTP induction (Isaac et al., 1995) or the insertion of new NR2A-containing NMDARs consecutive to PKC activation (Grosshans et al., 2002). Synaptic strengthening can also be due to changes of iGluRs channel properties following a phosphorylation. For instance, PKA phosphorylates GluA1 S845 and increases channel opening probability (Banke et al., 2000).

Long term depression (LTD)

In the area CA1 of the hippocampus low frequency stimulation induces a depression of the synaptic response due to the decrease of the number of AMPARs at the postsynaptic side (Collingridge et al., 2010). Postsynaptic AMPARs can be phosphorylated after mGluRI activation, resulting in an internalization of these receptors and/or alteration of the local translation of mRNA. LTD dependent on group II mGluR is well known in the CNS (Bellone et al., 2008). Here the intracellular cascade induced by presynaptic mGluRII activation results in a decrease of the release probability (Nicoll and Schmitz, 2005). Recently it has been observed that postsynaptic mGluRI activation induces synthesis and postsynaptic release of endocannabinoids, which activate their receptors (metabotropic CB1) on the presynaptic terminal, resulting in a decrease of neurotransmitter release, via a similar mechanism to the one triggered by mGluRII (Mato et al., 2008).

3.2.3.3. Role of synaptic plasticity

It has been proposed and it is widely accepted that cellular and molecular processes involved in synaptic plasticity are the basis for learning and memory.

Hippocampal plasticity and spatial learning

In the 70s, it was demonstrated that the area CA1 of the hippocampus contains a real spatial map of the animal environment (O'Keefe and Nadel, 1978). The “place cells” allow the formation of a precise cognitive map that can inform the animal on its location at anytime. Thus hippocampus has a preponderant role in spatial navigation. It has been reported that *in vivo* local perfusion of NMDAR antagonist alters the induction of CA1 LTP and spatial learning in rodent (Morris and Frey, 1997).

Synaptic plasticity associated pathologies

The mesocorticolimbic system has been associated to addiction processes. It has been proposed that addiction development is correlated to defective long term associative memory. Drug of abuse could impair the synaptic plasticity mechanisms normally in charge of reward-related learning. A direct relationship between addictive behavior and synaptic plasticity has been reported (Mameli and Lüscher, 2011). Drug of abuse could induce insertion of AMPAR in dopaminergic neurons from the tegmental ventral area, and occlude the normal LTP induction at glutamatergic synapses contacting with these neurons (Kauer and Malenka, 2007). “Addicted” patients would present incapacity to countervail the pathological modifications induced by these drugs.

The glutamatergic synapse presents remarkable complex morphofunctional plasticity. This element is highly structured and precisely regulated in order to generate an efficient and adaptable communication between neurons. In addition the activity of the excitatory synapses can be affected by the activation of another type of synapse: the inhibitory synapse.

3.3. The inhibitory synapse

3.3.1 Generalities

GABA is the main inhibitory neurotransmitter of the nervous system. Inhibitory transmitters are released by a special category of small projecting neurons named “interneurons”. These cells primarily contribute to local neural assemblies, where they provide inhibitory inputs and regulate excitability of the targets cells. At the opposite to excitatory synapses, the membrane differentiations located on each sides of the inhibitory synapses are symmetrical, therefore inhibitory synapses belong to the Type II in the Gray classification (Gray, 1969). GABA binding to its postsynaptic receptors

normally induces a hyperpolarization of the target neuron membrane. Hence, activation of inhibitory receptors decreases cell excitability.

3.3.2 The different type of inhibitory receptors

Ionotropic inhibitory receptors: GABA_AR

GABA_AR are ligand-gated anion channels permeable to Cl⁻ ions. This type of receptor produces very fast postsynaptic actions, falling within a couple of milliseconds after the presynaptic terminal activation. There are numerous subunit isoforms which determine the receptor's agonist affinity, opening probability, conductance, and other properties (Cossart et al., 2005). There are 4 different subunits: α , β , γ and δ , which presents various isoforms. A functional GABA_A receptor is composed by 2 α subunits and 1 β , 1 γ and 1 δ (GABA_A receptor formula: $\alpha_2\beta\gamma\delta$) (Bear et al., 2001).

Metabotropic inhibitory receptors: GABA_BR

Like mGluRs, GABA_BRs are G-protein-coupled receptors. Structure of these receptors is similar to mGluRs presented above. There are 2 GABA_BR subtypes: GABA_{B1} and GABA_{B2}, that can be assemble as heterodimers. Agonist binding provokes the release the G-protein from the receptor, that goes to interact with K⁺ channels or others proteins to open or close ion channels (Chen et al., 2005). For instance, GABA_BR activation triggers the opening of K⁺ channel inducing outward currents that hyperpolarizes the membrane potential. The generated postsynaptic responses are slow (from milliseconds to minutes) therefore GABA_BR can have a considerable influence on cell excitability (Bear et al., 2001).

3.3.3 Inhibitory synapses plasticity

Inhibition is also highly plastic, with multiple underlying cellular mechanisms (Kullmann et al., 2012). Despite the absence of an obvious local coincidence detector at the inhibitory synapse, several mechanisms act to regulate GABA release, like the depolarization-mediated suppression of inhibition (Llano et al., 1991) or also the spike-timing-dependent plasticity that induces changes in Cl⁻ current passing through the channel (Woodin et al., 2003). The plasticity at inhibitory synapses often implies retrograde signals that are release in the synaptic cleft by the postsynapse and regulate presynaptic GABA release (for review see Kullmann et al. 2012).

4. The kainate receptors

4.1. Generalities

Kainate or (2*S*,3*S*,4*S*)-3-(Carboxymethyl)-4-prop-1-en-2-ylpyrrolidine-2-carboxylic acid, is an excitotoxic molecule (~20Da) isolated from the red seaweed called "Kainin-sou" (*Digenea simplex*) in Japan. In traditional Japanese medicine, kainate is named "Makuri" and was used to kill parasitic worms (Mody, 1998). Kainate, like domoic acid (domoate) another molecule synthesized by diatoms *Pseudo-nitzschia* type, is a phycotoxin that produces amnesic shellfish poisoning (ASP) after consumption (Jeffery et al., 2004). The first case of massive intoxication was reported in 1961 in Capitola (California) when thousands of intoxicated seagulls attacked the seaside town. In 1987, on Prince Edward Island in Canada, 107 persons were poisoned after eating mussels intoxicated with diatom *Pseudo-nitzschia*. They presented gastrointestinal symptoms followed by neurological symptoms within 48 hours. All patients were confused and disoriented (Pulido, 2008). Nowadays, kainate and domoate concentrations are regularly controlled in shellfish of North Europe, Japan and North America.

Pharmacologically, kainate is able to activate both KARs and AMPARs. Thus, a crucial step forward in the study of KARs was the discovery of a compound, GYKI53655, that can selectively antagonize AMPARs, unmasking KAR-mediated responses (Paternain et al., 1995). Hence the availability of this compound has made possible functional studies for this class of iGluRs.

4.2. Structure and composition of KAR subunits

4.2.1. Structure and pharmacology

KAR subunits have the same membrane topology as AMPARs and NMDARs (Bennett and Dingledine, 1995). KARs are tetrameric combinations of five subunits. GluK1-3 can form functional homomeric or heteromeric receptors, whereas GluK4 and GluK5 only participate in heteromeric receptors partnering any of the GluK1-3 subunits (Lerma, 2006). KARs are activated and deeply desensitized by kainate ($EC_{50}=6-23 \mu\text{M}$). Domoate also activates and partially desensitizes these receptors ($EC_{50} \sim 1 \mu\text{M}$ for native KAR and $\sim 30 \mu\text{M}$ for recombinant KARs) (Lerma, 2003). ATPA (2-Amino-3-(3-hydroxy-5-*tert*-butylisoxazol-4-yl) propanoic acid) is a selective agonist of GluK1-









containing KARs ($EC_{50}=1 \mu\text{M}$). However it can also activate heteromeric KARs composed of GluK2 and GluK5 but with lower affinity ($EC_{50}= 20\mu\text{M}$) (Paternain et al., 2000).

KARs and AMPARs are difficult to distinguish pharmacologically. Again the most useful compound in the study of KARs has been GYKI53655 (AMPA selective antagonist) that shed light on the functional role of KARs (Paternain et al., 1995). CNQX (6-cyano-7-nitroquinoxaline), DNQX (6,7-dinitroquinoxaline-2,3-dione) and NBQX (2,3-dihydroxy-6-nitro-7-sulphamoyl-benzo(F) quinoxaline) are competitive selective antagonists for AMPARs at low concentrations (Lerma, 2003; Lerma et al., 2001), but are able to antagonize KARs at slightly higher concentrations. More recently, GluK1-containing KARs (GluK1-KARs) selective antagonists have been produced, such as the UBP302, UBP310 (More et al., 2004) and ACET (Dargan et al., 2009; Dolman et al., 2007). The contribution of each subunit to KAR pharmacology is not fully known. The use a dysiherbaine (KAR selective agonists) indicated that selective activation of the GluK1 subunit in a GluK1/K5 heteromeric KARs is sufficient to activate and open the channel (Swanson et al., 2002). Activation of KARs by glutamate depends on the nature and the stoichiometry of the subunits encompassing the receptor.

4.2.2. Molecular cloning and recombinant KARs

There are five genes coding for 5 different KAR subunits: *GRIK1* for GluK1, which maps in human chromosome 21q22.11 and 16 of mouse; , *GRIK2* for GluK2 (6q16.3-q21 in humans and 10 in mouse); *GRIK3* for GluK3 (1p34-p33 in humans and 4 in mouse), *GRIK4* for GluK4 (11q22.3 in humans and 9 in mouse) and *GRIK5* for GluK5 (19q13.2 in humans and 7 in mouse) (Barbon and Barlati, 2000; Barbon et al., 2001; Bettler et al., 1990; Egebjerg et al., 1991; Herb et al., 1992; Jamain et al., 2002; Kamboj et al., 1994, 1992; Sakimura et al., 1992; Schiffer et al., 1997). mRNA coding for KAR subunit undergo post-translational modifications (editing and or alternative splicing). GluK1 and GluK2 mRNA undergo editing at the so-called Q/R site of the M2 domain (Lerma, 2003). Except the alternative splicing of an exon coding for 15 amino acids insert in GluK1 N-terminal (GluK1-1 and GluK1-2), all the KAR subunit N-terminal present a large homology, whereas all KAR subunits C-terminal splicing variant are different. GluK1-1 and GluK1-2 exist in 4 different configurations of their C-terminal domain: GluK1-a, GluK1-b, GluK1-c and GluK1-d. Two mains isoforms has been

described for GluK2: GluK2a and GluK2b; as for GluK3 (GluK3a and GluK3b). The two other subunit types (GluK4 and GluK5) do not undergo any modifications (table 2) (Lerma, 2003). Hence, the conjugation of both editing and alternative splicing produces a large variety of KAR subunits isoforms with particular functional properties. Kinetic properties of KARs have been studied after the expression of recombinant receptors in heterologous systems where the amplitude of the measured currents depends on the number of receptors in the cell membrane and on their biophysical properties. The main characteristic of KARs is their rapid activation and desensitization in response to glutamate. Desensitization corresponds to a decrease of the current despite the presence of agonist. Homomeric receptors composed by GluK1-2b, GluK2a and GluK3a desensitize quickly in the presence of glutamate. GluK1-2b homomeric receptors desensitize partially in response to kainate (figure 5). Domoate does not activate GluK3a homomeric receptors, whereas it can activate GluK2a homomeric receptors that partially desensitize. The composition and the arrangement are determining factors of KARs functional properties (Lerma et al., 2001).

Subunit	RNA editing variants	Splice variants N terminus	Splice variants C terminus	Description	
GluR5 (GRIK1)	Q/R(M2)	GluR5-1 15 aa insert in the N-terminal domain (402-416)	a	856/871 aa polypeptide. A premature stop codon generates a 16 aa C terminus.	
			b	C-terminal domain is 49 aa longer than variant a; insert starts after Q854/869	
		c	GluR5-2 (402-416 insert missing)	C terminus is like variant b but with a 29 aa insert starting after Q854/869	
		d		Variant has a different C terminus that is not homologous to other C termini of GluR5, starting after Q854/869	
GluR6 (GRIK2)	I/V(M1) Y/C(M1) Q/R(M2)		GluR6	889 aa polypeptide	
			GluR6-2	The last 15 aa of the C terminus (after K854) are different from GluR6, and residues from 870 to 889 are missing.	
GluR7 (GRIK3)	No editing	GluR7		919 aa polypeptide	
		GluR7b		Presents a 13 aa insert at Q855 of GluR7, generating a new open reading frame that gives rise to a new C terminus, 9 aa shorter.	
KA1 (GRIK4)	No editing			No splice variants so far detected	
KA2 (GRIK5)	No editing			No splice variants so far detected	

aa, amino acid; C, carboxyl; N, amino.

Table 2: Kainate receptor subunits and their variant. GluR5= GluK1; GluR6= GluK2; GluR7= GluK3; KA1= GluK4; KA2= GluK5 (*adapted from Lerma, 2003*)

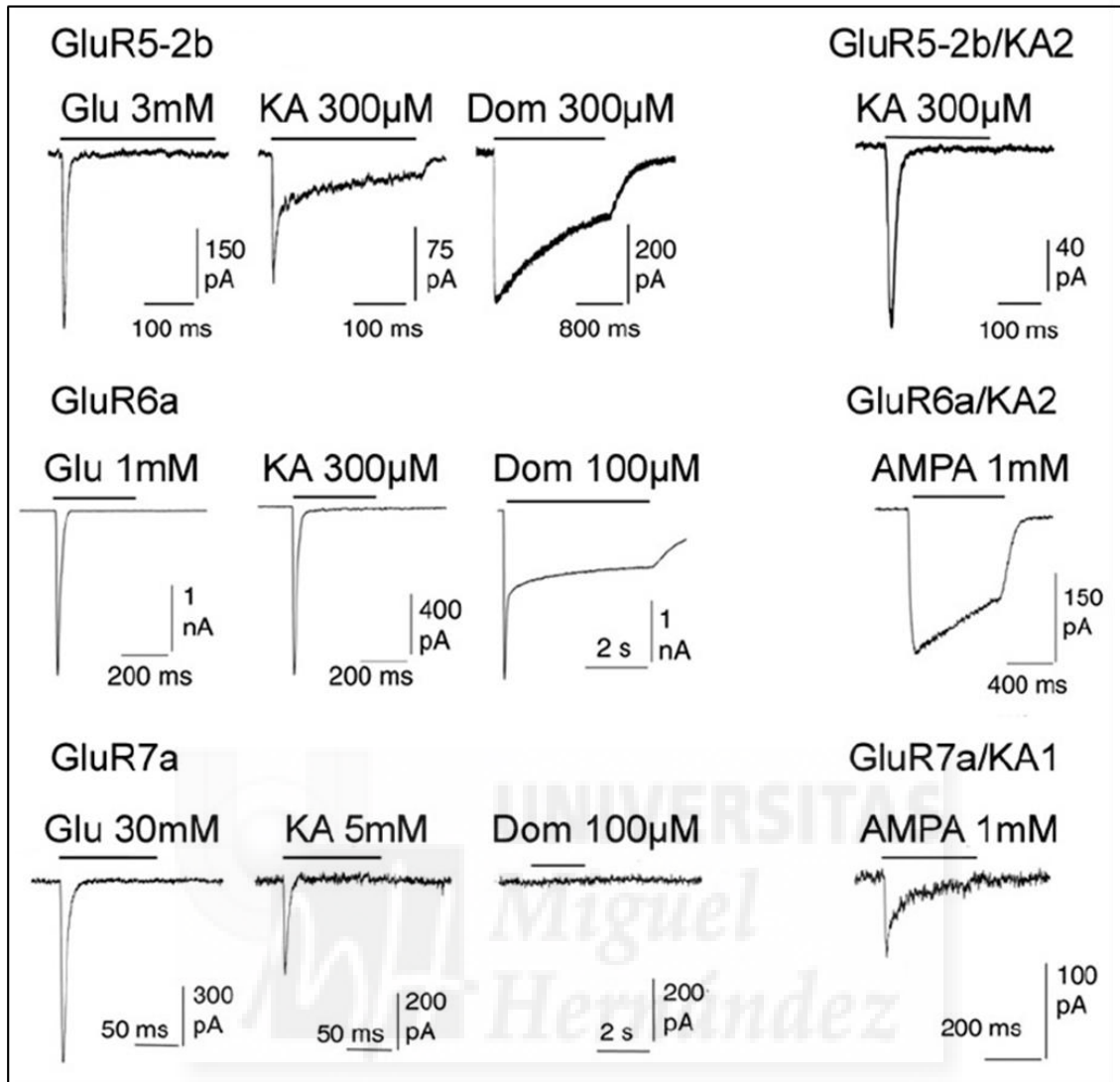


Figure 5: Electrophysiological response of different recombinant KARs. Homomeric (**left**) and heteromeric (**right**) are activated by the main agonists: glutamate (Glu), kainate (KA), domoate (Dom) and AMPA; GluR5= GluK1; GluR6= GluK2; GluR7= GluK3; KA1= GluK4; KA2= GluK5 (adapted from Lerma 2001)

4.2.3. Kainate receptors distribution

Study of KARs subcellular distribution by the classical electron microscopy (EM) method has been limited by the scarce availability of efficient selective antibodies. The best antibodies available label GluK3/4, GluK4 or GluK5. Unfortunately, any specific antibody for GluK1 subunits is available yet. Immunohistochemistry analysis reported the presence of GluK2, GluK4 and GluK5 at the mossy fiber synapses (Darstein et al., 2003). Studies using double *in situ* hybridization also permitted to localize KARs sites of expression. As an example, Paternain and colleagues did a mix of simple and double mRNA *in situ* staining against interneurons markers and KARs subunits. They

concluded that GluK1 and GluK2 subunits colocalize in a population of GABAergic neurons mainly out of the pyramidal cell layer in the CA1 and CA3 fields of the hippocampus (Figure 6) (Paternain et al., 2000).

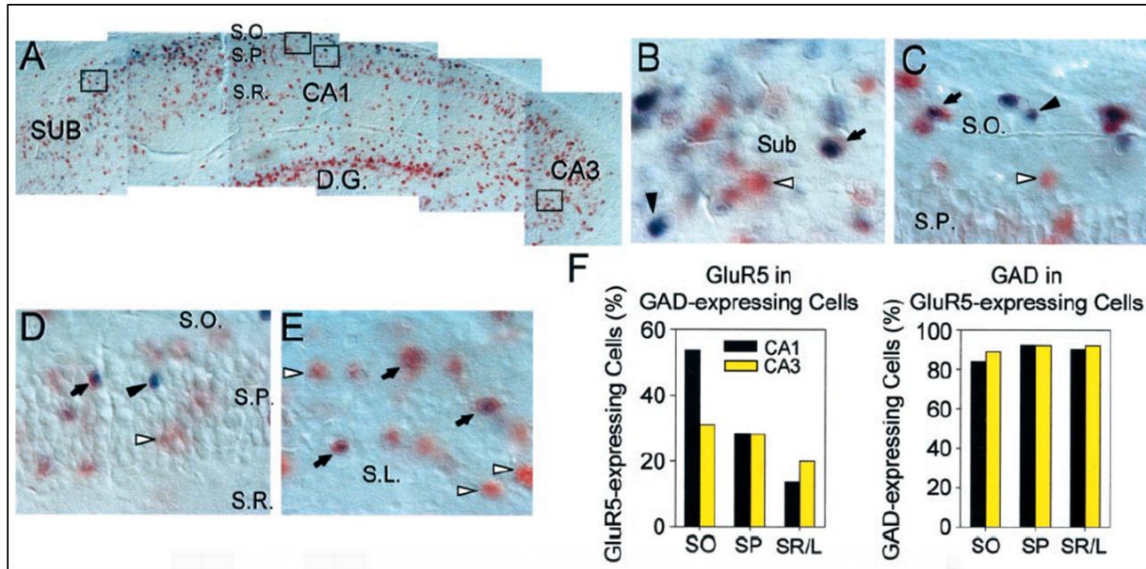


Figure 6: Coexpression of GluK1 subunit and GAD mRNAs in hippocampal neurons. (A) Composition of low-power pictures showing the hippocampus from the subiculum (SUB) to the CA3 field. Boxes in A from left to right are presented enlarged in B–E, respectively. GAD expression is labeled red (white arrowheads), whereas GluK1 mRNA is labeled blue (black arrowheads). Coexpression appears as a brown precipitate (black arrows). (F) Cells appearing blue, red, and brown were counted in the stratum oriens (SO), pyramidal (SP), and radiatum of CA1 or lucidum of CA3 (SR/L). The left histogram represents the fraction of interneurons (GAD-expressing cells) expressing GluK1 (GluR5) subunits, whereas the right histogram represents the fraction of GluK1-expressing cells that are GABA neurons (*adapted from Paternain et al 2000*).

The use of KARs knockout mouse models coupled to electrophysiology is a potent tool that helped localizing KARs subunit in the different cell compartments. At the mossy fiber-CA3 synapse, GluK2 and GluK5 are found pre- and postsynaptically (Contractor et al., 2003; Mulle et al., 1998). Using this approach, Christensen and colleagues reported that in CA1 interneurons of WT mice, heteromeric GluK2-K5 are found in the somatodendritic compartment of hippocampal interneurons. Whereas in the presynaptic domain combinations of GluK1-K2 or GluK1-K5 regulate GABA release (Christensen et al., 2004). In the nucleus accumbens, a structure involved in emotion regulation, the spiny neurons express GluK2 KAR subunits (Casassus and Mulle, 2002). Nonetheless, compensatory mechanisms can take place in the subunit deficient animals. Thus the data

emerging from KAR knockout models have to be interpreted carefully before reach a conclusion (Christensen et al., 2004).

Finally, the location (pre- or postsynaptic) of receptors with specific subunit composition cannot be predicted and, unfortunately, there is no knockout mouse model for each splicing variant, so the study of KARs subunit isoforms specific contribution is not possible.

4.3. Kainate receptors physiology

KARs play a large variety of roles in the glutamatergic synaptic transmission. They mediate part of the synaptic responses, modulate neurotransmitter release or regulate neuronal excitability.

4.3.1 Mediation of synaptic transmission

The contribution of KARs to the excitatory postsynaptic current (EPSC) has been reported for the first time in the synapse between mossy fibers and CA3 pyramidal cells in the hippocampus. After blocking AMPARs with GYKI53655, Castillo and colleagues observed KARs mediated EPSC showing a remarkable slow deactivation (figure 7) (Castillo et al., 1997; Vignes and Collingridge, 1997). Subsequently, contribution of KARs to synaptic transmission has been found at the synapse between Schaffer collaterals (SC) and CA1 interneurons (Cossart et al., 1998; Frerking et al., 1998), at the parallel fibers synapses in the cerebellum (Bureau et al., 2000; Delaney and Jahr, 2002), at the thalamocortical connexions (Kidd and Isaac, 1999), in the basolateral amygdale (Li and Rogawski, 1998) and at the synapse between afferent sensory fibers and dorsal horn neurons in the spinal cord (Li et al., 1999). Synaptic KARs presented a characteristic slow kinetics, probably providing integrative capacities to KARs in information transfer clearly unfulfilled by other glutamate receptors (Frerking and Ohliger-Frerking, 2002; Pinheiro et al., 2013). As an example, CA1 stratum oriens-lacunosum somatostatin interneurons receive glutamatergic inputs through KARs. Slow kinetics of this receptors permit to these cells to synchronize their activity with hippocampal theta frequency (Goldin et al., 2007). It has also been suggested that the role of KARs mediated EPSC would be to gate the threshold of theta-frequency-induced LTP (Clarke et al., 2012).

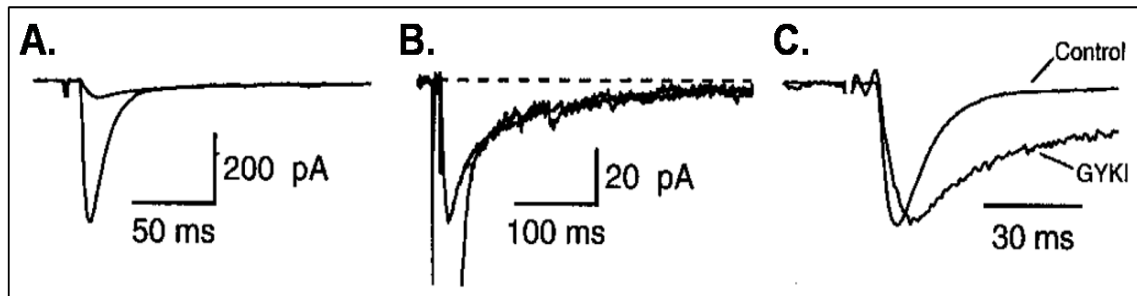


Figure 7: Characterization of the slow GYKI-resistant synaptic response (smaller peak) at normal (A) and higher gain (B). Scaling the GYKI-resistant component to the peak of AMPAR component allow the appreciation of the slow decay of the KAR-mediated component (*adapted from Castillo et al 1997*).

4.3.2 Regulation of the synaptic transmission

In addition to their postsynaptic role, KARs have been found to modulate transmitter release by presynaptic mechanisms. KARs are present at a subset of both excitatory and inhibitory terminals where they affect release by different mechanisms.

Dual signaling of KARs

An important particularity of KARs is that they can present two modes of signaling. Like others ligand-gated channels, KARs mediate the signal via a “canonical” pathway, by opening the ion channel and depolarizing the membrane. However, KARs also act through an unconventional metabotropic mechanism involving G proteins and second messengers, called the “noncanonical” pathway. This metabotropic activity of KARs was first described at inhibitory CA1 hippocampus synapses where activation of KARs result in a PKC-dependent inhibition of GABA release (figure 8) (Rodríguez-Moreno and Lerma, 1998). Later on, a coupling between KARs and an heteromeric G-protein was also reported in hippocampal synaptosomes (Cunha et al., 1999). Pure noncanonical activity has then been reported in dorsal root ganglion neurons where KARs metabotropic action can inhibit voltage-dependent Ca^{2+} channels (Rozas et al., 2003).

Regulation of inhibitory synaptic transmission

The implication of KARs in inhibitory transmission regulation has been investigated in several studies arriving to different somehow contradictory conclusions. On the one hand, at GABAergic terminals, activation of KARs can depress GABA release (Clarke et al., 1997; Rodríguez-Moreno et al., 1997; Vignes et al., 1998). Indeed, it has been

demonstrated that this effect was mediated by the metabotropic action of KARs (figure 8) (Rodríguez-Moreno and Lerma, 1998). Implication of KARs noncanonical pathway in reduction of GABA release was then reported in hippocampal synaptosomes (Cunha et al., 2000, 1999) and in other structures of the CNS such as the neocortex where KARs located on presynaptic fast-spiking interneurons terminals decrease GABA release and can be activated by ambient glutamate (Ali et al., 2001). On the other hand, some studies have reported that KARs located in synaptic terminals of hippocampal CA1 interneurons contacting other interneurons can increase GABA release (Cossart et al., 2001; Mulle et al., 2000). In these interneuron-interneuron synapses, activation of KARs increases miniature inhibitory frequency and decrease failure rate. It is also known for a long time, that the activation of KARs at the somatodendritic compartment produces a marked increase of spontaneous inhibitory activity (Cossart et al., 1998; Fisher and Alger, 1984; Frerking et al., 1998).

Taking together all these results suggest that presynaptic KARs regulate bidirectionally GABA release in hippocampus and neocortex and that the nature of this regulation depends on the cellular type. Moreover, in the supra optic nucleus, KARs are positively coupled to GABA release onto oxytocin and vasopressin neurons (Bonfardin et al., 2010). Here ambient glutamate tonically activates GluK1-KARs. This group demonstrated that in lactating rats, astrocytic glutamate reuptake is decreased, inducing an increase in ambient glutamate concentrations. Interestingly, this glutamate increase switches GluK1-KARs activity from facilitating GABAergic responses to inhibiting them. A role for GABA release regulation has also been reported in the amygdala (Aroniadou-Anderjaska et al., 2012; Braga et al., 2004) and the hypothalamus (Liu et al., 1999).

Regulation of excitatory synaptic transmission

The presence of KARs on excitatory presynaptic terminals was first reported in hippocampal synaptosomes preparation where kainate produces a dose-dependent decrease of glutamate release (Chittajallu et al., 1996). Then experiments performed on brain slices have provided evidence for the participation of KARs in SC excitatory synapses regulation (Chittajallu et al., 1996; Kamiya and Ozawa, 1998; Vignes et al., 1998). Perfusion of kainate to hippocampal slices in the presence of AMPARs antagonist produces a biphasic modulation of the NMDAR-mediated EPSC on CA1 neurons (Chittajallu et al., 1996).

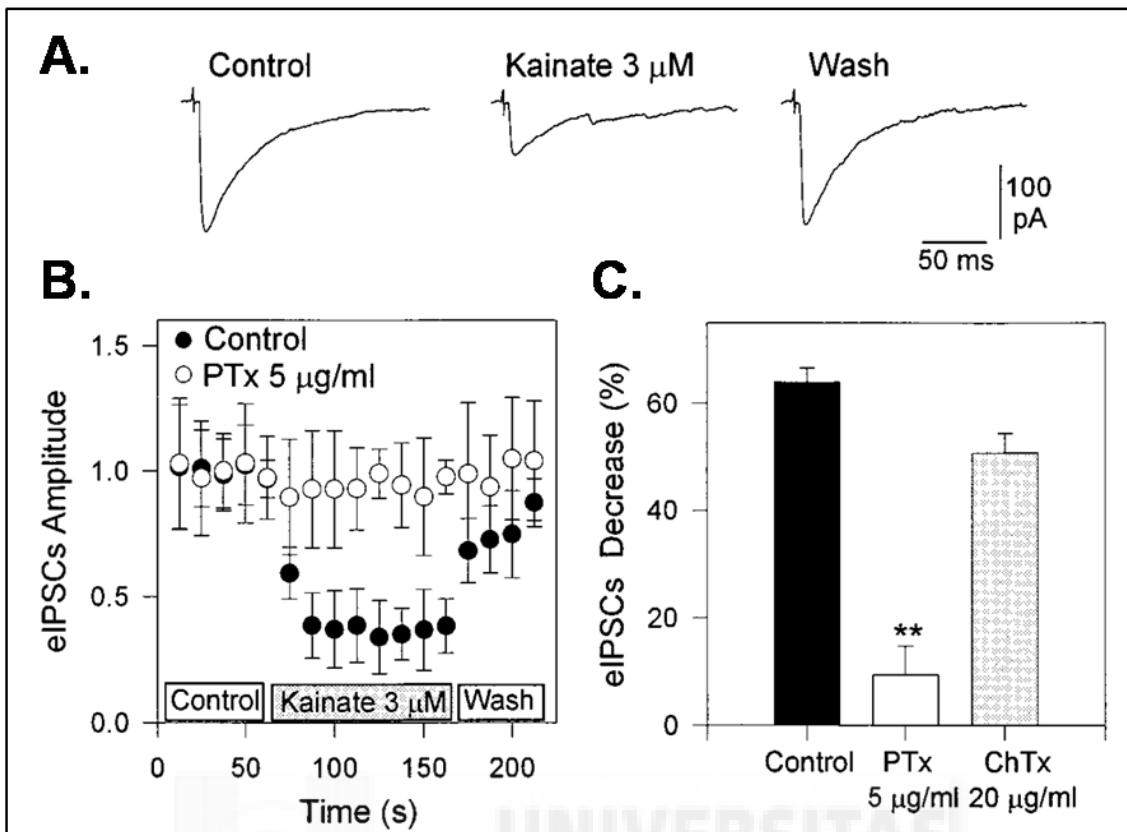


Figure 8: KARs modulation of GABA release involves a PTx-Sensitive G protein (A) Inhibition of IPSCs by 3mM kainate. eIPSCs were recorded from CA1 neurons and evoked by stimulation of the stratum oriens. (B) Time course of eIPSC amplitude before, during, and after bath application of kainate in an untreated (closed circles) and in a Ptx-treated (open circles) slice. (C) The effect of 3mM kainate on one IPSC amplitude in normal slices (Control) and slices treated with PTx or cholera toxin (ChTx) (adapted from Rodríguez-Moreno and Lerma 1998).

After an initial period of enhanced transmitter release, the agonist induced a reversible reduction of the excitatory response amplitude. This reduction was sensitive to LY294486, suggesting the involvement of GluK1-containing KARs (Vignes et al., 1998). This biphasic behavior can be explained by proposing an early depolarization of the terminal and the subsequent reduction of calcium influx due to the inactivation of the calcium channels involved in the release process (Chittajallu et al., 1996; Kamiya and Ozawa, 1998; Vignes et al., 1998). However, kainate-induced depression of glutamate release at SC terminal can be mediated by the metabotropic action of KARs, since it has been shown to be sensitive to G protein blockers (Frerking et al., 2001). Nevertheless, the resulting decrease of the excitatory drive is a surprising observation considering the known epileptogenic effects of kainate. Interestingly, lower concentrations of the agonist were effective in inducing only the increase of the synaptic response (Chittajallu et al., 1996).

At the mossy fiber-pyramidal CA3, presynaptic regulation of excitatory transmission by KARs has also been extensively studied. At this synapses KARs are involved in the characteristic frequency-dependent facilitation of excitatory transmission (Contractor et al., 2001; Lauri et al., 2001; Pinheiro et al., 2007; Schmitz et al., 2001), a phenomenon initially ascribed to the residual intraterminal Ca^{2+} . Indeed, blockade of KARs attenuates the potentiation of the second EPSC during high frequency stimulation (25Hz stimulation; Schmitz et al. 2001). This result also suggests that the presynaptic KARs activation must be fast to act between two pulses (10-30ms), indicating that KARs should be located near to the active zone. Frequency-facilitation could be due to an KARs-mediated increase of Ca^{2+} concentration that should amplify the AP-driven Ca^{2+} influx (Kamiya et al., 2002; Lauri et al., 2003). Indeed blockade of Ca^{2+} -permeable KARs reduced synaptic facilitation (Lauri et al., 2003) demonstrating that Ca^{2+} influx through KARs is necessary to induce this form of short-term plasticity. Nevertheless, mobilization of Ca^{2+} internal stores plays also a role in short-term facilitation of glutamate release (Lauri et al., 2003; Scott et al., 2008). However, another team demonstrated that presynaptic KARs were not sufficient to induce this form of plasticity and that CA3 network recurrent activity could also be responsible for the facilitation (Kwon and Castillo, 2008). Hence in the absence of further evidence against it, it should be concluded that KARs mediate part of the facilitation at mossy fiber-CA3 synapse. Moreover it is known that mossy fiber-CA3 synapse exhibit an NMDAR-independent LTP rather than the classical hippocampal NMDAR-dependent LTP. Indeed LY382884, a GluK1-KARs selective antagonist, was shown to block the induction of NMDARs-independent LTP in CA3 hippocampal neurons (figure 9) (Bortolotto et al., 1999), indicating the involvement of KARs in the phenomenon. It has been confirmed by the use of the more recently developed GluK1-KARs selective antagonist, UBP296 (More et al., 2004). Thus considering KARs properties here, one might think that KARs could bear the associative function necessary for long term plasticity.

At this synapse, activation of KARs receptors can also result in a depression of the glutamate release. Indeed, a long and strong stimulation of the mossy fiber induces a KARs-mediated depression of the synaptic transmission (Schmitz et al., 2000). In the CA3 associational/commissural pathway, KARs activation also depress transmitter release and it is accompanied with a reduction of presynaptic Ca^{2+} (Salmen et al., 2012). Like in Schaffer collaterals, this depression mechanism is sensitive to G-protein

blockers, thus most likely due to the noncanonical activation of KARs (Negrete-Díaz et al., 2006; Salmen et al., 2012).

During development KARs can have different roles and participate in shaping early hippocampal network by regulating transmitter release via their canonical (Lauri et al., 2005; Maingret et al., 2005) or noncanonical actions (Lauri et al., 2006; Sallert et al., 2007). KARs are not only active in the hippocampus during development. Indeed, it has also been demonstrated that KARs can be involved in plasticity mechanism at the thalamocortical junction in young animals (Kidd and Isaac, 1999) and in the basolateral amygdala (Li and Rogawski, 1998).

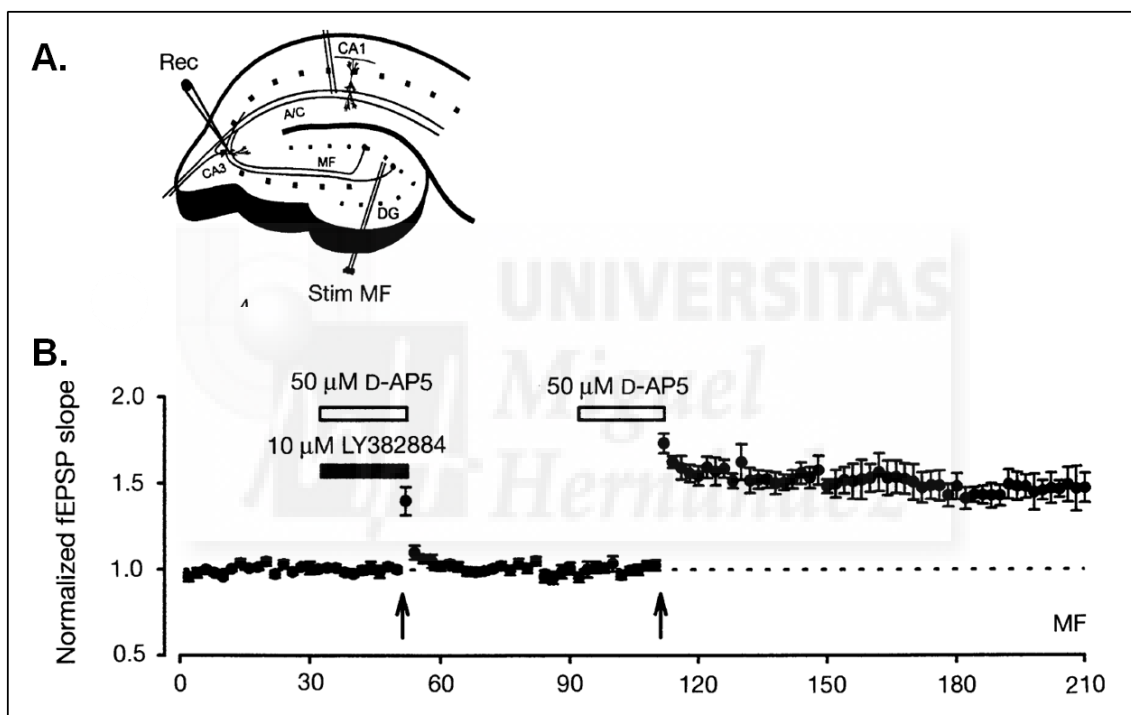


Figure 9: LY382884 (GluK1-KARs selective antagonist) specifically blocks the induction of mossy fiber LTP. (A) Position of the stimulating (stim MF) and recording (rec) electrode during the experiment. (B) A reversible block of the induction of mossy fiber LTP by LY382884. Note that the tetani were delivered in the presence of the NMDA receptor antagonist DAP5 (elicit NMDAR independent LTP). The traces in this and subsequent figures are averages of four successive records obtained at the times indicated on the graphs by the corresponding numbers. Inset, positions of the stimulating and recording electrodes (*adapted from Bortolotto et al, 1999*).

Finally it seems clear now that presynaptic KARs modulate transmitter release in a bidirectional way: facilitation occurs through their ionotropic activity, while inhibition seems to involve noncanonical signaling. The resulting physiological response would

possibly depend on the threshold to activate one or the other signaling pathway. Presynaptic modulation of glutamate and GABA release together with the postsynaptic regulation of neuronal excitability clearly demonstrate that KARs are responsible for the fine-tuning of synaptic function and network activity (Lerma and Marques, 2013).

4.3.3 Regulation of the neuronal excitability

Postsynaptic KARs directly increase neuronal excitability through their noncanonical activity on the slow after-hyperpolarization current (I_{SHAP}) (Melyan et al., 2004, 2002). I_{SHAP} was first observed in CA1 pyramidal cells (Lancaster and Adams, 1986). It is activated during a burst of AP and generated by voltage sensitive Ca^{2+} -dependent K^+ channels. This stimulus intensity-proportional K^+ current exhibits a slow decay and underlies spike frequency adaptation. At the SC-CA1 excitatory, glutamate cause a durable reduction of I_{SHAP} amplitude and this effect depends on the metabotropic activation of KARs (Melyan et al., 2004, 2002). This mechanism has been also documented at the mossy fiber-CA3 synapse (Fisahn et al., 2005; Ruiz et al., 2005). By reducing this hyperpolarizing current, KARs increase cell excitability. It has also been proposed that KARs located at the somatodendritic compartment could control the neuronal membrane potential. For instance, in CA1 interneurons ambient glutamate could activate these ionotropic KARs and consequently increase cell firing (Maingret et al., 2005).

4.4. Pathophysiology of kainate receptors

Some associations have been reported between KAR subunit-coding genes and pathologies of the CNS. For example, polymorphism of the GluK3-coding gene is related to Schizophrenia (Begni et al., 2002) whereas GluK2-coding gene polymorphism is associated with mental retardation (Motazacker et al., 2007). KARs have been also implicated in somatosensory signal transmission and pain (Li et al., 1999).

Glutamatergic synaptic transmission is considered to be an important factor in the development of neurodegenerative and mental disorders. KAR as an actor of this transmission have been logically involved in numerous neurological disorders (table 3) (Lerma and Marques, 2013).

Gene	Data	Linked Disease
<i>Grik1</i>	Upregulated expression	Epilepsy
<i>Grik2</i>	Modest linkage	Autism
<i>Grik2</i>	Deletion of exons 7 and 8	Mania, mild mental retardation
<i>Grik2</i>	Mapping susceptibility locus	Schizophrenia
<i>Grik2</i>	mapping	Huntington
<i>Grik3</i>	SNP T928G (rs6691840)	Schizophrenia
<i>Grik3</i>	SNP T928G (rs6691840)	Major depression
<i>Grik4</i>	Treatment response	Depression
<i>Grik4</i>	14 bp deletion/insertion variant	Bipolar disorder
<i>Grik4</i>	SNPs rs2282586 and rs1944522	Protection against Schizophrenia

Table 3: KARs most salient linkage to neurological disorders (adapted from Lerma and Marques, 2013)

Psychiatric disorders

All the studies cited earlier conclude that KARs are modulators of the synaptic transmission rather than major postsynaptic target for synaptically released glutamate, like NMDARs and AMPARs. Hence KARs are very attractive therapeutic targets when the aim of the treatment is to compensate an endogenous alteration of the synaptic transmission. Several conclusions after genetic analysis of human diseases and genetic manipulations in laboratory animals, relate KARs to psychiatric disorders pathophysiology.

In schizophrenic patient, some changes have been observed in tissues collected *postmortem*. First a preferential reduction of GluK1,2,3-immunoreactivity has been observed on apical dendrites of pyramidal neurons from schizophrenic patient hippocampus (Benes et al., 2001). Then an *in situ* hybridization-based work demonstrated a reduction of GluK1 and GluK2 transcription in limbic cortices of brains from bipolar patient (Beneyto et al., 2007), although another study revealed a reduction in number of GABAergic neurons expressing GluK1 KARs subunit (Woo et al., 2007). Whereas in another paper, a selective reduction of parvalbumin interneurons (fast spiking cells) was pointed out (Lewis et al., 2005). However another study based on quantitative analysis of glutamate receptors mRNA expression in different thalamus

nuclei, did not detect any changes (Dracheva et al., 2008). In animal models of Schizophrenia, a decreased of GluK1 and GluK2 KARs subunit expression has also been reported in the prefrontal cortex (Barbon et al., 2007). Other studies implicated GluK3 (Begni et al., 2002) and GluK4 (Pickard et al., 2006). Here also a decrease in parvalbumin interneurons number have been described (Lodge et al., 2009; Phillips et al., 2012). Considering all these results, it seems that changes in KARs and interneurons populations constitute a good lead for the following investigations. To date, there is only one pharmacological report showing a psychiatric indication for selective KAR antagonists. Indeed the GluK1-KARs antagonist, LY382884 produced anxiolytic type behaviour in the Vogel conflict test (Alt et al., 2007; Jane et al., 2009).

Epilepsy

In 1985, Ben Ari showed that kainate injection in awake animal induced epileptogenesis in hippocampus CA3, coupled with cellular loss and propagation to other structures (see Ben-Ari & Cossart 2000 for a review). Kainate injection is now a classical model to induce and study temporal lobe epilepsy. Activation of KARs could reduce GABA release and thus be responsible for network overexcitability. For example, in the area CA1 of the hippocampus perfusion of kainate reduced drastically the recurrent inhibition of the principal cells (figure 10) (Rodríguez-Moreno et al., 1997). Hence KARs became a lead in the research of therapeutic target for the treatment of epilepsy, but the precise mechanisms involved are not fully understood. On the one hand, it has been demonstrated that the blockade of GluK1-KARs prevents pilocarpine (muscarinic acetylcholine receptors agonist) epileptogenesis induction (Smolders et al., 2002). This effect was also observed *in vivo* where GluK1-KARs antagonist can even stop a started seizure. On the other hand, selective excitation of interneurons with GluK1-KARs agonists opens a new therapeutic approach for the epilepsies (Khalilov et al., 2002). It also has been reported that mice deficient for GluK2 subunit are less sensitive to kainate-induced epileptogenesis (Mulle et al., 1998). Even if KARs pharmacology have been linked to the disease, to our knowledge none of the anticonvulsant medication used to cure epilepsy in human are based on KAR activity.

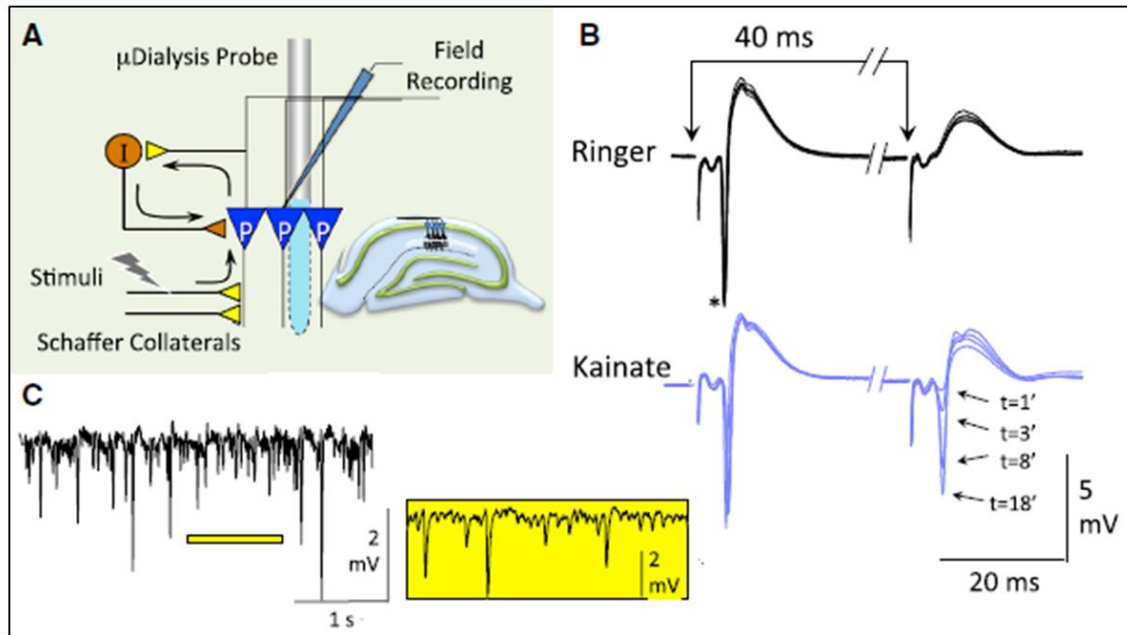


Figure 10: Kainate perfusion depresses hippocampal inhibition and generate epileptic activity. (A) Arrangement of recording and stimulating electrodes *in vivo*. In this experiment, a microdialysis probe implanted in the region allowed kainate to be slowly introduced into the extracellular fluid. The degree of GABAergic inhibition could be tested by the paired-pulse test, recording field potentials from the CA1 pyramidal layer through an extracellular electrode. (B) Stimulation of the SC pathway evokes the synchronous firing of a large number of CA1 pyramidal cells (the sharp negative wave indicated by an asterisk in the first evoked potential). This initial firing of the neuronal population activates a population of inhibitory interneurons that feedback onto the CA1 pyramidal neurons, such that a second stimulus arriving during the inhibitory phase (40 ms later) is unable to induce CA1 neuron firing, evident by the absence of a population spike in response to the second stimulus under control conditions. After perfusion of kainate through the dialysis probe (3 mM in the perfusate, probably 10% of this concentration reaches the extracellular fluid), the population spike in the second response progressively develops, indicating a failure in the inhibition of pyramidal cells. (C) After prolonged perfusion of kainate, ongoing epileptic activity develops that is characterized by the presence of interictal spikes in the EEG. The insert in yellow represents a 1 s period over an expanded time base. Adapted from Rodriguez-Moreno et al., 1997, Lerma and Marques, 2013

Neurodegeneration

As a mediator of glutamate excitotoxicity, KARs have been targeted in the study of ischemia-induced neuronal loss. A GluK1-KARs antagonist was able to protect efficiently against neuronal cell loss in rat model of ischemia (Gill and Lodge, 1994; O'Neill et al., 1998). This compound was even efficient when injected 1h after the beginning of the ischemia. But to date this product has never been tested for clinic applications. In another study, the authors neutralized expression of GluK2 and GluK5 (intracerebroventricular infusion of antisense-RNA) to test their implication in post-ischemia neuronal death. They observed an improvement of neuronal survival after

shunting GluK2 and GluK5 expression and concluded that these subunits are involved in delayed neuronal death by cerebral ischemia (Jane et al., 2009; Jiang et al., 2007).

Pain

The presence KARs is known in the dorsal root ganglions cells. Indeed, a pure population of KARs have been isolated from dorsal root ganglion that are likely to be C fiber nociceptors (Huettner, 1990). Different works made with selective KARs subunit deficient mice concluded that GluK1-KAR is the major iGluR expressed in these cells (Mulle et al., 2000; Rozas et al., 2003). In rodent, oral administration of a GluK1-KARs selective antagonist was able to reduced pain transmission during test (paw licking, carrageenan-induced thermal hyperalgesia, and capsaicin-induced mechanical hyperalgesia) (Dominguez et al., 2005; Jones et al., 2006; Simmons et al., 1998). In a primate model of neuropathic pain, LY382884 (GluK1-KARs antagonist) could diminish spinothalamic neurons nociceptive responses, confirming the implication of GluK1-KARs in pain signal transmission (Palecek et al., 2004). The only published study in humans shows a positive effect with the mixed AMPAR/GluK1-KARs antagonist (LY293558) in dental pain (Gilron et al., 2000). In another work on acute migraine made in humans, the same antagonist mix showed positive effects (Jane et al., 2009; Sang et al., 2004)

Other similar reports implicate genes coding for KARs to several disorders: GluK2/4 and anxiety/depression (Catches et al., 2012; Paddock et al., 2007), GluK2 with mental retardation, autism (Lanore et al., 2012; Motazacker et al., 2007b) and Huntington disease (Chattopadhyay et al., 2003; Diguët et al., 2004) (Lerma and Marques, 2013). These interesting associations await confirmation from molecular and mechanistic studies, but they clearly represent future research directions with potential application to human disease. To date no compounds developed as KARs antagonists became approved medicines. Indeed, as described above, only the GluK1 subunit have proved amenable to pharmaceutical chemists with a variety of chemical structures acting as agonists, antagonists and allosteric modulators (Jane et al., 2009).

5. Mouse models of Down syndrome

The balance between excitatory and inhibitory neurotransmission is crucial for the good network function. In Down syndrome pathology, this equilibrium seems to be at the

origin of the multiple alterations reported in the trisomics brain. The use of rodent models for the disease permits to go further in the understanding of the mechanisms responsible for this unbalance. Investigation on mouse model of DS is an advantage compare to human tissues. It allows working with a larger variety of tissues and functions with a possible access to CNS to try replicating DS and get a reliable model. Different types of mouse lines have been produced and can present a full chromosome triplication to monogenic triplication.

5.1 Transgenic models

Transchromosomic models

Transchromosomic (Tc) technology is based on the transfer of a large portion of human chromosome in an animal genome using microcell. As an example, Tc1 mouse comes from the insertion of the almost entire HSA21 in mouse embryonic stem cell. Ninety-two percent of HSA21 are triplicated in this animal but presents a mosaicism in the triplication. These mice are viable, with cardiac malformation (75% of the fetuses), facial morphological changes, motor and cognitive deficits (O'Doherty et al., 2005).

Chimeric mice

A model also coming from Tc technology, but here the inserted chromosome piece is free and lost in certain tissues. The result is a chimeric animal with variable degree of mosaicism. Nonetheless chromosome retention is good in the CNS. ES(#21)-10 model is an example emerging from the insertion of HSA21q. This animals have several learning deficits and morphological issues (Shinohara et al., 2001).

5.2 Partial and full models

A large choice of diverse DS mouse model is available at present. The main difference between models is the size of the triplicated segment and so the number of orthologous genes over represented in the animal (figure 11). Each one presents its pros and cons.

Ts16

It is the first generated rodent model of DS, obtained crossing double heterozygous males carrying Robertsonian translocations in MMU16 with diploid females. Despite Ts16 is syntenic for 80% of HSA21 genes, this model has not often been used because animals are not viable at birth and non-orthologous genes are also triplicated. Anyway some progress have been done working on Ts16 fetus that present cardiac, morphological and neurodevelopment problems (Haydar et al., 2000).

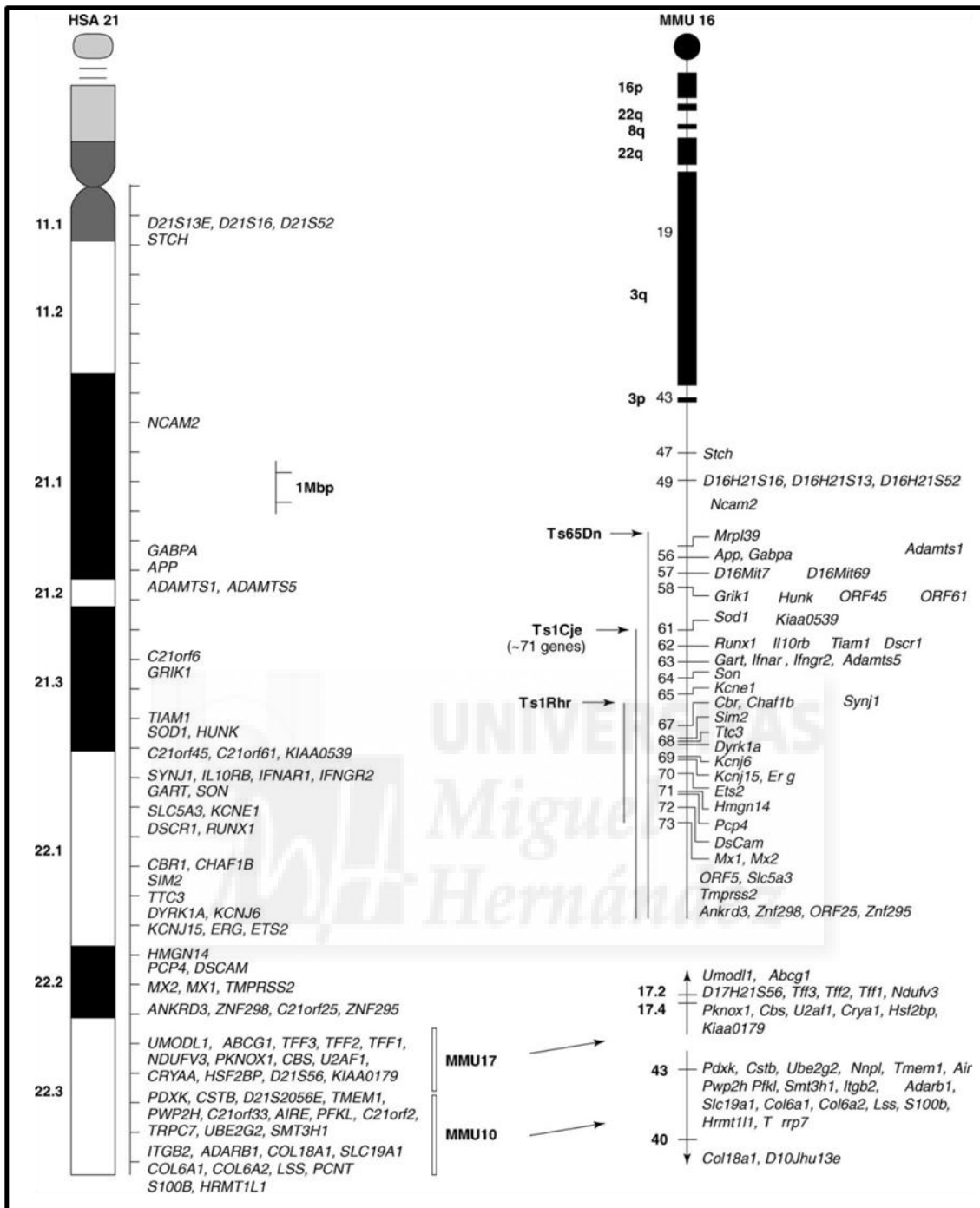


Figure 11: Comparative map of the segments conserved between human Chr 21 and mouse Chrs 10, 16 and 17 showing selected orthologous genes and the genetic extent of the trisomic segments present in Ts65Dn, Ts1Cje and Ts1Rhr mice. Arrows on the chromosomes 10 and 17 segments indicate the direction of the centromere. *Davissou, 2005*

Ts65Dn

This model is the “gold standard” for DS investigation nowadays. This partial model was produced at the beginning of the 80s by *The Jackson Laboratory*. Ts65Dn is formed from the translocation of the distal region of MMU16 (~13.4 Mb in total) onto

the of MMU17 centromere. This MMU16 region covers the genes *Mrpl39* to *Zfp295* and in total contains approximately 100 genes (including *Grik1*, the GluK1 protein-coding gene) that are orthologous to HSA21. Initially smaller, these animals usually become obese after 5 months (Kola and Hertzog, 1998). Ts65Dn mice show developmental delay and abnormalities in various organs, particularly the brain, that mimic those found in people with DS. These mice show delayed brain development, decreased cerebellar and hippocampal volume, altered density of specific cell types and alterations in the microstructure of pyramidal neurons and dendritic spines (Belichenko et al., 2004; Chakrabarti et al., 2010). The increase number of inhibitory neurons coupled to the decrease of excitatory neurons number, lead to an unbalance between excitation and inhibition (Chakrabarti et al., 2010). These animals also present abnormal synaptic plastic levels, with a decreased LTP and increased LTD (figure 12) (Costa and Grybko, 2005; Cramer and Galdzicki, 2012; Dierssen, 2012; Fernandez et al., 2007). Ts65Dn mice also show age-related atrophy, neurodegeneration of the basal forebrain cholinergic nucleus, neurotransmitter alterations and extensive astrocyte hypertrophy, which resembles the neuropathology of the Alzheimer-like disease that is observed in individuals with Down syndrome. Ts65Dn mice also show learning defects in spatial learning, hyperactivity and other cognitive and behavioural alterations (Dierssen, 2012).

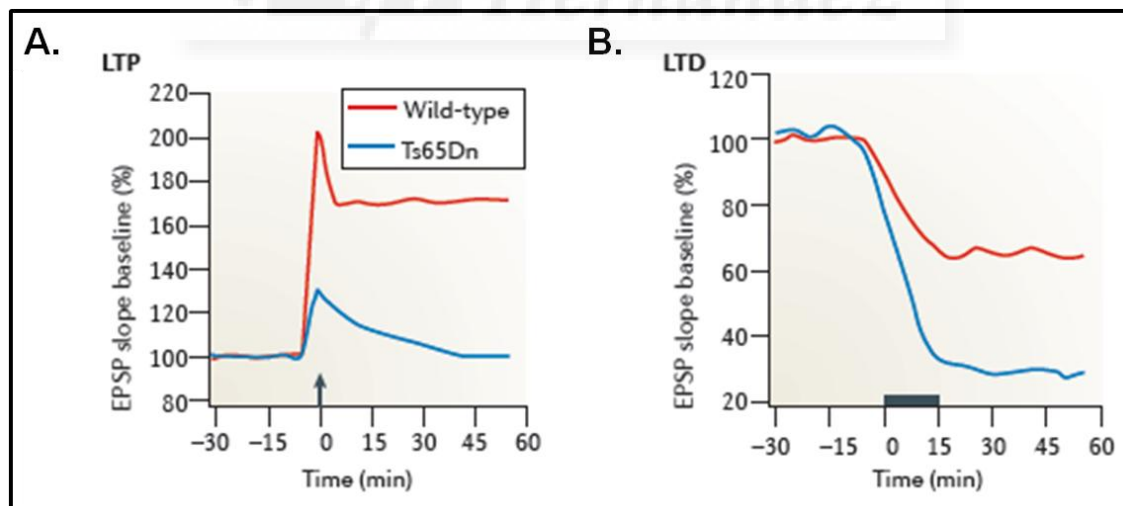


Figure 12: Excitation-inhibition imbalance in the hippocampal trisynaptic circuits of Ts65Dn mouse model of DS. (A) After HFS of the SC (time of onset is indicated by the arrow head), the field excitatory postsynaptic potential (EPSP) increases in both wild-type and Ts65Dn mice but fails to remain increased in the latter. (B) In Ts65Dn mice, there is an exaggerated depression of evoked EPSPs following LFS (which is indicated by the bar) of the SC. *Dierseen, 2012*

Ts1Cje

Ts(16C-tel)1Cje or Ts1Cje mice are trisomic for about 3/4 of the genes triplicated in Ts65Dn mice, lacking trisomy for the genes in the segment from *Mrpl39* to *Sod1*. Ts1Cje mice exhibit learning deficits in the Morris water maze, although impairment of spatial learning and memory in Ts1Cje mice is less severe than in Ts65Dn mice. Unlike Ts65Dn mice, they are able to perform well in the cued or non-spatial part of the test and only show moderate to severe impairment in the hidden platform, probe and reverse learning parts of the test. In addition, the age-dependent degeneration of basal forebrain cholinergic neurons, which is observed in Ts65Dn mice and individuals with DS, is absent in Ts1Cje mice. Craniofacial dysmorphology is also similar to Ts65Dn mice, but Ts1Cje mice lack the broadening of the cranium that confers brachycephaly in Ts65Dn mice. Ts1Cje mice have fewer similarities to DS than do Ts65Dn mice but are important to study the particular effects a subset of triplicated genes in Ts65Dn. The value of Ts1Cje mice for testing therapeutic interventions is for phenotypes related to genes in the triplicated segment (Belichenko et al., 2007; Sago et al., 1998).

Ms1Ts65

This model was designed to understand the role of the region present in Ts65Dn but not in Ts1Cje. Thus Ms1Ts65 mice come from the crossing of these two models and are trisomics for around 20 genes. Compare to Ts65Dn, they present less diminution of the cerebellum granular cell density and better performance during spatial memory test (Sago et al., 2000).

Ts1Rhr, Ms1Rhr and Ms1Rhr/Ts65Dn

Ts1Rhr and Ms1Rhr strains are respectively trisomics and monosomics for one segment of MMU16 corresponding to DSCR region. The Ms1Rhr/Ts65Dn strain is obtained crossing Ms1Rhr and Ts65Dn. This strain is disomic for DSCR and trisomic for the rest of the gene usually triplicated in Ts65Dn. These two strains allowed verifying that the exclusive triplication of the DSCR is able to generate the anomalies observed in Ts65Dn, Ts1Cje and human DS. With these models it has been deduced that DSCR is necessary to induce spatial learning and memory deficits, because it was absent in Ms1Rhr/Ts65Dn. But DSCR is not sufficient to generate these deficits considering that they were not observed in Ts1Rhr and Ms1Rhr (Olson et al., 2007). Therefore DSCR

genes participate in the elaboration of DS associated defects, but they need to interact with other triplicated genes out of this region.

Ts2Cje

Ts2Cje or Rb(12.Ts17¹⁶65Dn)2Cje is spontaneously derived from a natural mating between a Ts65Dn female and a diploid B6EiC3SnF1 male. This strain is genetically identical to the Ts65Dn strains, with trisomy of the MMU16, from *Mrpl39* to the distal telomere, which includes *Grik1*, the GluK1 protein-coding gene. Contrary to Ts65Dn, the extra chromosome is not free but translocated, via a Robertsonian translocation onto another chromosome (MMU12). Thus transmission of the MMU16 segmental trisomy through the female germline is significantly improved over Ts65Dn. Unlike Ts65Dn, males are fertile. *Ts2Cje* mice are 20% smaller in size than controls. *Ts2Cje* animals exhibit neurological features comparable with those of Ts65Dn mice (reduced spine density, spine size increased, enlarged ventricles) thereby validating the utility of this segmental trisomy model for the study of the molecular, genetic, and developmental mechanisms underlying DS. Furthermore because of their reproductive advantages, *Ts2cje* is a useful alternative to Ts65Dn to study DS (Ishihara et al., 2010; Villar et al., 2005).

Despite all these qualities, *Ts2Cje* model remains to be investigated (only 6 publications since 2005). In our project, we have considered using this model because of the previously presented advantages and the presence of our gene of interest GluK1 protein-coding gene in a triplicated region that is shorter than the one present in Ts65Dn.

6. Down syndrome as a synaptopathy

A synaptopathy is a pathology induced by a deregulation of the synaptic physiology. These functional disorders induce alteration of the organization and the function of neural circuitry that can be at the origin of pathological cognitive or emotional phenotype. Like for addiction and depression, the synaptic origin hypothesis for intellectual disability has been proposed recently (Vaillend et al., 2008). Genetic data, combined with functional studies, suggest that the delicate mechanism deregulations at the origin of the synaptic activity and plasticity are involved in diverse mental illnesses (Frankle et al., 2003). Considering that intellectual disability is the major DS phenotype

and that other cognitive or emotional disorders can be found in DS patient, can we associate DS to a synaptopathy?

Even if several drastic structural changes have been reported in the CNS of DS models and patients, it would be difficult to explain the deep disorders present in this disease by a simple change of brain volume. The literature currently available indicates that these structural anomalies are coupled to synaptic deregulations. In the first place, a study using transcranial magnetic stimulation in DS teenager patients, revealed that in the primary motor cortex the cortical excitability was normal but the induction of LTP-like changes was altered (Battaglia et al., 2008). Indeed, in Tc1 model, LTP is reduced in the DG (O'Doherty et al., 2005). In Ts65Dn mice, diverse studies pointed out plasticity changes using electrophysiological tools. In the area CA1, a lack of induction and maintenance of LTP and an increased LTD have been described (Dierssen, 2012). These defects could be due to alterations in proteins involved in synaptic plasticity, like CaMKII, ERK, PKA or PKC (Siarey et al. 1997; 2006). These mice also present LTP defect in the DG that can be restored by blocking fast inhibitory transmission (GABA_A antagonist) during LTP induction (Kleschevnikov et al., 2004). The author's conclusion was that in the DG of trisomic mice, the basal mechanisms responsible for the induction of LTP are still functional but an excessive inhibition prevents formation of long term plasticity. Another study, carried out in hippocampal CA3 from organotypic slice cultures, concludes that LTP machinery is not altered in Ts65Dn (Hanson et al., 2007). The most current hypothesis to explain this deficit is a change in excitation/inhibition ratio in the evoked transmission after electrical stimulation of the circuit. Increased inhibition would reduce the postsynaptic depolarization required to activate NMDAR and generate LTP.

In 2007, one study proposed for the first time an interesting therapeutic strategy to restore synaptic plasticity and cognitive defects observed in Ts65Dn. During this work, GABA_A antagonists were chronically administered to animals (injection or voluntary oral feeding). First *in vitro* electrophysiological study showed that this treatment can restore plasticity levels in the DG of Ts65Dn. Second, this treatment durably fixed the cognitive deficit observed in trisomic animals treated (Fernandez et al., 2007). This report demonstrates that the study of synaptic plasticity in DS mouse model could offer new perspectives to improve DS patient healthcare.

7. Aim of the thesis project

The principal objective of this project was to use the DS mouse model as a model of GluK1 gain of function to further understand the role of KARs in neurotransmission and try to assess their implication in normal and pathological synaptic mechanisms. As described earlier in this introduction, it has been demonstrated that GluK1-KARs are involved in mediating excitatory and regulating inhibitory synaptic transmission in the area CA1 of the hippocampus under non-pathological conditions. In addition, *in situ* hybridization reported the selective expression of GluK1 mRNA in interneurons of CA1 (Paternain et al., 2000). In human, the GluK1 protein-coding gene is located on the triplicated chromosome in DS, as it is in the triplicated segment in rodent models of this disease. Therefore, we expect that in DS, GluK1 subunit could represent an excess of function. If this is the case, the question is whether it could be related to the over-inhibition phenotype observed in DS. Thus this thesis work aimed at assessing the action of GluK1 overexpression on synaptic strength and plasticity in a DS animal model. With this work, we aspired to understand better the role of GluK1-KARs in synaptic transmission and to determine their level of implication in the pathophysiology of DS.

The main objectives of this thesis were:

- to find and to produce a DS model containing our gene of interest with the shortest triplicated region as possible.
- to set a reliable and fast genotyping method.
- to verify the actual overexpression of GluK1 protein in this animal model.
- to characterize the synaptic transmission phenotype in the hippocampus of these animals.
- to evaluate the implication of GluK1 protein overexpression in this phenotype.
- to restore putative alterations using GluK1-selective pharmacology.



MATERIALS AND METHODS

1. Animal model: Ts2Cje mouse

Rather than the gold standard “Ts65Dn” segmental trisomy mouse, in this study we used the “Ts2Cje” model (also called Rb(12.Ts17¹⁶65Dn)2Cje). This model presents reproductive advantages due to the chromosome aberration configuration. Rate of trisomy transmission is significantly increased in this model (43% vs 24%) (Villar et al., 2005). Ts2Cje presents a slightly smaller triplicated segment (from *Sod1* to *Mx1*) than Ts65Dn and this triplicated segment is fused to chromosome 12 (MMU12) via a Robertsonian translocation, contrary to Ts65Dn where the triplicated segment is freely segregated into the nucleus (figure 13).

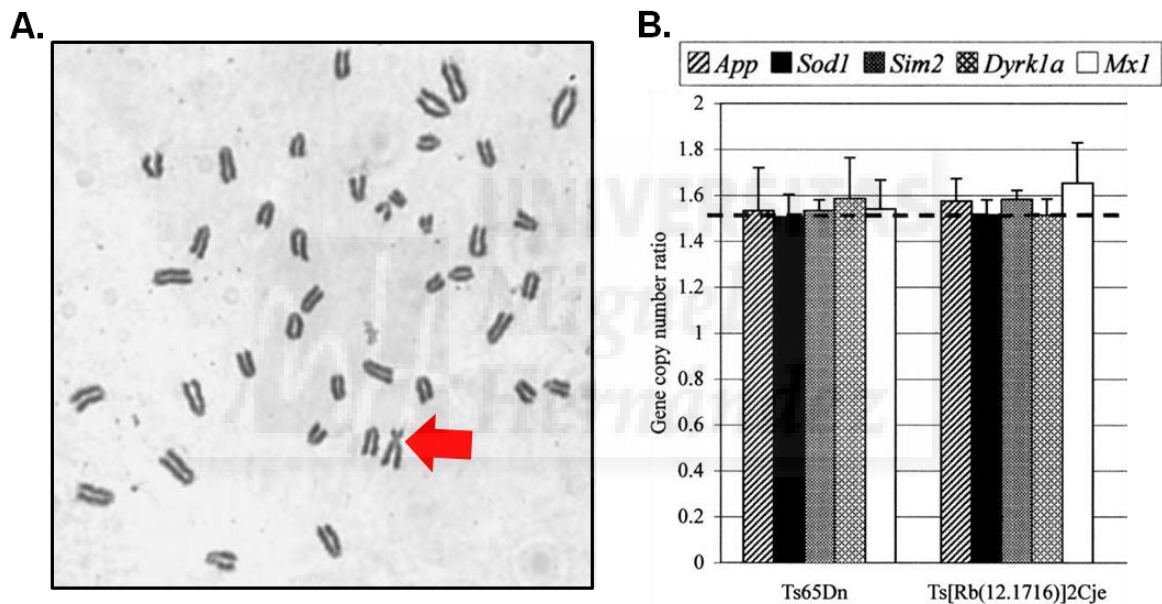


Figure 13: (A) Ts[Rb(12.1716)]2Cje metaphase stained with Giemsa showing the Robertsonian translocation chromosome (arrow), N = 40 chromosomes and 41 chromosome arms. (B) Gene copy number ratio (\pm SD) for *App*, *Sod1*, *Sim2*, *Dyrk1a*, and *Mx1* in DNA samples from Ts65Dn, Ts[Rb(12.1716)]2Cje, Ts1Cje<*Sod1a/a*>. Horizontal dashed line represents the position of a relative gene copy number of 1.5. Adapted from Villar et al, 2005

Villar and colleagues observed that Ts2Cje males present fertility contrary to Ts65Dn (normal spermatogenesis). It also exhibits a significant enlargement of spine volume and decrease spine density in dentate granule cells. Another study pointed out physiological abnormalities common with Ts65Dn (Ishihara et al., 2009) and described a short anteroposterior length of brain, enlarged ventricular volumes, impaired pre- and post-natal neurogenesis (figure 14).

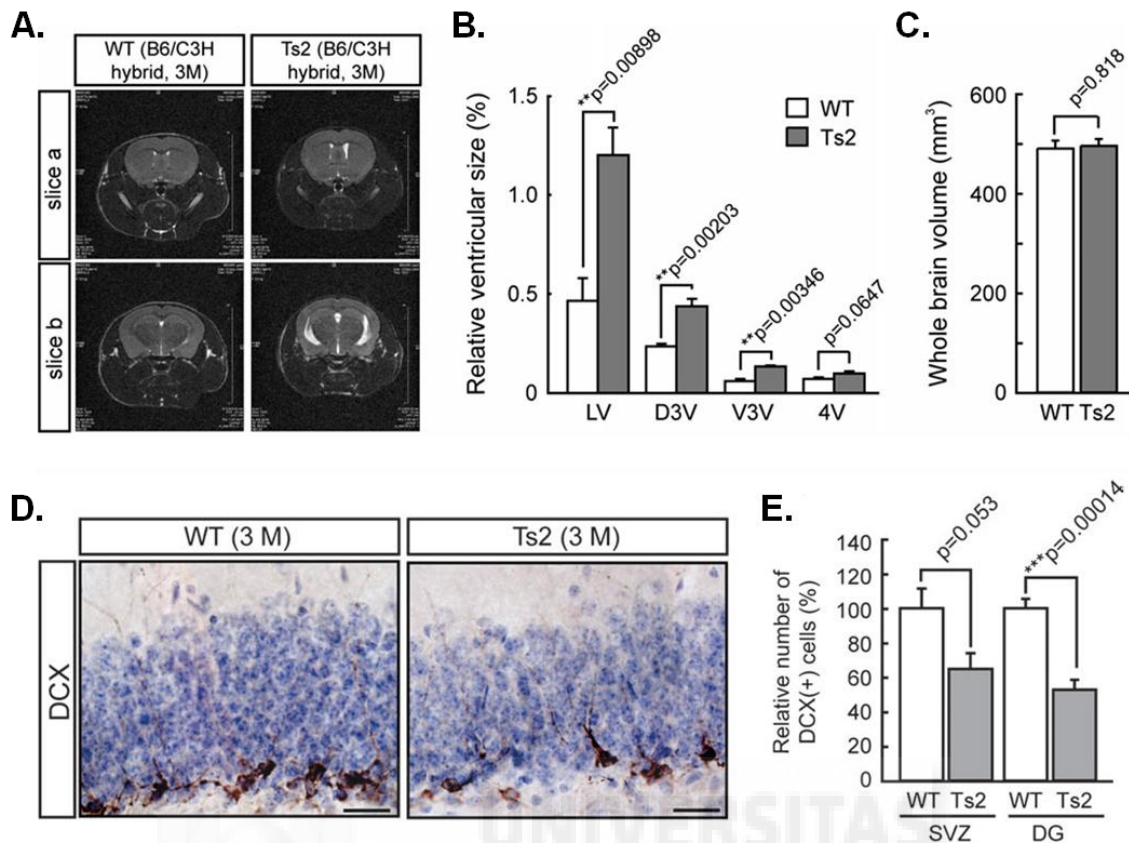


Figure 14: Enlarged brain ventricles in Ts2Cje. MRI analyses were performed on the brains from Ts2Cje and B6/C3H hybrid background at 3 months of age. (A) Coronal T2-weighted MRI images (slices a and b) of the brain from Ts2Cje and wild-type littermates. Expanded lateral and third ventricles were observed in Ts2Cje. (B) The ratios of each ventricular volume to whole brain volume indicate expansion of ventricles in Ts2Cje. (C) No significant change in whole brain volumes is detected. Decreased DCX-positive neuroblasts in the subventricular zone and dentate gyrus of Ts2Cje. (D) Magnified images of coronal sections of DG from WT and Ts2Cje. Scale bar: 50 μ m. (E) Quantification of DCX-positive cells in SVZ and DG by counting in a blinded manner shows that the number of DCX-positive neuroblasts are reduced in Ts2Cje. Adapted from Ishihara et al, 2009.

Two founders couples were purchased through *The Jackson Laboratory*, each couple was composed by one Ts2Cje female (JL stock number #4850) and a diploid B6EiC3SnF1/J male (JL stock number #1875). Animals were maintained in our animal facilities (Instituto de Neurociencias de Alicante), at 22-23°C, humidity 55±10% and under a 12h dark/12h light cycle. Animals had *ad libitum* access to food (pellet composition (%): 12 Moisture, 14.5 Protein, 4.5 Oils and Fats, 4.5 Fibers; Harlan®) and water. Animals couples were bred in separated cages and after weaning period (P14) animal facilities staff was collecting a small piece of tissue (tail or hear tagging residues) in order to proceed to qPCR genotyping. All animal experiments were approved by IN Bioethical Committee according to the “Real Decreto 1201/2005” and “Generalitat Valenciana 13/2007”.

2. Animal genotyping

Real time qPCR technique is a reliable method to genotype trisomic mice to differentiate three copies of a gene in trisomic from two copies in a disomic animal (Liu et al., 2003). Principle of this qPCR is illustrated and explained in figure 15. This technique can also be called “duplex qPCR” because it is possible to amplify two genes simultaneously in the same well during a unique run reaction using distinct fluorescent reporters for each probe. Another advantage of this duplex technique is that variation of the amount of input DNA is automatically normalized.

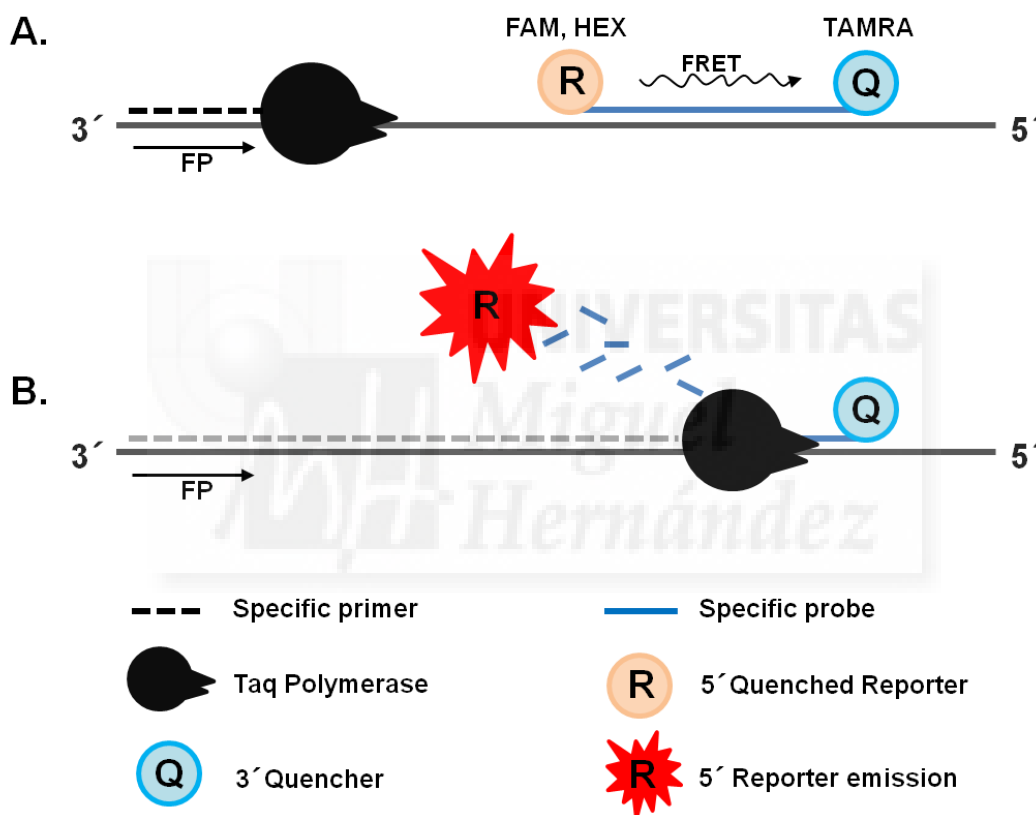


Figure 15: Real time qPCR principle. At the beginning of a PCR cycle, primer and TaqMan® probes link their specific sequences on DNA sequence coding for the gene of interest. Each probe (± 20 nucleotides) is tagged with a 5' fluorescent reporter (FAM, HEX) and a 3' quencher (TAMRA). Reporter emission spectrum covers the quencher absorption spectrum, so due to the proximity there is no fluorescence emission when the probe is entire and linked to its specific sequence, this phenomenon is called FRET (fluorescence resonance energy transfer) (A). Later in the cycle, Taq polymerase starts DNA replication from a double strand part (primer + DNA) from 3' to 5'. Once arrived in the probe region, Tap polymerase exonuclease activity denatures the probe. The consequence is an increase of the distance between reporter and quencher resulting in FRET neutralization and consequently a fluorescence emission from the reporter (B). For each DNA molecule synthesized, a fluorescent reporter is emitted. All of this occurs on each DNA strand and during each PCR cycle, so the fluorescence levels increase exponentially along the qPCR run. Using two different reporters allows following the amplification of two different genes in the same well during a run.

To genotype our animals, we used the Apolipoprotein B gene (*ApoB*) as a non-triplicated internal control (located on MMU12) and the Amyloid protein precursor gene (*App*) or GluK1 gene (*Grik1*) as triplicated genes (both located on MMU16 triplicated segment of Ts2Cje) (oligonucleotides sequences in table 4). Primers and probes were synthesized on demand by Sigma-Aldrich™.

Primer sequences	
<i>ApoB</i> forward	5'-CACGTGGGCTCCAGCATT
<i>ApoB</i> reverse	5'-TCACCAGTCATTTCTGCCTTTG
<i>App</i> forward	5'-TGCTGAAGATGTGGGTTCGA
<i>App</i> reverse	5'-GACAATCACGGTTGCTATGACAA
<i>Grik1</i> forward	5'-CTCTTCGGTCCTTCCCACAG
<i>Grik1</i> reverse	5'-GTCTGAATGTGTGGAAGTTCC
TaqMan® probe sequences	
<i>ApoB</i>	5'-HEX-CCAATGGTCGGGCACTGCTCAA-TAMRA
<i>App</i>	5'-FAM-CAAAGGCGCCATCATCGGACTCA-TAMRA
<i>Grik1</i>	5'-FAM-TGCTGTACAGTCTATTTGCAATGC-TAMRA

Table 4: Nucleotide sequences of the different primers and probes used during qPCR genotyping.

DNA was extracted from a small piece a tissue (tail and/or hear tagging residue) at P14. Samples were digested by 2x30min incubation with NaOH 50mM at 98°C followed by mechanical dissociation (vortex). Reaction was neutralized with TRIS 1M (pH=8), then the mix was centrifuged (6min, 14,000 rpm, MIKRO 120 Hettich®). Supernatant was transferred into a new tube and DNA concentration was determined (NanoDrop®) and normalized at 20ng/μl. Efficiency of each reaction was tested making standard curves for each qPCR. To do so, we used standard samples dilutions (1, 0.5, 0.25 and 0.125 ng/μl) from each animal type (1 DLM and 1 Ts2Cje), like illustrated in figure 16 B and C. Each DNA sample reaction was triplicated and test samples were used at 0.5 ng/μl. Then, PCR mix was prepared by mixing: DNA sample (10μl), 5x *HOTFIREPol*® *Probe qPCR mix Plus ROX* master mix (4μl), forward and reverse primers (0.25μl at 40μM), probes (0.75μl at 5μM) and DNA dilution solution (3.5μl of TRIS 10mM). Reactions were carried out on a 96-well plate in a StepOne Plus (Applied Biosystems). One full

real-time qPCR run was composed by a first initial denaturation step (95°C for 15min), followed by 40 cycles of denaturation/annealing-elongation (95°C for 15s / 60°C for 1min). At the end of the run, amplification curves (fluorescence/number of cycle) for the gene of interest were drawn automatically (figure 16A). StepOne Plus software determined automatically a cycle threshold (CT) for each well and generate a data file with all CTs values per gene and per well. CT is defined as the first PCR cycle at which an increase in reporter fluorescence can be detected above a basal signal. To determine zygosity of the animal, we calculated the average change (Δ) in CT of target gene (*App* or *Grik1*) from that of the internal control *ApoB* ($\Delta\text{CT} = \text{CT for } App \text{ or } Grik1 - \text{CT for } ApoB$) for each DNA sample. As triplicated gene presents 1.5 more DNA template at the starting of the PCR and theoretically quantity of amplified DNA is equal to 2^n (where n is the number of PCR cycle). Thus the expected difference between ΔCT for DLM and ΔCT for DLM ($\Delta\Delta\text{CT}$) should be 0.585 (if $2^n = 1.5$ then $n = 0.585$). The amplification of a triplicated gene present in three copies needs 0.585 less PCR cycles than a duplicated gene to emit sufficiently fluorescence in cross the cycle threshold.

The first set of experiments aimed to assess the reliability of Ts2Cje mouse as a model of GluK1 overexpression in CNS and more especially in our structure of interest, the hippocampus. With the duplex qPCR genotyping, we measured the copy number GluK1 protein-coding gene, the following step aimed to evaluate GluK1 gene products levels (mRNA and protein).

3. Evaluation of mRNA levels: RT-qPCR

It is often assumed that genes present in three copies in trisomic individuals will be expressed 1.5-fold relative to diploid state. However, it has been demonstrated that it is difficult to predict how changes in DNA copy-number affect gene expression relative to the diploid state (Lyle et al., 2004). To validate our model of GluK1 over expression, we first ran an mRNA quantification assay. Brains used for this experiment were collected from a total of 8 mice (1.5-2 months): 4 DLM and 4 Ts2Cje. Animals were anesthetized (Isoflurane, IsoVet[®]) and sacrificed. The brain was extracted immediately and the different structures of interest (cerebellum, cortex and hippocampus) dissected and dry ice frozen. Samples were then stored at -80°C until use.

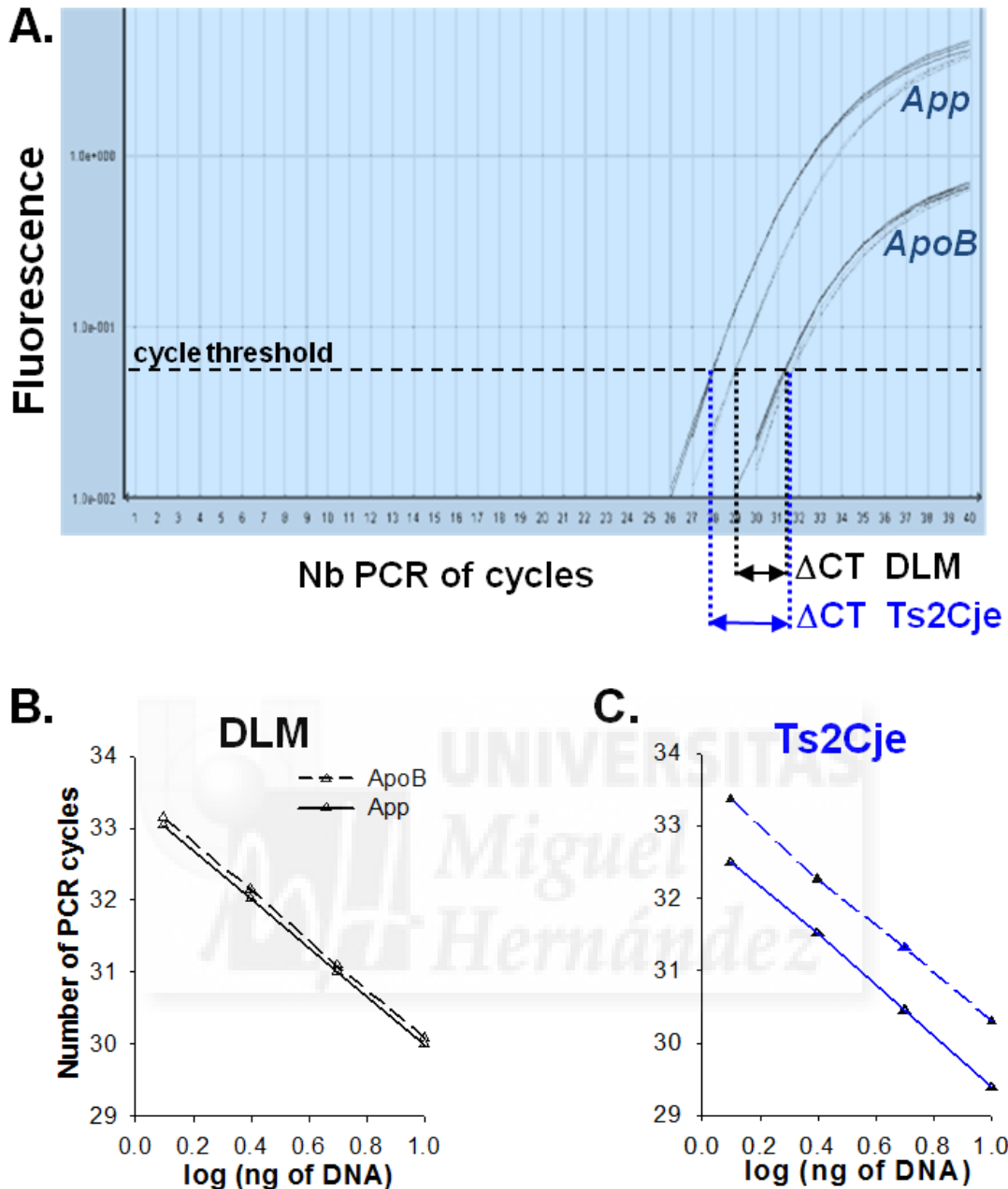


Figure 16: qPCR genotyping principle. (A) *ApoB* and *App* standards amplification curves obtained after 40 PCR cycles ($\Delta CT = CT_{App \text{ or } Grik1} - CT_{ApoB}$). Diploid (B) and trisomic (C) sample standard curves obtained from 4 different DNA concentrations (1, 0.5, 0.25 and 0.125 ng/ul).

To isolate total RNA, frozen tissues were homogenized (1ml of Ultraspec™ RNA solution) and stored 5 min at 4°C to finalized nucleoprotein complexes dissociation. Then to separate total RNA from DNA/protein by precipitation, chloroform (0.2 ml) was added to the tube and the preparation was shaken and placed at 4°C for 5min. This homogenate was centrifuged 15 min at 12,000 rpm. After this step, the homogenate formed two phases: one aqueous and one organic. The aqueous phase was carefully

transferred to a new tube where it was mixed with equal volume of isopropanol. The preparation was then stored 10 min at 4°C and RNA precipitation was finalized by a 10 min/12,000 rpm centrifugation. A white pellet of RNA was obtained at the bottom of the tube. Supernatant was removed and RNA pellet carefully washed three times with 75% ethanol and dried by vacuum (10 min) and later resuspended in DEPC treated water. This RNA solution was then treated with an RNase-free DNase set to digest contaminating DNA (RNeasy®, Qiagen). Finally RNA concentration was determined (NanoDrop®) and normalized at 0.1µg/µL. At this point, integrity of total RNA extracted could be assessed running an aliquot of the sample in denaturing agarose gel (1%) with ethidium bromide (EtBr). In these conditions, intact total RNA will present two sharp spots: one intense spot of 28S rRNA and one lighter, 18S rRNA, spot (figure 17). Total RNA was then used as a template to synthesize the complementary DNA (cDNA) during the Reverse Transcription (RT) phase (figure 18).

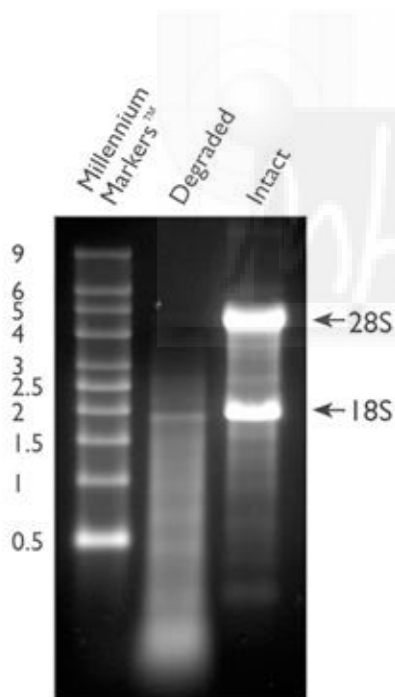


Figure 17: Intact vs. degraded RNA. Two µg of degraded total RNA and intact total RNA were run beside Ambion's RNA Millennium Markers™ on a 1.5% denaturing agarose gel. The 18S and 28S ribosomal RNA bands are clearly visible in the intact RNA sample. The degraded RNA appears as a lower molecular weight smear. *from Lifetechnologies.com*

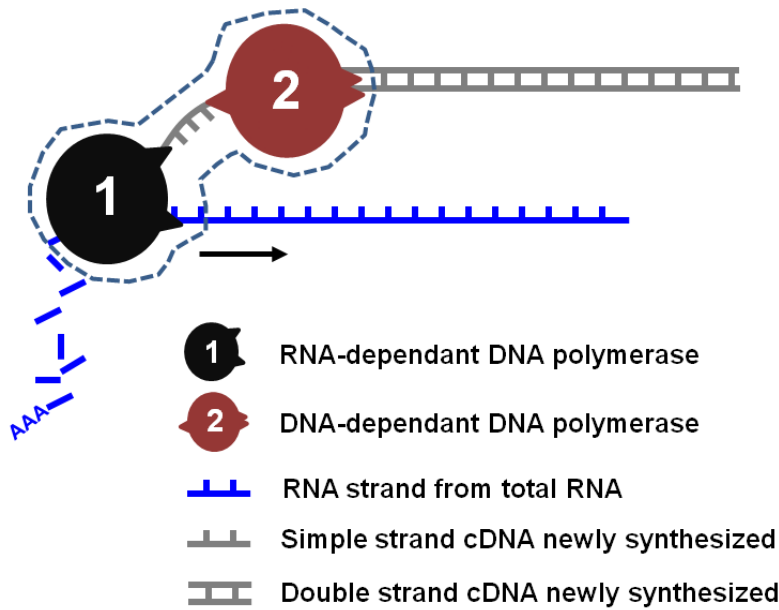


Figure 18: Reverse transcription principle, in tube containing total RNA, primers, dNTP mix and reverse transcriptase enzyme. Reverse transcriptase machinery produces a complementary double strand cDNA using single strand total RNA as template.

One μg of total RNA (diluted in $10\mu\text{l}$) was mixed with $10\mu\text{l}$ of RT master mix (composition in Table 5) and placed in a thermal cycler (Applied Biosystem model 2720) for annealing (10 min; 25°C), RT (30 min; 48°C) and RT inactivation (5 min; 95°C).

Component	Final concentration	Volume/Tube (μL)
10X RT buffer	1X	2
25 mM MgCl_2	5.5 mM	4.4
deoxyNTPs mixture (2.5 mM)	500 μM /dNTP	2
Random Hexamers (50 μL)	2.5 μM	1
Rnase inhibitor (20 U/L)	0.4 U/ μL	0.4
Multiscribe Reverse Transcriptase (50 U/L)	1.25 U/ μL	0.25

Table 5: Composition of RT master mix added to $10\mu\text{l}$ total RNA solution at $0.1\mu\text{g}/\mu\text{l}$. Final volume was $20\mu\text{l}$ (*Power SYBR[®] Green PCR Master Mix protocol*).

Second step is a selective amplification of the sequence coding for our gene of interest by qPCR. The procedure was similar to the one previously exposed in the figure 15, with the exception of the detection system. We used the fast SYBR[®] green system, which emits fluorescence when integrated in the double strand of DNA during amplification. Thus fluorescence detected during qPCR run is directly proportional to the number of DNA strand replicated. Here again logically if mRNA of interest was present in higher concentration at the beginning, there will be equally more cDNA transcripts and so more fluorescence emitted during qPCR cycle. In other words, fluorescence levels increase faster for an over-expressed mRNA than for a normal level mRNA. To selectively amplify our genes of interest, we used sequence specific couple of primers for all kainate receptors coding genes (*Grik1-5*) and Cyclophilin as an internal control (housekeeping gene) (Table 6).

Proteins	Genes	Forward (5'-3')	Reverse (5'-3')
Cyclophilin A (CC)	<i>Ppia</i>	AGGTCCTGGCATCTTGCCAT	GAACCGTTTGTGTTTGGTCCA
App	<i>App</i>	TGCTGAAGATGTGGGTTTCGA	GACAATCACGGTTGCTATGACA
GluK1	<i>Grik1</i>	ACTCAGGATCGGAGGGATTTT	GGTGA CTGCAA ACTTGAAAGC
GluK2	<i>Grik2</i>	AGCGTCGGTTAAACATAAGCC	GTTTCTTTACCTGGCAACCTTCT
GluK3	<i>Grik3</i>	AGAGAGCAGCGTTCCTTCTG	CGGCGGTCATTGAATGTGT
GluK4	<i>Grik4</i>	TGAGGATCGCTGCTATCTTGG	CGTACTCGCTGTCTCTGAGAA
GluK5	<i>Grik5</i>	GATCAACGGGATCATCGAGGT	GTGTCCGTGGTCTCGTACTG

Table 6: Primers couples sequences used during qPCR.

For the qPCR reaction, 1µl of cDNA template (0.05 µg/µl) was mixed with primers couples (0.5 µl at 5 µM), fast SYBR[®] green Master mix (5 µl) and RNase free water for a total volume of 10 µl. Reactions were run on a 96-well plate in a StepOne Plus (Applied Biosystems). Fast qPCR run was composed by an enzyme activation step (95°C for 20s) followed by 40 cycles of denaturation/annealing-elongation (95°C for 3s / 60°C for 30s). Here also reaction efficiency and couples of primers quality was verified making standard curves with samples dilutions (25, 12.5, 7.25, 3.125, 1.56 and 0.781 ng/µl) from a pool of cDNA (figure 19).

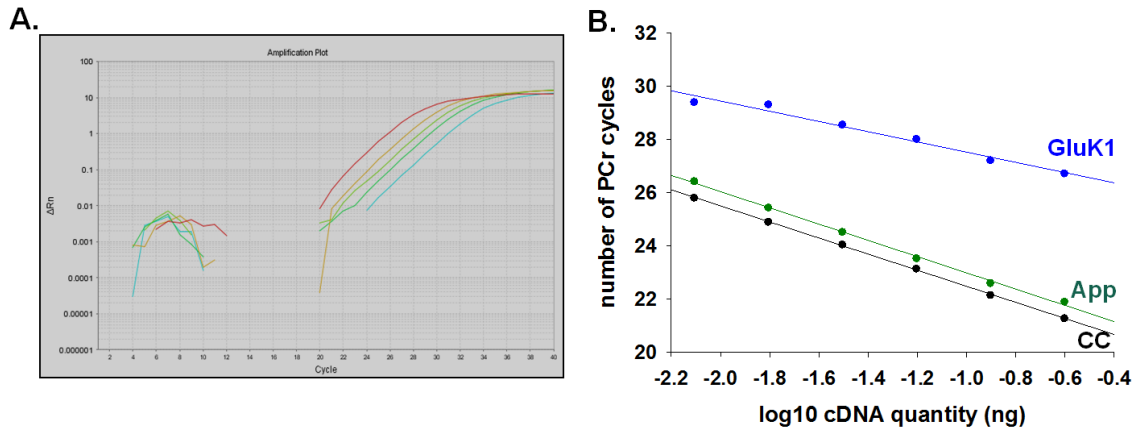


Figure 19: Primer testing. (A) Examples of amplification curves obtained after a PCR run with GluK1 primers. A range of cDNA dilutions (higher concentration on the left) produces constant amplification rate. (B) Plot CT (when fluorescence levels were higher than noise) against cDNA quantity in the PCR mix with different primers pair (CC, App and GluK1). Reaction was good quality when the coefficient of determination (R^2) of linear regression was >0.98 . This parameter informed us about the stability and the specificity of the primers along the qPCR run. In this example, R^2 CC, App and GluK1 were equal to 0.999, 0.997 and 0.994 respectively.

4. Quantification of KARs protein levels

With this procedure we wanted to quantify KARs protein levels in the CNS. Unfortunately a specific anti-GluK1 antibody is not available, making it impossible to assess directly GluK1 protein levels in the tissue. However, a few antibodies raised against KARs subunits: GluK2/3, GluK4 and GluK5 are available.

Four DLM and four Ts2Cje were anaesthetized (Isoflurane, IsoVet[®]) and sacrificed for this experience. The CNS was dissected and pons/medulla oblongata were taken out. The cerebellum was isolated from the rest of the brain as kainate receptors have a strong cerebellar pattern of expression (Darstein et al., 2003; Lerma, 2003) and was analyzed separately from the rest of the brain. Tissues were quickly frozen on dry-ice and stored at -80°C .

The day of the experiment, tissue were thawed very slowly on ice and homogenized in 2X volume of sheep buffer containing protease inhibitors and then centrifuged (4,000 rpm at 4°C). Then supernatant was transferred to a new tube and centrifuged (18,000rpm at 4°C). From there, the supernatant was removed and the bottom pellet resuspended with MKM buffer containing protease inhibitors and agitated to dissolve protein pellet (1h at 4°C in a rotator). This solution was then centrifuged (4,000 rpm, 10 min, 4°C) to pellet out undissolved fractions. Protein concentrations were measured by

Bradford quantification (Pierce™ BCA Protein Assay Kit) and samples concentrations were normalized (10 µg/µl). Proteins were separated by electrophoresis (1h 30 min at 30 mA) and transferred overnight to nitrocellulose membranes. Correct protein transfer was confirmed by staining membranes with Ponceau red.

Membranes containing the proteins were blocked for 1 h at room temperature with 5% milk in TBS containing Tween 20 (TBS/T) and incubated overnight at 4°C with one of the following primary antibodies: Tubuline (1:5000; Abcam®), App (1:5000; Sigma-Aldrich®), GluK2/3 (1:1000; Millipore™), GluK4 (1:2000; gently provided by Darstein's laboratory (Germany; Darstein et al, 2003)), GluK5 (1:3000; Millipore™). After washing in TBS/T, membranes were incubated for 2 hours at room temperature with secondary antibody conjugated with horseradish peroxidase (goat anti-rabbit (1:10000; Pierce®) or goat anti-mouse (15000; Pierce®)). The immunoblotted proteins were detected using enhanced chemiluminescence reagents (SuperSignal® West Pico Chemiluminescent Substrate, ThermoScientific) and revealing them with a luminescent image analyser (Fujifilm Intelligent Dar Box II). Finally spots intensity was quantify with ImageJ image processing program. To enrich the use of our sample, certain membranes were reused after a stripping. To remove antibodies (primary and secondary), membrane was put in a bath of chemiluminescence stripping buffer (Tris 62.5 mM, SDS 2%, β-mercaptoethanol for 30 pH 6.7) for 30 min at 60°C.

As mentioned previously, it does not exist any specific antibody raise against GluK1 subunit, so we were not able to measure directly GluK1 levels. So we approach this question with an electrophysiological tool.

5. *In vitro* Electrophysiology

5.1. Setting up the experiment

Animals were deeply anaesthetized using Isoflurane (IsoVet®), decapitated and brain was taken out an immediately place in an ice-cold high sucrose buffer (in mM: 124 NaCl, 8 NaHCO₃, 10 Glucose, 3 KCl, 1.25 NaH₂PO₄, 1 MgSO₄, 2 CaCl₂, saturated with 95% O₂ – 5% CO₂). Cerebellum/pons/medulla was removed and the brain was cut on the sagittal lane (figure 20). Right and left hemispheres were glued on the brain holder (proximal side facing the holder), put in the cutting chamber of the vibroslicer

(Leica VT1200S) and immediately immersed in ice-cold sucrose buffer. Hippocampal slices (320 μm) were cut in an anteroposterior way and directly transferred into a 37°C bath of extracellular solution (in mM: 124 NaCl, 8 NaHCO₃, 10 Glucose, 3 KCl, 1.25 NaH₂PO₄, 1 MgSO₄, saturated with 95% O₂ – 5% CO₂).

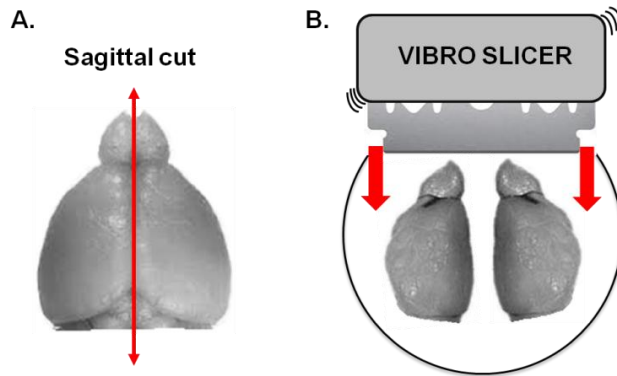


Figure 20: Brain preparation before slicing. (A) First, brain was separated in 2 parts cutting on the sagittal lane with a razor blade. (B) Then both hemisphere were glued on a holder and put in the vibro slicer. Slices were cut in an anteroposterior way.

After at least 45 min of recovery, brain slices were immersed in a recording chamber filled with extracellular buffer constantly renewed (1ml/min). Recordings were made on a classical *in vitro* setup to record bioelectrical activity in hippocampal slices (figure 21) at room temperature (around 22°C) or 32 °C depending on the experiment. Once the slice was under the microscope objective, it was gently anchored in the bottom of the recording chamber to avoid slice movement during recording due to fluid streaming.

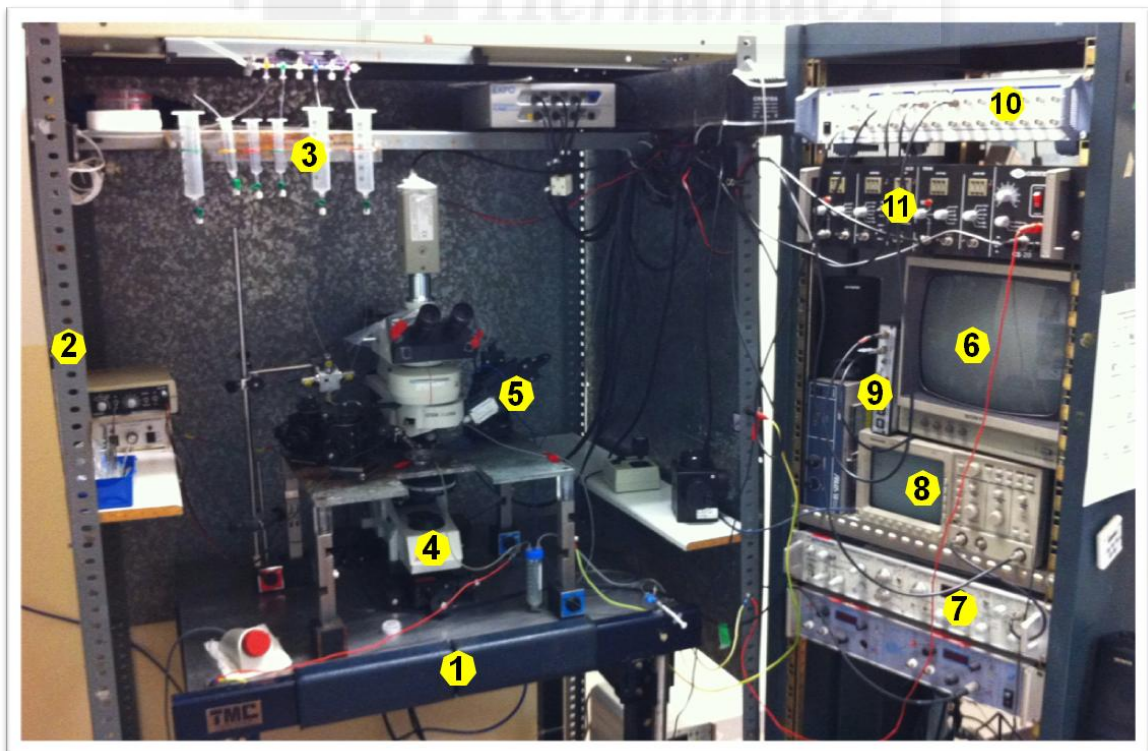


Figure 21: Main components of the recording rig. -1- Anti-vibration table. -2- Faraday cage. -3- Gravity perfusion system. General Valve Corporation. -5- Recording pipette holder and micromanipulator piezo (Burleigh PCS-6000). -6- Visualization system (Sony CCD-IRIS camera and Hamamatsu Argus50 + Minitor). -7- Amplifier Axopatch 200A. -8- Oscilloscope (Tektronik). -9- Noise eliminator (HumBug Quest Scientific). -10- Data acquisition system (Digidata 1400A Axon instruments) coupled to pClamp10 acquisition software on set-up computer. -11- Stimulation system (Cibertec CS20 and ISU165).

5.2. Whole cell patch clamp experiments

Hippocampal slices from P19-21 were used for those recordings. The area CA1 was localized under a 10X objective, but cells were visually identified at higher magnification (X40). We recorded pyramidal cells located in the pyramidal layer and interneurons in stratum radiatum or stratum oriens (figure 22). Recordings from pyramidal cells and interneurons were both made with 3-5M Ω borosilicate electrodes (Kwik-Fil™, WPI) filled with a specific internal solution depending on experiment type.

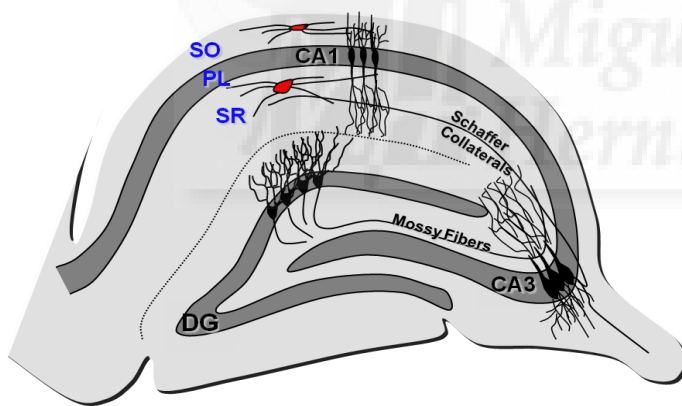


Figure 22: Trisynaptic organization of the hippocampus. Briefly, input arrives on dentate gyrus (DG), then goes to CA3 via mossy fibers. Then from CA3 to CA1 through Schaffer Collaterals. Finally output goes out of the structure to cortical area. (SO: stratum oriens; PL: pyramidal layer; SR: stratum radiatum)

Recordings made in interneurons or pyramidal cells were done with a chloride-based internal solution (in mM: 130 CsCl, 8 NaCl, 10 HEPES, 3 Qx, 0.5 EGTA, 4 Na-ATP, 0.4 Na-GTP and 5 phosphocreatine) or Gluconate-based solution (in mM: 140 K-Gluconate, 10 NaCl, 10 HEPES, 0.3 EGTA, 2 ATP-Mg and 0.5 GTP) depending on the experiment. External solution was supplemented with D(-)-2-amino-5-phosphonopentanoic (D-AP5; 25 μ M) to block NMDA receptors and GYKI53655 (LY303070; 25 μ M) to selectively block AMPARs. For recordings mIPSC, tetrodotoxine (TTX; 1 μ M) was also perfused to prevent action potential propagation

and record only spike-independent neurotransmitter release. This configuration allowed recording of inhibitory events under KARs influence only. Evoked IPSC in pyramidal cells or interneurons were evoked by local extracellular bipolar stimulation (theta tube borosilicate pipette) and recorded under the same pharmacological conditions as sIPSC (figure 23). To get more information about the neurotransmission characteristic we did paired-pulse stimulation (25Hz). For control experiments, inhibitory events were fully blocked using picrotoxine (50 μ M). Conditions of each experiment will be summarized in the “Results” chapter. Data were recorded using an Axopatch 200A amplifier and filtered at 2 kHz and acquired to a personal computer at 5 kHz of sampling frequency.

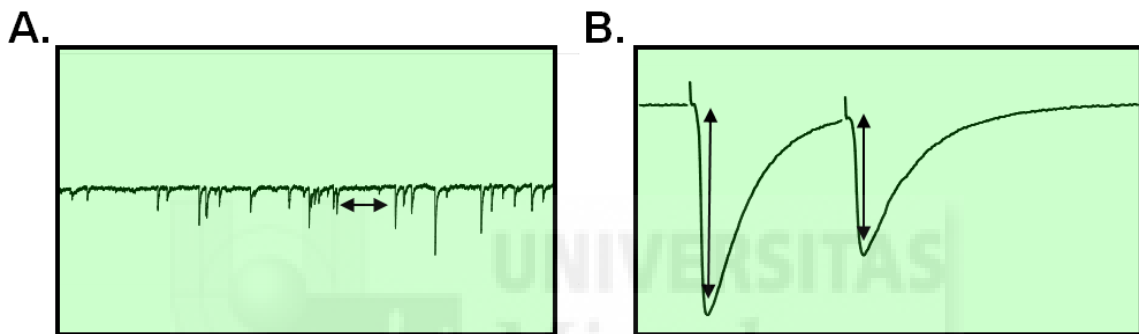


Figure 23: Example of traces obtained during whole cell patch clamp. (A) Frequency and amplitude of mIPSC and sIPSC was evaluated. (B) Amplitude and Paired-pulse ratio were monitored during study of eIPSC.

5.3. Extracellular field recording experiments

Hippocampal slices from 2 months old animals were prepared in the same conditions as for patch clamp experiments. Field excitatory post synaptic potentials (fEPSP) were recorded with 3-5M Ω borosilicate electrodes filled with 1M NaCl to improve signal detection and stability. A bipolar stimulation electrode was placed on Schaffer collaterals to evoke field responses recorded in the middle of CA1 pyramidal cell dendritic tree (SR).

For long term potentiation (LTP) protocol, first the maximal fEPSP amplitude was determined and then the stimulation intensity was adjusted to yield approximately 50% of the maximal amplitude. After a stable 20 minutes baseline, high frequency stimulation (HFS) potentiation protocol (1 or 3 trains of 1 sec pulses at 100Hz) was applied, resulting in a persistent increase of fEPSP size. This potentiated response often lasted as long as the slice preparation remained viable (Figure 24A) (Bortolotto et al.,

2011). The parameters assessed during LTP were the amplitude of the fiber volley (FV) and both slope and amplitude of fEPSPs. FV represents the number of fibers activated by the stimulation and it should remain stable during all the assay. Depression of the fEPSP response could also be induced *in vitro* using specific stimulation protocol depending on the age of the animal. In young animals (P15-17), *de novo* long term depression (LTD) was induced by low frequency stimulation (LFS; 900 pulses at 1Hz). The consequence was a persistent reduction of the fEPSP amplitude that lasted for many hours (figure 24B). As in LTP experiments, FV amplitude, fEPSP slope and amplitude were the parameters quantified. Since in old animals (e.g. 2 months), induction of a persistent *de novo* depression is difficult, rather we applied a depotentiation protocol. The first step of this protocol was to apply a standard LTP-inducing protocol (HFS) to obtain a stable potentiated fEPSP and then to depotentiate these responses.

5.4. Kainate receptors selective pharmacology

To test the implication of GluK1 kainate receptors in CA1 synaptic physiology, we challenged our preparations with several drugs. KARs agonists were kainate (3 μM) and ATPA (1, 3 and 10 μM); KARs antagonists were CNQX (20 μM), UBP310 (10 μM) and ACET (1 μM). All those compounds were prepared at desired concentrations in external solution.

5.5. Data analysis

Data were acquired using Clampex 10.0 to a personal computer where they could be analyzed with Mini Analysis (Synaptosoft Inc.) software (basal activity analysis) or Clampfit 10.0 (evoked activities). Statistical analyses were run with the analysis tools provided with SigmaPlot 12.0 analysis software. We mainly used Student t-test or Paired t-test (confidence interval 95%), and variability represented by standard error of the mean ($\pm\text{SEM}$).

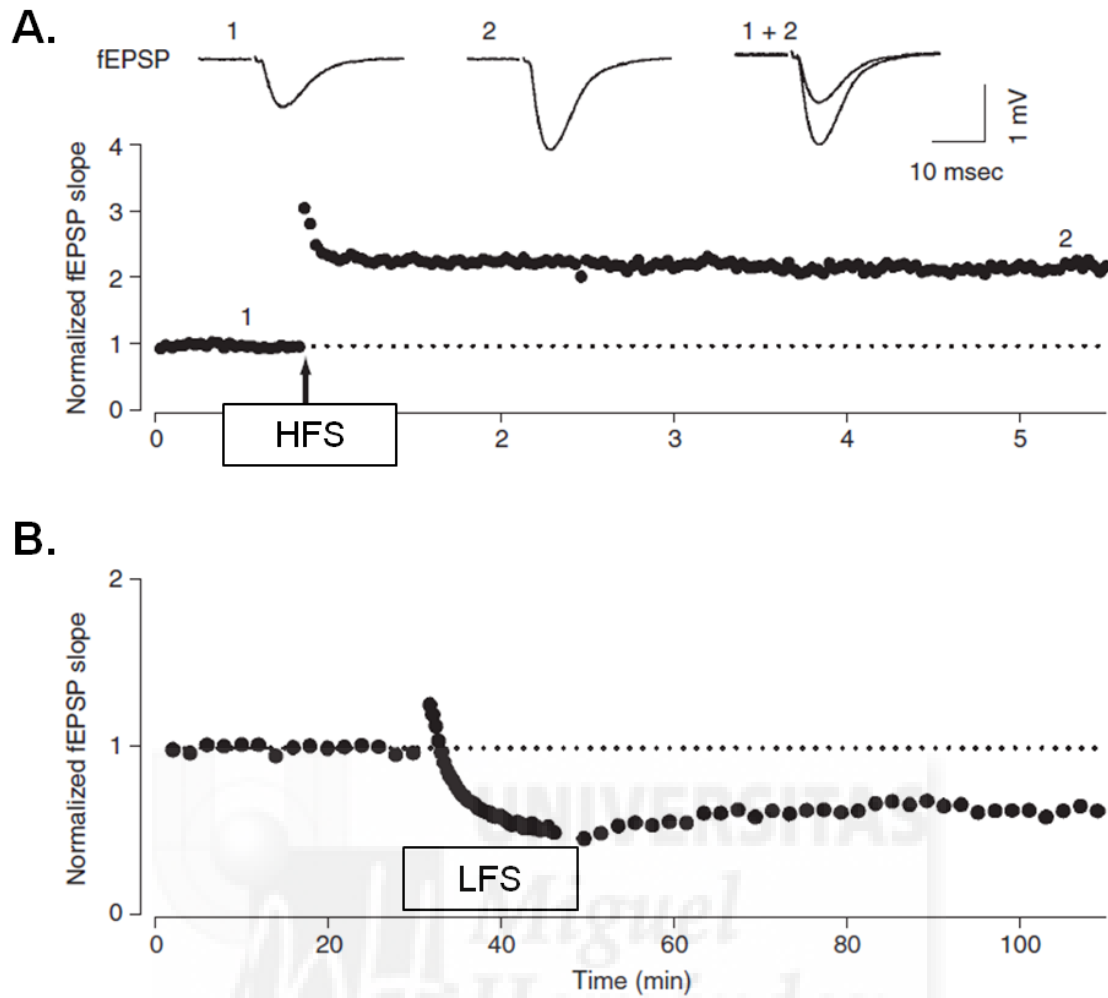


Figure 24: LTP and LTD studied using field potential recording. **(A)** A typical LTP experiment in a slice obtained from an adult rat. The traces at the top of the graph show the field excitatory postsynaptic potential (fEPSP) responses extracted from the plot at the times indicated on the graph (1, 2). These responses are superimposed in the third trace. A single tetanus (100 Hz, 1 sec, test intensity) was delivered at the time indicated by the arrow. Note that this induced LTP showed no sign of abatement after >4 hr. **(B)** A typical de novo LTD experiment in a slice obtained from a 14-day-old rat induced by low-frequency stimulation (LFS; 900 shocks at 1 Hz, test intensity). Adapted from Bortolotto *et al*, 2011



RESULTS

1. Ts2Cje production and genotyping

Extracting DNA from P15 pups and using a real-time qPCR method furnished us a ΔCT (= $CT_{App \text{ or } Grik1} - CT_{ApoB}$) for each sample tested. As previously described (Liu et al., 2003), two different types of animals were easily identified within each litter, the ones with a low ΔCT (DLM) and the others with a high ΔCT (Ts2Cje) (figure 25). ΔCT was significantly increased in DNA samples coming from trisomic animals ($p < 0.0001$), reaching differential values of 0.60, very close to the theoretical value of 0.58.

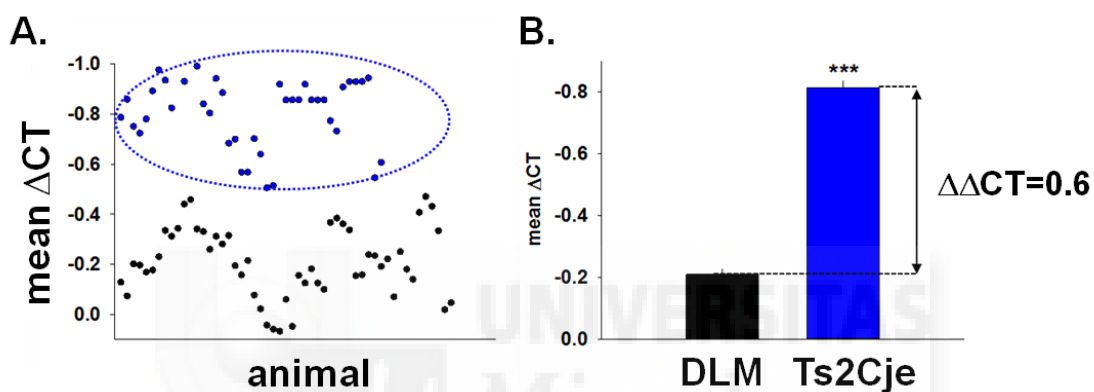


Figure 25: qPCR allowed a clear discrimination between DLM and Ts2Cje pups. (A) Mean ΔCT from several animals (53 DLM and 42 Ts2Cje) were plotted. Two distinct populations were coming out. (B) DLM and Ts2Cje mean ΔCT . $\Delta\Delta CT$ was significantly increased in DNA samples coming from trisomic animals ($***p < 0.0001$; Student t-test).

Between April 2011 and November 2013, 450 animals were born in our animal house premises. 28.7% were genotyped as Ts2Cje. Focusing on the female germline, Ts2Cje represented 34.6% of the new pups ranging from 0% to 75%. Both genders were represented in the same proportions and trisomy transmission affected both male and female in the same way (figure 26). By simple eye observation animal facilities staff was able to predict pups genotype comparing animal size within the litter (figure 26D). These observations were always confirmed by qPCR genotyping. Before starting the experiments, animals were weighed resulting that Ts2Cje were significantly lighter than DLM ($p < 0.001$; figure 26C).

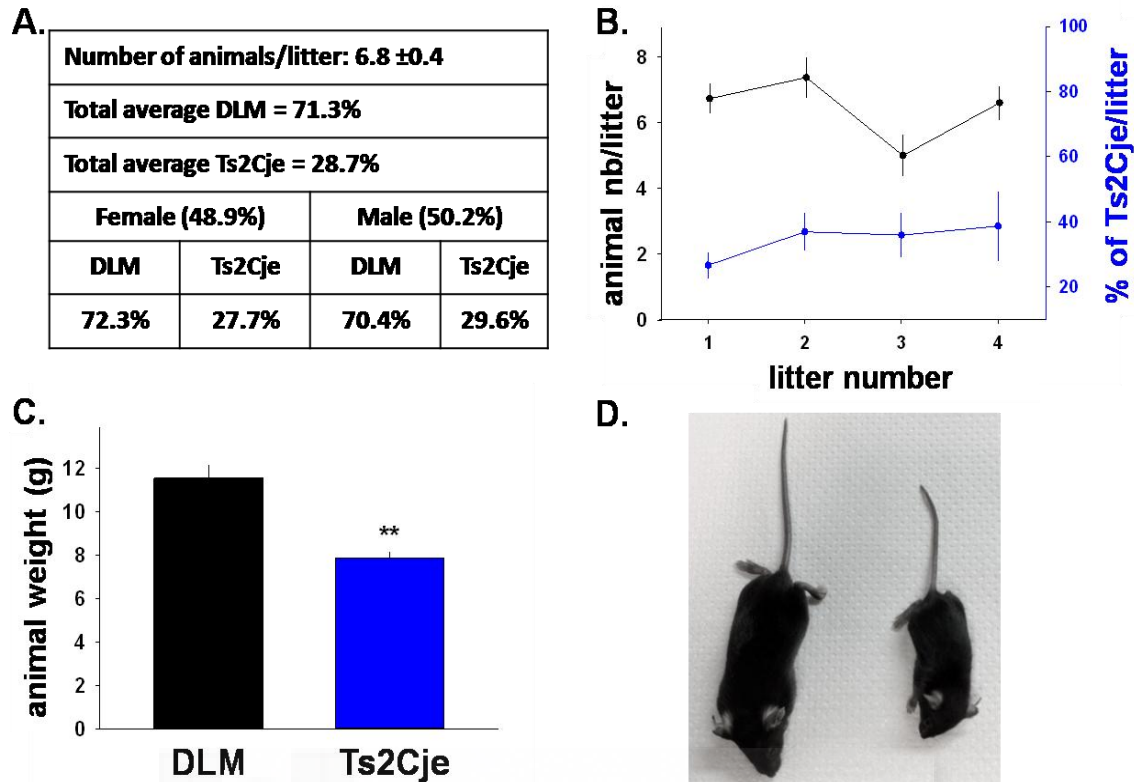


Figure 26: Animal production statistics from April 2011 to November 2013. (A) Table presenting several relevant numbers on animal production. (B) No difference was observed between 1st and the 4th litter in term of number of animal or % of Ts2Cje (C) At P20 Ts2Cje animals were significantly lighter than DLM; ** $p < 0.001$ (D) Trisomic animals were also smaller than diploid littermates.

2. Increased GluK1 mRNA levels

To confirm that Ts2Cje could actually be a model for GluK1 overexpression, the first step consisted in GluK1-coding mRNA quantification. In the different brain structures tested, we observed that mRNA levels coding for triplicated genes (*App* and *Grik1*) were significantly increased in Ts2Cje (figure 27). KARs are tetrameric combinations composed by GluK1 and others subunits, we wanted to know if a putative GluK1 overexpression could affect mRNA levels of genes coding for others KARs subunits. We evaluated mRNA levels for all KARs subunits from RNA samples isolated from cerebellum and we did not find any significant changes (figure 28).

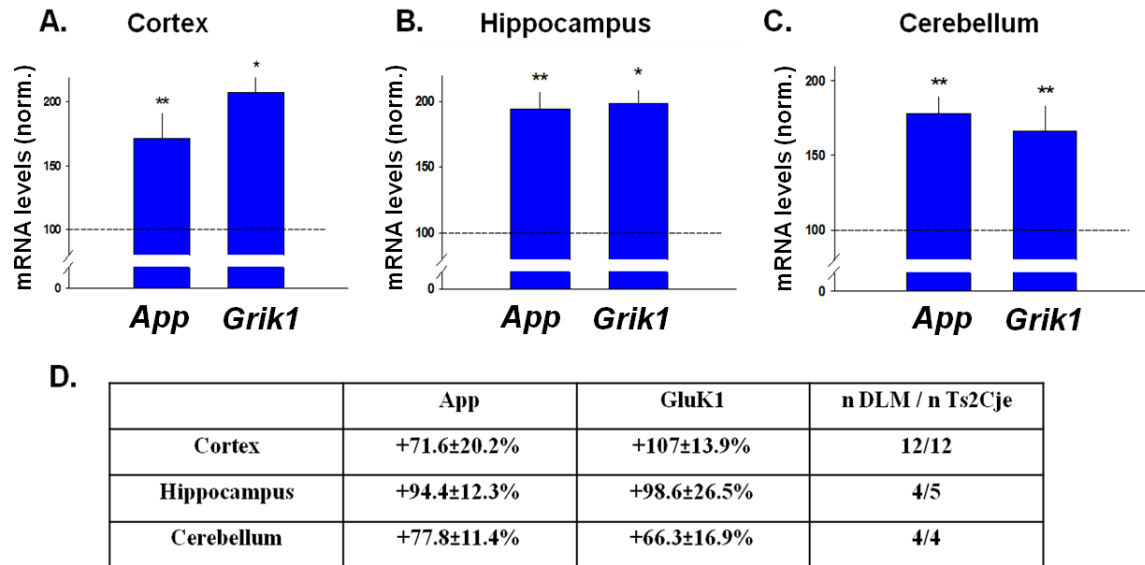


Figure 27: mRNA levels of gene transcript from triplicated genes were significantly increased in the cortex (A), the hippocampus (B) and the cerebellum (C) of Ts2Cje animals. (D) RT-qPCR data compilation. (* $p < 0.01$, ** $p < 0.001$; Student t-test)

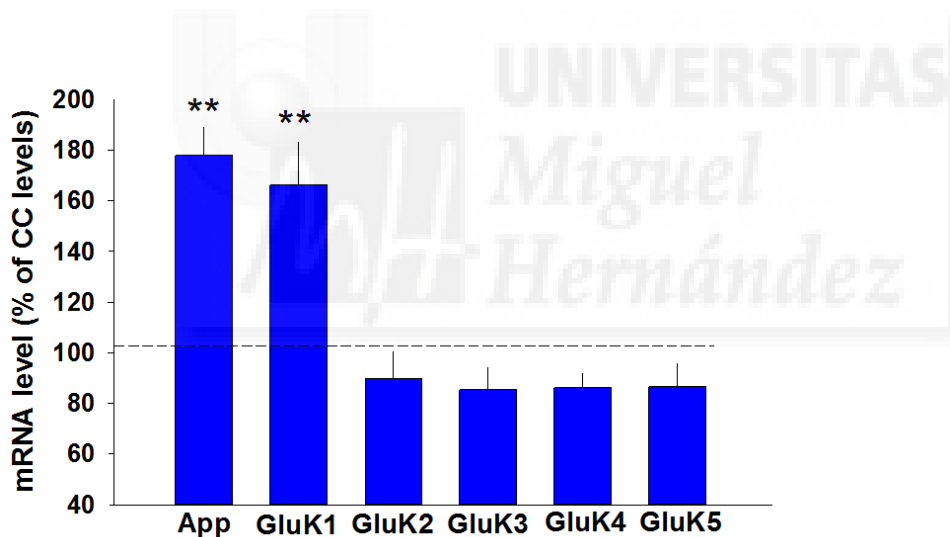


Figure 28: In the cerebellum, mRNA levels of gene coding for the others KARs subunit were not changed (** $p < 0.001$; Student t-test).

3. Changes in KARs protein levels

Functional GluK1-containing KARs could be either homomeric or heteromeric if GluK1 is combined with other KARs subunits (Lerma, 2003). Although no GluK1 specific antibody was available on the market, we wanted to look at the protein levels for other KARs subunits in the CNS to assess if the increase of GluK1 expression could

affect the level of other subunits. We made three different hypotheses about the effect of GluK1 overexpression: (i) it has no effect on other KARs subunit levels; (ii) increase of GluK1 homomeric receptors produces a compensatory decrease of heteromeric KARs, so we should observe a decrease of others KARs subunit levels; (iii) increase of GluK1 containing heteromeric KARs induces an increase of others subunits levels. To challenge our hypotheses we quantified GluK2/3, GluK4 and GluK5 in the cerebellum and in the rest of the brain. Protein levels were normalized to α -tubuline levels and App (coded by a triplicated gene) was used as an internal positive control. App levels were significantly increased in cerebellum ($+49.5 \pm 8.1\%$) and the rest of the brain ($+31.5 \pm 6.9\%$). Levels of GluK2/3, however, did not change (Cb: $+6 \pm 5.7\%$; brain: $-11.8 \pm 5.2\%$). GluK4 levels were significantly reduced in both the cerebellum and the brain ($-21.6 \pm 5.8\%$ and $-35.8 \pm 5.4\%$, respectively, $p < 0.05$). The same result was observed for GluK5 (Cb: $-34.3 \pm 5.5\%$; Brain: $-21.8 \pm 6.1\%$; $p < 0.05$) (figure 29).

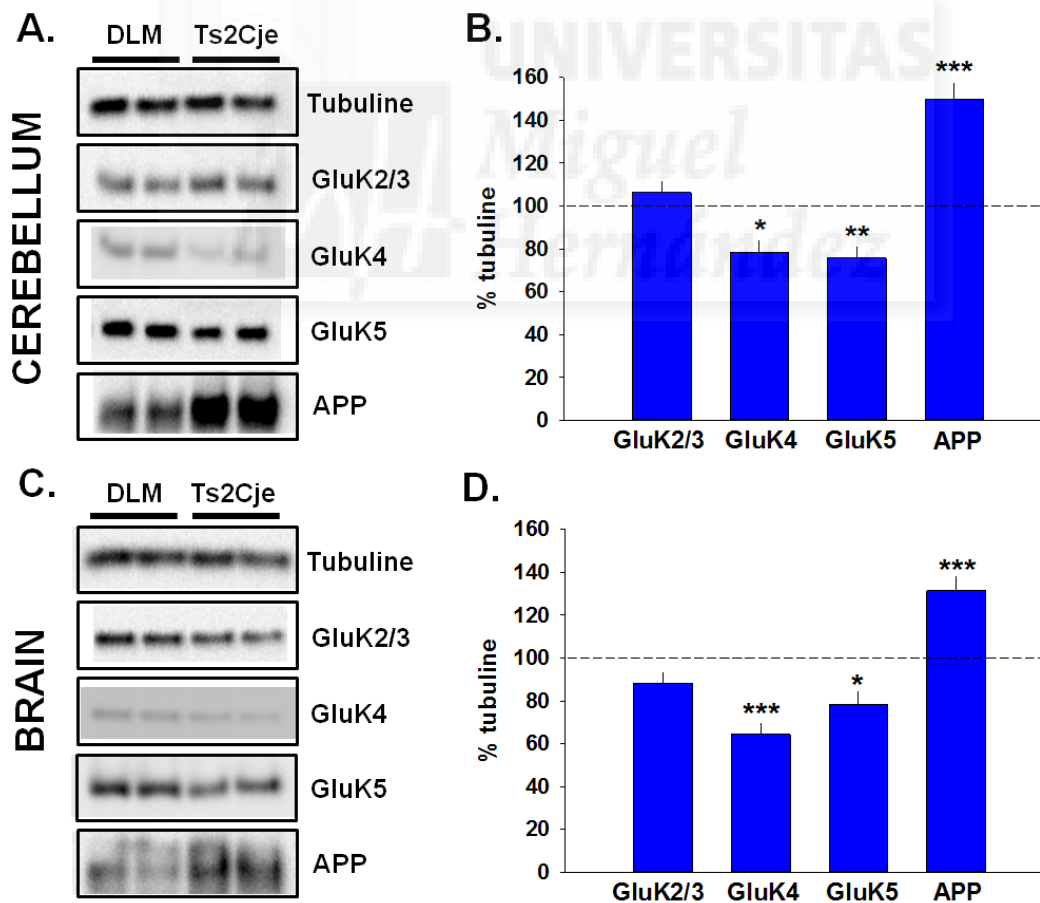


Figure 29: Trisomy affects KARs receptors levels of expression in Cerebellum (A, B) and Brain (C, D). Same profile is observed in both structures, App levels are increased whereas GluK4 and GluK5 are decreased. GluK2/3 are not changed (* $p < 0.01$, ** $p < 0.001$, *** $p < 0.0001$; Student t-test).

4. Overexpression of functional GluK1 protein in CA1 interneurons

As explained, we were unable to measure the protein levels given the lack of specific antibody against GluK1 subunit. We used an electrophysiological approach to evaluate the excess of functional GluK1 channels at the membrane of CA1 interneurons in Ts2Cje as compared to DLM. This experiment was run in interneurons of CA1 SR where the presence of GluK1 mRNA has been previously reported (figure 4) (Paternain et al., 2000).

While recording holding currents in voltage clamp configuration, activation of KARs will produce an inward current that will be reflected by a change of in holding current. The amount of current induced is directly proportional to the number of functional channels at the membrane. In this case our hypothesis was that if GluK1 is overexpressed at the membrane, inward current induced in a CA1 interneuron by a selective agonist of GluK1-KARs (ATPA 1 μ M, 30 seconds) must be greater in Ts2Cje than in DLM. In order to record exclusively current due to GluK1-containing KARs, we blocked GABA_ARs, AMPARs and NMDARs with their respective antagonists (picrotoxine 50 μ M, GYKI 25 μ M and D-AP5 25 μ M). After a 10 minutes washing with normal ringer, we perfused a larger concentration of ATPA (3 μ M) able to activate also other KARs types (e.g. GluK2/GluK5). With this experiment, we wanted to get an estimation of the proportion of GluK1-containing over all KARs.

In DLM animals perfusion of ATPA 1 μ M induced 2.7 ± 0.9 pA/pF (n=11) and in Ts2Cje it was 15.6 ± 3.3 pA/pF (n=12) (figure 30A, B; p=0.001). Using 3 μ M ATPA, we observed larger inward currents (DLM: 5 ± 2.1 pA/pF and Ts2Cje: 21 ± 3.8 pA/pF; DLM p=0.01 and Ts2Cje p=0.003; figure 30C). To compare the proportion of GluK1-containing KARs in one or another situation, we calculated the ratio of currents induced by 3 μ M over 1 μ M ATPA. In DLM, ATPA 3 μ M produced $103 \pm 26\%$ more inward current than ATPA 1 μ M. This increase was significantly reduced in Ts2Cje ($+44.6 \pm 6.8\%$, p=0.02; figure 30D).

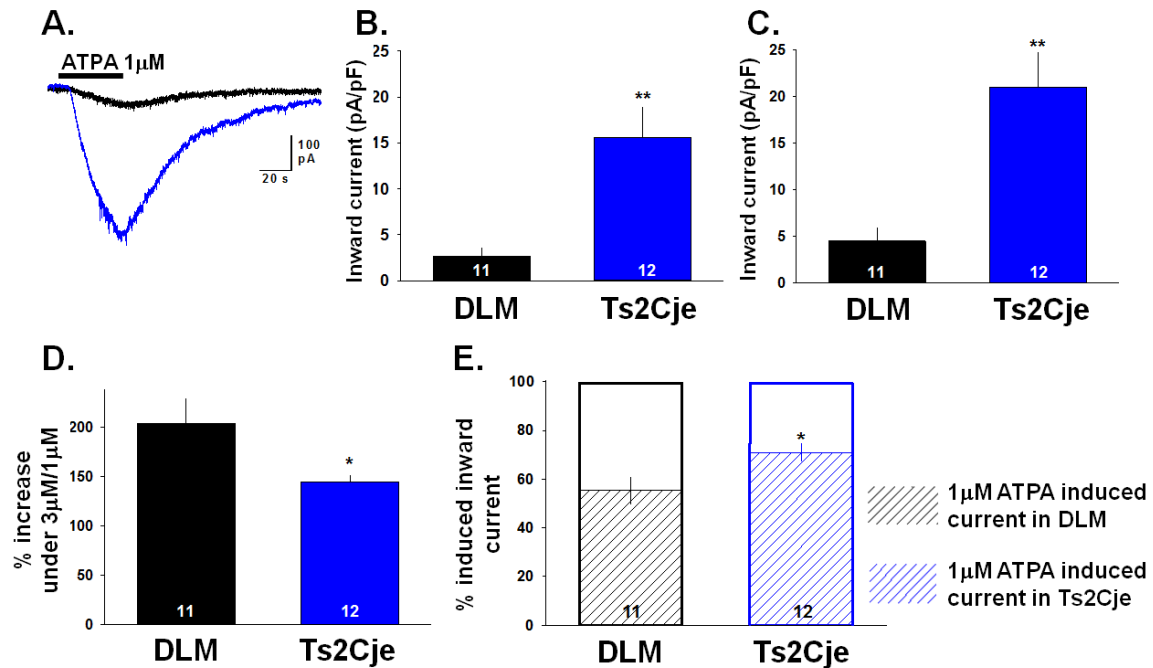


Figure 30: GluK1 channel overexpression in Ts2Cje interneurons. (A) Example of 1 μM ATPA induced inward current in interneuron of CA1 (black line=DLM, blue line= Ts2Cje). (B) In DLM, ATPA 1 μM induces significantly more inward currents in Ts2Cje, the same effect was observed with 3 μM ATPA (C). (D) Comparing the effect of 1 and 3 μM in the same cell. Increase caused by 3 μM ATPA over 1 μM was significantly reduced in Ts2Cje compared to DLM. (E) Proportion of current activated by 1 μM ATPA over 3 μM was significantly increased in Ts2Cje (* p <0.05; ** p <0.001; Student t-test).

Thus in Ts2Cje, the fraction of current mediated by GluK1-KARs was significantly higher ($70.9 \pm 3.4\%$ vs $55.3 \pm 5.6\%$; $p=0.02$). The same experiment was also done using K-gluconate based internal solution and with longer ATPA applications (2 min). Again, inward current induced in Ts2Cje were significantly greater than in DLM (2.13 ± 0.6 vs 0.24 ± 0.1 pA/pF, $p=0.02$). These results indicate that more functional GluK1-containing KARs are present at the membrane of neurons in Ts2Cje animals.

5. Increased basal inhibitory synaptic transmission of CA1 pyramidal cells

mIPSC frequency and amplitude were higher in Ts2Cje

For these experiments we used TTX (1 μM) to record only action potential independent release of GABA. We also perfused the slices with GYKI53655 25 μM and D-AP5 25 μM to block AMPARs and NMDARs. The recording pipette was filled with a chloride-

based solution and recording chamber was kept at 32°C. Patched pyramidal cells were clamped at -70mV. The frequency and amplitude of mIPSC were significantly larger in Ts2Cje neurons compared to DLM cells (11.05 ± 0.8 vs 6.52 ± 0.7 Hz; +69.5% $p=0.0004$ for frequency; 62.1 ± 5.3 vs 46.4 ± 3.3 pA; +33.8% $p=0.02$ for amplitude) (figure 31). Interestingly, a GluK1-KARs selective antagonist (ACET 100 nM) significantly increased mIPSC frequency in both DLM ($+155.2 \pm 18.3\%$, $n=13$ $p=0.004$) and Ts2Cje ($+130.7 \pm 6.1\%$, $n=14$; $p=0.001$) but it did not have effect on mIPSC amplitude (figure 31). Note that picrotoxine application fully abolished transmission demonstrating that those events were only due to GABA_A activation.

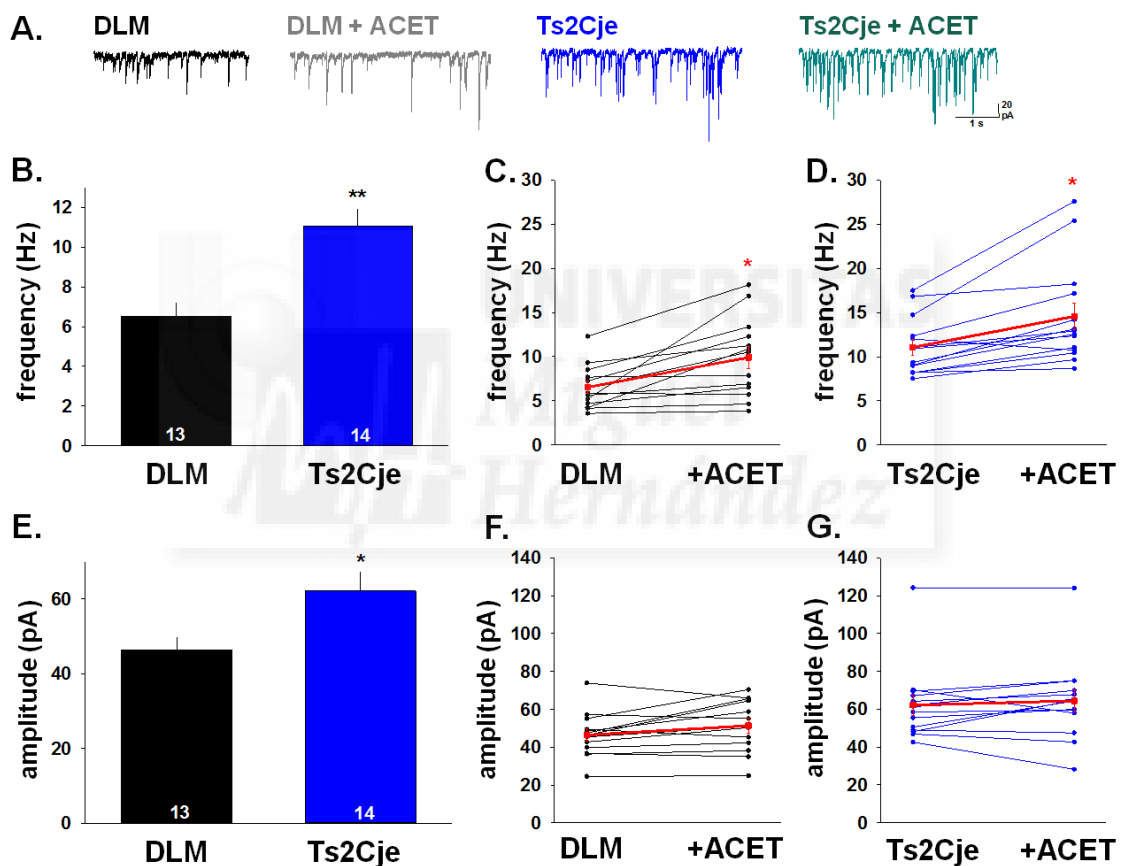


Figure 31: mIPSC frequency and amplitude were larger in Ts2Cje CA1 pyramidal cells. (A) mIPSC recording for each conditions. With normal external solution, mIPSC frequency and amplitude was significantly larger in Ts2Cje (B,E). ACET application enhanced significantly frequency in both models (C,D) and had no effect on amplitude (F,G). In B,C,E,F: black line = individual cell data, red line = all cells mean (* $p<0.05$; ** ($p<0.001$); Student t-test).

In another set of experiments, we also assessed the effect of another GluK1-KARs selective antagonist: UBP310 (10 μ M). In these experiments, the frequency of the mIPSCs was still higher in Ts2Cje than in DLM under control conditions (without UBP310) (9.7 ± 0.9 vs 7.1 ± 0.5 Hz; $p=0.02$). The amplitude was also significantly larger

in Ts2Cje (36.3 ± 6.5 vs 27.6 ± 2.3 pA; $p=0.03$) (figure 32). UBP310 perfusion significantly increased mIPSC frequency in both DLM ($+131.2 \pm 8.9\%$, $n=16$, $p=0.004$) and Ts2Cje ($+119 \pm 5.6\%$, $n=16$, $p=0.003$) to a similar extent ($p=0.35$), having no effect on mIPSC amplitude.

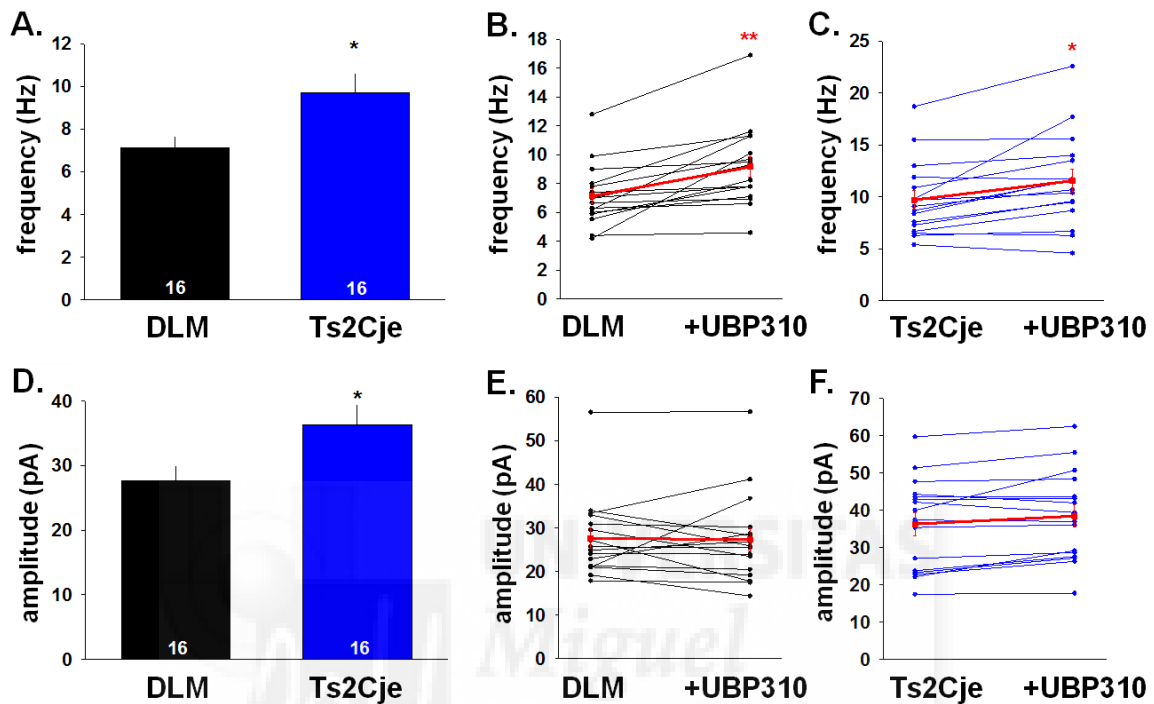


Figure 32: Higher mIPSC frequency in Ts2Cje CA1 pyramidal cells. (A) In normal conditions, mIPSC frequency was significantly higher in Ts2Cje. UBP310 application induced a significant increase of frequency in both models (B,C). (D) Amplitude mIPSC in Ts2Cje was significantly larger compare to DLM in normal ringer. UBP310 had no effect on mIPSC amplitude recorded in pyramidal cells of CA1 (E,F). In B,C,E,F: black line = individual cell data, red line = all cells mean) (* $p<0.05$; ** $p<0.001$; Student t-test).

sIPSC frequency was larger in Ts2Cje

In CA1 pyramidal cells, we monitored the characteristic of the sIPSC, i.e. without AP blockade, under several pharmacological conditions. These experiments were carried out a room temperature and we pooled data from 4 different sets of experiments to have a more representative picture (DLM $n=52$ and Ts2Cje= 58). As it happened with mIPSCs, the frequency of spontaneous events was significantly higher in Ts2Cje than in DLM (11.25 ± 0.4 vs 8.54 ± 0.3 Hz; $p=3.10^{-6}$; figure 33). We also observed that the average amplitude of sIPSC was significantly smaller in Ts2Cje (46.7 ± 2.2 vs 55.8 ± 3.1 pA; $p=0.01$).

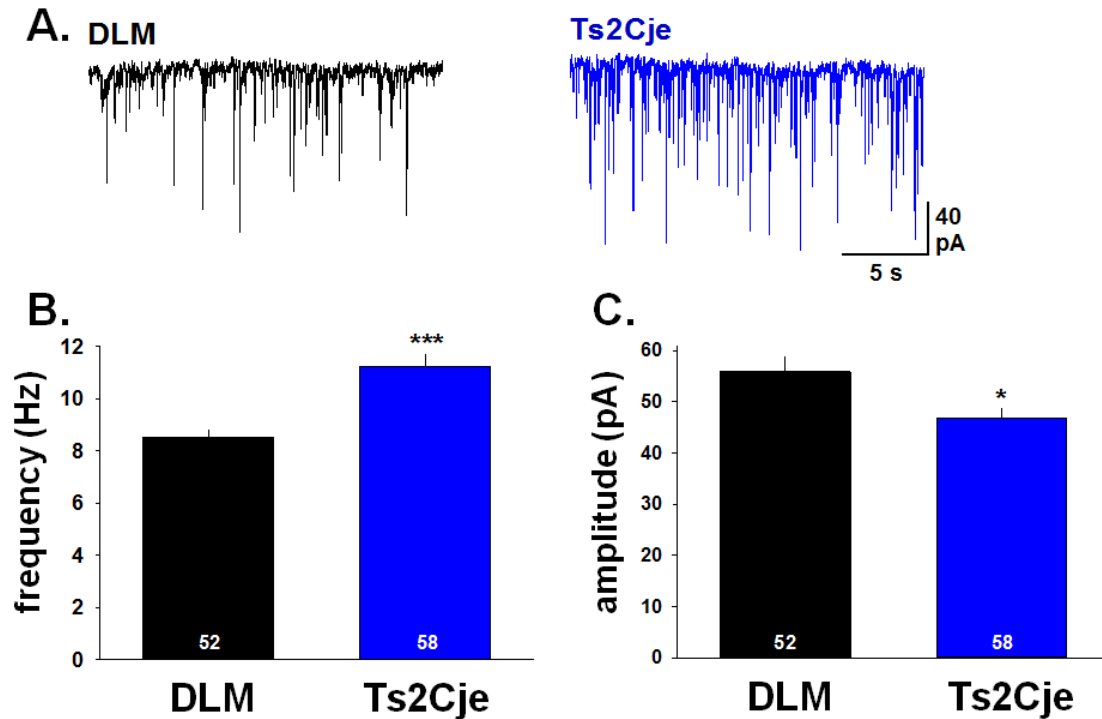


Figure 33: sIPSC were changed in Ts2Cje CA1 pyramidal cells. (A) In control conditions, sIPSC frequency was significantly higher in Ts2Cje. (B) Amplitude of sIPSC was smaller (* $p < 0.05$; *** $p < 0.0001$; Student t-test).

Then we pharmacologically blocked GluK1-KARs using UBP310 at 10 μ M. This antagonist significantly enhanced frequency in DLM (control: 10 ± 0.5 Hz, UBP310: 11.8 ± 0.6 Hz, $p = 0.003$) and in Ts2Cje (control: 12.3 ± 0.7 Hz, UBP310: 13.7 ± 0.6 Hz, $p = 0.02$) (figure 34). Frequency was equally increased in both models (DLM: $+20.2 \pm 5.9\%$, Ts2Cje: $+14.8 \pm 5.1\%$, $p = 0.5$). UBP310 had the same effect on sIPSC amplitude in DLM (control: 47.5 ± 4.3 pA, UBP310: 61.7 ± 4.6 pA, $n = 16$, $p = 0.001$) and Ts2Cje (control: 37.2 ± 2.6 pA, UBP310: 47.8 ± 3.4 pA, $n = 16$, $p = 0.00003$) (figure 34). The fractional increase in amplitude was similar in DLM and Ts2Cje (DLM: $+35.3 \pm 8.8\%$, Ts2Cje: $+29 \pm 5.1\%$, $p = 0.6$).

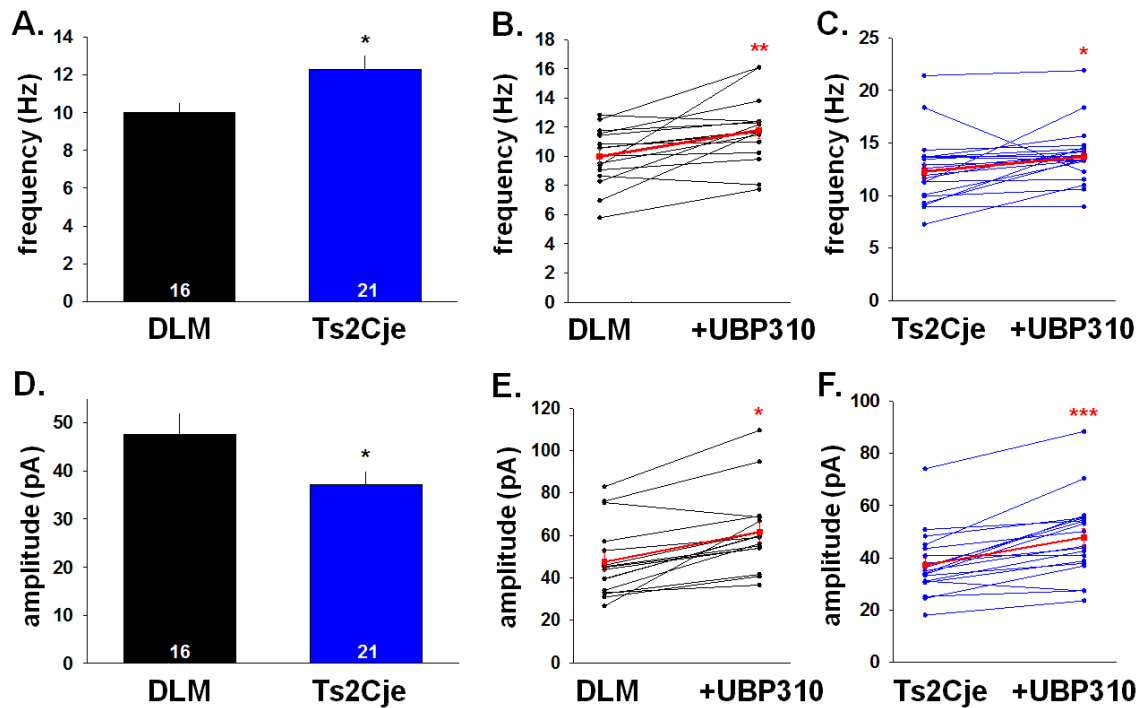


Figure 34: In CA1 pyramidal cells GluK1 blockade increased sIPSC frequency and amplitude. In control conditions, sIPSC frequency was significantly larger in Ts2Cje (A) whereas amplitude (D) was smaller. UBP310 perfusion enhanced frequency (B,C) and amplitude (E,F) in both animal types. In B,C,E,F: black line = individual cell data, red line= all cells mean (* $p < 0.05$; ** $p < 0.001$; *** $p < 0.0001$; Student t-test).

Perfusion of a large spectrum KAR/AMPA antagonists (CNQX $20\mu\text{M}$) also induced a significant increase of sIPSC frequency in DLM (10.5 ± 0.7 Hz; $n=6$; $p=0.002$) and Ts2Cje (13.2 ± 0.9 Hz; $n=8$; $p=0.01$). Effect of CNQX was similar in both models (DLM: $+20.1 \pm 3.7\%$ and Ts2Cje: $+12.8 \pm 4.3\%$; $p=0.24$). However, this experiment did not reveal any significant changes in sIPSC amplitude (figure 35).

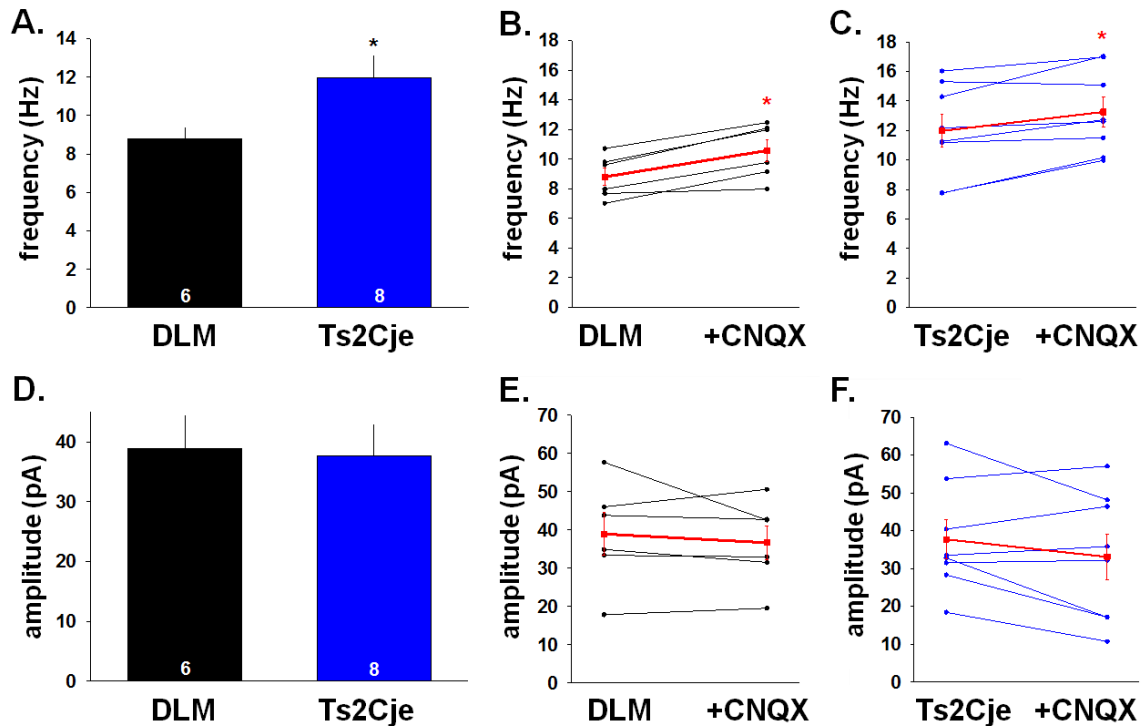


Figure 35: KARs blockade increased sIPSC frequency in CA1 pyramidal cells. In control conditions, sIPSC frequency was increased in Ts2Cje compare to DLM (A) CNQX enhanced frequency in both animal types (B,C). No changes in amplitude were observed in control conditions nor under CNQX. (D,E;F). In B,C,E,F: black line = individual cell data, red line= all cells mean (* $p < 0.05$; Student t-test).

GluK1 activation enhanced sIPSC frequency

ATPA $1\mu\text{M}$ induced a massive increase of sIPSC frequency and amplitude in DLM (frequency: 13.5 ± 0.8 Hz; $p = 4.10^{-8}$; amplitude: 81 ± 6.7 pA; $n = 24$; $p = 0.004$) and Ts2Cje (frequency: 20.4 ± 1.4 Hz; $p = 7.10^{-7}$; amplitude: 90.1 ± 8.4 pA; $n = 23$; $p = 0.0001$). However, the induced increase of sIPSC frequency was significantly greater in Ts2Cje than in DLM ($+126.9 \pm 23.3\%$ vs $+74.7 \pm 10.1\%$; $p = 0.04$). Amplitude was enhanced to the same extent in both types of animal (figure 36).

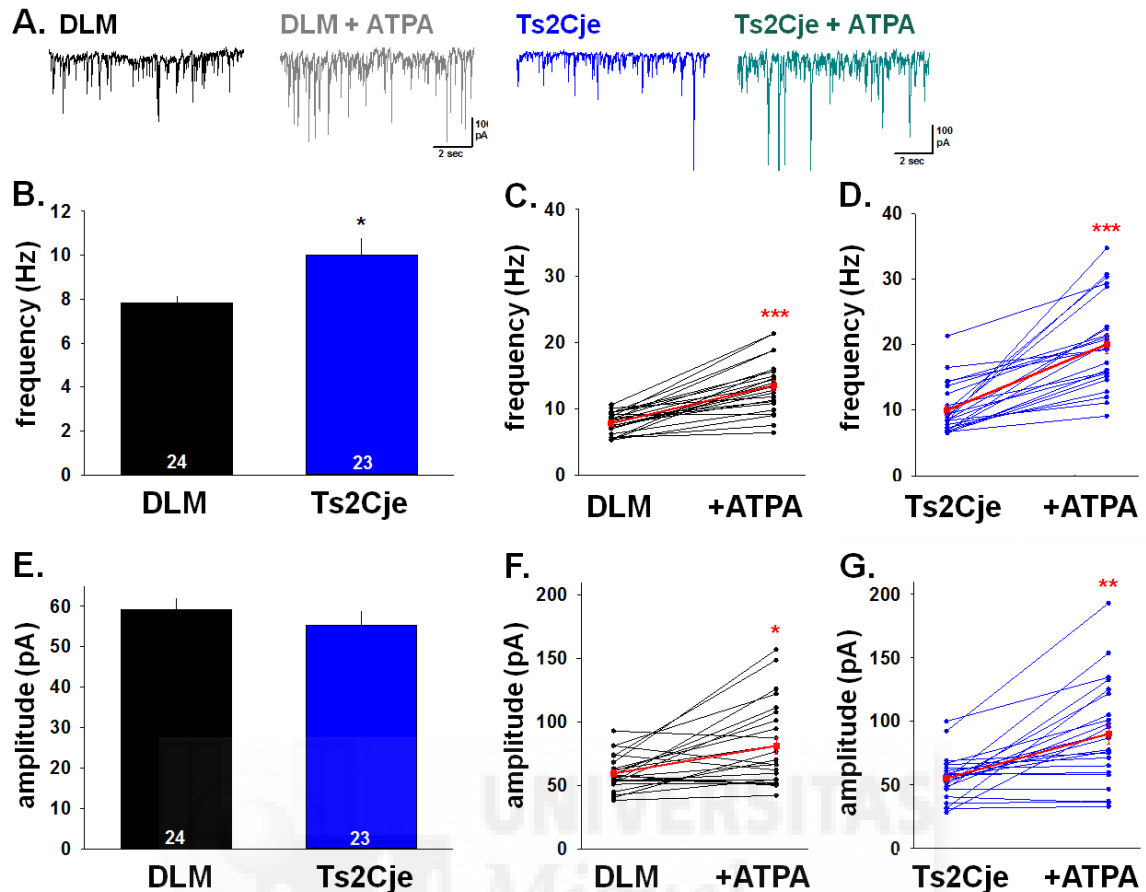


Figure 36: In CA1 pyramidal cells ATPA $1\mu\text{M}$ increased sIPSC frequency and amplitude. (A) In control conditions, sIPSC frequency was larger in Ts2Cje, whereas amplitude was identical to DLM (D). (B,C,E,F) ATPA enhanced frequency and amplitude in DLM and Ts2Cje (significantly more effect in Ts2Cje, $+126.9\pm 23.3\%$ vs $+74.7\pm 10.1\%$; $p=0.04$). In B,C,E,F: black line = individual cell data, red line = all cells mean (* $p<0.05$; ** $p<0.001$ Student t-test).

We also tested the effect of ATPA at concentration activating KARs incorporating other subunits than GluK1 ($3\mu\text{M}$). As in previous experiments, in control conditions, sIPSCs frequency and amplitude were larger in Ts2Cje (frequency: 10.7 ± 0.7 vs 7.5 ± 1.2 Hz; $p=0.02$ / amplitude: 49.9 ± 2.9 vs 38.9 ± 2.2 pA; $p=0.01$) (figure 37). Activation of KARs with ATPA $3\mu\text{M}$ produced significant increase of sIPSC frequency (DLM: 12.8 ± 1.8 Hz; $n=6$; $p=0.009$ and Ts2Cje 18.8 ± 3 Hz; $n=5$; $p=0.03$) and amplitude (DLM: 54.2 ± 4.7 pA; $p=0.02$ and Ts2Cje 73.3 ± 8.2 pA; $p=0.01$). The incremental effect of ATPA $3\mu\text{M}$ on frequency and amplitude was the same in DLM and Ts2Cje.

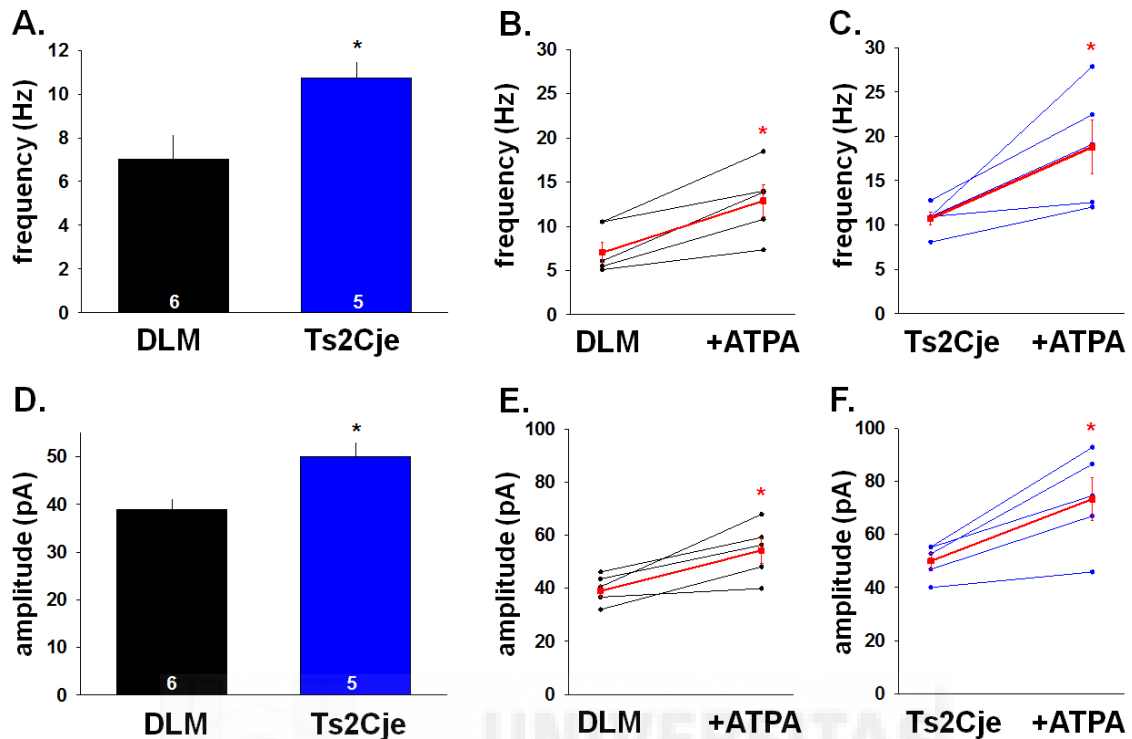


Figure 37: ATPA 3 μ M increased sIPSC frequency and amplitude in CA1 pyramidal cells. In control conditions, sIPSC frequency and amplitude were larger in Ts2Cje compare to DLM (A,D). ATPA enhanced frequency and amplitude in both animal types (B,C,E,F). In B,C,E,F: black line = individual cell data, red line= all cells mean (* $p < 0.05$; Student t-test).

6. Enhanced basal inhibitory synaptic transmission in stratum radiatum interneurons

mIPSC frequency was higher in CA1 SR interneurons in Ts2Cje

In Ts2Cje animals, the mIPSC frequency recorded from stratum radiatum interneurons was larger than in normal animals (7.8 ± 1.1 vs 3.9 ± 1.1 Hz; $p = 0.03$) whereas amplitude was not different (figure 38). Blockade of GluK1-KARs UBP310 had no significant effect on DLM mIPSC frequency or amplitude in DLM ($n = 5$) and Ts2Cje ($n = 7$).

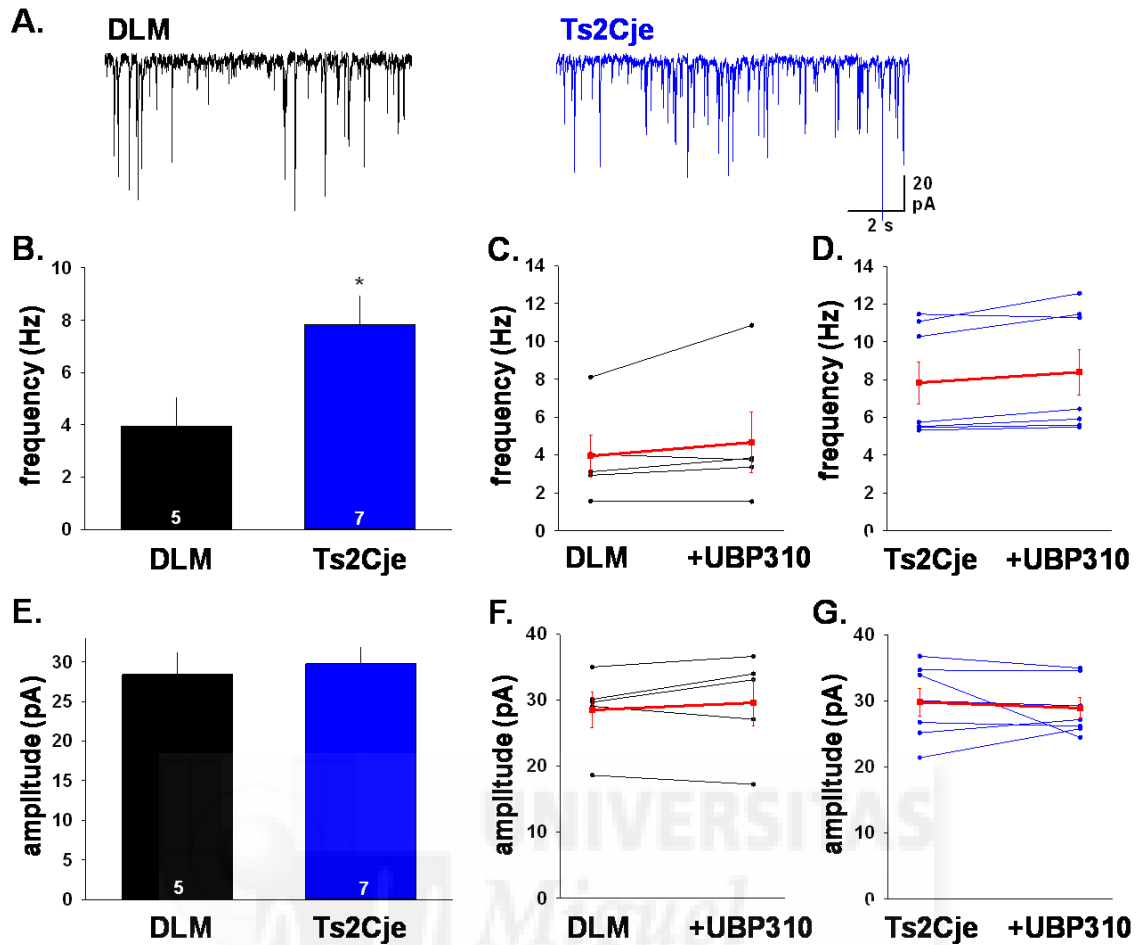


Figure 38: (A) Example of mIPSC recordings in SR interneurons. (B) In control conditions, mIPSC frequency was larger in Ts2Cje. (E) No significant changes were observed in amplitude and after UBP310 perfusion (C,D,F,G). In C,D,F,G: black line = individual cell data, red line = all cells mean (* $p < 0.05$; Student t-test).

sIPSC frequency was larger in SR interneurons from Ts2Cje

Recording sIPSC in interneurons of SR, we observed a significant larger frequency (13.6 ± 1.2 vs 7.3 ± 1.4 Hz; $p = 0.001$) and amplitude (28.4 ± 3 vs 19 ± 1.6 pA; $p = 0.04$) in Ts2Cje compare to DLM mice (figure 39). Perfusion of CNQX did not affect sIPSC frequency or amplitude of these events (DLM $n = 4$, Ts2Cje $n = 6$). In another set of experiments we used a potassium-gluconate based internal solution to try to reduce sIPSC frequency to discard smallest events, decrease frequency and be able to get a better resolution of peak amplitudes. Here we also observed a larger sIPSC frequency (1.43 ± 0.2 vs 3.1 ± 0.4 Hz; $p = 0.002$) in interneurons of SR in Ts2Cje (figure 40) but amplitude was similar (DLM: 7.8 ± 0.4 pA; Ts2Cje: 8 ± 0.5 pA; $p = 0.9$).

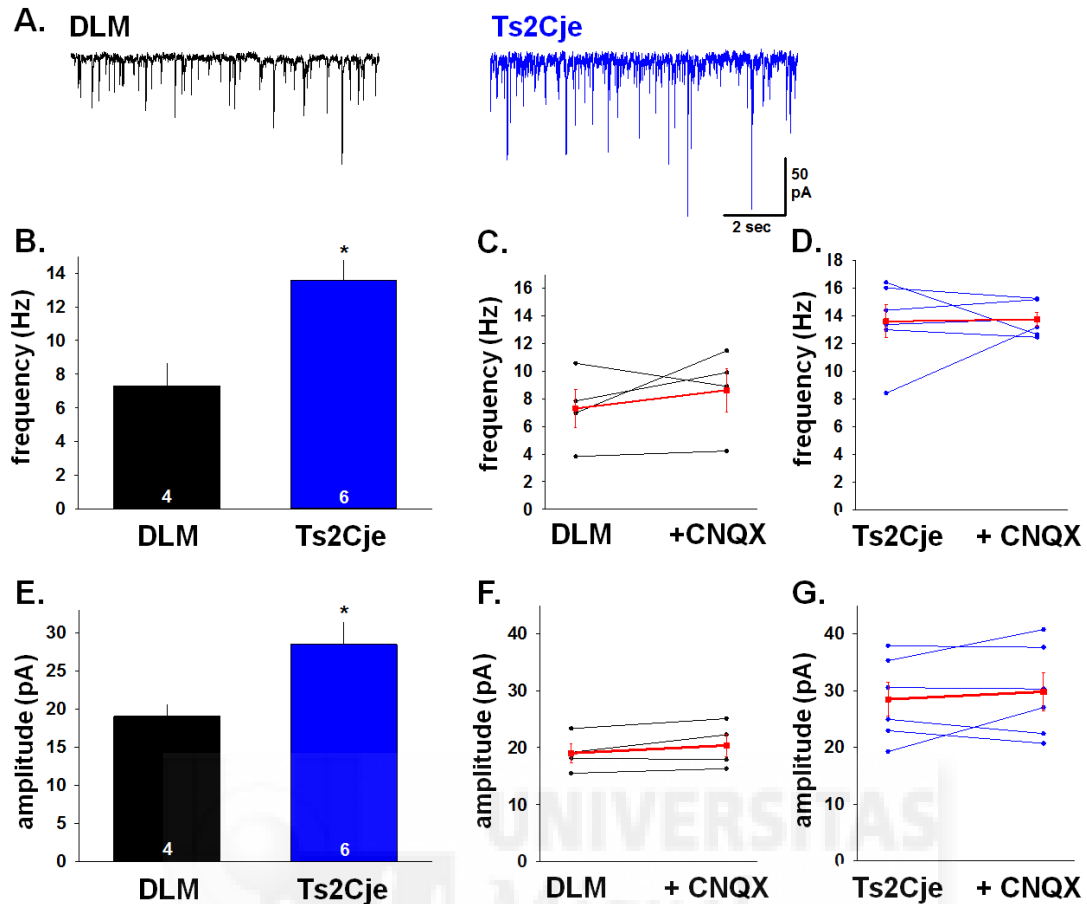


Figure 39: (A) Example traces of sIPSC in interneurons. (B,E) In SR interneurons sIPSC frequency and amplitude were larger in Ts2Cje. (C,D,F,G) Perfusion of CNQX did not induce changes on sIPSC parameters. In C,D,F,G: black line = individual cell data, red line= all cells mean (* $p < 0.05$; Student t-test).

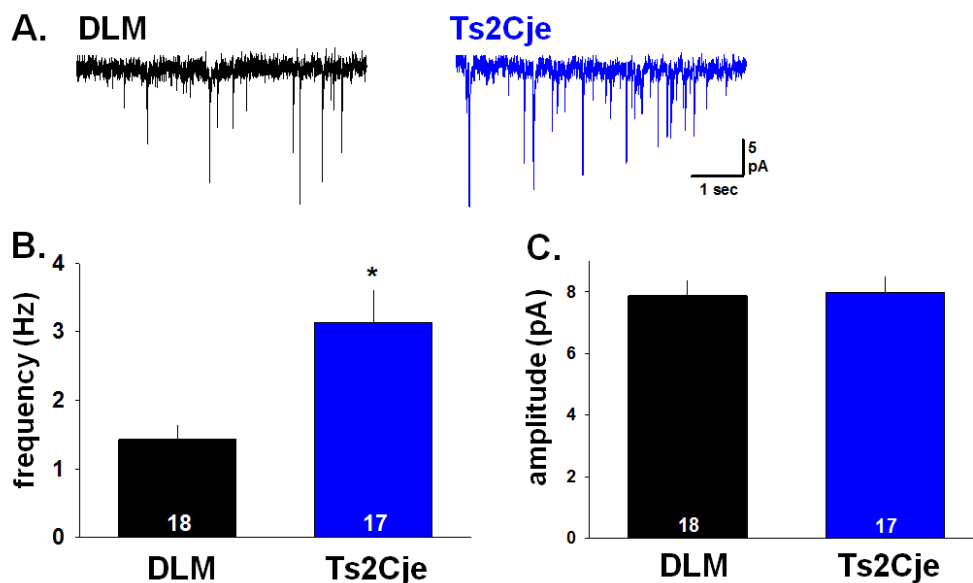


Figure 40: (A) Traces examples recording with a K^+ -gluconate-based internal solution (B) sIPSC frequency in interneurons of SR was larger in Ts2Cje. (C) No significant changes in amplitude were observed when K-Gluconate was used as internal solution (* $p < 0.05$; Student t-test).

7. Augmented basal inhibitory synaptic transmission in Stratum Oriens interneurons

mIPSC frequency was higher in SO interneurons of Ts2Cje

In control conditions, mIPSC frequency recorded from interneurons placed in stratum oriens was higher in Ts2Cje (11.5 ± 1.5 Hz) comparing to DLM (6.5 ± 1.2 Hz; $p=0.02$), whereas amplitude of the events was not (DLM: 23.7 ± 2.6 pA; Ts2Cje: 21 ± 2.7 pA; $p=0.5$). Blockade of GluK1-KARs with UBP310 did not induced significant changes in mIPSC frequency and amplitude neither in DLM nor in Ts2Cje. Although clear augmentation of frequency was observed in a few neurons, when pooling all recorded cells there was a no significant changes (figure 41).

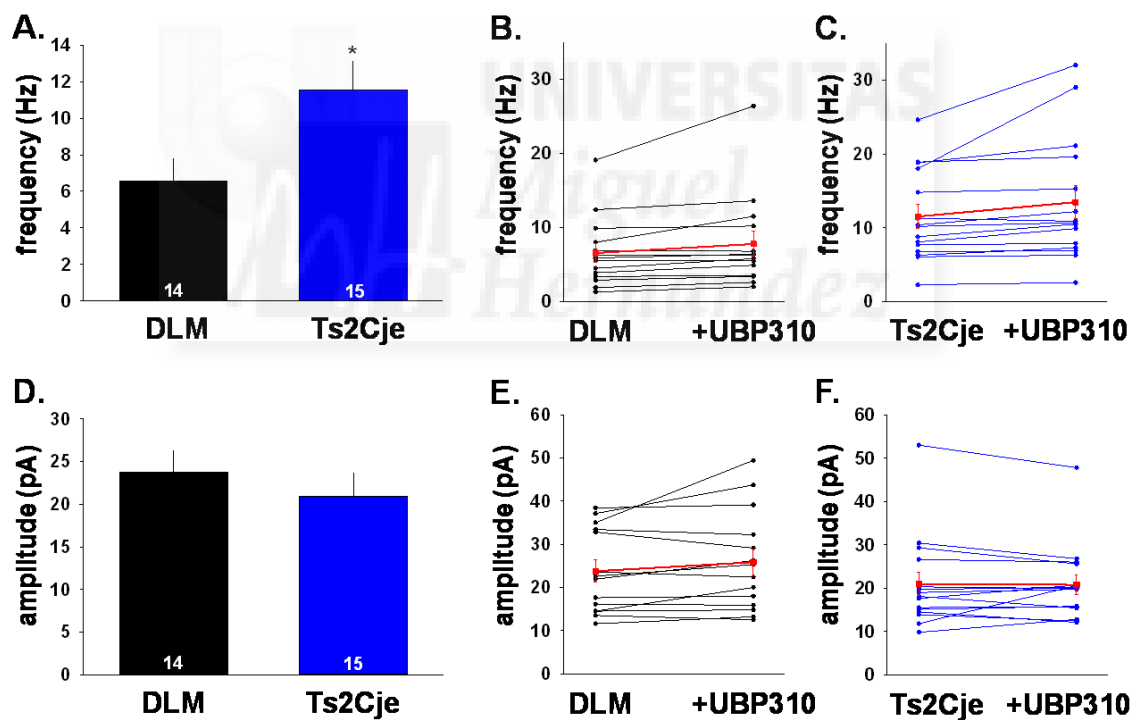


Figure 41: (A) mIPSC frequency was larger in SO interneurons of Ts2Cje. (B,C) UBP310 perfusion had no clear effect on mIPSC frequency in DLM and Ts2Cje, this effect was similar in both models. Amplitude did not changed with genotype nor UBP310 perfusion (D,E,F) (* $p < 0.05$; Student t-test).

In contrast, frequency and amplitude of sIPSC in SO interneurons were similar in Ts2Cje and DLM (figure 42). Perfusion of ACET induced a significant increase of

frequency in Ts2Cje (13.5 ± 0.8 Hz vs 9.1 ± 0.9 Hz; $p=0.0001$) but not in DLM (12.9 ± 2.3 Hz vs 9.7 ± 1.3 Hz; $p=0.02$). The amplitude of events was not affected by ACET.

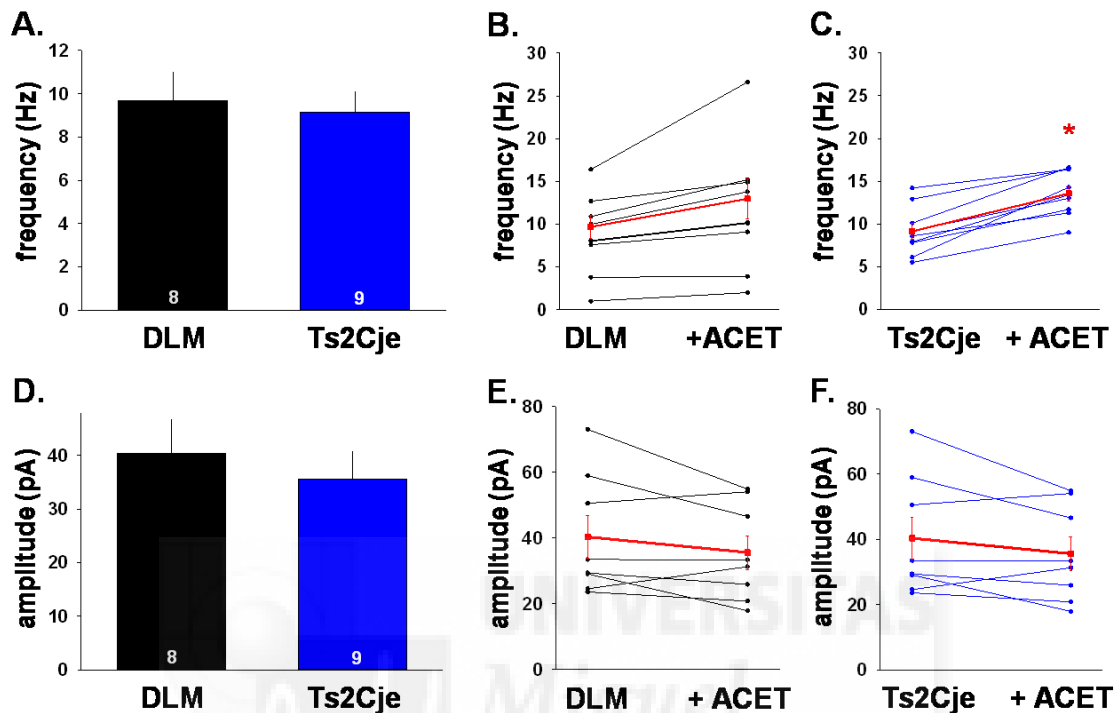


Figure 42: Frequency (A) and amplitude (D) of sIPSC recorded in SO interneurons were similar in DLM and Ts2Cje. ACET perfusion effect on sIPSC frequency in DLM (B) and Ts2Cje (C). Amplitude did not change during ACET perfusion (D,E,F). In B,C,E,F: black line = individual cell data, red line = all cells mean ($*p<0.01$; Student t-test).

In these interneurons ATPA $1\mu\text{M}$ significantly increased both frequency and amplitude of sIPSC in DLM (frequency: 20.3 ± 2.1 Hz vs 9.3 ± 1 Hz; +118%; $p=6.10^{-5}$; amplitude: 52.2 ± 6.6 vs 38.2 ± 16.2 pA; $p=0.05$) and Ts2Cje (19.7 ± 1.7 Hz vs 10 ± 1.6 Hz; +97%; $p=9.10^{-5}$; amplitude: 52.2 ± 8.3 vs 35.2 ± 3.3 pA; $p=0.01$). This effect, however, was similar between models (Figure 42).

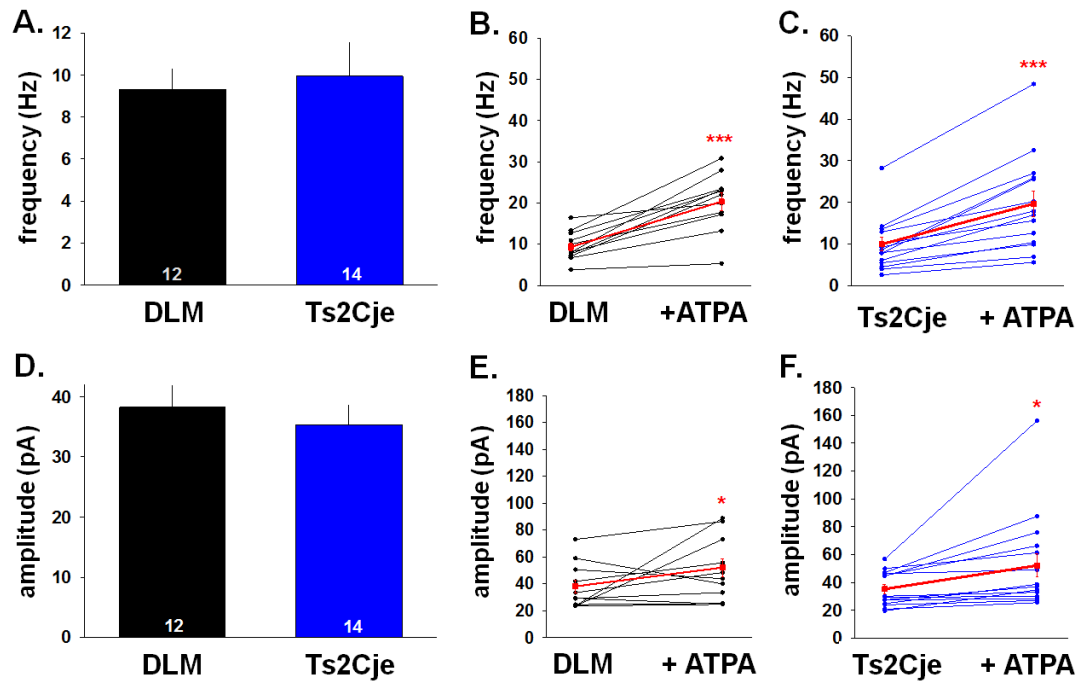


Figure 43: Frequency (A) and amplitude (D) of sIPSC recorded in SO interneurons were similar in DLM and Ts2Cje. ATPA perfusion increased significantly sIPSC frequency and amplitude in DLM (B,E) and Ts2Cje (C,F), this effect was similar in both models. In B;C;E;F: black line = individual cell data, red line = all cells mean (* $p < 0.05$; ** $p < 0.0001$; $p < 0.0001$; Student t-test).

8. Impaired evoked inhibitory synaptic transmission

After having studied basal activity, the aim of the following experiments was to compare dynamic inhibitory synaptic transmission between DLM and Ts2Cje. First a pyramidal cell or an interneuron in the area CA1 was patched and kept at -70 mV and AMPARs/NMDARs were blocked to isolate GABAergic events. Stimulating electrode was placed close to the cell of interest and paired-pulse stimulation (40 ms interval) was applied to induce short term synaptic plasticity of evoked inhibitory response which was assessed by measuring the PPR. The influence of GluK1-KARs on these eIPSCs was evaluated by activating them with ATPA 1 μ M.

eIPSC PPD is decreased in CA1 pyramidal cells

In control conditions, we first observed that eIPSC PPR was significantly larger in Ts2Cje CA1 pyramidal cells compared to DLM (0.79 ± 0.02 vs 0.70 ± 0.02 ; $p = 0.01$) (figure 44). Perfusion of ATPA 1 μ M significantly decreased eIPSC amplitude in DLM (-30.6 ± 4.6 %, $p = 8.10^{-5}$) and Ts2Cje (-24.3 ± 4.4 %, $p = 2.10^{-5}$) (figure 45). However, there was no difference on the effect of ATPA on eIPSC amplitude between DLM and

Ts2Cje mice. Applying paired-pulse stimulation, we observed that ATPA increased PPR, i.e. reduced PPD (DLM: 0.80 ± 0.06 ; $p=0.03$; Ts2Cje: 0.87 ± 0.03 ; $p=0.002$) (figure 45). The effect of ATPA on PPR was similar in DLM and Ts2Cje.

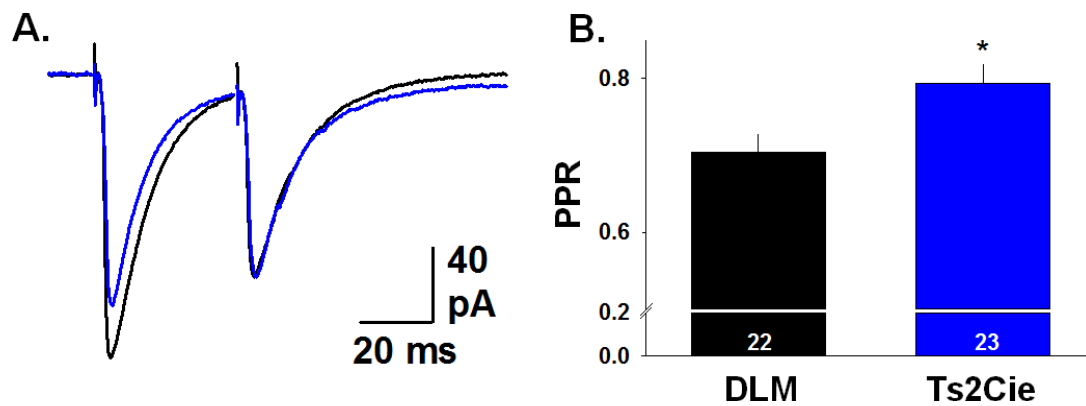


Figure 44: PPR of eIPSCs was augmented in Ts2Cje CA1 pyramidal cell. (A) Superimposed and normalized eIPSC recordings example from a pyramidal cell in DLM (black line) and Ts2Cje (blue line). Ts2Cje trace was normalized on the DLM second peak. (B) eIPSC PPR was significantly increase in Ts2Cje ($*p < 0.05$; Student t-test).

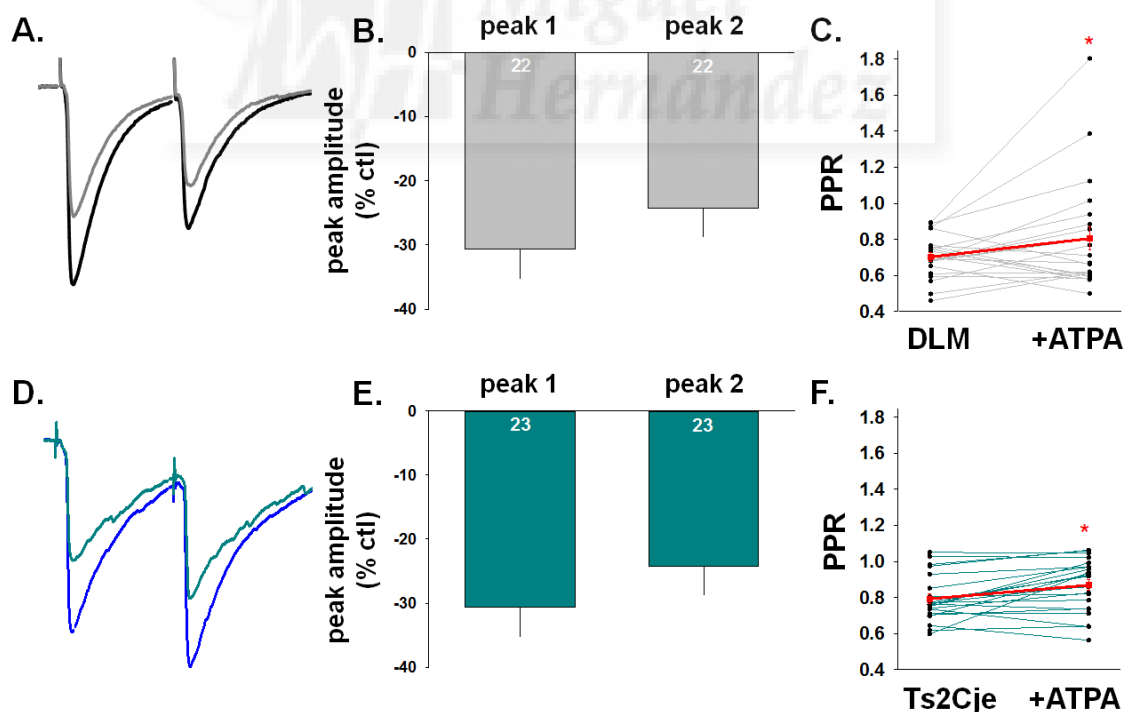


Figure 45: ATPA $1 \mu\text{M}$ decreased eIPSC amplitude and augmented PPR in Ts2Cje CA1 pyramidal cells. (A, D) Superposed eIPSC recordings from CA1 pyramidal cells in DLM (control: black line; ATPA: gray line) and Ts2Cje (control: blue line; ATPA: cyan line). Effect of ATPA on eIPSC amplitude in DLM (B) and Ts2Cje (E). ATPA perfusion induced an increase of PPR in DLM (C) and Ts2Cje (F) ($*p < 0.05$; Student t-test).

eIPSC PPR is abolished in Stratum Radiatum interneurons of Ts2Cje

In control conditions, we first observed that eIPSC PPR was significantly augmented in Ts2Cje CA1 pyramidal cell (1.08 ± 0.08 vs 0.85 ± 0.04 ; $p=0.01$) compared to DLM (figure 46). Perfusion of ATPA $1 \mu\text{M}$ decreased very significantly eIPSC amplitude in DLM (-39.3 ± 5.7 , $p=3.10^{-4}$) and Ts2Cje (-38.7 ± 6.2 , $p=1.10^{-4}$). Here again there was no difference on the effect of ATPA on eIPSC amplitude between DLM and Ts2Cje. ATPA perfusion did not affect PPR (DLM: 0.90 ± 0.07 ; $p=0.4$ / Ts2Cje: 1.2 ± 0.06 ; $p=0.19$) (figure 47).

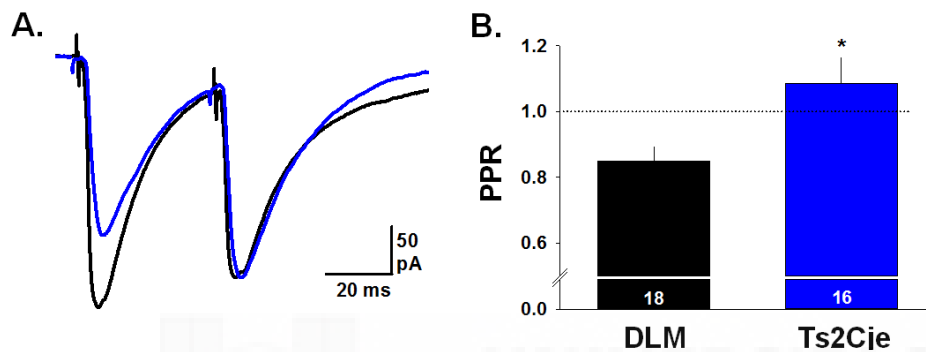


Figure 46: Inhibitory PPR was augmented in Ts2Cje SR interneurons in CA1. (A) Superposed and normalized eIPSC recordings example from a SR interneuron in DLM (black line) and Ts2Cje (blue line). Ts2Cje trace was normalized on the DLM second peak. (B) eIPSC PPR was significantly increase in Ts2Cje (* $p<0.05$; Student t-test).

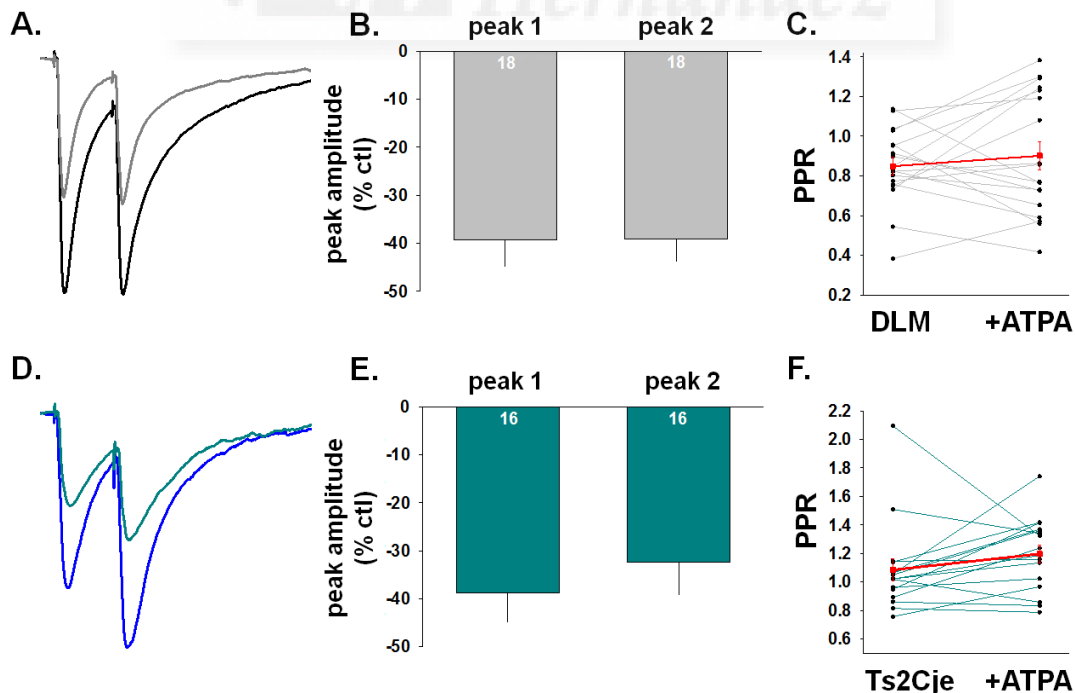


Figure 47: In SR interneurons ATPA $1 \mu\text{M}$ decreased eIPSC amplitude and did not affect PPR. (A,D) Superposed eIPSC recordings example from SR interneuron in DLM (control: black line; ATPA: gray line) and Ts2Cje (control: blue line; ATPA: cyan line). Effect of ATPA on eIPSC amplitude in (B) DLM and (E) Ts2Cje. ATPA did not change DLM (C) or Ts2Cje (F) PPR.

PPR of eIPSCs remains unchanged in Stratum Oriens interneurons

In control conditions, DLM and Ts2Cje eIPSC PPRs were not different (0.82 ± 0.06 and 0.77 ± 0.03 ; $p=0.45$) (figure 48). ATPA $1 \mu\text{M}$ diminished very significantly eIPSC amplitude in DLM ($-33.2 \pm 5\%$, $p=0.006$) and Ts2Cje ($-41.8 \pm 6.8\%$, $p=1.10^{-4}$) (figure 58). Like for other cellular types there was no difference on the effect of ATPA on eIPSC amplitude between DLM and Ts2Cje. ATPA did not affect PPR (DLM: 0.77 ± 0.05 ; $p=0.77$ / Ts2Cje: 0.74 ± 0.05 ; $p=0.58$) (figure 49).

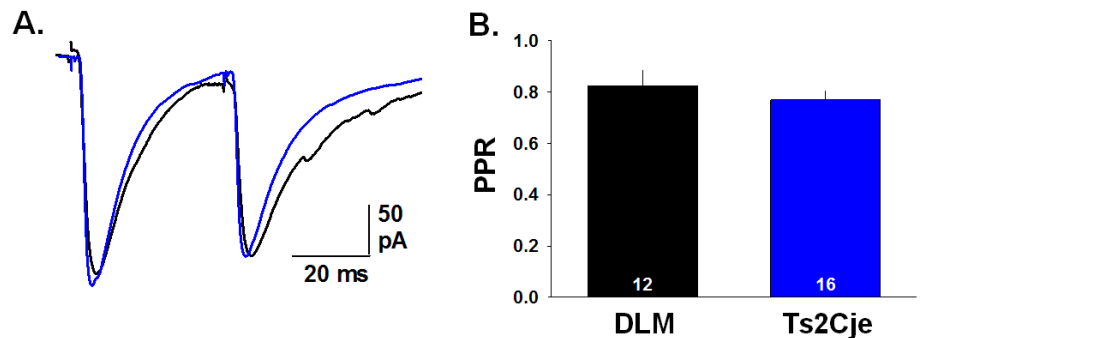


Figure 48: In SO interneurons, PPR was similar between DLM and Ts2Cje. (A) Superposed and normalized eIPSC recordings example from SO interneuron in DLM (black line) and Ts2Cje (blue line). Ts2Cje trace was normalized on the DLM second peak. (B) eIPSC PPR was significantly increase in Ts2Cje ($*p < 0.05$; Student t-test).

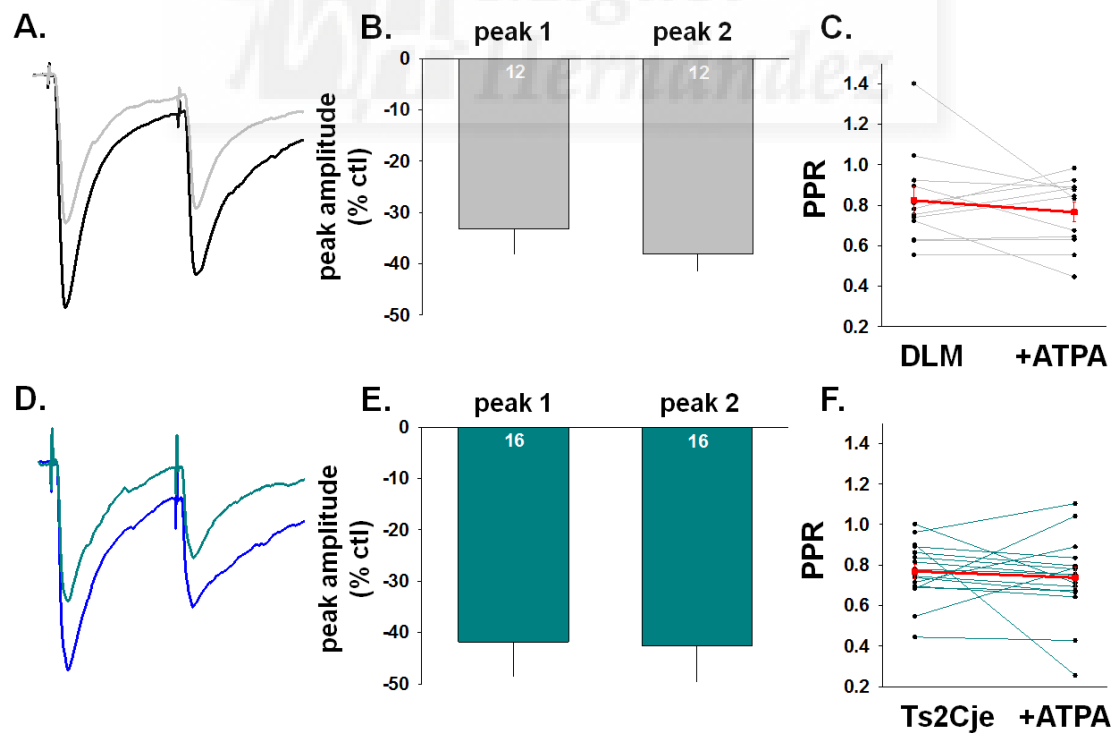


Figure 49: In SO interneurons ATPA $1 \mu\text{M}$ decreased eIPSC amplitude and did not affect PPR. (A, D) Superposed eIPSC recordings example from SO interneuron in DLM (control: black line; ATPA: gray line) and Ts2Cje (control: blue line; ATPA: cyan line). Effect of ATPA on eIPSC amplitude in DLM (B) and Ts2Cje (E). ATPA perfusion did not change PPR in DLM (C) nor in Ts2Cje (F).

9. Altered synaptic plasticity in Ts2Cje hippocampus

LTP is impaired in area CA1 of the hippocampus of Ts2Cje

Study of LTP mechanisms should provide insights into the cellular and molecular basis of learning and memory. It has been established that in hippocampus CA1, LTP induction requires the transient activation of the NMDARs system (Collingridge et al., 1983). During basal low-frequency transmission, activation of this system is prevented by synaptic inhibition (GABA) which hyperpolarizes neurons into a region where NMDAR-operated channels are substantially blocked by Mg^{2+} (Collingridge et al., 1988). But during high-frequency transmission, a sufficient depolarization of the postsynaptic membrane removes Mg^{2+} block, activates NMDARs and thereby triggers the induction of LTP. The consequence of NMDARs activation is a persistent increase of AMPARs at the postsynapse that produces an increase of fEPSP amplitude. It has been reported that this depolarization is attained because during high-frequency transmission GABA depresses its own release by an action on $GABA_B$ autoreceptors, which permits sufficient NMDARs activation for LTP induction (Davies et al., 1991). LTP mechanisms have been studied in DS model to try to link deficits in learning and memory to a molecular/cellular alteration (Dierssen, 2012). In this study we also wanted to get more information about Ts2Cje CA1 hippocampal synaptic plasticity in a larger scale.

We started the characterization looking at the CA1 input-output relationship doing a ramp of stimulation intensity and plotting fEPSP amplitude and fiber volley amplitude on the same graph (figure 50). For each slice we fitted the different points to a linear regression and calculated the slope of this line. To compare both animal types, the mean of all slopes was calculated within each group. We did not observe any significant differences between DLM (0.43 ± 0.07 , $n=10$) and Ts2Cje (0.32 ± 0.06 , $n=14$), although Ts2Cje slope was slightly smaller than DLM slope without reaching statistical significance ($p=0.25$).

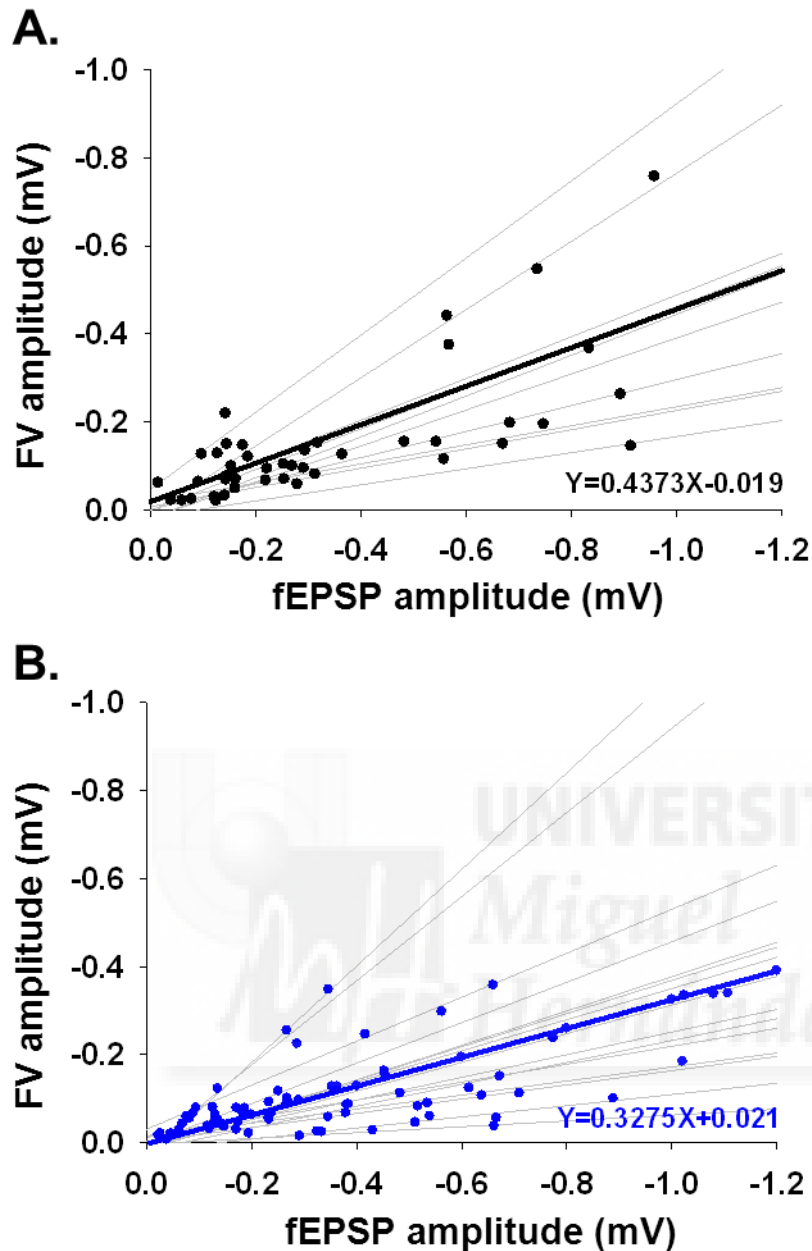


Figure 50: Input-output relationship was not changed in Ts2Cje. Plot of the fEPSP amplitude function of fiber volley amplitude in DLM (A) and Ts2Cje (B). Fine grey line = linear regression fit on one slice input-output values; black and blue thick lines are the respective linear regression means for DLM (A) and Ts2Cje (B), their respective equation is precised in the bottom right corner.

Then we studied LTP in CA1 stimulating Schaffer Collaterals pathway and recorded field responses in stratum radiatum. In the first set of experiments LTP was induced using a classical and robust protocol composed by 3 trains (1 sec at 100Hz) at a 10 sec interval, and with a test intensity producing 50% of the maximal fEPSP amplitude. In control conditions (normal aCSF), LTP induced in Ts2Cje was significantly smaller

than in DLM mice (Ts2Cje +33±2%, DLM: +51±3%, $p=0.0002$) (figure 51). We previously observed that perfusion of a GluK1-KARs selective agonist (ATPA 1 μ M) significantly decreased evoked inhibitory transmission (figure 45, 47 and 49). Additionally it has been reported that GABA_A antagonism can restore deficient LTP levels in Ts65Dn (Fernandez et al., 2007; Kleschevnikov et al., 2004). So we thought that if LTP defect observed in Ts2Cje was due to the previously described excess of inhibition, perfusion of ATPA could improve LTP induction in Ts2Cje hippocampus.

The effect of 1 μ M ATPA was first observed on the basal response (fEPSP before LTP induction). After 10 min, ATPA decreased fEPSP amplitude in DLM (-33±3%) and Ts2Cje (-20±2%) (figure 52). The effect of ATPA was significantly smaller in Ts2Cje ($p=1.10^{-5}$). Once the fEPSP was stable, a baseline of 10 min was taken prior to HFS LTP induction. Under ATPA, the magnitude of LTP induced in DLM was not different from the one observed in control conditions (+44±2%) whereas in Ts2Cje ATPA significantly increased LTP magnitude compared to control conditions (+46±3%; $p=0.002$) (figure 53).

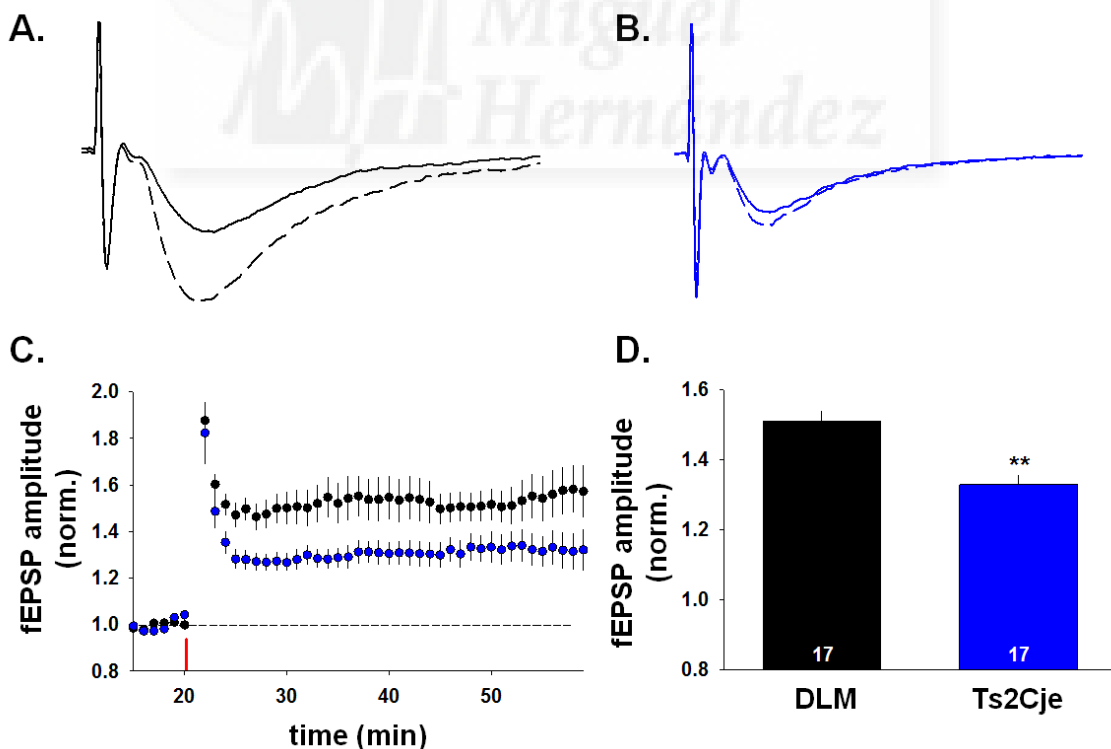


Figure 51: LTP was reduced in Ts2Cje. fEPSP traces example in DLM (A) and Ts2Cje (B); solid line = basal fEPSP and dashed line = potentiated fEPSP. (C) Time course of normalized fEPSP amplitude during LTP experiment (vertical red line = HFS (3x1sec at 100Hz)). (D) Quantification of fEPSP amplitudes 30 min after HFS, in Ts2Cje fEPSP amplitude LTP was significantly reduced (** $p<0.001$; Student t-test).

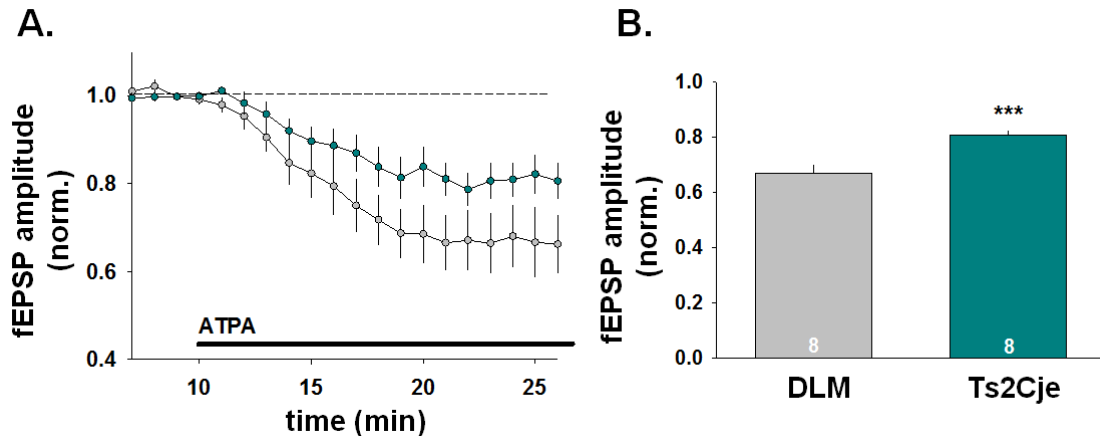


Figure 52: ATPA 1µM diminished fEPSP amplitude. (A) Normalized fEPSP amplitude during ATPA perfusion (at 10min). After 15 min fEPSP amplitude was decreased in DLM and Ts2Cje, this effect was smaller in Ts2Cje (B) (***) $p < 0.0001$; Student t-test).

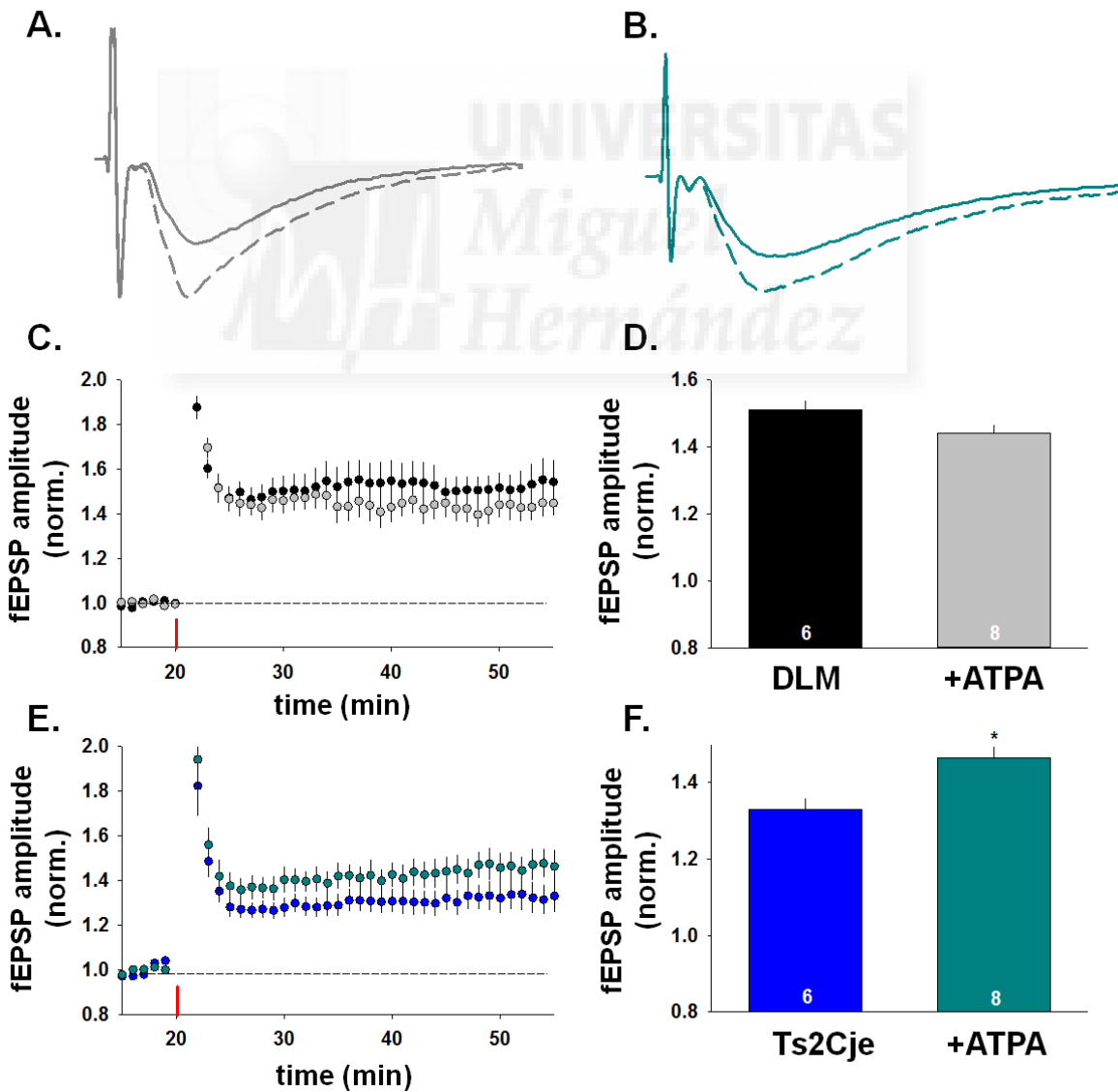


Figure 53: ATPA 1 μ M restored LTP levels in Ts2Cje. Traces examples of fEPSP in DLM (A) and Ts2Cje (B) in presence of ATPA; solid line = basal fEPSP and dashed line = potentiated fEPSP). Time course of normalized fEPSP amplitude during LTP experiment in (C) DLM and (E) Ts2Cje (vertical red line = HFS (3x1sec at 100 Hz)). (D) In DLM ATPA did not induced changes in LTP levels, but (F) in Ts2Cje fEPSP amplitude was significantly increased under ATPA (black = DLM with normal ringer, gray = DLM with ATPA added ringer, blue = Ts2Cje with normal ringer, cyan = Ts2Cje with ATPA added ringer) (* $p < 0.05$; Student t-test).

Depotentialization is altered in area CA1 of the hippocampus of Ts2Cje

LTD (long-term depression) is the inverse of LTP, namely a persistent decrease in AMPAR-mediated synaptic transmission. In adult animals, *de novo* LTD is difficult to induce. Therefore, we started by potentiating synaptic transmission with a classical HFS-LTP induction protocol and subsequently apply the LTD protocol. This process is generally referred to as “depotentialization” (Bortolotto et al., 2011) rather than LTD. Here we used a low frequency stimulation (LFS, test intensity during 15 min at 1Hz) to depotentialize a previously HFS-potentiated response. For this experiment we followed a LTP induction stimulation protocol of just 1 train of stimuli (1 second at 100Hz at test intensity) (Bortolotto et al 2011). Using this HFS protocol fEPSP was potentiated by $+35 \pm 2\%$ in DLM and by $+21 \pm 2\%$ in Ts2Cje (figure 54). Here again LTP magnitude was significantly smaller in Ts2Cje compare to DLM ($p = 5.10^{-6}$). Thirty minutes after LTP induction, depotentialization protocol was run for 15 min and depression evaluated 30 min after. In DLM, fEPSP amplitude was decreased by $-9.03 \pm 2\%$ whereas it was not changed in Ts2Cje ($-1.09 \pm 2\%$) (figure 54). However, activation of GluK1-containing receptors (ATPA 1 μ M) did not affect depotentialization in DLM ($-8 \pm 3\%$) but significantly increased it in Ts2Cje ($-17 \pm 2\%$, $p = 7.10^{-5}$) (figure 55).

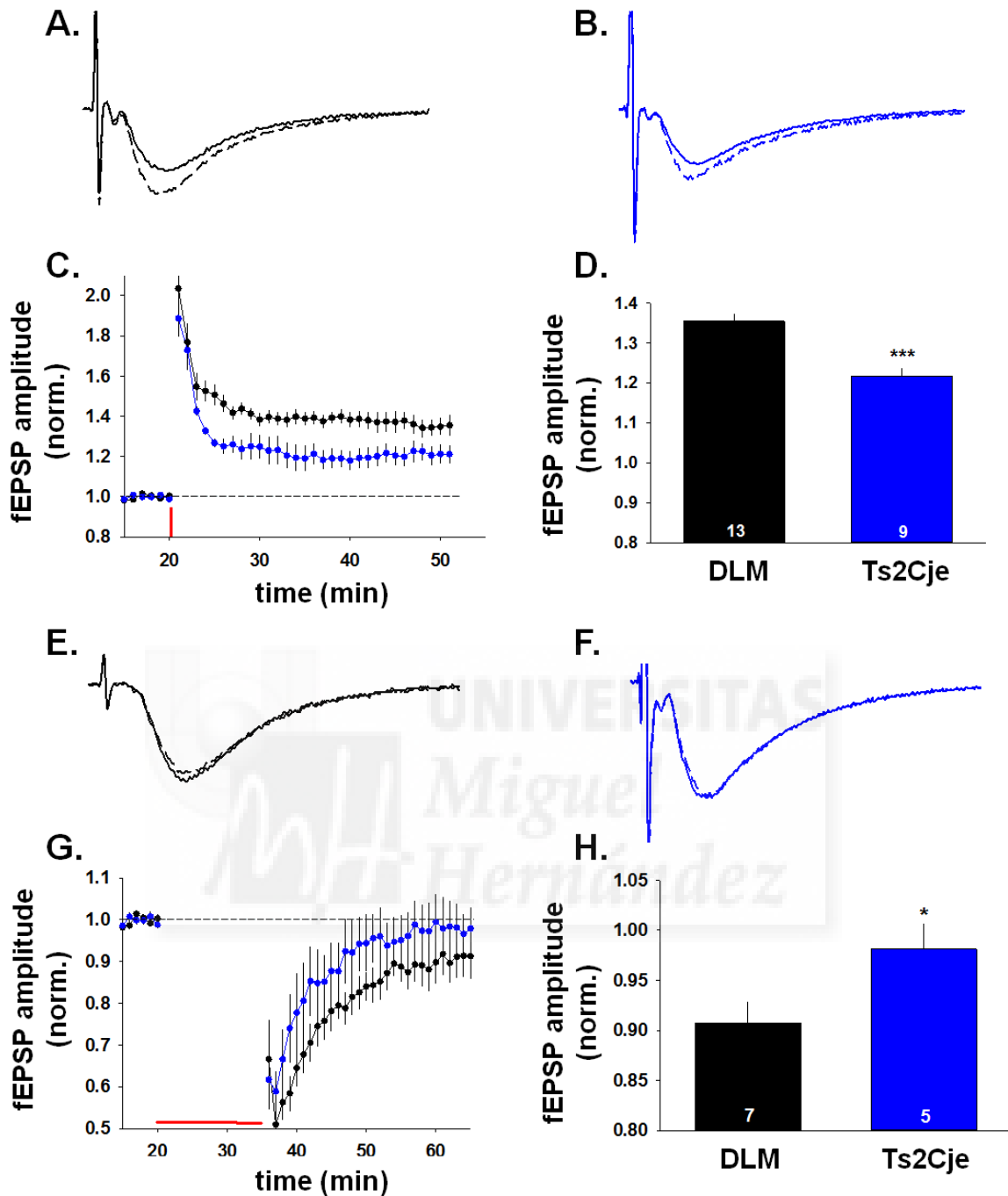


Figure 54: LTP and Depotentiation were impaired in Ts2CJe. fEPSP traces example in DLM (A/E) and Ts2CJe (B/F); solid line = basal fEPSP and dashed line = potentiated fEPSP). (C/G) Time course of normalized fEPSP amplitude during (C) LTP experiment (vertical red line = HFS (1x1sec at 100Hz)) and (G) depotentiation experiment (horizontal red line = LFS (15min at 1Hz)). (D) Quantification of fEPSP amplitudes 30 min after HFS, in Ts2CJe fEPSP amplitude LTP was significantly reduced. (H) Quantification of fEPSP amplitudes 30 min after LFS, in Ts2CJe depotentiation was significantly reduced compare to DLM (* $p < 0.05$, *** $p < 0.0001$; Student t-test).

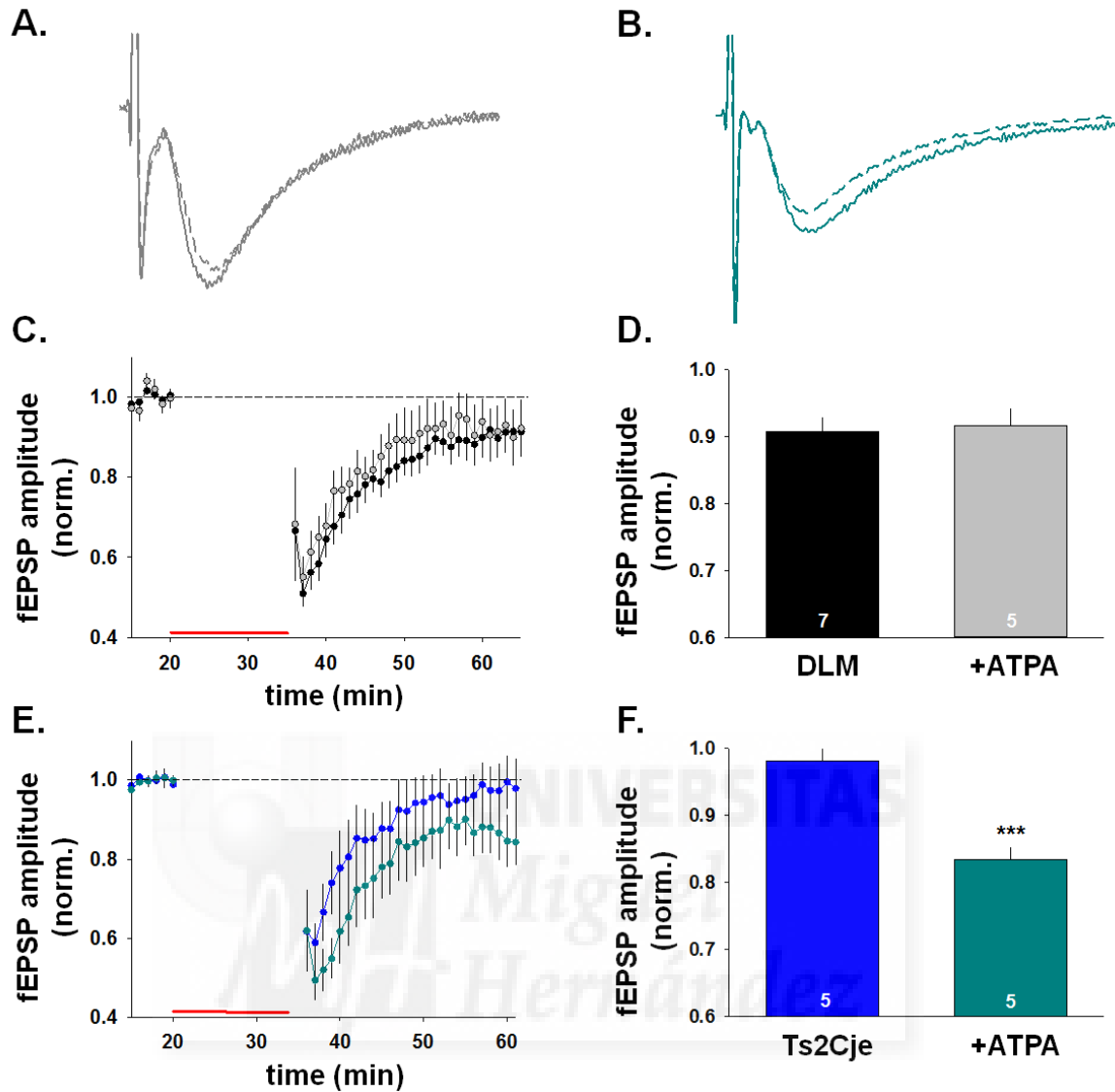


Figure 55: ATPA 1 μ M increased depotentiation levels in Ts2Cje. Traces examples of fEPSP in DLM (A) and Ts2Cje (B) in presence of ATPA; solid line = basal fEPSP and dashed line = depotentiated fEPSP). Time course of normalized fEPSP amplitude during depotentiation experiment in (C) DLM and (E) Ts2Cje (horizontal red line = LFS (15min, 1Hz)). (D) In DLM ATPA did not induced changes in depotentiation levels, but (F) in Ts2Cje fEPSP amplitude was significantly decreased under ATPA after depotentiation (black = DLM with normal ringer, gray = DLM with ATPA added ringer, blue = Ts2Cje with normal ringer, cyan = Ts2Cje with ATPA added ringer) (***)p<0.0001; Student t-test).



DISCUSSION
GENERAL CONCLUSION

Discussion

This work aimed at figuring out a putative link between DS pathophysiology and GluK1 coding gene triplication. Using Ts2Cje DS mouse model, we found an overexpression of GluK1 protein in the brain and confirmed the existence of an over-inhibition in the hippocampus of trisomic mice. Considering our results the supernumerary GluK1-KARs would be more likely located in the somatodendritic/axonal compartment of CA1 interneurons where they increase cell excitability. We also demonstrated a lower capacity for long term plasticity in Ts2Cje. Interestingly, activating GluK1 could counterbalance this deficit, restoring the magnitude of plasticity.

Animal production and genotyping

Two founder couples from The Jackson laboratory produced litters that we successfully genotyped using a duplex quantitative PCR method. This technique constitutes a reliable alternative to other laborious genotyping methods like chromosomal analysis from cultured peripheral lymphocytes or fluorescent in situ hybridization. As described previously, measuring ΔCT we were clearly able to discriminate DLM from Ts2Cje pups within the same litter. Our mean $\Delta\Delta\text{CT}$ of 0.6 was very close to the theoretical value (0.58), indicating adequacy of the procedure. We detected that 34.6% of trisomy transmission in the female germline. This number is comparable from to the 43% exhibited in the female germline in papers describing Ts2Cje model (Villar et al., 2005). Males and females were equally represented in Ts2Cje pups, demonstrating that trisomy affects individuals independently from the gender.

After genotyping we noticed that Ts2Cje animals were smaller and lighter than DLM. This observation has also been reported for Ts65Dn. Moreover other authors observed that after 5 months trisomics animals became obese and the weight difference was not visible any longer (Kola and Hertzog, 1998). Animal facilities staff was able to predict pups genotype by simple eye observation of the animal size and face shape. This “by eye genotyping” could be interesting in order to discard litters free from trisomic animals and then save time and effort. With these results, we confirmed successful breeding of Ts2Cje animals in our facilities and that TaqMan real-time qPCR

genotyping is a reliable and simple method to estimate gene copy number (Liu et al., 2003).

GluK1 mRNA levels are increased in Ts2Cje

We found that the mRNA coding for our protein of interest, GluK1 KAR subunit, was expressed in higher quantity in Ts2Cje mice. It has been demonstrated, however, that it is difficult to predict how changes in DNA copy-number affect gene expression because there is a complex regulation of gene expression that is not only related to the number of gene copies (Lyle et al., 2004). It has also been shown that gene expression is not systematically triplication-sensitive (Prandini et al., 2007). Here RTqPCR carried out from material from different brain structures confirmed that mRNAs coding for triplicated genes are present in higher quantity in Ts2Cje. *App* and *Grik1* mRNA levels were significantly higher in trisomics brain. The 1.5/2-fold increase relative to DLM observed here is comparable to what it has been published previously for Ts2Cje or other DS models (Lyle et al., 2004; Villar et al., 2005). Our analysis of mRNA levels for the other KARs subunits, carried out from cerebellum samples, did not detect any significant change in their levels. Therefore, the increase of gene copy-number for one subunit (GluK1) does not influence levels of transcription of the others.

From these experiments, we can conclude that *Grik1* mRNA levels are significantly increased in Ts2Cje animals. This confirms that GluK1 transcription is sensitive to gene copy number and that Ts2Cje constitutes a good model to study GluK1 overexpression and its implication in DS pathophysiology.

Protein quantification highlights changes in KARs levels in Ts2Cje

Since there is no specific GluK1 antibody available, direct quantification of GluK1 protein was not possible. However, available antibodies can readily detect others kainate receptor subunits. In agreement with mRNA expression data, we found that *App* levels (positive control) were increased in the whole CNS of Ts2Cje animals, in keeping with data from Ts65Dn model (Salehi et al., 2006; Seo and Isacson, 2005). In spite of the unchanged levels of mRNA, we found diminished protein levels of GluK4 and GluK5 in Ts2Cje animals, but not of GluK2/3 subunits. Therefore, a kind of down regulation happens for these subunits upon overexpression of GluK1. Since GluK4 and GluK5 only form functional receptors in combination with GluK1, GluK2 or GluK3, it

can be suggested that in the presence of an excess of GluK1, heteromerization of GluK4/5 with GluK2/3 is disfavored, likely inducing degradation of GluK4 and GluK5 subunits. Indeed, in GluK2 KO mice, the protein levels of GluK5 falls below to detection limits (Christensen et al., 2004). The fact that GluK1 and GluK2 readily form heteromeric receptors (Cui and Mayer, 1999; Paternain et al., 2000) lead us to postulate that GluK1 competes with GluK4/5 for heteromerization with GluK2/3. Therefore, Ts2Cje neurons present a compensatory mechanism in favor of GluK1/GluK2 and GluK1/GluK3 heteromeric receptors. Such a mechanism would be important in terms of determining cell intrinsic properties and excitability because channel gating (conductance and desensitization) depends on subunit composition (Swanson et al., 1996).

GluK1 levels are increased at interneuron membrane

To assess the excess of functional GluK1 receptors in the neuronal membranes in Ts2Cje, we used electrophysiology. In these experiments, perfusion of a GluK1 selective agonist (ATPA at 1 μ M) induced larger currents in Ts2Cje interneurons than in DLM cells. This result demonstrates that in Ts2Cje, CA1 interneurons present more functional GluK1-KARs than in DLM. Perfusion of ATPA on the same cells at a concentration of 3 μ M to activate other receptor combinations (e.g. GluK2/GluK5) induced larger currents. However the fraction of 3 μ M-induced current that was already activated at ATPA 1 μ M was larger in Ts2Cje, indicating the existence of more GluK1-containing receptors in the neuronal membrane. This result again argues in favor to conclude that the global subunit composition of KAR population is modified in favor of GluK1 subunit in CA1 interneurons from Ts2Cje mice.

Increased basal inhibitory neurotransmission in the area CA1

In CA1 pyramidal cells and interneurons from Ts2Cje, the frequency of both mIPSC and sIPSC were larger than in DLM animals. The higher mIPSC frequency was surprising since it had not been observed before in area CA1 of a DS mouse model (Chakrabarti et al., 2010). However, an increase of mIPSC frequency has also been described in the granule cells of the dentate gyrus of Ts65Dn (Kleschevnikov et al., 2004). Our data indicate that in Ts2Cje mice, CA1 pyramidal cells and interneurons receive more inhibitory contacts than in DLM. This agrees well with the finding of a widespread over-abundance of interneurons throughout the forebrain in Ts65Dn mouse

model (Chakrabarti et al. 2010). In addition, an increase of interneuronal excitability due to GluK1 overexpression could account for sIPSC frequency increase in Ts2Cje. Indeed the presence of supernumerary GluK1-KARs at the somatodendritic/axonal compartment could increase cell sensitivity to ambient glutamate and make it more excitable. The consequence of such an increase of basal GABA release input onto a pyramidal cell is the decrease of cell excitability in Ts2Cje. Taking into account that hippocampal signals have to go through CA1 pyramidal cells, a global decrease of pyramidal cells excitability could alter the information processing through the hippocampal trisynaptic circuit.

On the one hand, introduction of KARs antagonists produced an increase of mIPSC frequency in CA1 pyramidal cells in the same range in both animal types. This result is consistent with the existence of a presynaptic population of GluK1-KARs that tonically down-regulates GABA release at the interneuron- pyramidal cells synapse in the area CA1. As GluK1 antagonist effect is similar in DLM and Ts2Cje, we can say that the number of GluK1-KARs present at the presynaptic terminals to control GABA release remains unchanged in Ts2cje. In both SR and SO interneurons, TTX-insensitive basal inhibitory transmission was not sensitive to GluK1 antagonism. This indicates that GluK1-KARs are not be involved in the regulation of GABA release in interneuron-interneuron synapses.

Blockade of GluK1-KARs also increases sIPSC recorded in pyramidal cells. This result points out the involvement of GluK1-KARs in GABA release down-regulation at the interneuron-pyramidal cell synapse. In interneurons, GluK1-KARs blockade only produced a significant increase of sIPSC frequency when tested in SO interneurons of Ts2Cje. This observation could be explained by a higher number of presynaptic GluK1-KARs at the interneuron-interneuron synapse in Ts2Cje SO. This excess of GABA down regulation would create a disinhibition of SO interneurons in Ts2Cje compared to DLM and then could explain in part the over-inhibition observed in pyramidal layer. Another explanation could emerge from the recent discovery that the willardiine derivative molecule (UBP310) could behave as a positive allosteric modulator of heteromeric receptors containing GluK2 subunits, rather than being a GluK1/3 antagonist (Pinheiro et al., 2013). Experiments subsequently carried out in our lab to test this aspect, revealed similar properties for the other willardiine derivative (ACET)

(Valbuena and Lerma, unpublished) used in this study. In our study, the application of both molecules could actually activate a KARs subpopulation present at the somatodendritic compartment, producing membrane depolarization and a subsequent increase of sIPSC frequency. Here again the presence of supernumerary GluK1-KARs in Ts2Cje interneurons could explain that this class of antagonists have more effect in Ts2cje than in DLM. However, we also observed that application of another class of large spectrum antagonist (CNQX; quinoxalinedione derivatives) had a similar effect as UBP310 and ACET on basal inhibitory activity in pyramidal cells. Finally, in absence of more evidence about this paradoxical effect of willardiine derivatives, we conclude that the observed effect on mIPSCs is likely due to the blockade of the GluK1-KAR-mediated depression of GABA release, while the action of sIPSC could be due to their allosteric action on somatodendritic/axonal receptors.

On the other hand, the application of a GluK1-KARs selective agonist provoked a “massive” increase of sIPSC frequency in CA1 pyramidal cells of both DLM and Ts2Cje. This effect is due to the activation of GluK1-KARs present in the somatodendritic/axonal compartment of CA1 interneurons projecting onto CA1 pyramidal cells and is consistent with the presence of an excess of GluK1 receptors in this compartment in trisomics. The effect of ATPA observed here agrees with previous findings (Rodriguez Moreno et al., 2000; Clarke et al. 1997; Cossart et al. 1998). This population of GluK1-KARs would allow detection of ambient glutamate and permits adapting cell excitability to the context. According to the presence of a larger population of membrane receptors due to the gene extra copy, the effect of ATPA 1 μ M on sIPSC frequency increase was significantly larger in Ts2Cje than in DLM. This is also in keeping with the observation that ATPA depolarized significantly more the interneurons from Ts2Cje mice. Physiologically, the presence of more GluK1-KARs in the somatodendritic compartment confers to Ts2Cje CA1 interneurons more sensitivity to ambient glutamate levels. As the frequency of synaptic events depends on the membrane potential, the same concentration of ambient glutamate will generate more depolarizing current and consequently more GABA release in Ts2cje than in DLM.

Changes in the amplitude of spontaneous synaptic events were also observed, first between animal types and then between pharmacological treatments in some experiments. We would like to precise that under these recording conditions evaluation

of amplitude was rather unreliable. The frequent summation of synaptic events in our recordings made accurate amplitude measurement unlikely. As a proof of this, we recorded some cells using K-gluconate rather than a chloride based solution (figure 40). Under these circumstances, IPSCs were smaller, as membrane potential was closer to the IPSC reversal potential. This procedure allowed detection of sIPSC with significant amplitude, demonstrating that the amplitude of these events was equal in Ts2Cje and DLM. Therefore, we prefer to not conclude about the action of agonists and antagonists on events amplitude, since changes in frequency would impact amplitude measurements, making conclusion difficult.

Impaired evoked inhibitory synaptic transmission in the area CA1

Inhibitory synapses at the hippocampus and other cortical structures exhibit PPD (Bortolotto et al., 2011). The relationship between release probability and PPR is inverted: a large PPR (i.e. PPF) reflects low release probability, whereas low PPR (i.e. PPD) indicates high probability of release (Zucker, 1989). Consistent with a constitutively larger tonic downregulation of GABA release, we observed that PPD was significantly lower (larger PPR) in Ts2Cje compared to DLM in pyramidal cells. Indeed, in Ts2Cje SR interneurons, eIPSC PPR revealed paired-pulse facilitation (PPF) rather than depression, as it was observed in DLM. An increased PPR has also been previously observed in dentate gyrus granule cells in Ts65Dn model (Kleschevnikov et al., 2004), indicating that the basal probability of release is reduced in trisomy. However, PPR was similar between DLM and Ts2Cje mice in SO interneurons. This means that during repeated stimulation, the inhibition in Ts2Cje CA1, has lower frequency induced attenuation in pyramidal cells and SR interneurons. Another group working with Ts65Dn model did also observe modifications of GABA_B-mediated inhibition within CA1 but did not report any significant changes in basal GABA release probability in hippocampal CA1 (Best et al., 2012).

Activation of GluK1-KARs with selective agonist (ATPA at 1 μ M) drastically decreases eIPSC amplitude in both DLM and Ts2Cje. These data is in keeping with the existence of presynaptic KARs depressing GABA release in a concentration dependent manner (Clarke et al., 1997; Clarke and Collingridge, 2004; Rodríguez-Moreno et al., 1998, 1997). As the same effect was observed in both DLM and Ts2Cje, it suggests that the GluK1-KARs presynaptic subpopulation is not modified in trisomic hippocampus. The

activation of GluK1-KARs also decreased the PPD recorded in pyramidal cells of both DLM and Ts2Cje. This result indicates that activation of presynaptic GluK1-KARs could decrease GABA release onto pyramidal cells and confirms that GluK1-antagonists could produce an increase of basal inhibitory transmission in pyramidal cells as described previously. Like in CA1 principal cells, GluK1-KARs selective agonist considerably depressed eIPSC in DLM and Ts2Cje SR/SO interneurons, but does not affect eIPSC PPR.

Deficient synaptic plasticity in area CA1

LTP is a well studied synaptic model of learning and memory (Bortolotto et al., 2011; Malenka and Nicoll, 1999). Reports from various groups working with Ts65Dn have indicated a link between learning and memory deficits exhibited by these animals and impairment of hippocampal synaptic plasticity (Costa and Grybko, 2005; Fernandez et al., 2007; Kleschevnikov et al., 2004; Siarey et al., 1999, 1997). However, the mechanisms responsible for this deficit in synaptic plasticity observed in Ts65Dn have not been elucidated. We found that in Ts2Cje DS model, LTP is attenuated in hippocampal CA1 field and that LTD generation is abnormal. However, LTP levels become comparable to the ones observed in DLM when GluK1-KARs are stimulated. Interestingly in DLM, GluK1-KARs activation does not affect the LTP induction. This result is the first description of LTP induction restoration via activation of GluK1-KARs in a trisomics model.

Since tonic activation of GluK1-KARs (ATPA 1 μ M) is enough to restore LTP and LTD in Ts2Cje mice. We believe that LTP induction impairment in this model can be due to the exacerbated inhibition. It has been shown that suppression of inhibition, with GABA_A antagonists, can normalize impaired LTP induction in Ts65Dn dentate gyrus cells (Fernandez et al., 2007; Kleschevnikov et al., 2004) and CA1 area (Costa and Grybko, 2005). Therefore, we propose that a reduction of inhibition of neuronal networks by activation of GluK1-KARs in Ts2Cje mice allows LTP to develop.

The level of inhibition is also important for the induction of another type of hippocampal synaptic plasticity, the LTD. During LTD, reduction of the fEPSP is induced by prolonged low-frequency stimulation. During preliminary tests, we did not

manage to induce a direct NMDAR-dependent LTD in adults (2 months old) via the classical LFS protocol. This observation has also been reported previously and the authors proposed to use a depotentiation protocol to induce an mGluR-dependent depotentiation of LTP (Bashir and Collingridge, 1994). Even if the depotentiation was variable between animals during preliminary experiments, this protocol gave us more success than *de novo* LTP induction. In DLM we managed to get a small but significant LTP-depotentiation, while it was not seen in Ts2Cje. Activation of GluK1-KARs did not alter depotentiation in DLM animals but restored it in Ts2Cje mice. Like for LTP, selective activation of GluK1-KARs could relieve the excessive inhibitory tonus present in Ts2Cje CA1 and restore normal plasticity levels.



General conclusion

Several groups have suggested that synaptic plasticity defects observed in trisomics brains are due to the existence of over-inhibition (Belichenko et al., 2009, 2004; Fernandez et al., 2007; Kleschevnikov et al., 2004; Siarey et al., 1999, 1997). Other studies demonstrated that GluK1-KARs selective pharmacological agents can reduced inhibitory transmission (Christensen et al., 2004; Clarke et al., 1997; Clarke and Collingridge, 2004; Maingret et al., 2005; Rodríguez-Moreno et al., 1998, 1997). Despite GluK1-encoding gene triplication and a promising effect of a pharmacologically-induced GABA release depression on DS mice cognition (Fernandez et al, 2007), the link between GluK1-KARs activity and inhibitory neurotransmission in the trisomics brain has been under-investigated. In this study we present a detailed report of basal inhibitory neurotransmission and associated plasticity in Ts2Cje model.

In summary, in this study we demonstrate that Ts2Cje is a good model to investigate on GluK1-KARs implication in DS pathophysiology. Our molecular biology results point out an increase of GluK1 mRNA quantities associated to some global rearrangements of KARs subunits composition in favor to GluK1-KARs in Ts2Cje brain. Indeed using an electrophysiological approach, we demonstrate the overexpression of GluK1 subunits in Ts2Cje hippocampal interneurons. For the first time in this model, we report an exaggerated inhibitory tonus due to the increase of GABAergic basal neurotransmission in different hippocampal CA1 cellular types. Application of GluK1-selective pharmacology confirms the implication of these receptors in the control of GABA release onto pyramidal cells. At the same time, activation of GluK1-KARs can be either pro-GABA release by increasing basal inhibition or anti-GABA release by decreasing evoked inhibitory response amplitude. This idea of bidirectional KAR-mediated modulation of transmitter release has already been reported in synaptosomes (Perkinton and Sihra, 1999), in cerebellar cortex interneurons (Delaney and Jahr, 2002) and in hippocampus interneurons (Maingret et al., 2005). In neonatal hippocampus interneurons, the existence of two distinct KARs populations that can have distinct functional role has been suggested. Somatodendritic/axonal KARs would be pro-GABAergic, involved in the detection of large scale activity. Meanwhile KARs located at GABAergic terminals would be anti-GABAergic, sensitive to local glutamate spill

over from neighboring glutamatergic afferents (Maingret et al., 2005). Considering our results, it appears that the excess of GluK1-KARs is more likely located in the somatodendritic/axonal compartments in Ts2Cje hippocampus CA1. The direct consequence is an increase of the pro-GABA release influence participating in the over-inhibition phenotype. Then we observed that the capacity to generate long term plasticity is diminished in Ts2Cje. Nevertheless perfusion of GluK1-KARs selective agonist restores normal plasticity levels. This effect points out that the fundamental molecular mechanisms necessary to produce normal plasticity remains present and functional in Ts2Cje CA1 area. Finally, these results draw a line between GluK1 protein level and the LTP levels in area CA1.

In order approach the global functioning of this network, we can imagine a simple model, considering only the interneurons connected to CA1 pyramidal cells (Figure 56). In DLM, during basal activity stages, ambient glutamate levels are low, somatodendritic/axonal GluK1-KARs are inactive and presynaptic GluK1-KARs lightly down regulate GABA release onto CA1 pyramidal cells. Under these conditions, the only effect of an antagonist would be a small increase of elementary GABA release. But during sustained activity in the hippocampus, ambient glutamate levels would activate somatodendritic/axonal GluK1-KARs producing a massive increase of GABA release due to action potential generation that overcomes the action of presynaptic GluK1-KARs. This scenario also confers a “security break” role to somatodendritic/axonal GluK1-KARs in case of hyperexcitation.

If now we can consider a similar scenario in Ts2Cje, keeping in mind that in Ts2Cje the number of interneuron is larger (Chakrabarti et al., 2010) and that each interneuron overexpresses GluK1-KARs at the somatodendritic/axonal compartment. Under basal condition, tonic GABA release is increased because interneurons are more numerous and more excitable. The main difference with DLM appears during sustained activity phases. Here the “security break” is more sensitive and more powerful than in DLM. In trimosy, the increase of ambient glutamate concentration quickly activates the numerous somatodendritic/axonal GluK1-KARs located at the interneuron membrane and launch a massive inhibitory input onto the pyramidal cells.

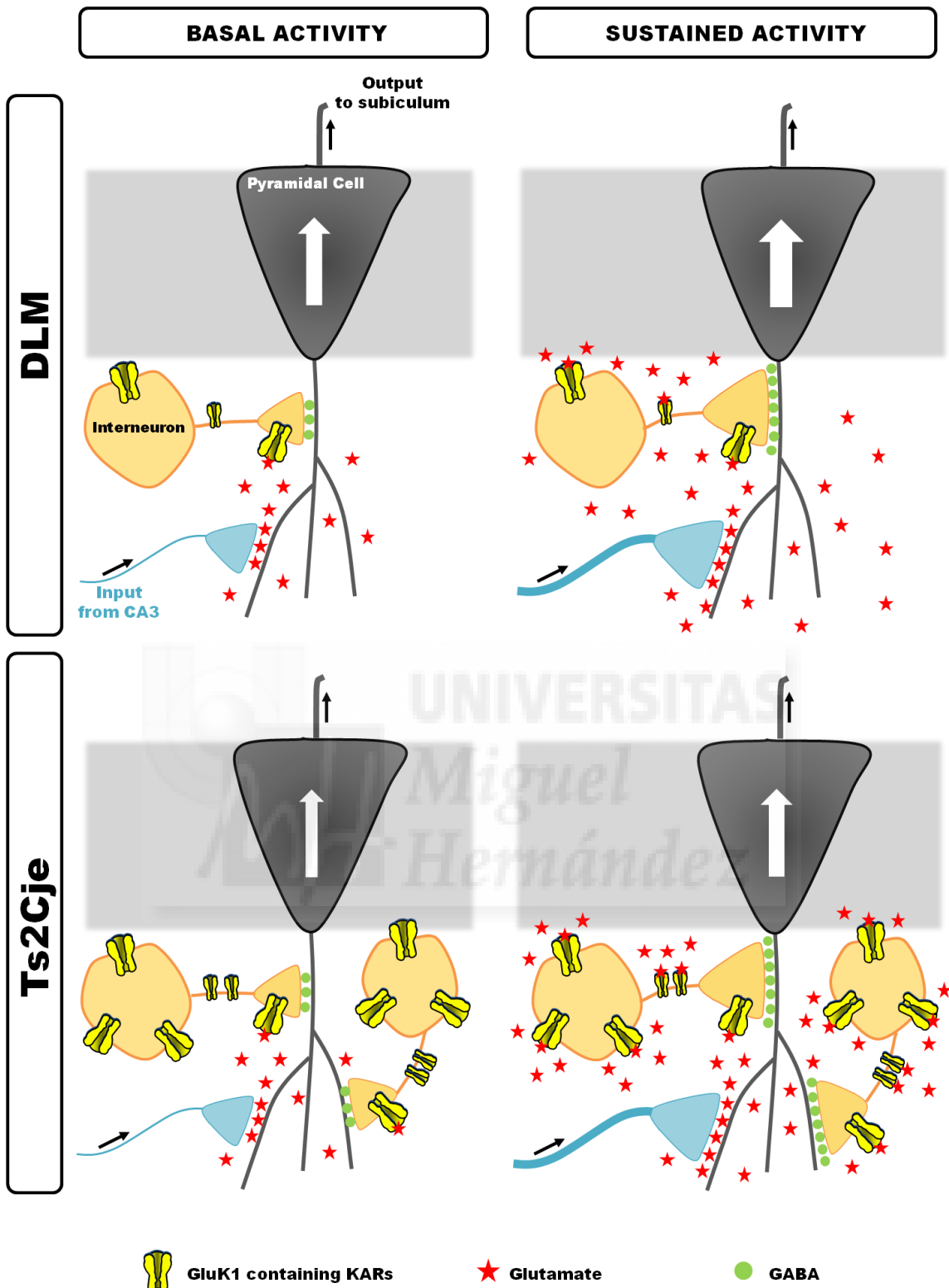


Figure 56: Simple modelisation of putative consequences of GluK1 overexpression in Ts2Cje area CA1 of the hippocampus. During basal activity in DLM ambient glutamate levels are low, somatodendritic/axonal GluK1-KARs are inactive and presynaptic GluK1-KARs down regulate GABA release onto CA1 pyramidal cells. Sustained activity increase ambient glutamate level, activates somatodendritic/axonal GluK1-KARs. Interneuron excitation produces a massive increase of GABA release that controls the excitatory input arriving in CA1 pyramidal cell. In Ts2Cje, where there are more interneurons with more GluK1-KARs, basal GABA release is slightly increased. During sustained activity, the opening of the numerous somatodendritic/axonal GluK1-KARs massively enhanced the inhibitory drive onto principal cells.

This simple model only tries to understand the pathophysiological changes present in Ts2Cje. However it does not explain how GluK1-KARs selective activation can regulate eIPSC amplitude and restore impaired LTP in Ts2Cje. To explain the effect of agonist perfusion, we have to consider two scenarios. Firstly, GluK1 agonist would strongly activate presynaptic KARs, blocking GABA release. Or secondly, agonist perfusion could also activate further interneurons in charge of the inhibition of the previously described interneuron (the one that fires directly onto pyramidal cells). The putative result would be an inhibition of the inhibitor, in other words a reduction of the inhibitory drive onto the pyramidal cells. It may be that a computational approach could help us to predict what happen in Ts2Cje hippocampus.

Because DS is a multigenic disease, it is important to go deeper in the analysis to understand better the “specific” role of GluK1-KARs. It could be interesting to selectively reduce GluK1 protein levels in a trisomic brain. In order to evaluate the specific implication of a gene of interest in DS pathophysiology, “gene dosage normalization” approach has been used (Chakrabarti et al., 2010; Salehi et al., 2006). In our case, we can imagine a selective gene dosage normalization for GluK1, breeding a Ts2Cje female with a male heterozygous for GluK1 deletion ($\text{GluK1}^{+/-}$). Four different genotypes could emerge from this cross: DLM mouse with two copies of GluK1 ($\text{GluK1}^{+/+}$), DLM mouse with one copy of GluK1 ($\text{GluK1}^{+/-}$) and Ts2Cje mouse with three copies of GluK1 ($\text{GluK1}^{+/+/+}$) and Ts2Cje mouse with two copies of GluK1 ($\text{GluK1}^{+/+/-}$). The $\text{GluK1}^{+/+/-}$ genotype would present a real control to test the specific effect of GluK1 triplication in the over-inhibition phenotype observed in TS2Cje. Another option could be to reduce of GluK1 transcription products using interfering RNA system (Canzonetta 2008; Ortiz-Abalia 2008) and repeat the electrophysiological experiments done during this project and compare them. Results coming out from such project could build a strong link between GluK1 gene dosage imbalance and the observed over-inhibition phenotype observed in Ts2Cje.

Considering that the reported over-inhibition could contribute to the deficits in learning and memory presented by both trisomic mice and DS patient, it is important to run behavioral experiments with Ts2Cje. Indeed in Ts65Dn, it has been shown that chronic administration of noncompetitive GABA_A antagonists ameliorates cognitive deficits in Ts65Dn mice for a period of months (Fernandez et al., 2007). Thus it would be

interesting to challenge adult Ts2Cje animals with different learning and memory dependent tasks, like novel object recognition or spontaneous alternation. In case of performance deficit it would be smart to attempt a rescue with a GluK1-KARs agonist-based treatment.

To our knowledge GABA receptor antagonism is considered to be the main therapeutic strategies in DS for restoring both memory and LTP in Ts65Dn mice (Fernandez et al., 2007). Considering that epilepsy is more common in DS patient than in the rest of the population (Stafstrom, 1993) and that DS patient present more sensitivity to epilepsy-inducing drugs (Dierssen, 2012), blockade of inhibitory synaptic transmission appears to further enhance risk to provoke epileptic episodes in DS patient. Alternatively a selective targeting of GluK1-KARs could allow a therapeutical regulation of inhibitory synaptic transmission in Ts2Cje CA1 hippocampus. The final objective is the development specific drugs to improve cognitive performance of DS patient. To finish, in this project we have characterized the utility of Ts2Cje mouse model in the study of functional synaptic impairments at the basis of mental retardation observed in DS patient. This model could also be useful for preclinical testing of putative therapies and in our case the potential clinical utility of GluK1-KARs selective pharmacology in the improvement of DS pathophysiology.

Conclusiones

El objetivo de este trabajo fue verificar la existencia de una relación entre la fisiopatología del síndrome de Down y la triplicación del gen que codifica para GluK1. Usando un modelo atípico del síndrome de Down, Ts2Cje, hemos alcanzado las siguientes conclusiones:

- La RTqPCR es un método simple y rápido para genotipar individuos dentro de una misma camada
- Los niveles de ARNm codificante para GluK1 están incrementados en el sistema nervioso central de los ratones Ts2Cje.
- La distribución global de los receptores al kainato en la membrana de las interneuronas de hipocampo está modificada a favor de GluK1, existiendo una sobreexpresión de los receptores al kainato conteniendo la subunidad GluK1
- La transmisión inhibitoria basal es mayor en la zona CA1 del hipocampo de los ratones trisómicos.
- La transmisión inhibitoria está regulada por los receptores de kainato que contienen la subunidad GluK1 en el área CA1 del hipocampo
- La inducción de plasticidad a largo plazo está desfavorecida en el área CA1 del hipocampo de los ratones trisómicos.
- La activación selectiva de los receptores al kainato conteniendo la subunidad GluK1 permite recuperar los niveles de plasticidad normales en estos ratones.



BIBLIOGRAPHY

- Ali, A.B., Rossier, J., Staiger, J.F., Audinat, E., 2001. Kainate receptors regulate unitary IPSCs elicited in pyramidal cells by fast-spiking interneurons in the neocortex. *J. Neurosci. Off. J. Soc. Neurosci.* 21, 2992–2999.
- Alt, A., Weiss, B., Ornstein, P.L., Gleason, S.D., Bleakman, D., Stratford, R.E., Jr, Witkin, J.M., 2007. Anxiolytic-like effects through a GLUK5 kainate receptor mechanism. *Neuropharmacology* 52, 1482–1487.
- Antonarakis, S.E., Lyle, R., Dermitzakis, E.T., Reymond, A., Deutsch, S., 2004. Chromosome 21 and down syndrome: from genomics to pathophysiology. *Nat. Rev. Genet.* 5, 725–738.
- Aroniadou-Anderjaska, V., Pidoplichko, V.I., Figueiredo, T.H., Almeida-Suhett, C.P., Prager, E.M., Braga, M.F.M., 2012. Presynaptic Facilitation of Glutamate Release in the Basolateral Amygdala: A Mechanism for the Anxiogenic and Seizurogenic Function of Gluk1 Receptors. *Neuroscience*.
- Banke, T.G., Bowie, D., Lee, H., Haganir, R.L., Schousboe, A., Traynelis, S.F., 2000. Control of GluR1 AMPA receptor function by cAMP-dependent protein kinase. *J. Neurosci. Off. J. Soc. Neurosci.* 20, 89–102.
- Barbon, A., Barlati, S., 2000. Genomic organization, proposed alternative splicing mechanisms, and RNA editing structure of GRIK1. *Cytogenet. Cell Genet.* 88, 236–239.
- Barbon, A., Fumagalli, F., La Via, L., Caracciolo, L., Racagni, G., Riva, M.A., Barlati, S., 2007. Chronic phencyclidine administration reduces the expression and editing of specific glutamate receptors in rat prefrontal cortex. *Exp. Neurol.* 208, 54–62.
- Barbon, A., Vallini, I., Barlati, S., 2001. Genomic organization of the human GRIK2 gene and evidence for multiple splicing variants. *Gene* 274, 187–197.
- Bashir, Z.I., Collingridge, G.L., 1994. An investigation of depotentiation of long-term potentiation in the CA1 region of the hippocampus. *Exp. Brain Res.* 100, 437–443.
- Battaglia, F., Quartarone, A., Rizzo, V., Ghilardi, M.F., Di Rocco, A., Tortorella, G., Girlanda, P., 2008. Early impairment of synaptic plasticity in patients with Down's syndrome. *Neurobiol. Aging* 29, 1272–1275.
- Bear, M.F., Connors, B.W., Paradiso, M.A., 2001. *Neuroscience: exploring the brain*. Lippincott Williams & Wilkins.
- Begni, S., Popoli, M., Moraschi, S., Bignotti, S., Tura, G.B., Gennarelli, M., 2002. Association between the ionotropic glutamate receptor kainate 3 (GRIK3) ser310ala polymorphism and schizophrenia. *Mol. Psychiatry* 7, 416–418.
- Belichenko, P.V., Kleschevnikov, A.M., Masliah, E., Wu, C., Takimoto-Kimura, R., Salehi, A., Mobley, W.C., 2009. Excitatory-inhibitory relationship in the fascia dentata in the Ts65Dn mouse model of Down syndrome. *J. Comp. Neurol.* 512, 453–466.
- Belichenko, P.V., Kleschevnikov, A.M., Salehi, A., Epstein, C.J., Mobley, W.C., 2007. Synaptic and cognitive abnormalities in mouse models of Down syndrome: exploring genotype-phenotype relationships. *J. Comp. Neurol.* 504, 329–345.
- Belichenko, P.V., Masliah, E., Kleschevnikov, A.M., Villar, A.J., Epstein, C.J., Salehi, A., Mobley, W.C., 2004. Synaptic structural abnormalities in the Ts65Dn mouse model of Down Syndrome. *J. Comp. Neurol.* 480, 281–298.
- Bellone, C., Lüscher, C., Mamei, M., 2008. Mechanisms of synaptic depression triggered by metabotropic glutamate receptors. *Cell. Mol. Life Sci. CMLS* 65, 2913–2923.
- Ben-Ari, Y., Cossart, R., 2000. Kainate, a double agent that generates seizures: two decades of progress. *Trends Neurosci.* 23, 580–587.

- Benes, F.M., Todtenkopf, M.S., Kostoulakos, P., 2001. GluR5,6,7 subunit immunoreactivity on apical pyramidal cell dendrites in hippocampus of schizophrenics and manic depressives. *Hippocampus* 11, 482–491.
- Beneyto, M., Kristiansen, L.V., Oni-Orisan, A., McCullumsmith, R.E., Meador-Woodruff, J.H., 2007. Abnormal glutamate receptor expression in the medial temporal lobe in schizophrenia and mood disorders. *Neuropsychopharmacol. Off. Publ. Am. Coll. Neuropsychopharmacol.* 32, 1888–1902.
- Bennett, J.A., Dingledine, R., 1995. Topology profile for a glutamate receptor: three transmembrane domains and a channel-lining reentrant membrane loop. *Neuron* 14, 373–384.
- Best, T.K., Cramer, N.P., Chakrabarti, L., Haydar, T.F., Galdzicki, Z., 2012. Dysfunctional hippocampal inhibition in the Ts65Dn mouse model of Down syndrome. *Exp. Neurol.* 233, 749–757.
- Bettler, B., Boulter, J., Hermans-Borgmeyer, I., O'Shea-Greenfield, A., Deneris, E.S., Moll, C., Borgmeyer, U., Hollmann, M., Heinemann, S., 1990. Cloning of a novel glutamate receptor subunit, GluR5: expression in the nervous system during development. *Neuron* 5, 583–595.
- Bliss, T.V., Lomo, T., 1973. Long-lasting potentiation of synaptic transmission in the dentate area of the anaesthetized rabbit following stimulation of the perforant path. *J. Physiol.* 232, 331–356.
- Bonfardin, V.D.J., Fossat, P., Theodosis, D.T., Oliet, S.H.R., 2010. Glia-dependent switch of kainate receptor presynaptic action. *J. Neurosci. Off. J. Soc. Neurosci.* 30, 985–995.
- Bortolotto, Z.A., Amici, M., Anderson, W.W., Isaac, J.T.R., Collingridge, G.L., 2011. Synaptic plasticity in the hippocampal slice preparation. *Curr. Protoc. Neurosci.* Editor. Board Jacqueline N Crawley A1 Chapter 6, Unit 6.13.
- Bortolotto, Z.A., Clarke, V.R., Delany, C.M., Parry, M.C., Smolders, I., Vignes, M., Ho, K.H., Miu, P., Brinton, B.T., Fantaske, R., Ogden, A., Gates, M., Ornstein, P.L., Lodge, D., Bleakman, D., Collingridge, G.L., 1999. Kainate receptors are involved in synaptic plasticity. *Nature* 402, 297–301.
- Braga, M.F.M., Aroniadou-Anderjaska, V., Li, H., 2004. The physiological role of kainate receptors in the amygdala. *Mol. Neurobiol.* 30, 127–141.
- Bureau, I., Dieudonne, S., Coussen, F., Mulle, C., 2000. Kainate receptor-mediated synaptic currents in cerebellar Golgi cells are not shaped by diffusion of glutamate. *Proc. Natl. Acad. Sci. U. S. A.* 97, 6838–6843.
- Burnashev, N., Villarroel, A., Sakmann, B., 1996. Dimensions and ion selectivity of recombinant AMPA and kainate receptor channels and their dependence on Q/R site residues. *J. Physiol.* 496 (Pt 1), 165–173.
- Carroll, R.C., Beattie, E.C., von Zastrow, M., Malenka, R.C., 2001. Role of AMPA receptor endocytosis in synaptic plasticity. *Nat. Rev. Neurosci.* 2, 315–324.
- Carroll, R.C., Zukin, R.S., 2002. NMDA-receptor trafficking and targeting: implications for synaptic transmission and plasticity. *Trends Neurosci.* 25, 571–577.
- Casassus, G., Mulle, C., 2002. Functional characterization of kainate receptors in the mouse nucleus accumbens. *Neuropharmacology* 42, 603–611.
- Castillo, P.E., Malenka, R.C., Nicoll, R.A., 1997. Kainate receptors mediate a slow postsynaptic current in hippocampal CA3 neurons. *Nature* 388, 182–186.

- Catches, J.S., Xu, J., Contractor, A., 2012. Genetic ablation of the GluK4 kainate receptor subunit causes anxiolytic and antidepressant-like behavior in mice. *Behav. Brain Res.* 228, 406–414.
- Chakrabarti, L., Best, T.K., Cramer, N.P., Carney, R.S.E., Isaac, J.T.R., Galdzicki, Z., Haydar, T.F., 2010. Olig1 and Olig2 triplication causes developmental brain defects in Down syndrome. *Nat. Neurosci.* 13, 927–934.
- Chattopadhyay, B., Ghosh, S., Gangopadhyay, P.K., Das, S.K., Roy, T., Sinha, K.K., Jha, D.K., Mukherjee, S.C., Chakraborty, A., Singhal, B.S., Bhattacharya, A.K., Bhattacharyya, N.P., 2003. Modulation of age at onset in Huntington's disease and spinocerebellar ataxia type 2 patients originated from eastern India. *Neurosci. Lett.* 345, 93–96.
- Chen, K., Li, H.-Z., Ye, N., Zhang, J., Wang, J.-J., 2005. Role of GABAB receptors in GABA and baclofen-induced inhibition of adult rat cerebellar interpositus nucleus neurons in vitro. *Brain Res. Bull.* 67, 310–318.
- Chittajallu, R., Vignes, M., Dev, K.K., Barnes, J.M., Collingridge, G.L., Henley, J.M., 1996. Regulation of glutamate release by presynaptic kainate receptors in the hippocampus. *Nature* 379, 78–81.
- Choquet, D., Triller, A., 2003. The role of receptor diffusion in the organization of the postsynaptic membrane. *Nat. Rev. Neurosci.* 4, 251–265.
- Christensen, J.K., Paternain, A.V., Selak, S., Ahring, P.K., Lerma, J., 2004. A mosaic of functional kainate receptors in hippocampal interneurons. *J. Neurosci. Off. J. Soc. Neurosci.* 24, 8986–8993.
- Clarke, V.R., Ballyk, B.A., Hoo, K.H., Mandelzys, A., Pellizzari, A., Bath, C.P., Thomas, J., Sharpe, E.F., Davies, C.H., Ornstein, P.L., Schoepp, D.D., Kamboj, R.K., Collingridge, G.L., Lodge, D., Bleakman, D., 1997. A hippocampal GluR5 kainate receptor regulating inhibitory synaptic transmission. *Nature* 389, 599–603.
- Clarke, V.R.J., Collingridge, G.L., 2004. Characterisation of the effects of ATPA, a GLU(K5) kainate receptor agonist, on GABAergic synaptic transmission in the CA1 region of rat hippocampal slices. *Neuropharmacology* 47, 363–372.
- Clarke, V.R.J., Collingridge, G.L., Lauri, S.E., Taira, T., 2012. Synaptic kainate receptors in CA1 interneurons gate the threshold of theta-frequency-induced long-term potentiation. *J. Neurosci. Off. J. Soc. Neurosci.* 32, 18215–18226.
- Collingridge, G.L., Herron, C.E., Lester, R.A., 1988. Synaptic activation of N-methyl-D-aspartate receptors in the Schaffer collateral-commissural pathway of rat hippocampus. *J. Physiol.* 399, 283–300.
- Collingridge, G.L., Kehl, S.J., McLennan, H., 1983. Excitatory amino acids in synaptic transmission in the Schaffer collateral-commissural pathway of the rat hippocampus. *J. Physiol.* 334, 33–46.
- Collingridge, G.L., Peineau, S., Howland, J.G., Wang, Y.T., 2010. Long-term depression in the CNS. *Nat. Rev. Neurosci.* 11, 459–473.
- Contractor, A., Sailer, A.W., Darstein, M., Maron, C., Xu, J., Swanson, G.T., Heinemann, S.F., 2003. Loss of kainate receptor-mediated heterosynaptic facilitation of mossy-fiber synapses in KA2^{-/-} mice. *J. Neurosci. Off. J. Soc. Neurosci.* 23, 422–429.
- Contractor, A., Swanson, G., Heinemann, S.F., 2001. Kainate receptors are involved in short- and long-term plasticity at mossy fiber synapses in the hippocampus. *Neuron* 29, 209–216.
- Cossart, R., Bernard, C., Ben-Ari, Y., 2005. Multiple facets of GABAergic neurons and synapses: multiple fates of GABA signalling in epilepsies. *Trends Neurosci.* 28, 108–115.

- Cossart, R., Esclapez, M., Hirsch, J.C., Bernard, C., Ben-Ari, Y., 1998. GluR5 kainate receptor activation in interneurons increases tonic inhibition of pyramidal cells. *Nat. Neurosci.* 1, 470–478.
- Cossart, R., Tyzio, R., Dinocourt, C., Esclapez, M., Hirsch, J.C., Ben-Ari, Y., Bernard, C., 2001. Presynaptic kainate receptors that enhance the release of GABA on CA1 hippocampal interneurons. *Neuron* 29, 497–508.
- Costa, A.C.S., Grybko, M.J., 2005. Deficits in hippocampal CA1 LTP induced by TBS but not HFS in the Ts65Dn mouse: a model of Down syndrome. *Neurosci. Lett.* 382, 317–322.
- Cramer, N., Galdzicki, Z., 2012. From abnormal hippocampal synaptic plasticity in down syndrome mouse models to cognitive disability in down syndrome. *Neural Plast.* 2012, 101542.
- Cui, C., Mayer, M.L., 1999. Heteromeric kainate receptors formed by the coassembly of GluR5, GluR6, and GluR7. *J. Neurosci. Off. J. Soc. Neurosci.* 19, 8281–8291.
- Cunha, R.A., Malva, J.O., Ribeiro, J.A., 1999. Kainate receptors coupled to G(i)/G(o) proteins in the rat hippocampus. *Mol. Pharmacol.* 56, 429–433.
- Cunha, R.A., Malva, J.O., Ribeiro, J.A., 2000. Pertussis toxin prevents presynaptic inhibition by kainate receptors of rat hippocampal [(3)H]GABA release. *FEBS Lett.* 469, 159–162.
- Dargan, S.L., Clarke, V.R.J., Alushin, G.M., Sherwood, J.L., Nisticò, R., Bortolotto, Z.A., Ogden, A.M., Bleakman, D., Doherty, A.J., Lodge, D., Mayer, M.L., Fitzjohn, S.M., Jane, D.E., Collingridge, G.L., 2009. ACET is a highly potent and specific kainate receptor antagonist: characterisation and effects on hippocampal mossy fibre function. *Neuropharmacology* 56, 121–130.
- Darstein, M., Petralia, R.S., Swanson, G.T., Wenthold, R.J., Heinemann, S.F., 2003. Distribution of kainate receptor subunits at hippocampal mossy fiber synapses. *J. Neurosci. Off. J. Soc. Neurosci.* 23, 8013–8019.
- Davies, C.H., Starkey, S.J., Pozza, M.F., Collingridge, G.L., 1991. GABA autoreceptors regulate the induction of LTP. *Nature* 349, 609–611.
- Delaney, A.J., Jahr, C.E., 2002. Kainate receptors differentially regulate release at two parallel fiber synapses. *Neuron* 36, 475–482.
- Dermitzakis, E.T., Reymond, A., Lyle, R., Scamuffa, N., Ucla, C., Deutsch, S., Stevenson, B.J., Flegel, V., Bucher, P., Jongeneel, C.V., Antonarakis, S.E., 2002. Numerous potentially functional but non-genic conserved sequences on human chromosome 21. *Nature* 420, 578–582.
- Dierssen, M., 2012. Down syndrome: the brain in trisomic mode. *Nat. Rev. Neurosci.* 13, 844–858.
- Dierssen, M., Herault, Y., Estivill, X., 2009. Aneuploidy: from a physiological mechanism of variance to Down syndrome. *Physiol. Rev.* 89, 887–920.
- Diguet, E., Fernagut, P.-O., Normand, E., Centelles, L., Mulle, C., Tison, F., 2004. Experimental basis for the putative role of GluR6/kainate glutamate receptor subunit in Huntington's disease natural history. *Neurobiol. Dis.* 15, 667–675.
- Dolman, N.P., More, J.C.A., Alt, A., Knauss, J.L., Pentikäinen, O.T., Glasser, C.R., Bleakman, D., Mayer, M.L., Collingridge, G.L., Jane, D.E., 2007. Synthesis and pharmacological characterization of N3-substituted willardiine derivatives: role of the substituent at the 5-position of the uracil ring in the development of highly potent and selective GLUK5 kainate receptor antagonists. *J. Med. Chem.* 50, 1558–1570.
- Dominguez, E., Iyengar, S., Shannon, H.E., Bleakman, D., Alt, A., Arnold, B.M., Bell, M.G., Bleisch, T.J., Buckmaster, J.L., Castano, A.M., Del Prado, M., Escribano, A., Filla,

- S.A., Ho, K.H., Hudziak, K.J., Jones, C.K., Martinez-Perez, J.A., Mateo, A., Mathes, B.M., Mattiuz, E.L., Ogden, A.M.L., Simmons, R.M.A., Stack, D.R., Stratford, R.E., Winter, M.A., Wu, Z., Ornstein, P.L., 2005. Two prodrugs of potent and selective GluR5 kainate receptor antagonists actives in three animal models of pain. *J. Med. Chem.* 48, 4200–4203.
- Down, J.L.H., 1866. Observations on an ethnic classification of idiots. *Lond. Hosp. Rep.*
- Dracheva, S., Byne, W., Chin, B., Haroutunian, V., 2008. Ionotropic glutamate receptor mRNA expression in the human thalamus: absence of change in schizophrenia. *Brain Res.* 1214, 23–34.
- Egebjerg, J., Bettler, B., Hermans-Borgmeyer, I., Heinemann, S., 1991. Cloning of a cDNA for a glutamate receptor subunit activated by kainate but not AMPA. *Nature* 351, 745–748.
- Fernandez, F., Morishita, W., Zuniga, E., Nguyen, J., Blank, M., Malenka, R.C., Garner, C.C., 2007. Pharmacotherapy for cognitive impairment in a mouse model of Down syndrome. *Nat. Neurosci.* 10, 411–413.
- Fisahn, A., Heinemann, S.F., McBain, C.J., 2005. The kainate receptor subunit GluR6 mediates metabotropic regulation of the slow and medium AHP currents in mouse hippocampal neurones. *J. Physiol.* 562, 199–203.
- Fisher, R.S., Alger, B.E., 1984. Electrophysiological mechanisms of kainic acid-induced epileptiform activity in the rat hippocampal slice. *J. Neurosci. Off. J. Soc. Neurosci.* 4, 1312–1323.
- FitzPatrick, D.R., Ramsay, J., McGill, N.I., Shade, M., Carothers, A.D., Hastie, N.D., 2002. Transcriptome analysis of human autosomal trisomy. *Hum. Mol. Genet.* 11, 3249–3256.
- Frankle, W.G., Lerma, J., Laruelle, M., 2003. The synaptic hypothesis of schizophrenia. *Neuron* 39, 205–216.
- Frerking, M., Malenka, R.C., Nicoll, R.A., 1998. Synaptic activation of kainate receptors on hippocampal interneurons. *Nat. Neurosci.* 1, 479–486.
- Frerking, M., Ohliger-Frerking, P., 2002. AMPA receptors and kainate receptors encode different features of afferent activity. *J. Neurosci. Off. J. Soc. Neurosci.* 22, 7434–7443.
- Frerking, M., Schmitz, D., Zhou, Q., Johansen, J., Nicoll, R.A., 2001. Kainate receptors depress excitatory synaptic transmission at CA3→CA1 synapses in the hippocampus via a direct presynaptic action. *J. Neurosci. Off. J. Soc. Neurosci.* 21, 2958–2966.
- Gill, R., Lodge, D., 1994. The neuroprotective effects of the decahydroisoquinoline, LY 215490; a novel AMPA antagonist in focal ischaemia. *Neuropharmacology* 33, 1529–1536.
- Gilron, I., Max, M.B., Lee, G., Boher, S.L., Sang, C.N., Chappell, A.S., Dionne, R.A., 2000. Effects of the 2-amino-3-hydroxy-5-methyl-4-isoxazole-propionic acid/kainate antagonist LY293558 on spontaneous and evoked postoperative pain. *Clin. Pharmacol. Ther.* 68, 320–327.
- Goldin, M., Epsztein, J., Jorquera, I., Represa, A., Ben-Ari, Y., Crépel, V., Cossart, R., 2007. Synaptic kainate receptors tune oriens-lacunosum moleculare interneurons to operate at theta frequency. *J. Neurosci. Off. J. Soc. Neurosci.* 27, 9560–9572.
- Gray, E.G., 1969. Electron microscopy of excitatory and inhibitory synapses: a brief review. *Prog. Brain Res.* 31, 141–155.
- Grosshans, D.R., Clayton, D.A., Coultrap, S.J., Browning, M.D., 2002. LTP leads to rapid surface expression of NMDA but not AMPA receptors in adult rat CA1. *Nat. Neurosci.* 5, 27–33.

- Hanson, J.E., Blank, M., Valenzuela, R.A., Garner, C.C., Madison, D.V., 2007. The functional nature of synaptic circuitry is altered in area CA3 of the hippocampus in a mouse model of Down's syndrome. *J. Physiol.* 579, 53–67.
- Harris, E.W., Ganong, A.H., Cotman, C.W., 1984. Long-term potentiation in the hippocampus involves activation of N-methyl-D-aspartate receptors. *Brain Res.* 323, 132–137.
- Harris, K.M., 1999. Structure, development, and plasticity of dendritic spines. *Curr. Opin. Neurobiol.* 9, 343–348.
- Hattori, M., Fujiyama, A., Taylor, T.D., Watanabe, H., Yada, T., Park, H.S., Toyoda, A., Ishii, K., Totoki, Y., Choi, D.K., Groner, Y., Soeda, E., Ohki, M., Takagi, T., Sakaki, Y., Taudien, S., Blechschmidt, K., Polley, A., Menzel, U., Delabar, J., Kumpf, K., Lehmann, R., Patterson, D., Reichwald, K., Rump, A., Schillhabel, M., Schudy, A., Zimmermann, W., Rosenthal, A., Kudoh, J., Schibuya, K., Kawasaki, K., Asakawa, S., Shintani, A., Sasaki, T., Nagamine, K., Mitsuyama, S., Antonarakis, S.E., Minoshima, S., Shimizu, N., Nordsiek, G., Hornischer, K., Brant, P., Scharfe, M., Schon, O., Desario, A., Reichelt, J., Kauer, G., Blocker, H., Ramser, J., Beck, A., Klages, S., Hennig, S., Riesselmann, L., Dagand, E., Haaf, T., Wehrmeyer, S., Borzym, K., Gardiner, K., Nizetic, D., Francis, F., Lehrach, H., Reinhardt, R., Yaspo, M.L., Chromosome 21 mapping and sequencing consortium, 2000. The DNA sequence of human chromosome 21. *Nature* 405, 311–319.
- Haydar, T.F., Nowakowski, R.S., Yarowsky, P.J., Krueger, B.K., 2000. Role of founder cell deficit and delayed neurogenesis in microencephaly of the trisomy 16 mouse. *J. Neurosci. Off. J. Soc. Neurosci.* 20, 4156–4164.
- Herb, A., Burnashev, N., Werner, P., Sakmann, B., Wisden, W., Seeburg, P.H., 1992. The KA-2 subunit of excitatory amino acid receptors shows widespread expression in brain and forms ion channels with distantly related subunits. *Neuron* 8, 775–785.
- Hollmann, M., O'Shea-Greenfield, A., Rogers, S.W., Heinemann, S., 1989. Cloning by functional expression of a member of the glutamate receptor family. *Nature* 342, 643–648.
- Huettnner, J.E., 1990. Glutamate receptor channels in rat DRG neurons: activation by kainate and quisqualate and blockade of desensitization by Con A. *Neuron* 5, 255–266.
- Isaac, J.T., Nicoll, R.A., Malenka, R.C., 1995. Evidence for silent synapses: implications for the expression of LTP. *Neuron* 15, 427–434.
- Ishihara, K., Amano, K., Takaki, E., Ebrahim, A.S., Shimohata, A., Shibazaki, N., Inoue, I., Takaki, M., Ueda, Y., Sago, H., Epstein, C.J., Yamakawa, K., 2009. Increased lipid peroxidation in Down's syndrome mouse models. *J. Neurochem.* 110, 1965–1976.
- Ishihara, K., Amano, K., Takaki, E., Shimohata, A., Sago, H., Epstein, C.J., Yamakawa, K., 2010. Enlarged brain ventricles and impaired neurogenesis in the Ts1Cje and Ts2Cje mouse models of Down syndrome. *Cereb. Cortex N. Y. N* 1991 20, 1131–1143.
- Jamain, S., Betancur, C., Quach, H., Philippe, A., Fellous, M., Giros, B., Gillberg, C., Leboyer, M., Bourgeron, T., Paris Autism Research International Sibpair (PARIS) Study, 2002. Linkage and association of the glutamate receptor 6 gene with autism. *Mol. Psychiatry* 7, 302–310.
- Jane, D.E., Lodge, D., Collingridge, G.L., 2009. Kainate receptors: pharmacology, function and therapeutic potential. *Neuropharmacology* 56, 90–113.
- Jeffery, B., Barlow, T., Moizer, K., Paul, S., Boyle, C., 2004. Amnesic shellfish poison. *Food Chem. Toxicol. Int. J. Publ. Br. Ind. Biol. Res. Assoc.* 42, 545–557.

- Jiang, H.-X., Guan, Q.-H., Pei, D.-S., Zhang, G.-Y., 2007. Functional cooperation between KA2 and GluR6 subunits is involved in the ischemic brain injury. *J. Neurosci. Res.* 85, 2960–2970.
- Johnson, J.W., Ascher, P., 1987. Glycine potentiates the NMDA response in cultured mouse brain neurons. *Nature* 325, 529–531.
- Jones, C.K., Alt, A., Ogden, A.M., Bleakman, D., Simmons, R.M.A., Iyengar, S., Dominguez, E., Ornstein, P.L., Shannon, H.E., 2006. Antiallodynic and antihyperalgesic effects of selective competitive GLUK5 (GluR5) ionotropic glutamate receptor antagonists in the capsaicin and carrageenan models in rats. *J. Pharmacol. Exp. Ther.* 319, 396–404.
- Kamboj, R.K., Schoepp, D.D., Nutt, S., Shekter, L., Korczak, B., True, R.A., Rampersad, V., Zimmerman, D.M., Wosnick, M.A., 1994. Molecular cloning, expression, and pharmacological characterization of humEAA1, a human kainate receptor subunit. *J. Neurochem.* 62, 1–9.
- Kamboj, R.K., Schoepp, D.D., Nutt, S., Shekter, L., Korczak, B., True, R.A., Zimmerman, D.M., Wosnick, M.A., 1992. Molecular structure and pharmacological characterization of humEAA2, a novel human kainate receptor subunit. *Mol. Pharmacol.* 42, 10–15.
- Kamiya, H., Ozawa, S., 1998. Kainate receptor-mediated inhibition of presynaptic Ca²⁺ influx and EPSP in area CA1 of the rat hippocampus. *J. Physiol.* 509 (Pt 3), 833–845.
- Kamiya, H., Ozawa, S., Manabe, T., 2002. Kainate receptor-dependent short-term plasticity of presynaptic Ca²⁺ influx at the hippocampal mossy fiber synapses. *J. Neurosci. Off. J. Soc. Neurosci.* 22, 9237–9243.
- Kandel, E., Schwartz, J., Jessell, T., 2000. *Principles of Neural Science*, Fourth Edition. McGraw-Hill Companies, Incorporated.
- Kauer, J.A., Malenka, R.C., 2007. Synaptic plasticity and addiction. *Nat. Rev. Neurosci.* 8, 844–858.
- Khalilov, I., Hirsch, J., Cossart, R., Ben-Ari, Y., 2002. Paradoxical anti-epileptic effects of a GluR5 agonist of kainate receptors. *J. Neurophysiol.* 88, 523–527.
- Kidd, F.L., Isaac, J.T., 1999. Developmental and activity-dependent regulation of kainate receptors at thalamocortical synapses. *Nature* 400, 569–573.
- Kleschevnikov, A.M., Belichenko, P.V., Villar, A.J., Epstein, C.J., Malenka, R.C., Mobley, W.C., 2004. Hippocampal long-term potentiation suppressed by increased inhibition in the Ts65Dn mouse, a genetic model of Down syndrome. *J. Neurosci. Off. J. Soc. Neurosci.* 24, 8153–8160.
- Kola, I., Hertzog, P.J., 1998. Down syndrome and mouse models. *Curr. Opin. Genet. Dev.* 8, 316–321.
- Korenberg, J.R., Bradley, C., Disteche, C.M., 1992. Down syndrome: molecular mapping of the congenital heart disease and duodenal stenosis. *Am. J. Hum. Genet.* 50, 294–302.
- Korenberg, J.R., Chen, X.N., Schipper, R., Sun, Z., Gonsky, R., Gerwehr, S., Carpenter, N., Daumer, C., Dignan, P., Disteche, C., 1994. Down syndrome phenotypes: the consequences of chromosomal imbalance. *Proc. Natl. Acad. Sci. U. S. A.* 91, 4997–5001.
- Kullmann, D.M., Moreau, A.W., Bakiri, Y., Nicholson, E., 2012. Plasticity of Inhibition. *Neuron* 75, 951–962.
- Kwon, H.-B., Castillo, P.E., 2008. Role of glutamate autoreceptors at hippocampal mossy fiber synapses. *Neuron* 60, 1082–1094.
- Lancaster, B., Adams, P.R., 1986. Calcium-dependent current generating the afterhyperpolarization of hippocampal neurons. *J. Neurophysiol.* 55, 1268–1282.

- Lanore, F., Labrousse, V.F., Szabo, Z., Normand, E., Blanchet, C., Mulle, C., 2012. Deficits in morphofunctional maturation of hippocampal mossy fiber synapses in a mouse model of intellectual disability. *J. Neurosci. Off. J. Soc. Neurosci.* 32, 17882–17893.
- Lauri, S.E., Bortolotto, Z.A., Nistico, R., Bleakman, D., Ornstein, P.L., Lodge, D., Isaac, J.T.R., Collingridge, G.L., 2003. A role for Ca²⁺ stores in kainate receptor-dependent synaptic facilitation and LTP at mossy fiber synapses in the hippocampus. *Neuron* 39, 327–341.
- Lauri, S.E., Delany, C., J Clarke, V.R., Bortolotto, Z.A., Ornstein, P.L., T R Isaac, J., Collingridge, G.L., 2001. Synaptic activation of a presynaptic kainate receptor facilitates AMPA receptor-mediated synaptic transmission at hippocampal mossy fibre synapses. *Neuropharmacology* 41, 907–915.
- Lauri, S.E., Segerstråle, M., Vesikansa, A., Maingret, F., Mulle, C., Collingridge, G.L., Isaac, J.T.R., Taira, T., 2005. Endogenous activation of kainate receptors regulates glutamate release and network activity in the developing hippocampus. *J. Neurosci. Off. J. Soc. Neurosci.* 25, 4473–4484.
- Lauri, S.E., Vesikansa, A., Segerstråle, M., Collingridge, G.L., Isaac, J.T.R., Taira, T., 2006. Functional maturation of CA1 synapses involves activity-dependent loss of tonic kainate receptor-mediated inhibition of glutamate release. *Neuron* 50, 415–429.
- Lerma, J., 2003. Roles and rules of kainate receptors in synaptic transmission. *Nat. Rev. Neurosci.* 4, 481–495.
- Lerma, J., 2006. Kainate receptor physiology. *Curr. Opin. Pharmacol.* 6, 89–97.
- Lerma, J., Marques, J.M., 2013. Kainate receptors in health and disease. *Neuron* 80, 292–311.
- Lerma, J., Paternain, A.V., Rodríguez-Moreno, A., López-García, J.C., 2001. Molecular physiology of kainate receptors. *Physiol. Rev.* 81, 971–998.
- Lewis, D.A., Hashimoto, T., Volk, D.W., 2005. Cortical inhibitory neurons and schizophrenia. *Nat. Rev. Neurosci.* 6, 312–324.
- Li, H., Rogawski, M.A., 1998. GluR5 kainate receptor mediated synaptic transmission in rat basolateral amygdala in vitro. *Neuropharmacology* 37, 1279–1286.
- Li, P., Wilding, T.J., Kim, S.J., Calejesan, A.A., Huettner, J.E., Zhuo, M., 1999. Kainate-receptor-mediated sensory synaptic transmission in mammalian spinal cord. *Nature* 397, 161–164.
- Lisman, J., Yasuda, R., Raghavachari, S., 2012. Mechanisms of CaMKII action in long-term potentiation. *Nat. Rev. Neurosci.*
- Liu, D.P., Schmidt, C., Billings, T., Davisson, M.T., 2003. Quantitative PCR genotyping assay for the Ts65Dn mouse model of Down syndrome. *BioTechniques* 35, 1170–1174, 1176, 1178 passim.
- Liu, G., 2003. Presynaptic control of quantal size: kinetic mechanisms and implications for synaptic transmission and plasticity. *Curr. Opin. Neurobiol.* 13, 324–331.
- Liu, Q.S., Patrylo, P.R., Gao, X.B., van den Pol, A.N., 1999. Kainate acts at presynaptic receptors to increase GABA release from hypothalamic neurons. *J. Neurophysiol.* 82, 1059–1062.
- Llano, I., Leresche, N., Marty, A., 1991. Calcium entry increases the sensitivity of cerebellar Purkinje cells to applied GABA and decreases inhibitory synaptic currents. *Neuron* 6, 565–574.
- Lockstone, H.E., Harris, L.W., Swatton, J.E., Wayland, M.T., Holland, A.J., Bahn, S., 2007. Gene expression profiling in the adult Down syndrome brain. *Genomics* 90, 647–660.

- Lodge, D.J., Behrens, M.M., Grace, A.A., 2009. A loss of parvalbumin-containing interneurons is associated with diminished oscillatory activity in an animal model of schizophrenia. *J. Neurosci. Off. J. Soc. Neurosci.* 29, 2344–2354.
- Luscher, C., Frerking, M., 2001. Restless AMPA receptors: implications for synaptic transmission and plasticity. *Trends Neurosci.* 24, 665–670.
- Lyle, R., Gehrig, C., Neergaard-Henrichsen, C., Deutsch, S., Antonarakis, S.E., 2004. Gene Expression From the Aneuploid Chromosome in a Trisomy Mouse Model of Down Syndrome. *Genome Res.* 14, 1268–1274.
- Maingret, F., Lauri, S.E., Taira, T., Isaac, J.T.R., 2005. Profound regulation of neonatal CA1 rat hippocampal GABAergic transmission by functionally distinct kainate receptor populations. *J. Physiol.* 567, 131–142.
- Malenka, R.C., Nicoll, R.A., 1999. Long-term potentiation--a decade of progress? *Science* 285, 1870–1874.
- Mameli, M., Lüscher, C., 2011. Synaptic plasticity and addiction: learning mechanisms gone awry. *Neuropharmacology* 61, 1052–1059.
- Mato, S., Lafourcade, M., Robbe, D., Bakiri, Y., Manzoni, O.J., 2008. Role of the cyclic-AMP/PKA cascade and of P/Q-type Ca⁺⁺ channels in endocannabinoid-mediated long-term depression in the nucleus accumbens. *Neuropharmacology* 54, 87–94.
- McGee, A.W., Brecht, D.S., 2003. Assembly and plasticity of the glutamatergic postsynaptic specialization. *Curr. Opin. Neurobiol.* 13, 111–118.
- Meldrum, B.S., 2000. Glutamate as a neurotransmitter in the brain: review of physiology and pathology. *J. Nutr.* 130, 1007S–15S.
- Melyan, Z., Lancaster, B., Wheal, H.V., 2004. Metabotropic regulation of intrinsic excitability by synaptic activation of kainate receptors. *J. Neurosci. Off. J. Soc. Neurosci.* 24, 4530–4534.
- Melyan, Z., Wheal, H.V., Lancaster, B., 2002. Metabotropic-mediated kainate receptor regulation of IsAHP and excitability in pyramidal cells. *Neuron* 34, 107–114.
- Mody, I., 1998. Interneurons and the ghost of the sea. *Nat. Neurosci.* 1, 434–436.
- More, J.C.A., Nistico, R., Dolman, N.P., Clarke, V.R.J., Alt, A.J., Ogden, A.M., Buelens, F.P., Troop, H.M., Kelland, E.E., Pilato, F., Bleakman, D., Bortolotto, Z.A., Collingridge, G.L., Jane, D.E., 2004. Characterisation of UBP296: a novel, potent and selective kainate receptor antagonist. *Neuropharmacology* 47, 46–64.
- Morris, R.G., Frey, U., 1997. Hippocampal synaptic plasticity: role in spatial learning or the automatic recording of attended experience? *Philos. Trans. R. Soc. Lond. B. Biol. Sci.* 352, 1489–1503.
- Motazacker, M.M., Rost, B.R., Hucho, T., Garshasbi, M., Kahrizi, K., Ullmann, R., Abedini, S.S., Nieh, S.E., Amini, S.H., Goswami, C., Tzschach, A., Jensen, L.R., Schmitz, D., Ropers, H.H., Najmabadi, H., Kuss, A.W., 2007b. A defect in the ionotropic glutamate receptor 6 gene (GRIK2) is associated with autosomal recessive mental retardation. *Am. J. Hum. Genet.* 81, 792–798.
- Mulle, C., Sailer, A., Pérez-Otaño, I., Dickinson-Anson, H., Castillo, P.E., Bureau, I., Maron, C., Gage, F.H., Mann, J.R., Bettler, B., Heinemann, S.F., 1998. Altered synaptic physiology and reduced susceptibility to kainate-induced seizures in GluR6-deficient mice. *Nature* 392, 601–605.
- Mulle, C., Sailer, A., Swanson, G.T., Brana, C., O’Gorman, S., Bettler, B., Heinemann, S.F., 2000. Subunit composition of kainate receptors in hippocampal interneurons. *Neuron* 28, 475–484.

- Negrete-Díaz, J.V., Sihra, T.S., Delgado-García, J.M., Rodríguez-Moreno, A., 2006. Kainate receptor-mediated inhibition of glutamate release involves protein kinase A in the mouse hippocampus. *J. Neurophysiol.* 96, 1829–1837.
- Nicoll, R.A., Kauer, J.A., Malenka, R.C., 1988. The current excitement in long-term potentiation. *Neuron* 1, 97–103.
- Nicoll, R.A., Schmitz, D., 2005. Synaptic plasticity at hippocampal mossy fibre synapses. *Nat. Rev. Neurosci.* 6, 863–876.
- Nowak, L., Bregestovski, P., Ascher, P., Herbet, A., Prochiantz, A., 1984. Magnesium gates glutamate-activated channels in mouse central neurones. *Nature* 307, 462–465.
- O'Doherty, A., Ruf, S., Mulligan, C., Hildreth, V., Errington, M.L., Cooke, S., Sesay, A., Modino, S., Vanes, L., Hernandez, D., Linehan, J.M., Sharpe, P.T., Brandner, S., Bliss, T.V.P., Henderson, D.J., Nizetic, D., Tybulewicz, V.L.J., Fisher, E.M.C., 2005. An aneuploid mouse strain carrying human chromosome 21 with Down syndrome phenotypes. *Science* 309, 2033–2037.
- O'Neill, M.J., Bond, A., Ornstein, P.L., Ward, M.A., Hicks, C.A., Hoo, K., Bleakman, D., Lodge, D., 1998. Decahydroisoquinolines: novel competitive AMPA/kainate antagonists with neuroprotective effects in global cerebral ischaemia. *Neuropharmacology* 37, 1211–1222.
- Olson, L.E., Roper, R.J., Sengstaken, C.L., Peterson, E.A., Aquino, V., Galdzicki, Z., Siarey, R., Pletnikov, M., Moran, T.H., Reeves, R.H., 2007. Trisomy for the Down syndrome “critical region” is necessary but not sufficient for brain phenotypes of trisomic mice. *Hum. Mol. Genet.* 16, 774–782.
- Orth, A., Tapken, D., Hollmann, M., 2013. The delta subfamily of glutamate receptors: characterization of receptor chimeras and mutants. *Eur. J. Neurosci.* 37, 1620–1630.
- Paddock, S., Laje, G., Charney, D., Rush, A.J., Wilson, A.F., Sorant, A.J.M., Lipsky, R., Wisniewski, S.R., Manji, H., McMahon, F.J., 2007. Association of GRIK4 with outcome of antidepressant treatment in the STAR*D cohort. *Am. J. Psychiatry* 164, 1181–1188.
- Palecek, J., Neugebauer, V., Carlton, S.M., Iyengar, S., Willis, W.D., 2004. The effect of a kainate GluR5 receptor antagonist on responses of spinothalamic tract neurons in a model of peripheral neuropathy in primates. *Pain* 111, 151–161.
- Paternain, A.V., Herrera, M.T., Nieto, M.A., Lerma, J., 2000. GluR5 and GluR6 kainate receptor subunits coexist in hippocampal neurons and coassemble to form functional receptors. *J. Neurosci. Off. J. Soc. Neurosci.* 20, 196–205.
- Paternain, A.V., Morales, M., Lerma, J., 1995. Selective antagonism of AMPA receptors unmasks kainate receptor-mediated responses in hippocampal neurons. *Neuron* 14, 185–189.
- Perkinton, M.S., Sihra, T.S., 1999. A high-affinity presynaptic kainate-type glutamate receptor facilitates glutamate exocytosis from cerebral cortex nerve terminals (synaptosomes). *Neuroscience* 90, 1281–1292.
- Phillips, K.G., Cotel, M.C., McCarthy, A.P., Edgar, D.M., Tricklebank, M., O'Neill, M.J., Jones, M.W., Wafford, K.A., 2012. Differential effects of NMDA antagonists on high frequency and gamma EEG oscillations in a neurodevelopmental model of schizophrenia. *Neuropharmacology* 62, 1359–1370.
- Pickard, B.S., Malloy, M.P., Christoforou, A., Thomson, P.A., Evans, K.L., Morris, S.W., Hampson, M., Porteous, D.J., Blackwood, D.H.R., Muir, W.J., 2006. Cytogenetic and genetic evidence supports a role for the kainate-type glutamate receptor gene, GRIK4, in schizophrenia and bipolar disorder. *Mol. Psychiatry* 11, 847–857.

- Pinheiro, P.S., Lanore, F., Veran, J., Artinian, J., Blanchet, C., Crépel, V., Perrais, D., Mulle, C., 2013. Selective block of postsynaptic kainate receptors reveals their function at hippocampal mossy fiber synapses. *Cereb. Cortex N. Y. N* 1991 23, 323–331.
- Pinheiro, P.S., Perrais, D., Coussen, F., Barhanin, J., Bettler, B., Mann, J.R., Malva, J.O., Heinemann, S.F., Mulle, C., 2007. GluR7 is an essential subunit of presynaptic kainate autoreceptors at hippocampal mossy fiber synapses. *Proc. Natl. Acad. Sci. U. S. A.* 104, 12181–12186.
- Pinter, J.D., Brown, W.E., Eliez, S., Schmitt, J.E., Capone, G.T., Reiss, A.L., 2001. Amygdala and hippocampal volumes in children with Down syndrome: a high-resolution MRI study. *Neurology* 56, 972–974.
- Prandini, P., Deutsch, S., Lyle, R., Gagnebin, M., Vivier, C.D., Delorenzi, M., Gehrig, C., Descombes, P., Sherman, S., Bricarelli, F.D., Baldo, C., Novelli, A., Dallapiccola, B., Antonarakis, S.E., 2007. Natural Gene-Expression Variation in Down Syndrome Modulates the Outcome of Gene-Dosage Imbalance. *Am. J. Hum. Genet.* 81, 252–263.
- Pulido, O.M., 2008. Domoic Acid Toxicologic Pathology: A Review. *Mar. Drugs* 6, 180–219.
- Rachidi, M., Lopes, C., 2007. Mental retardation in Down syndrome: from gene dosage imbalance to molecular and cellular mechanisms. *Neurosci. Res.* 59, 349–369.
- Rodríguez-Moreno, A., Herreras, O., Lerma, J., 1997. Kainate receptors presynaptically downregulate GABAergic inhibition in the rat hippocampus. *Neuron* 19, 893–901.
- Rodríguez-Moreno, A., Lerma, J., 1998. Kainate receptor modulation of GABA release involves a metabotropic function. *Neuron* 20, 1211–1218.
- Rodríguez-Moreno, A., Sistiaga, A., Lerma, J., Sánchez-Prieto, J., 1998. Switch from facilitation to inhibition of excitatory synaptic transmission by group I mGluR desensitization. *Neuron* 21, 1477–1486.
- Roizen, N.J., Patterson, D., 2003. Down's syndrome. *Lancet* 361, 1281–1289.
- Romano, C., Yang, W.L., O'Malley, K.L., 1996. Metabotropic glutamate receptor 5 is a disulfide-linked dimer. *J. Biol. Chem.* 271, 28612–28616.
- Rosenmund, C., Stern-Bach, Y., Stevens, C.F., 1998. The tetrameric structure of a glutamate receptor channel. *Science* 280, 1596–1599.
- Rowe, J., Lavender, A., Turk, V., 2006. Cognitive executive function in Down's syndrome. *Br. J. Clin. Psychol. Br. Psychol. Soc.* 45, 5–17.
- Rozas, J.L., Paternain, A.V., Lerma, J., 2003. Noncanonical signaling by ionotropic kainate receptors. *Neuron* 39, 543–553.
- Ruiz, A., Sachidhanandam, S., Utvik, J.K., Coussen, F., Mulle, C., 2005. Distinct subunits in heteromeric kainate receptors mediate ionotropic and metabotropic function at hippocampal mossy fiber synapses. *J. Neurosci. Off. J. Soc. Neurosci.* 25, 11710–11718.
- Sago, H., Carlson, E.J., Smith, D.J., Kilbridge, J., Rubin, E.M., Mobley, W.C., Epstein, C.J., Huang, T.T., 1998. Ts1Cje, a partial trisomy 16 mouse model for Down syndrome, exhibits learning and behavioral abnormalities. *Proc. Natl. Acad. Sci. U. S. A.* 95, 6256–6261.
- Sago, H., Carlson, E.J., Smith, D.J., Rubin, E.M., Crnic, L.S., Huang, T.T., Epstein, C.J., 2000. Genetic dissection of region associated with behavioral abnormalities in mouse models for Down syndrome. *Pediatr. Res.* 48, 606–613.
- Sakimura, K., Morita, T., Kushiya, E., Mishina, M., 1992. Primary structure and expression of the gamma 2 subunit of the glutamate receptor channel selective for kainate. *Neuron* 8, 267–274.

- Salehi, A., Delcroix, J.-D., Belichenko, P.V., Zhan, K., Wu, C., Valletta, J.S., Takimoto-Kimura, R., Kleschevnikov, A.M., Sambamurti, K., Chung, P.P., Xia, W., Villar, A., Campbell, W.A., Kulnane, L.S., Nixon, R.A., Lamb, B.T., Epstein, C.J., Stokin, G.B., Goldstein, L.S.B., Mobley, W.C., 2006. Increased App expression in a mouse model of Down's syndrome disrupts NGF transport and causes cholinergic neuron degeneration. *Neuron* 51, 29–42.
- Sallert, M., Malkki, H., Segerstråle, M., Taira, T., Lauri, S.E., 2007. Effects of the kainate receptor agonist ATPA on glutamatergic synaptic transmission and plasticity during early postnatal development. *Neuropharmacology* 52, 1354–1365.
- Salmen, B., Beed, P.S., Ozdogan, T., Maier, N., Johenning, F.W., Winterer, J., Breustedt, J., Schmitz, D., 2012. GluK1 inhibits calcium dependent and independent transmitter release at associational/commissural synapses in area CA3 of the hippocampus. *Hippocampus* 22, 57–68.
- Sang, C.N., Ramadan, N.M., Wallihan, R.G., Chappell, A.S., Freitag, F.G., Smith, T.R., Silberstein, S.D., Johnson, K.W., Phebus, L.A., Bleakman, D., Ornstein, P.L., Arnold, B., Tepper, S.J., Vandenhende, F., 2004. LY293558, a novel AMPA/GluR5 antagonist, is efficacious and well-tolerated in acute migraine. *Cephalalgia Int. J. Headache* 24, 596–602.
- Schiffer, H.H., Swanson, G.T., Heinemann, S.F., 1997. Rat GluR7 and a carboxy-terminal splice variant, GluR7b, are functional kainate receptor subunits with a low sensitivity to glutamate. *Neuron* 19, 1141–1146.
- Schmitz, D., Frerking, M., Nicoll, R.A., 2000. Synaptic activation of presynaptic kainate receptors on hippocampal mossy fiber synapses. *Neuron* 27, 327–338.
- Schmitz, D., Mellor, J., Nicoll, R.A., 2001. Presynaptic kainate receptor mediation of frequency facilitation at hippocampal mossy fiber synapses. *Science* 291, 1972–1976.
- Scott, R., Lalic, T., Kullmann, D.M., Capogna, M., Rusakov, D.A., 2008. Target-cell specificity of kainate autoreceptor and Ca²⁺-store-dependent short-term plasticity at hippocampal mossy fiber synapses. *J. Neurosci. Off. J. Soc. Neurosci.* 28, 13139–13149.
- Scoville, W.B., Milner, B., 2000. Loss of recent memory after bilateral hippocampal lesions. 1957. *J. Neuropsychiatry Clin. Neurosci.* 12, 103–113.
- Seo, H., Isacson, O., 2005. Abnormal APP, cholinergic and cognitive function in Ts65Dn Down's model mice. *Exp. Neurol.* 193, 469–480.
- Shi, S.H., Hayashi, Y., Petralia, R.S., Zaman, S.H., Wenthold, R.J., Svoboda, K., Malinow, R., 1999. Rapid spine delivery and redistribution of AMPA receptors after synaptic NMDA receptor activation. *Science* 284, 1811–1816.
- Shinohara, T., Tomizuka, K., Miyabara, S., Takehara, S., Kazuki, Y., Inoue, J., Katoh, M., Nakane, H., Iino, A., Ohguma, A., Ikegami, S., Inokuchi, K., Ishida, I., Reeves, R.H., Oshimura, M., 2001. Mice containing a human chromosome 21 model behavioral impairment and cardiac anomalies of Down's syndrome. *Hum. Mol. Genet.* 10, 1163–1175.
- Siarey, R.J., Carlson, E.J., Epstein, C.J., Balbo, A., Rapoport, S.I., Galdzicki, Z., 1999. Increased synaptic depression in the Ts65Dn mouse, a model for mental retardation in Down syndrome. *Neuropharmacology* 38, 1917–1920.
- Siarey, R.J., Kline-Burgess, A., Cho, M., Balbo, A., Best, T.K., Harashima, C., Klann, E., Galdzicki, Z., 2006. Altered signaling pathways underlying abnormal hippocampal synaptic plasticity in the Ts65Dn mouse model of Down syndrome. *J. Neurochem.* 98, 1266–1277.

- Siarey, R.J., Stoll, J., Rapoport, S.I., Galdzicki, Z., 1997. Altered long-term potentiation in the young and old Ts65Dn mouse, a model for Down Syndrome. *Neuropharmacology* 36, 1549–1554.
- Simmons, R.M., Li, D.L., Hoo, K.H., Deverill, M., Ornstein, P.L., Iyengar, S., 1998. Kainate GluR5 receptor subtype mediates the nociceptive response to formalin in the rat. *Neuropharmacology* 37, 25–36.
- Smolders, I., Bortolotto, Z.A., Clarke, V.R.J., Warre, R., Khan, G.M., O'Neill, M.J., Ornstein, P.L., Bleakman, D., Ogden, A., Weiss, B., Stables, J.P., Ho, K.H., Ebinger, G., Collingridge, G.L., Lodge, D., Michotte, Y., 2002. Antagonists of GLU(K5)-containing kainate receptors prevent pilocarpine-induced limbic seizures. *Nat. Neurosci.* 5, 796–804.
- Stafstrom, C.E., 1993. Epilepsy in Down syndrome: clinical aspects and possible mechanisms. *Am. J. Ment. Retard. AJMR* 98 Suppl, 12–26.
- Swanson, G.T., Feldmeyer, D., Kaneda, M., Cull-Candy, S.G., 1996. Effect of RNA editing and subunit co-assembly single-channel properties of recombinant kainate receptors. *J. Physiol.* 492 (Pt 1), 129–142.
- Swanson, G.T., Green, T., Sakai, R., Contractor, A., Che, W., Kamiya, H., Heinemann, S.F., 2002. Differential Activation of Individual Subunits in Heteromeric Kainate Receptors. *Neuron* 34, 589–598.
- Ulrich, D.A., Ulrich, B.D., Angulo-Kinzler, R.M., Yun, J., 2001. Treadmill training of infants with Down syndrome: evidence-based developmental outcomes. *Pediatrics* 108, E84.
- Vaillend, C., Poirier, R., Laroche, S., 2008. Genes, plasticity and mental retardation. *Behav. Brain Res.* 192, 88–105.
- Vignes, M., Clarke, V.R., Parry, M.J., Bleakman, D., Lodge, D., Ornstein, P.L., Collingridge, G.L., 1998. The GluR5 subtype of kainate receptor regulates excitatory synaptic transmission in areas CA1 and CA3 of the rat hippocampus. *Neuropharmacology* 37, 1269–1277.
- Vignes, M., Collingridge, G.L., 1997. The synaptic activation of kainate receptors. *Nature* 388, 179–182.
- Villar, A.J., Belichenko, P.V., Gillespie, A.M., Kozy, H.M., Mobley, W.C., Epstein, C.J., 2005. Identification and characterization of a new Down syndrome model, Ts[Rb(12.1716)]2Cje, resulting from a spontaneous Robertsonian fusion between T(171)65Dn and mouse chromosome 12. *Mamm. Genome Off. J. Int. Mamm. Genome Soc.* 16, 79–90.
- Walker, J.C., Dosen, A., Buitelaar, J.K., Janzing, J.G.E., 2011. Depression in Down syndrome: a review of the literature. *Res. Dev. Disabil.* 32, 1432–1440.
- Woo, T.-U.W., Shrestha, K., Amstrong, C., Minns, M.M., Walsh, J.P., Benes, F.M., 2007. Differential alterations of kainate receptor subunits in inhibitory interneurons in the anterior cingulate cortex in schizophrenia and bipolar disorder. *Schizophr. Res.* 96, 46–61.
- Woodin, M.A., Ganguly, K., Poo, M., 2003. Coincident pre- and postsynaptic activity modifies GABAergic synapses by postsynaptic changes in Cl⁻ transporter activity. *Neuron* 39, 807–820.
- Yoon, P.W., Freeman, S.B., Sherman, S.L., Taft, L.F., Gu, Y., Pettay, D., Flanders, W.D., Khoury, M.J., Hassold, T.J., 1996. Advanced maternal age and the risk of Down syndrome characterized by the meiotic stage of chromosomal error: a population-based study. *Am. J. Hum. Genet.* 58, 628–633.
- Yuzaki, M., 2003. The delta2 glutamate receptor: 10 years later. *Neurosci. Res.* 46, 11–22.

Zucker, R.S., 1989. Short-term synaptic plasticity. *Annu. Rev. Neurosci.* 12, 13–31.

Zucker, R.S., Regehr, W.G., 2002. Short-term synaptic plasticity. *Annu. Rev. Physiol.* 64, 355–405.





APPENDIX



Eli Lilly and Company

Erl Wood Manor
Surrey, United Kingdom

Title of the project:

**Characterizing abnormal network
activity in a rat model of Schizophrenia**



Supervised by:

Dr. Keith G. Phillips

Six months private internship report

From April to September 2013

1. Introduction

How does the brain control behavior? This is an important question in neuroscience. One of the main functions of the brain is its capacity to promote behavioral adaptation according to internal or environmental cues. This function is, in part, sustained by learning and memory processes that are supported by specific cellular and molecular mechanisms within dedicated neuronal circuits. In contrast to a quite detailed understanding of these mechanisms, the involvement of specific neuronal circuits deregulations in the non-adapted behavior observed in pathological cases, like Schizophrenia are poorly understood.

The proper functioning of CNS is dependent on the communication ability of the different entities composing its network. Communications have to be clear within and between the different structures of the brain to ensure that the individual have an adapted behaviour.

Classically the core element involved in the signal transmission within a neural network is the “neuron”. The neuron does not function in isolation. Whatever its type a neuron is always an electrically excitable cell that processes and transmits information through electrical and chemical signals to another neuron. These signals between neurons occur via specialized connections with other cells, the “synapses”. One neuron can be highly connected to others, as it is the case in the Hippocampus. In this structure neurons from the CA3-CA1 system belong to a strongly connected network (figure 56) (Wittner et al., 2006). For example one CA3 can have a half meter of axon and more than 40 000 presynaptic boutons that are all putative contacts. One pyramidal cell can access almost all the others within the structure.

However cells are only connected to each other via one unique synapse. Thus only one cell cannot stimulate its partner enough to make it fire. Neurons need to come together and generate cell assemblies to activate their targets. Neuronal oscillations are thought to provide this synchronized activity. In order to work together, in “phase”, neurons involved in a network need to be rhythmically activated and inhibited. “Phase synchronisation” (PS) between different brain regions have a pivotal role in supporting neural communication and plasticity involved in memory processes (figure 57) (Fell and Axmacher, 2011). During a working memory related task, like memorizing a telephone

number, communications are established between material-specific storage systems (hippocampus; HPC) and attentional executive center (prefrontal cortex; PFC).

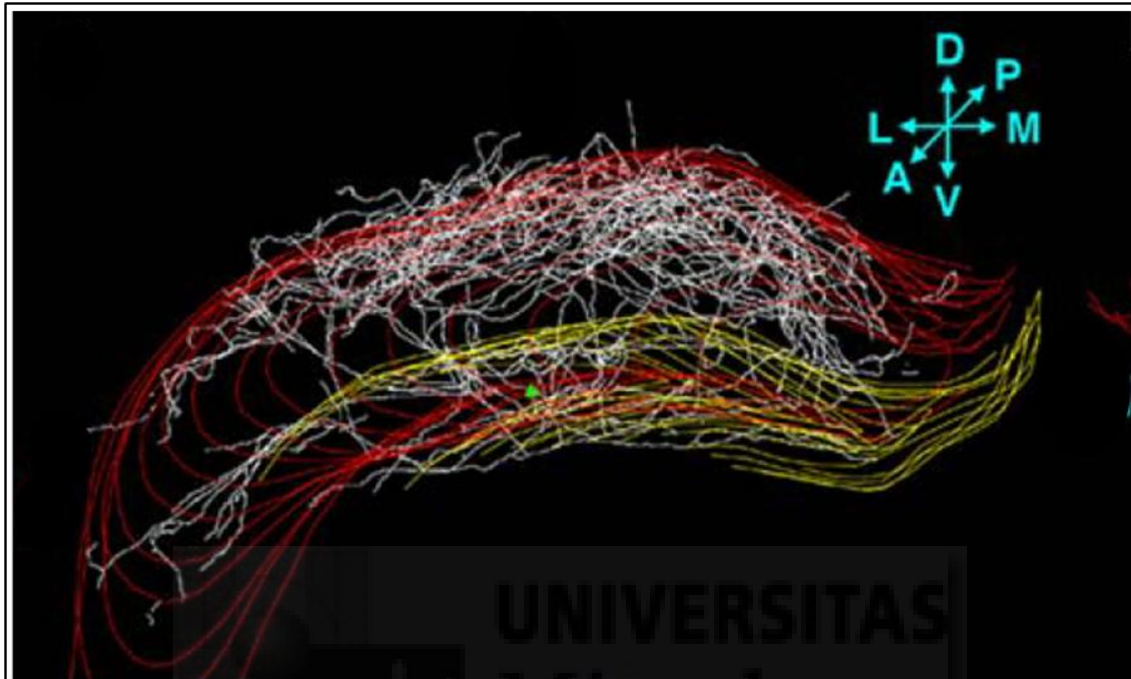


Figure 56: NeuroLucida reconstruction of the CA3 pyramidal cell. Coronal view of the entire axon arbor. Green triangle shows the location of the cell body, the axons are white, the dentate granule cell layer is marked with yellow line, CA1-3 pyramidal cell layer with red line. D dorsal, V ventral, L lateral, M medial, A anterior, P posterior (*adapted from Wittner et al, 2007*).

Some human scalp EEG recordings made during working memory task, revealed theta synchronization (4 to 12Hz) between temporal lobe (HPC) and PFC (figure 58A). It has also been reported that in rats, similar mechanism of synchrony between CA1 and CA3 hippocampus region can be observed during a ‘delayed alternate choice task’ (figure 58B) (Fell and Axmacher, 2011).

Another study recoding simultaneously intracellular and extracellular dynamics in the area CA1 of the hippocampus revealed that theta oscillations recorded in the structure underlie intracellular primary features of firing rate and temporal codes (Harvey et al., 2009). Thus individual cell activity is dependent on the activity of the neuronal assembly where it belongs. On a larger scale, during working memory dependent task, the phase synchronization of neural assemblies can coordinates the timing of synaptic inputs to a common target region. Some studies went further and recorded

simultaneously the activity of medial PFC (mPFC; (Ongür and Price, 2000)) and HPC involved in learning and memory during an alternation task in rats. Note that the mPFC in rodents is homologous to dorsolateral PFC in primates. This works demonstrated that at choice point (when the animal has to decide which side to go in the maze), there was a coherence peak between mPFC and HPC.

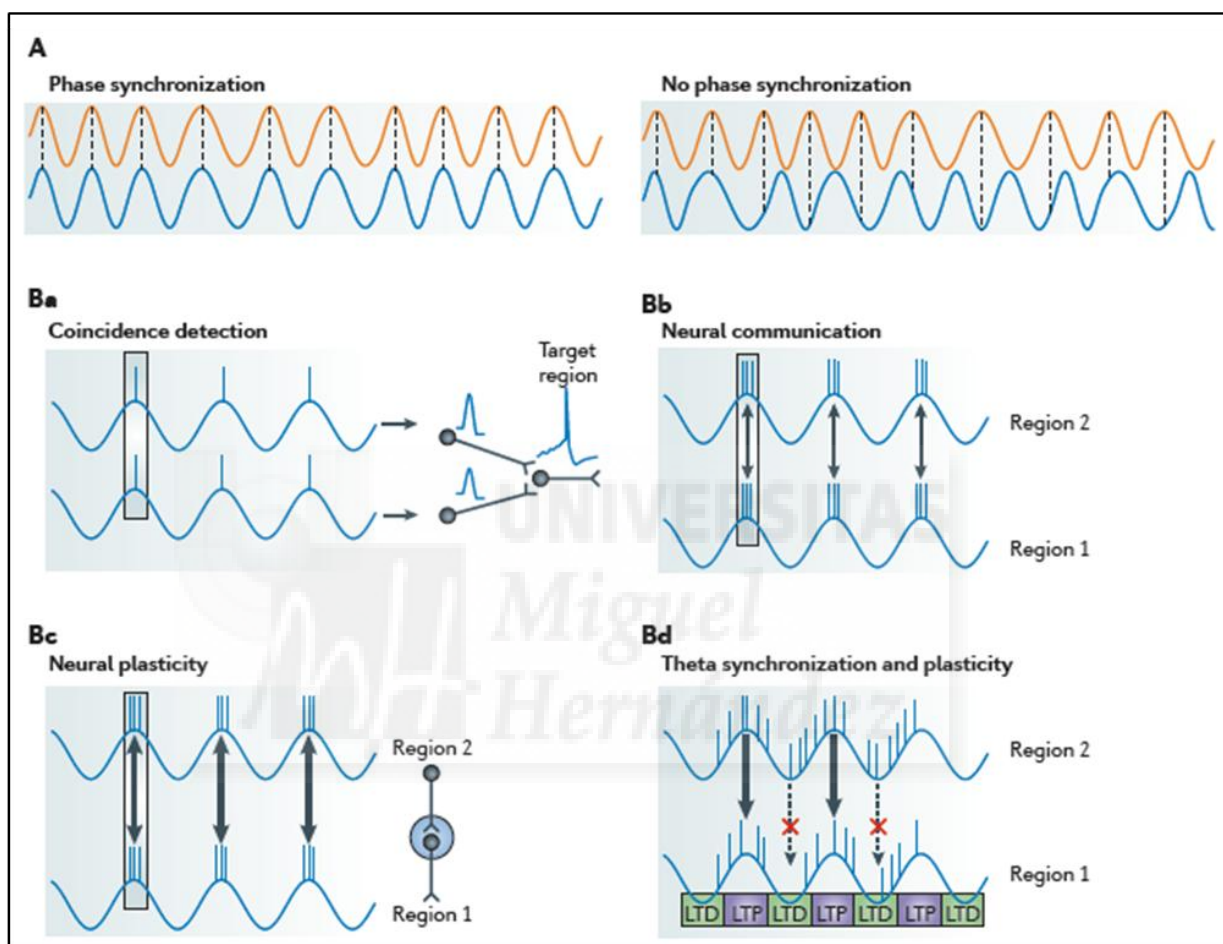


Figure 57: Putative functions of PS. (A) Neural oscillations may show PS (left; stable phase relationships) or may show no PS (right; variable phase relationships). (B) Blue curves represent oscillations of neural assemblies in two brain regions, arrows denote interregional information transfer. (Ba) PS coordinates the timing of synaptic inputs to a common target region. Coincident activity thus reliably induces action potential (AP). (Bb) PS between multiple brain regions allows for efficient information transfer during excitable periods. (Bc) Precise timing of AP resulting from PS between two regions can induce spike timing-dependent plasticity of the synaptic connections between these regions. Consequently, communication is facilitated further. (Bd) The putative function of theta PS between two regions. The propensity of AP that are propagated from region 2 to region 1 to induce synaptic plasticity in region 1 depends on the theta phase in region 1 during which the AP arrive. Therefore, PS in the theta range may serve to recruit memory-related regions (for example, the hippocampus) during periods of high susceptibility to synaptic potentiation (solid arrows). LTD, long-term depression; LTP, long-term potentiation (adapted from Fell et Axmacher 2011).

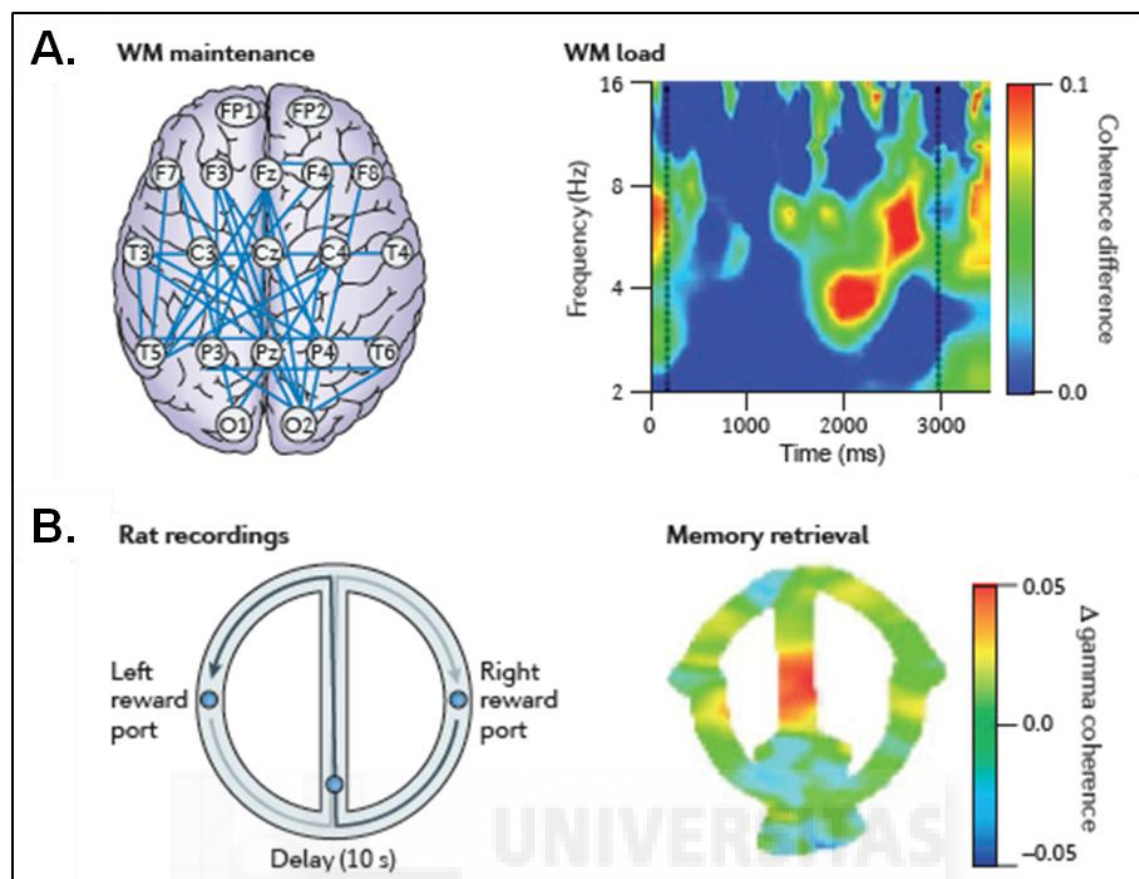


Figure 58: Patterns of phase synchronization during working and long-term memory. **(A)** Theta coherence between brain regions. In the left panel, the blue lines are based on data from scalp electroencephalography (EEG) recordings and reflect changes in inter-regional coherence during a working memory (WM) task compared with a control task. The middle panel shows that fronto-temporal EEG coherence in scalp EEG data increases further when memory load is enhanced. The figure shows the difference in coherence between the 6 versus 4 letter conditions, with warm and cold colours indicating increases and decreases in coherence, respectively. Increases were most obvious at 4 Hz and ~2000 ms and at ~6 Hz and ~2500 ms after stimulus presentation. This increase in theta coherence may be related to the recruitment by the frontal cortex of synaptic plasticity in the temporal lobe at appropriate theta phases, inducing LTP rather than LTD. **(B)** The left panel shows a spatial memory task in which rats alternate left and right turns in each trial at the junction point of a modified T-maze to retrieve a reward. In this ‘delayed alternate choice task’, intrahippocampal gamma coherence between CA1 and CA3 was elevated just before rats reached the decision point (indicated by the warm colour on the central arm), when they presumably used previously acquired information to determine in which direction to turn (right panel). Mechanistically, this increase in coherence may facilitate neural communication and plasticity between CA1 and CA3 (*adapted from Fell and Axmacher 2011*).

Simultaneously, mPFC pyramidal neurons reorganized their preferred firing phase, with higher firing rates during the hippocampal theta trough, and synchronous cell assemblies emerged (figure 59) (Benchenane et al., 2010; Jones and Wilson, 2005). Authors hypothesized that this synchronous state could result from increased inhibition

exert by interneurons onto pyramidal cells. Considering all these results, phase synchronization between the different involved structures is at the origin of the apparition of an adapted behaviour. In pathological conditions, like during schizophrenia, the quality of these mechanisms could be impaired and responsible of the disease symptoms.

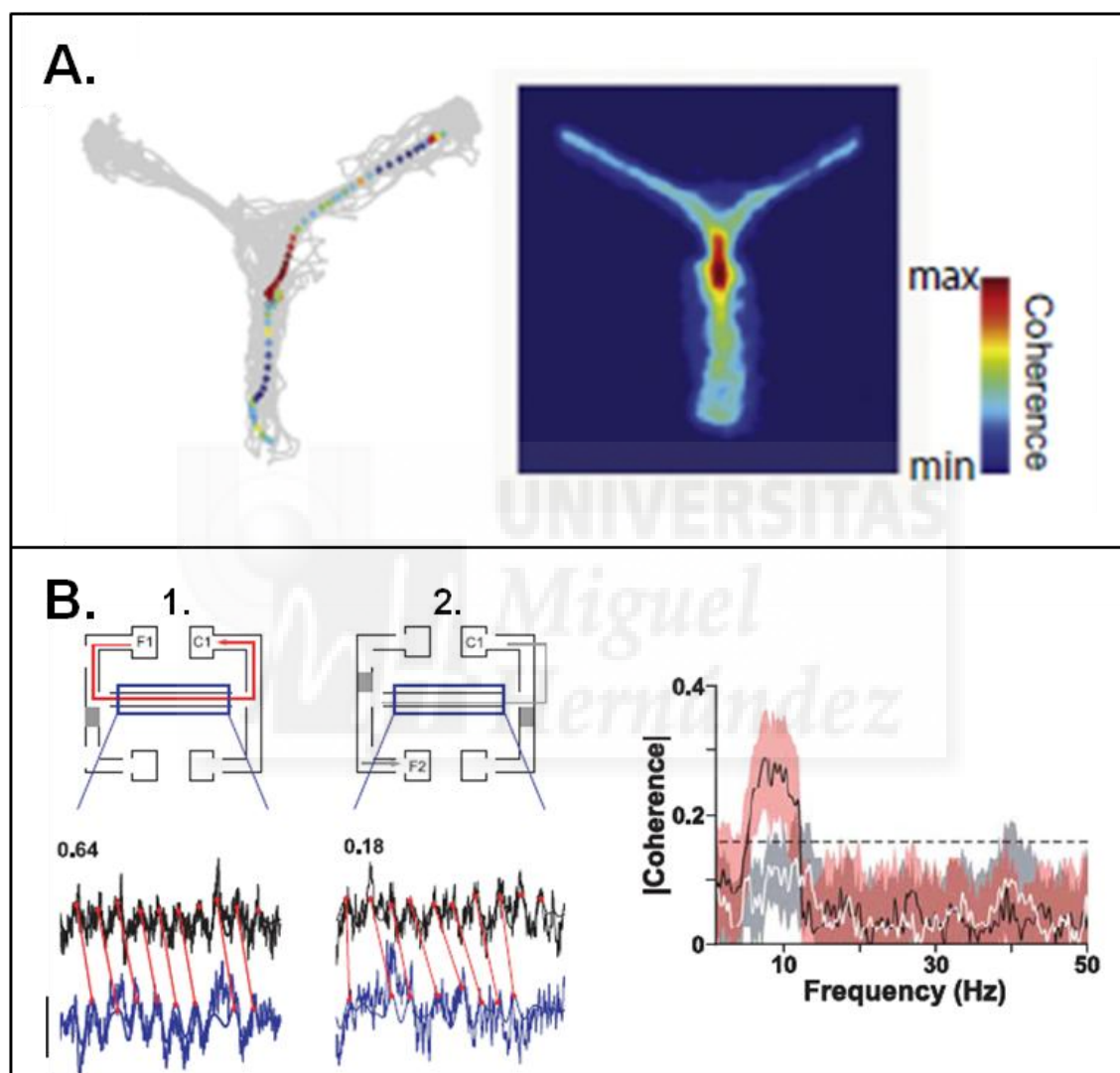


Figure 59: (A) (left panel) Instantaneous HPC-mPFC theta coherence (color coded) for one trial (overhead view). Each color point represents the average value over a 100 ms sample. (right panel) “Coherence map” average HPC-PFC theta coherence recorded at each point on the maze (*adapted from Benchenane et al, 2010*). (B) (left panel) Raw LFP from dorsal CA1 (black) and mPFC (blue) during consecutive single central-arm crossings in the choice (1) and forced-turn (2) directions. Thick lines show theta-filtered LFP. Red lines highlight the timing relationship between CA1 and mPFC theta peaks. Numbers above raw LFP traces give coherence in the theta range during these two example trials. (right panel) Trial-averaged, central-arm coherence during a single run-session. Central-arm coherence is subdivided into forced-turn (grey) and choice (red) directions. Significant coherence was seen only in the theta-frequency range, and only during choice epochs on the central arm (*adapted from Jones and Wilson, 2005*).

Schizophrenia is a mental disorder characterized by a breakdown of thought processes and by impaired emotional responses. Common symptoms include delusions (such as paranoid beliefs); hallucinations; disorganized thinking; and negative symptoms, such as blunted affect and avolition. Schizophrenia causes significant social and vocational dysfunction. Symptom onset typically occurs in young adulthood. Diagnosis is based on observed behaviour and the person's reported experiences. Schizophrenia is probably a neurodevelopmental disorder with evidence of brain changes before clinical onset. This hypothesis is supported by the behavioural and intellectual abnormalities observed in children who later developed schizophrenia. Anatomically some changes have been observed in patients, like an enlargement of the ventricles, a decrease of the cerebral cortex volume due to a loss of neuronal processes, a diminution of grey matter part. For example, they reported a consistent and significant reduction in the number of dendritic spines on pyramidal neurons of which soma is in layer III (involved in cortico-cortical connectivity). The greatest reduction was observed in temporal and frontal association cortex. Overall there seems to be a loss of cerebral tissue (for review Garey, 2010). A study from 2006, also pointed out a dysfunction in the coordination of the distributed neural activity in schizophrenic patients (Uhlhaas et al., 2006). They compared the synchronization of neural responses (EEG recordings) from schizophrenic to the ones of healthy control subjects during a perception task. And they observed that the deficit in perception exhibited by schizophrenic patients was associated with reduced phase synchrony in the beta-band. This result revealed a core deficit in coordination of the neural activity that could underlie specific cognitive dysfunctions associated with schizophrenia (figure 60) (Uhlhaas et al., 2006). In order to understand the observed deficit in phase synchrony in schizophrenic patient and determine if it can be related to the illness aetiology, some animal models have been developed, *Df(16)A*^{+/-} mouse is one of them. It reproduces a microdeletion on human chromosome 22 (22q11.2) that constitutes one of the largest known genetic risk factors for schizophrenia. *Df(16)A*^{+/-} mice present a microdeletion in the region of MMU16 syntenic to the core 1.5Mb microdeletion found in patients with schizophrenia (Stark et al., 2008). These animals exhibit strong working memory impairment. In 2010, Sigurdsson and colleagues, measured synchronization of neural activity between the HPC and the mPFC during a working memory-related task. First in WT animals, they recorded an increase HPC-mPFC synchrony after learning period and that PFC cells firing was locked to HPC theta oscillations.

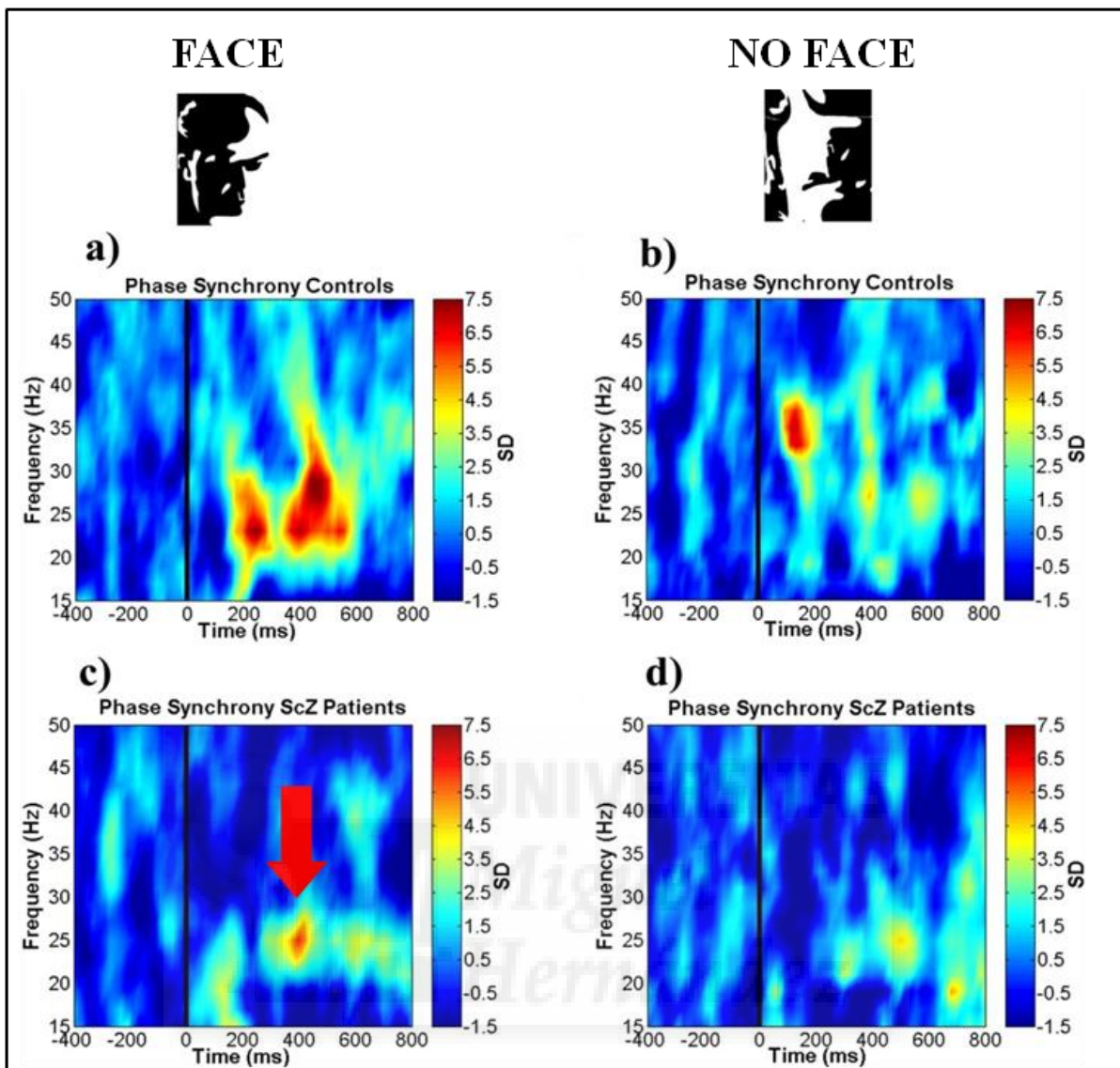


Figure 60: Group average of phase synchrony for all EEG electrodes and correct trials during a Gestalt perception test. **(a)** Face condition for controls, normal synchrony levels. **(b)** No-face condition for controls, levels of synchrony are decreased. **(c)** Face condition for patients with schizophrenia, compare to control patient the level of synchrony is clearly diminished (red arrow) **(d)** No-face condition for patients with schizophrenia, almost no synchrony (*adapted from Uhlhass et al, 2006*).

Then, in accord to what have been observed in schizophrenic patients, their results pointed out a diminution of HPC-PFC synchrony in $Df(16)A^{+/-}$ compare to WT (figure 61) (Sigurdsson et al., 2010). Here again the authors suggested that an increase in HPC-mPFC synchrony during learning enables animals to acquire the working memory task successfully. Whereas the synchronization alterations reported in $Df(16)A^{+/-}$ could be link to a connectivity issue between HPC and PFC that could explain the decreased performance exhibited by these animals.

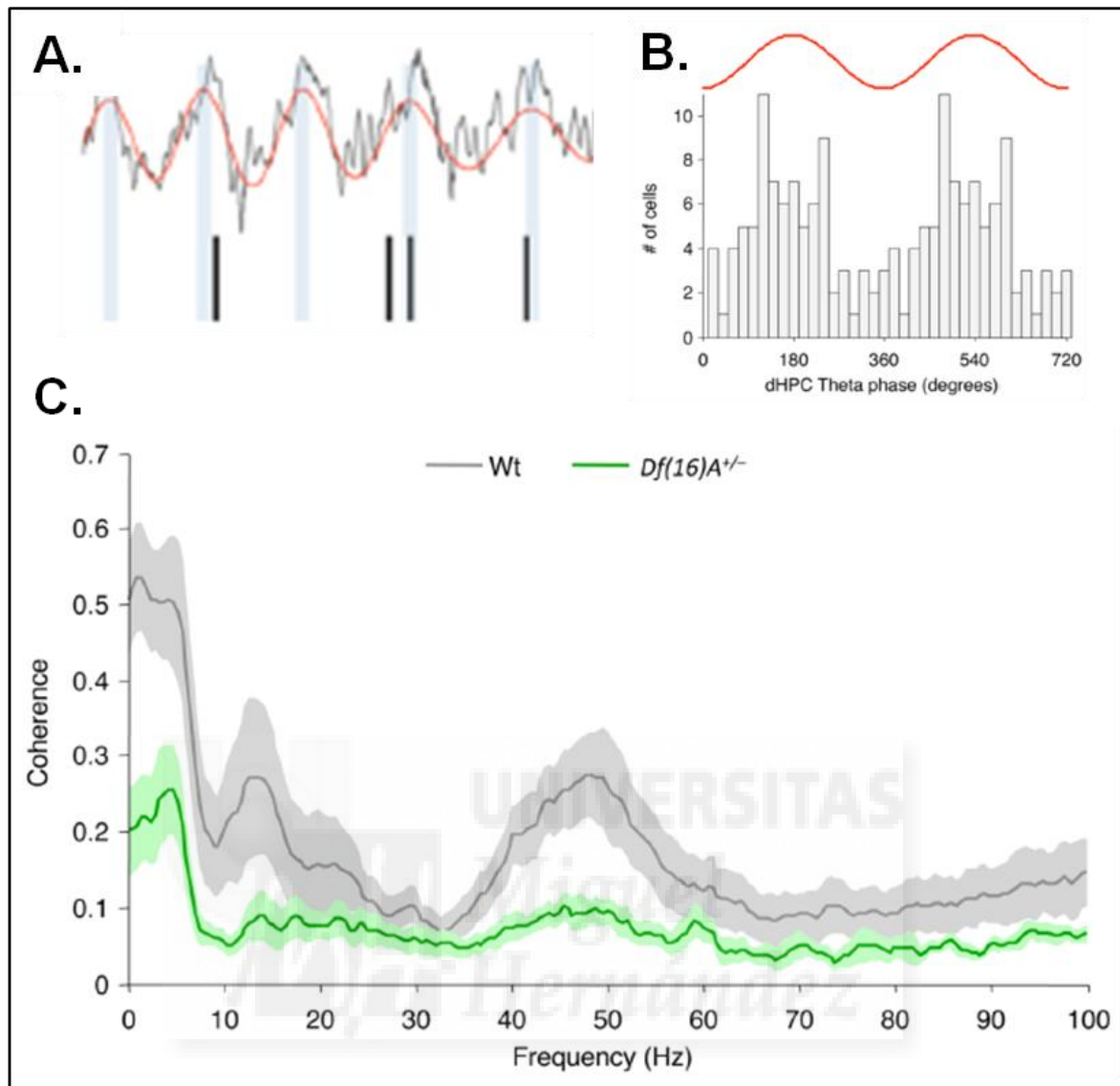


Figure 61: HPC-mPFC synchrony during a spatial memory task. (A) Example of field potential recording from HPC (black trace) showing theta oscillations (red trace) and spikes recorded simultaneously from a PFC neuron (ticks). (B) Distribution of HPC theta phases to which PFC neurons are phase-locked. Red trace= theta cycle. (C) Coherence between HPC and PFC field potentials at choice point of the maze. (adapted from Sigurdsson et al, 2010).

The lack of connectivity between different brain areas could be related to neuroanatomical issues resulting from developmental alterations. To test the hypothesis that schizophrenia can be due to an abnormal developed brain, a rat model of the disease is particularly useful: the methylazoxymethanol acetate embryonic day 17 (MAM-E17). This model is based on administration of a mitotoxin MAM (methylazoxymethanol-acetate) to pregnant rats to induce a neurodevelopmental disruption, selectively targeting limbic-cortical circuits by timing embryonic day 17 MAM injections to coincide with hippocampal and prefrontal cortical embryogenesis (Lodge and Grace

2007). Although no single intervention can model all aspects of schizophrenia in a rodent, the MAM-E17 model is therefore particularly useful in studying limbic-cortical dysfunction in neurodevelopmental disorders. MAM-E17 exposed rats show cognitive changes reminiscent of those seen in schizophrenia (table 7) (Moore et al., 2006), including impairments in spatial working memory (Gourevitch et al., 2004), attentional set-shifting (Featherstone et al., 2007), and reversal learning (Gastambide et al., 2012). MAM-E17 exposed rats also exhibit glutamatergic dysfunction, interneuronal dysfunction reflected by regionally restricted reductions in parvalbumin expression (Phillips et al. 2012) and reductions in the cortical up-state down-state transitions that underlie sleep slow oscillations (Moore et al. 2006). Previous work in the lab showed by using EEG, local field potential (LFP), and unit recordings in rats, that anteroposterior propagation of neocortical slow-waves during sleep coordinates timing of hippocampal ripples and prefrontal cortical spindles during NREM sleep. This coordination is selectively disrupted in the MAM rats: fragmented NREM sleep and impaired slow-wave propagation in the model culminate in deficient ripple-spindle coordination and disrupted spike timing, potentially as a consequence of interneuronal abnormalities reflected by reduced parvalbumin expression (K.G. Phillips et al., 2012). Interestingly it has been shown that mGlu5 positive allosteric modulator (PAM) may act as a cognitive enhancer and have beneficial effects on the deficits reported in this model (Gastambide et al., 2012).

Imaging or Neuropathological Findings in Schizophrenia	References	Present Findings in MAM-E17 Model
Reduction in tissue volume or thickness Reliability/severity: Hippocampus/parahippocampal region > frontal lobe > parietal or lateral frontal	Harrison 1999 Selemon et al 2003 Wright et al 2000	Reduced cortical thickness or area significant in HIPP, parahippocampal cortex, and mPFC but not in frontoparietal
Correlations between reduction in hippocampal volume and size and/or function of frontal lobe	Wible et al 1995 Bilder et al 1995	HIPP size correlates with PFC thickness and degree of orofacial dyskinesia
Selective reduction of size and/or cell number in anterior/medial dorsal thalamus	Ananth et al 2002 Thune and Pakkenberg 2000	Reduced size of medial dorsal thalamus but not medial geniculate body
Increased neuron packing density in dorsal frontal cortex (Brodmann area 9) and occipital cortex but not in ventrolateral frontal cortex (Brodmann area 45)	Selemon et al 1995, 2003	Increased neuron packing density in mPFC and OCC but not frontoparietal cortex
No difference in neocortical neuron number	Thune and Pakkenberg 2000	No difference in neocortical neuron number

MAM, methylazoxymethanol acetate; mPFC, medial prefrontal cortex; HIPP, hippocampus; PFC, prefrontal cortex; OCC, occipital.

Table 7: Comparison of neuroanatomical characteristics reported in Schizophrenia patients with findings in MAM-E17 model. (*adapted from Moore et al, 2006*).

As discussed above, Sigurdsson et al. 2010, showed that hippocampal and prefrontal synchrony was disrupted in a genetic mouse model of schizophrenia (Sigurdsson et al., 2010). The objective of this project was to attempt to replicate these observations in the MAM-E17 and try to reverse any deficits with pharmacological tools. We aimed to reveal the mechanisms underlying synchrony disruption in schizophrenia and improve our knowledge on the anatomical and neurophysiological dysfunctions responsible for this disorder.

The main objectives of this internship were:

- to surgically implant control and MAM-E17 animals with dual HPC-mPFC LFP recording probe.
- to perform wireless recordings as the rat learn a working memory-based task.
- to correlate electrophysiological measurements with behavioural performance.
- if a deficit is seen, attempt a reversal with pharmacology (ex: mGlu5 PAM)

Results of this project will be exposed after a brief presentation of the materials and methods necessary for this work. And finally results will be discussed at the end of this report.

2. Material and Methods

Animals

MAM and SHAM (=control coming from the litter of a saline-treated dam) were provided by Charles River (UK). Briefly MAM pups were obtained by injecting Sprague-Dawley pregnant dams on E17 with MAM mitotoxin (22 mg/kg i.p.; Midwest research institute, Missouri) or saline. For this project, we used 6 SHAM and 7 MAM male rats.

Surgery

Animals were anaesthetized (Isoflurane (2-3%) administered with O₂/CO₂ mix), head shaved and placed inside a stereotaxical frame. Along the surgery, anaesthetic depth was controlled following pinch paw reflex and body temperature. To prevent dehydration, animal were injected with Saline (5ml, before, during if more than 2 hours surgery and after). After skin surface cleaning (Chlorhexidine Gluconate 4%. HibiScrub, then ethanol 70%), a 3 cm window was opened at the top skin to get access to the bones. Bones surface was cleaned by scratching (scalpel blade) and 5% H₂O₂ washing. Then Bregma and the emplacement of for 2 electrodes and 5 stabilizing screws were pointed (pen or cauterizer) on the different bone plates. Five stabilizing screws were placed in the different bone plates, taking care to leave enough space for the implant. Good location of the prefrontal and hippocampal point was checked by placing the implant (from Bregma). Like for stabilizing screws, insertion windows were done with a hand drill to expose Dura matter surface. Dual site implants were moved onto the dura mater to determine the dorso-ventral zero. Dura mater was opened with a small bent needle (characteristic little eruption of CSF). Then the 32 channels dual silicon probe (CM32, 2x16; NeuroNexus Technologies) was placed down into the medial prefrontal cortex (A/P 3.20 mm, M/L 0.60 mm, D/V 3.25 mm) and the hippocampus (A/P -3.60 mm, M/L 2.20 mm, D/V 3.25mm) (figure 62). Paraffin was apply around the top of the silicon shank to prevent closure of the exposure and contact between the acrylic UV composite cement (Revolution, Formula 2, KERR). Cement was placed around the implant and the screws to stabilize the implant. Then skin was rehydrated, and closed tightly (absorbable suture, Ethicon) and cleaned (Betadine, Iodine).

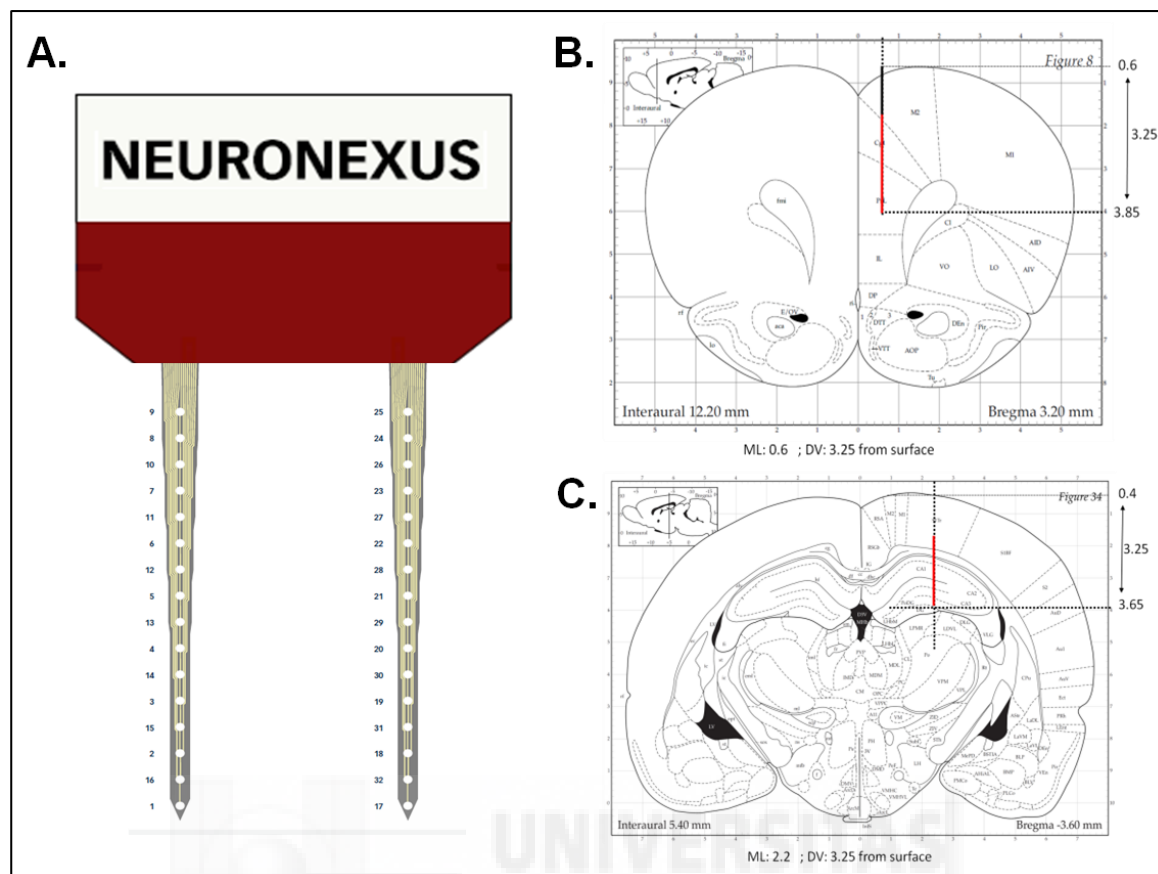


Figure 62: (A) Schema of a dual silicon probe, 2 times 16 channels. Implantation sites of the probe in the PFC (B) and the HPC (C).

The animal was injected with analgesics (Buprenorphine 0.05 mg/kg) and antibiotics (Covenia, 8 mg/kg) and placed in a recovery chamber (37°C). The animal's condition was checked every 30 min during the 2 hours recovery period. Finally, animals were placed in individual cages for a recovery period (at least 14 days) during which animal care was maintained daily (analgesics, anti-inflammatory, body weight measure).

In vivo Electrophysiology

To record long field potential (LFP) from mPFC and HPC during the task, a wireless headstage (32 channel neural systems, TBSI) was plugged and fixed into the implant on the head of the animal (figure 63). Antennas for the analogue receivers were placed in the maze room and linked to the receiver located in the experimenter room. The signal was digitised (Micro1401 v3, Expansion ADC64, Cambridge Electronic Design) and sent to the signal analysis software (Spike 2, Cambridge Electronic Design).

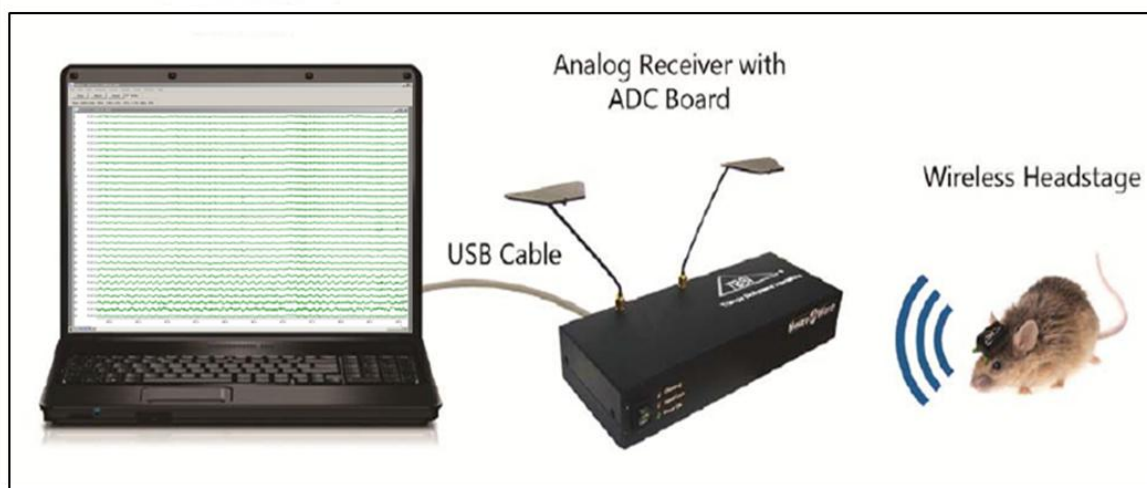


Figure 63: Organization of the electrophysiological data collection with the standard TBSI Wireless recording system.

Food deprivation

A food deprivation protocol aims to increase the motivation of the animal during the behaviour task. Maximum weight after surgery recovery period was considered as the initial weight to start the food deprivation protocol. All the animals were then daily weighed and appropriately fed to maintain them between 85 and 90% of the initial weight (middle food deprivation). Animals had *ad libitum* access to water.

Working memory continuous alternation task

The maze was located in a separate room from the experimenter, with constant light and temperature. Doors, rewards dispenser system and performance were controlled and recorded via custom MATLAB (The MathWorks, Inc., Natick, MA) scripts.

Training period (6 sessions): Initially rat was placed in the waiting area, after a 2 seconds delay door 1 was open to give access onto the central arm (figure 64). Once in the central arm the animal was exposed to two different situations: First the “forced-turn” where door 2 or 4 was open, so the animal get access to one side or the other and get rewarded (5x12 sucrose pellets, Janssen Pharmaceutica) while the opened door (2 or 4) was closed and the one giving access to the waiting room (3 or 5) opened.

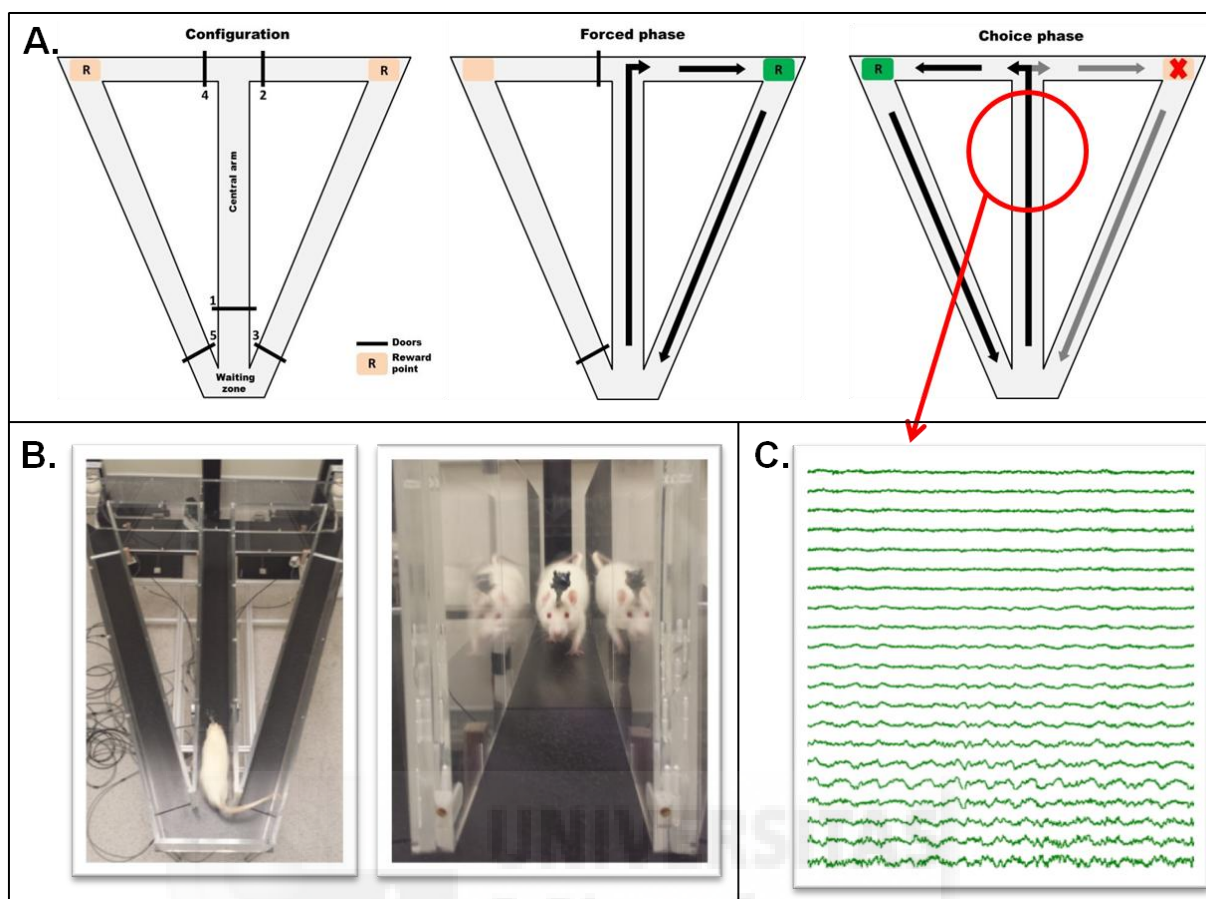


Figure 64: (A) Schema of the automated maze organization and task principle. (B) Two photographs of a equipped run into the maze. (C) Example of multichannel recording during the task. Note the characteristic hippocampal theta frequency in channel of lower half.

Once back in the waiting zone, the animal was exposed to a 5 seconds delay before door 1 opened to start the second part of the test phase, the “choice-turn”. In this case, doors 2 and 4 were opened, so the animal had the choice to turn left or right. To be rewarded, the animal must turn in the opposite side from the precedent “forced-turn” (alternation). Then the animal came back in the waiting zone and started a new trial after a 2 seconds delay (figure 64). Forced-turn direction was randomly varied, with no more than three consecutive trials in one direction (Jones and Wilson 2005).

One trial is composed of one “forced-turn” followed by a “choice-turn”. During one training session, the animal had to run 20 trials in a maximum of 45 minutes. Six training sessions were done.

Pharmacological study

All animals were submitted to the training paradigm (alternation task, 5 seconds delay). Thirty minutes prior running, animals were injected with a compound. Here we tested an NMDARs antagonist (Ketamine 10 mg/kg).

Data Analysis

Data from maze and electrophysiological signals were collected and analyzed simultaneously. LFP oscillatory events were detected using custom MATLAB (The MathWorks, Inc., Natick, MA) routines. All LFP traces were first band pass filtered (EEGLab toolbox, Delorme and Makeig, 2004) and then transformed to z-scores. A multi-taper spectral analysis was used to calculate power spectra and coherence for LFP data between the two cortical recording locations (Chronux toolbox, www.chronux.org). To investigate the temporal relationship between hippocampal and prefrontal events on a slow time scale, cross-correlation between the respective powers was computed. Spectral power in these frequency bands was calculated in overlapping 1s windows, providing a time series, which were log-transformed and cross-correlated. Statistical analysis was done using Prism (Graph Pad).

All this experiments were done under the Home office UK accord, respecting the Animal Scientific Procedures Act 1986 (PPL: 70/7430; PIL: 70/21195) and Lilly UK ethical review.

3. Results

Issues with MAME17 batch of animals and task learning

During the six days training sessions, we did not notice any difference between SHAM and MAM. On day 1, they were running the same number of trials (SHAM: 11.6 ± 2.3 ; MAM: 8.6 ± 2.3 ; $p=0.2$) with the same performance (SHAM: 77 ± 8.8 ; MAM: 62.1 ± 9.7 ; $p=0.2$). After 6 training sessions we did not observe any difference between groups in term of number of attempts (SHAM: 20 ± 0 ; MAM: 20 ± 0 ; $p=1$) or performance (SHAM: 81 ± 6 ; MAM: 86.3 ± 3 ; $p=0.3$). We were initially surprised by this result, as published data had previously suggested MAM animals have deficits in hippocampal dependent tasks (Gourevitch et al., 2004). However results from the *in vitro* electrophysiological department (Dr. Steve Fitzjohn) that was working with MAM's littermates also failed to see any MAM effect. Previous studies had shown a strong hyperexcitability phenotype has been reported in the area CA1 of the hippocampus in these animals (Lodge and Grace, 2007). In this batch however, this phenotype was not present suggesting a problem with the MAM production in this case. The decision was taken to stop working with the MAM animals and stay focus on the SHAM for the rest of the project.

Thus in SHAM animals, we observed that animals had good scores all along the training period (around 80% of success). The parameter that was significantly augmented was the number of trials. After 5 days 100% of the rats were running their 20 trials during the session (figure 65).

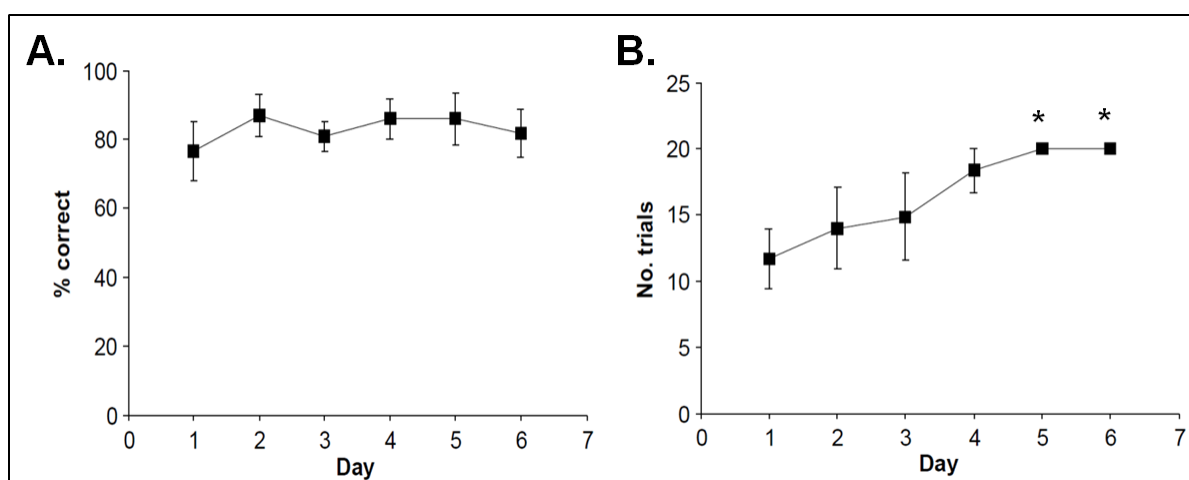


Figure 65: Rats spontaneously alternate and therefore show no significant increase in performance following training (A). Training does however increase the number of trials completed within a recording session (B). * $p < 0.05$ vs. day 1.

Theta coherence increase with training

As introduced earlier, the synchronization of HPC and PFC in the theta rhythm has been associated with working memory. Hence we started looking at the spectral powers of both structures at the moment when the animal was crossing the central arm: the choice point. Then we used these results to have an idea of the levels of coherence between the two structures at this point. We observed that from the second days, there is already a tendency of coherence between HPC and PFC within the theta range. Then across further training days significant theta coherence develops (day 4) and then continued to increase in magnitude (n= 6 animals, figure 66A). Looking selectively at the spectral power of LFP activity coming from one animal, we noted that hippocampal LFP showed a clear and persistent theta band that increases in both frequency and magnitude as the rat approaches the choice point. In the PFC, low frequency oscillations were preponderant with an acute change just before to make the choice. Here again at the scale of one animal, when we crossed these results, a clear increase in coherence between HPC and PFC LFP oscillations within the theta frequency band was appearing as the rat approaches the choice point. Another important point that we controlled here, is the correlation between the animal running speed and the theta frequency. Because with training the animals had a tendency to go faster every session so we were thinking that increased speed of the motor activity could be influence the detected signal in the both structures. Our analysis revealed that the levels of theta coherence were not correlated with animal running speed ($R^2=0.1$) (figure 66D).

As we had this issue with our model of schizophrenia, we adopted another strategy to simulate the disease. Blocking of NMDARs allows decreasing the excitability of interneurons expressing these receptors. Such a decrease of interneural excitability can simulate the hyperexcitability phenotype observed in MAM. Indeed it has been observed that blockade of the NMDARs induce schizophrenia-like psychotic state in human (LUBY et al. 1959; D. Lodge and Anis 1982) and can mimic NMDARs hypofunction during schizophrenia study (Olney et al 1999). Here used ketamine 10mg/kg to block NMADRs.

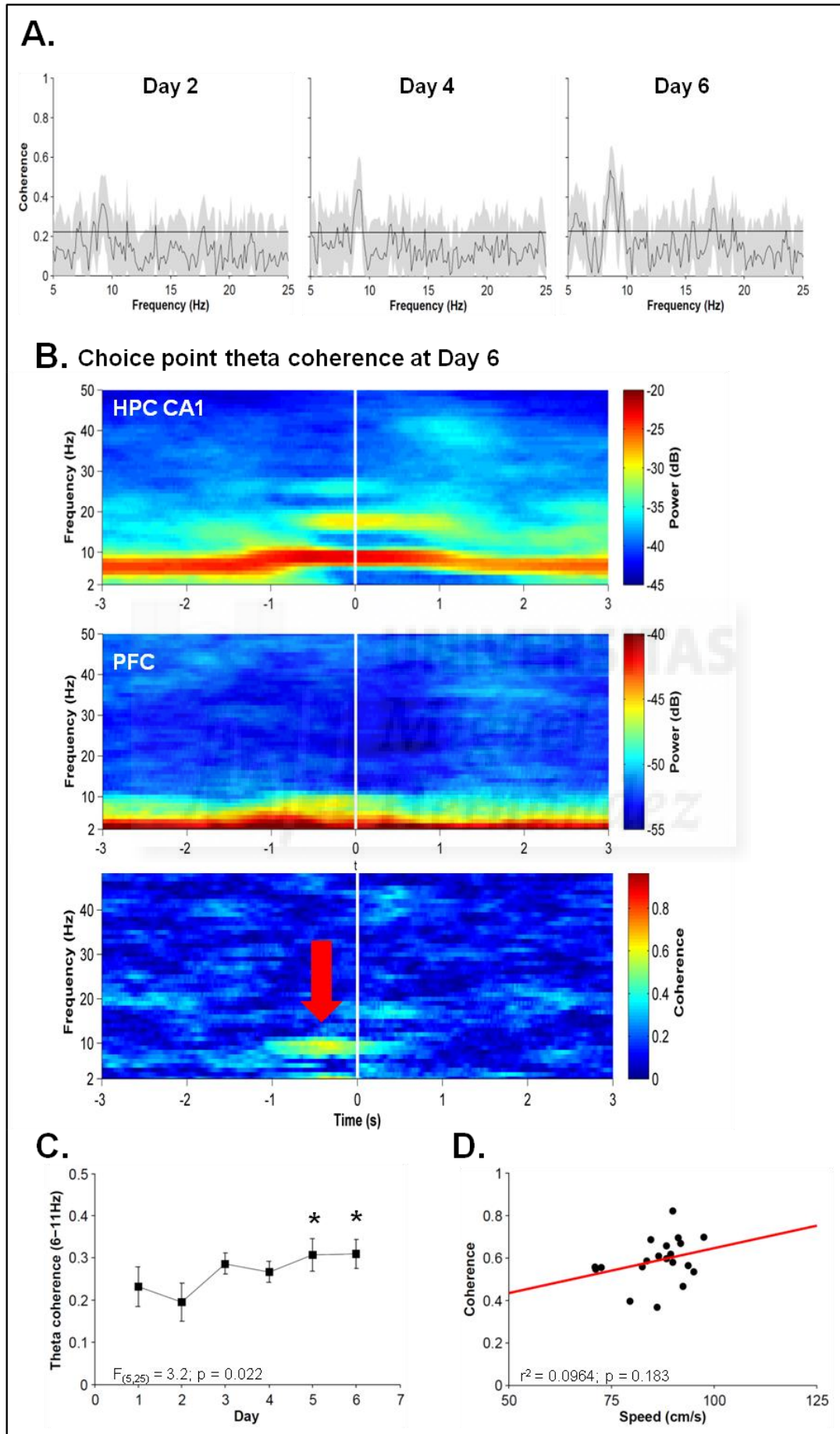


Figure 66: (A) Trial averaged HPC CA1-PFC coherence on training days 2, 4 and 6 from the same rat. Significant levels of coherence are indicated where Jackknife error horizontal bars do not overlap the 95% confidence marker (coherence = 0.222). (B) Spectral analysis of LFP activity recorded from a single rat on day 6 of recording centered on the choice point of the maze. *TOP*: Spectrogram of hippocampal LFP showed a clear and persistent theta band that increases in both frequency and magnitude as the rat approaches the choice point. *MIDDLE*: Low frequency power predominates in PFC, with little clear task relevant modulation in power. *BOTTOM*: A coherogram illustrates an increase in coherence between HPC and PFC LFP oscillations within the theta frequency band as the rat approaches the choice point (red arrow). (C) Mean theta coherence for all rats increased with training and is significantly elevated by day 5 of training. (D) Theta coherence changes were independent from running speed.

Ketamine reduced theta synchrony and reduction of theta synchrony was correlated to performance

Animals were injected 30 minutes prior to the beginning of the session. A short latency before the test is necessary to reach ketamine peak of activity on brain oscillations (Keith G. Phillips et al., 2012). Under ketamine, the running speed and the number of trials per session were diminished. The proportion of good choices has a clear tendency to be reduced (figure 67). Electrophysiological changes are produced after ketamine injection. In the HPC theta power was reduced whereas mPFC gamma power was increased. The theta range coherence between PFC and HPC was significantly decreased at the choice point. Statistical analysis revealed that theta coherence and performance reduction were correlated in the reduction (figure 67).

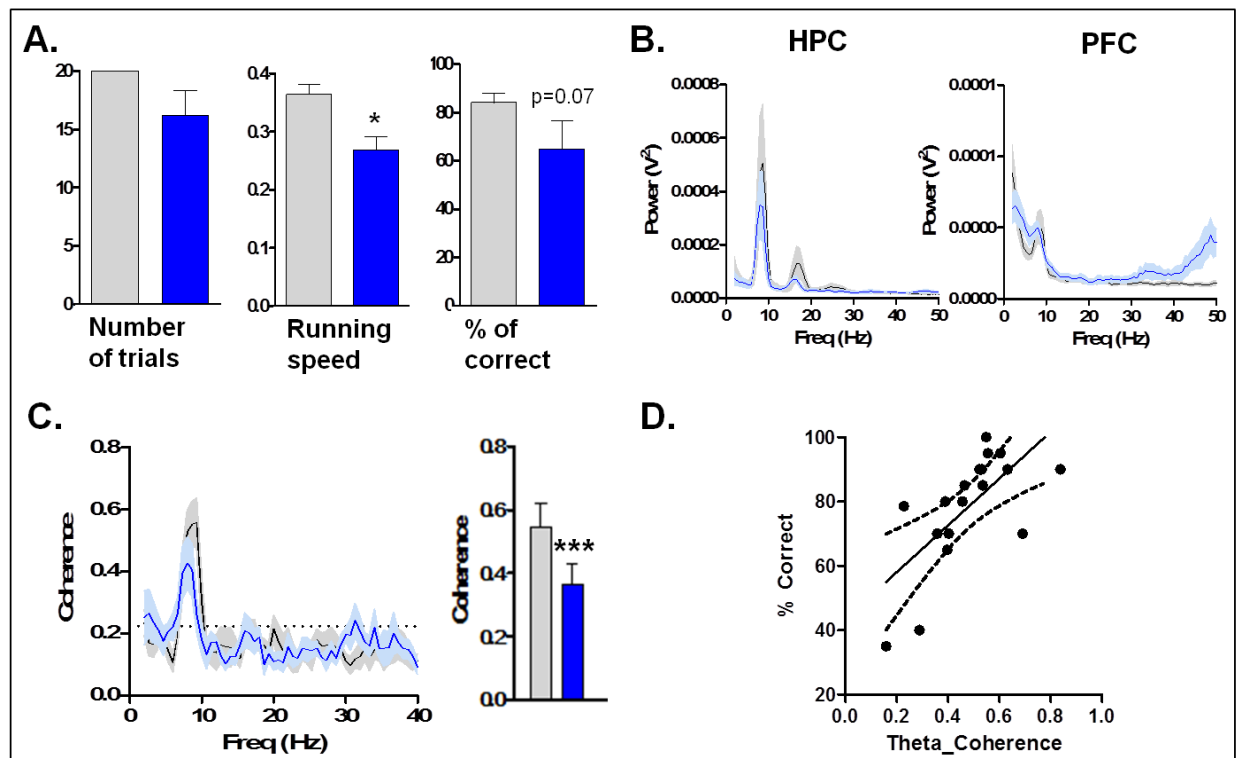


Figure 67: (A) Ketamine impaired performance and decreased the number of trials and the mean running speed of the rat on the centre arm. (B) Ketamine affects neural oscillations: Power spectrum from centre arm data pointed out a decrease in power in the theta band. (C) Ketamine significantly reduced theta coherence between HPC and PFC (D) Theta coherence reduction is correlated to performance. Grey= vehicle, blue= Ketamine 10mg/kg. * $p < 0.05$; *** $p < 0.001$

4. Discussion

The original aim of this internship project was to work on MAM-E17 rat model of schizophrenia. During the very first step of behavioural experiments, we realize that suspiciously ours MAM animals were not exhibiting any alteration in task completion. In fact electrophysiological *in vitro* data confirmed that there was a problem with this batch of MAM animals. Considering that it was too late to restart the project from the beginning and that we had implanted animals, we decided to stay focus on the SHAM animals and induce schizophrenia-like deficit pharmacologically.

During training we did not observed any improvement of the behaviour performance. In fact, rodents present a spontaneous alternation behaviour and have a natural tendency to goal in the arm that has been least recently explored (Still, 1966). As the animals had to alternate to get rewarded it is normal to not find any changes in alternation tendency during learning phase. However as the task was rewarded, we observed that the animal were running significantly more trials in the same time after 4 sessions. This result demonstrates that the animals learned and get motivated along the training period. As all these animals were implanted, hence it was possible to see if learning influence electrophysiological parameters in mPFC and HPC of these animals.

Previously it has been postulated that the interaction between mPFC and HPC is important for gating of attentional states (Grace, 2012; Sesack and Grace, 2010) and it has been demonstrated that mPFC-HPC theta synchrony is linked to spatial memory performance in rodent (Jones and Wilson, 2005; Sigurdsson et al., 2010). Here we also report a clear increase of the mPFC-HPC synchrony in the theta range at choice point during a working memory dependent task. For the first time we observe that theta synchrony between structures is “gradually” augmented at the choice point along training period. Importantly, we controlled that this augmentation is not correlated with an increase of animal motor activity.

Ketamine injection prior to the behavioural test decrease the performance and it is coupled to an increase of HPC theta power and an increase of mPFC gamma power. Increase of gamma oscillation is in accordance to what have been reported previously in visual cortex after NMDAR blockade (Keith G. Phillips et al., 2012). Ketamine injection drastically alters mPFC-HPC theta synchrony at the choice point. This result

points out the importance of the NMDARs component of the glutamatergic neurotransmission during execution of working memory-based task and also account for the glutamatergic hypofunction hypothesis as an origin of schizophrenia. Further experiments to test the implication of NMDARs in the elaboration of mPFC-PFC synchrony could be to expose one part of the animals to NMDARs antagonists during the whole learning period and see if the learning deficit and the lack of synchrony are persistent. In effect it is known that long term exposure to NMDARs antagonists is the most reliable way to model schizophrenia (Jentsch and Roth, 1999). Furthermore it would be possible to run other pharmacological experiments simultaneously to rescue the putative defects. Considering the reported hyperexcitability, a good strategy could be to enhance the inhibition pharmacologically or at the opposite try to control the excitatory transmission. As an example we can cite the study of Belujon and colleagues that reinstate normal synchrony in MAM with administration of sulpiride, an antipsychotic drug (antagonist of D2 dopamine receptors) (Belujon et al., 2013). In fact dopaminergic transmission onto nucleus accumbens is also increased in schizophrenia. Using this antagonist they managed to restore balance between structures. Finally they also suggest that lack of interaction between these structures in this model could explain the attentional deficits in schizophrenia patients and shed light onto their inability to focus a single task.

Taking together our results confirm that the theta synchrony constitutes a functional link between HPC and mPFC necessary for the acquisition of a spatial memory based task. It would be important to repeat this study with a proper batch of MAM-E17 rats. Main objectives would be to confirm the lack of reciprocal interaction between HPC and mPFC during working memory task in MAM and correlates it to the levels of performance. Also pharmacological experiments during this behavioural paradigm could help to improve our knowledge about the physiological alterations underlying behavioral and cognitive deficits observed in schizophrenia.

5. Appendix bibliography

- Belujon, P., Patton, M.H., Grace, A.A., 2013. Disruption of prefrontal cortical–hippocampal balance in a developmental model of schizophrenia: reversal by sulpiride. *Int. J. Neuropsychopharmacol.* 16, 507–512.
- Benchenane, K., Peyrache, A., Khamassi, M., Tierney, P.L., Gioanni, Y., Battaglia, F.P., Wiener, S.I., 2010. Coherent theta oscillations and reorganization of spike timing in the hippocampal–prefrontal network upon learning. *Neuron* 66, 921–936.
- Featherstone, R.E., Rizos, Z., Nobrega, J.N., Kapur, S., Fletcher, P.J., 2007. Gestational methylazoxymethanol acetate treatment impairs select cognitive functions: parallels to schizophrenia. *Neuropsychopharmacol. Off. Publ. Am. Coll. Neuropsychopharmacol.* 32, 483–92.
- Fell, J., Axmacher, N., 2011. The role of phase synchronization in memory processes. *Nat. Rev. Neurosci.* 12, 105–118.
- Garey, L., 2010. When cortical development goes wrong: schizophrenia as a neurodevelopmental disease of microcircuits. *J. Anat.* 217, 324–333.
- Gastambide, F., Cotel, M.-C., Gilmour, G., O’Neill, M.J., Robbins, T.W., Tricklebank, M.D., 2012. Selective remediation of reversal learning deficits in the neurodevelopmental MAM model of schizophrenia by a novel mGlu5 positive allosteric modulator. *Neuropsychopharmacol. Off. Publ. Am. Coll. Neuropsychopharmacol.* 37, 1057–1066.
- Gourevitch, R., Rocher, C., Le Pen, G., Krebs, M.-O., Jay, T.M., 2004. Working memory deficits in adult rats after prenatal disruption of neurogenesis. *Behav. Pharmacol.* 15, 287–92.
- Grace, A.A., 2012. Dopamine system dysregulation by the hippocampus: implications for the pathophysiology and treatment of schizophrenia. *Neuropharmacology* 62, 1342–1348.
- Harvey, C.D., Collman, F., Dombeck, D.A., Tank, D.W., 2009. Intracellular dynamics of hippocampal place cells during virtual navigation. *Nature* 461, 941–946.
- Jentsch, J.D., Roth, R.H., 1999. The Neuropsychopharmacology of Phencyclidine: From NMDA Receptor Hypofunction to the Dopamine Hypothesis of Schizophrenia. *Neuropsychopharmacology* 20, 201–225.
- Jones, M.W., Wilson, M.A., 2005. Theta rhythms coordinate hippocampal–prefrontal interactions in a spatial memory task. *PLoS Biol.* 3, e402.
- Lodge, D.J., Grace, A.A., 2007. Aberrant Hippocampal Activity Underlies the Dopamine Dysregulation in an Animal Model of Schizophrenia. *J. Neurosci.* 27, 11424–11430.
- Moore, H., Jentsch, J.D., Ghajarnia, M., Geyer, M.A., Grace, A.A., 2006. A neurobehavioral systems analysis of adult rats exposed to methylazoxymethanol acetate on E17: implications for the neuropathology of schizophrenia. *Biol. Psychiatry* 60, 253–264.
- Ongür, D., Price, J.L., 2000. The organization of networks within the orbital and medial prefrontal cortex of rats, monkeys and humans. *Cereb. Cortex N. Y. N* 1991 10, 206–219.

- Phillips, K.G., Bartsch, U., McCarthy, A.P., Edgar, D.M., Tricklebank, M.D., Wafford, K.A., Jones, M.W., 2012. Decoupling of Sleep-Dependent Cortical and Hippocampal Interactions in a Neurodevelopmental Model of Schizophrenia. *Neuron* 76, 526–533.
- Phillips, K.G., Cotel, M.C., McCarthy, A.P., Edgar, D.M., Tricklebank, M., O’Neill, M.J., Jones, M.W., Wafford, K.A., 2012. Differential effects of NMDA antagonists on high frequency and gamma EEG oscillations in a neurodevelopmental model of schizophrenia. *Neuropharmacology* 62, 1359–1370.
- Sesack, S.R., Grace, A.A., 2010. Cortico-Basal Ganglia reward network: microcircuitry. *Neuropsychopharmacol. Off. Publ. Am. Coll. Neuropsychopharmacol.* 35, 27–47.
- Sigurdsson, T., Stark, K.L., Karayiorgou, M., Gogos, J.A., Gordon, J.A., 2010. Impaired hippocampal-prefrontal synchrony in a genetic mouse model of schizophrenia. *Nature* 464, 763–767.
- Stark, K.L., Xu, B., Bagchi, A., Lai, W.-S., Liu, H., Hsu, R., Wan, X., Pavlidis, P., Mills, A.A., Karayiorgou, M., Gogos, J.A., 2008. Altered brain microRNA biogenesis contributes to phenotypic deficits in a 22q11-deletion mouse model. *Nat. Genet.* 40, 751–760.
- Still, A.W., 1966. Spontaneous Alternation and Exploration in Rats. *Nature* 210, 657–658.
- Uhlhaas, P.J., Linden, D.E.J., Singer, W., Haenschel, C., Lindner, M., Maurer, K., Rodriguez, E., 2006. Dysfunctional long-range coordination of neural activity during Gestalt perception in schizophrenia. *J. Neurosci. Off. J. Soc. Neurosci.* 26, 8168–8175.
- Wittner, L., Henze, D.A., Záborszky, L., Buzsáki, G., 2006. Hippocampal CA3 pyramidal cells selectively innervate aspiny interneurons. *Eur. J. Neurosci.* 24, 1286–1298.

Front page picture

Prefrontal cortex biocytin-labeled interneuron and pyramidal neuron. Gao Lab,
Department of Neurobiology and Anatomy, Drexel University (www.conncad.com)



